212

Source Apportionment of Volatile Organic Compounds and Aerosols on Sable Island

Attribution des sources de composés organiques volatiles et des aérosols sur l'Ile de Sable

Canada

July 2018

ENVIRONMENTAL
STUDIES
RESEARCH
FUNDS

SOURCE APPORTIONMENT OF VOLATILE ORGANIC COMPOUNDS AND AEROSOLS
ON SABLE ISLAND: 2017 Final Report

Contract number: 3000469926

Submitted by Dr. Mark Gibson P.Chem P.Eng and Dr. Susanne Craig

Contributing authors:
Alex Hayes, B.Eng MASc P.Eng
Jason Hopper, B.Sc
James Kuchta, B.Sc
Gavin King, B.Sc MSc
Yunchen Li, B.Sc MASc
Loay Jabre, B.Sc MASc
Codey Barnett, B.Eng MASc
Ellen Patrick B.Eng MASc
Courtney Wilson B.Eng

Atmospheric Forensics Research Group
Department of Civil and Resource Engineering
Dalhousie University
Sexton House
1360 Barrington Street
Halifax, Nova Scotia, B3J 24X Canada

TABLE OF CONTENTS

LIST OF TABLES

LIST OF FIGURES

ACKNOWLEDGEMENTS

EXECUTIVE SUMMARY

Air pollution can have varying health and environmental impacts which are not limited to the point of release, making it important to identify and quantify sources of air pollution and their fate and transport globally. Most studies are conducted in urban areas with few studies taking place at sea or near offshore oil and gas (O&G) production facilities, resulting in a paucity of data in these environments. This ESRF funded project aims to examine the different sources of air pollution/atmospheric chemistry affecting the air quality on Sable Island, a remote marine site, with the aim of better understanding the impacts of emissions from nearby offshore O&G activities, on island anthropogenic emissions (e.g. trash burning, diesel generator emissions, aircraft emissions and supply vessel emissions) directly from the ocean (e.g. sea salt spray, volatile organic compounds from phytoplankton and other marine organisms) and from continental outflow of anthropic (e.g. primarily fossil fuel combustion related emissions), and biogenic emissions (e.g. wildfire smoke and vegetative volatile organic compound emissions).

Gaseous and size-resolved particulate matter data obtained from Sable Island between May 7th and October 30th of 2013 was used to perform statistical analysis, source apportionment, and meteorological analysis. Further monitoring continued after this preliminary data capture providing a total of 541 days of data. The project finished on December 31st 2017.

The models used to identify and quantify sources of air pollution included the National Oceanic and Atmospheric Administration (NOAA) Hybrid Single-Particle Lagrangian Integrated Trajectory (HYSPLIT) model and the United States Environmental Protection Agency (USEPA) Positive Matrix Factorization (PMF) model v 3.0.2.2 and v 5.0. The air pollutants measured included non-methane hydrocarbons (NMHCs), black carbon (BC), hydrogen sulfide (H_2S), mono-nitrogen oxides (NO_x), nitrogen oxide (NO), nitrogen dioxide (NO_2), ozone (O_3), particulate matter with a median aerodynamic diameter less than or equal to 10/4/2.5/1 microns ($PM_{10/4/2.5/1}$), size-resolved particle number counts between 20 nm and 20 microns over 58 size bins, and sulphur dioxide (SO_2). NMHCs and BC measurements had a temporal resolution of 5 minutes, ultrafine particles 15 minutes with the remaining data averaged hourly.

Results from Data Collected May to October 2013

Between May 7th and October 30th of 2013 the average concentration of O_3 (30.4 ppb) was below the annual average concentration of O_3 in ambient air in Canada, which was 33 ppb in 2011 (Environment Canada, 2013). All of the average and maximum concentrations for pollutants governed by The Air Quality Regulations from Nova Scotia Environment (including O_3) fell below maximum permissible levels. The mean values (min:max) for NMHC, BC, $PM_{2.5}$, SO_2, H_2S, O_3, NO, NO_x, and NO_2 were 0.034 ppm (0.0 : 1.13), 0.092 $\mu g/m^3$ (0.0 : 13), 14.1 $\mu g/m^3$ (0 : 43), 0.168 ppb (0.0 : 3), 0.361ppb (0.0 : 13.7), 30.4 ppb (8.24 : 61.1), 2.17 ppb (0.0 : 3.5), 1.12 ppb (0.0 : 28.7), 0.998 ppb (0.0 : 14.6). During this study, a new gas production facility came on line on July 22nd 2013. Significant differences ($P<0.05$) between concentrations of BC, $PM_{2.5}$, SO_2, H_2S, O_3, NO, NO_x, and NO_2 were seen after July 22nd 2013. The median values and upper percentiles for BC, $PM_{2.5}$, NO, and NO_x show decreases after July 22nd, while those for SO_2, H_2S, and NO_2 show increases. For the preliminary data between May 7th 2013 and October 30th of 2013, PMF identified 4 sources contributing to the air quality on Sable Island that included long range transport, offshore O&G activities, marine emissions and on-island combustion were the sources associated with these 4 factors. However, during this period, a lack of a full suite of instruments, caused by numerous contract amendments to replace instruments that were to be supplied from research partners or removed from the Island by Nova Scotia Environment, meant that the mass contributions from these sources could not be determined due to insufficient aerosol and VOC chemical speciation data. The loss of these instruments, the vital data they would have provided and the inability to identify these sources ran contrary to the aims and objectives of the study. Having these data would have allowed the project to be completed sooner, or to provide a larger data set upon which to gain further insights into the drivers of air emission sources impacting Sable Island.

Results from 2016 Data Set

After the full suite of instruments were finally in place in late 2015, monitoring was conducted for the entirety of 2016 (and still ongoing). This report also contains the analysis and modelling of the 2016 data set. The summary descriptive statistics for the 2016 data set are provided in Table 1 below.

Table 1 Descriptive Statistics for the 2016 data set

Variables	n	Missing Data	Data Completeness	Min	Median	Mean	Max	IQR	Std. Dev.
DRX_PM$_1$ [mg/m^3]						0.011	0.087	0.01	0.009
DRX_PM$_{2.5}$ [mg/m^3]						0.012	0.093	0.01	0.01
DRX_PM$_4$ [mg/m^3]	32866	739	97.75%	0	0.009	0.011	0.124	0.011	0.010
DRX_PM$_{10}$ [mg/m^3]						0.012	0.124	0.011	0.010
DRX PM$_{Total}$ [mg/m^3]						0.012	0.127	0.011	0.010
UFP 20-30 nm [Particle #/cm^3]					185	328	34766	354	597
UFP 30-50 nm [Particle #/cm^3]					214	360	35441	394	595
UFP 50-70 nm [Particle #/cm^3]	32502	2634	92.5%	0	138	227	20213	266	339
UFP 70-100 nm [Particle #/cm^3]					129	205	17333	241	286
UFP 100-200 nm [Particle #/cm^3]					191	252	32469	261	321
UFP 200-800 nm [Particle #/cm^3]					25	43	4261	57	66
APS_PM$_1$ [Particle #/cm^3]				1879	18360	21249	79590	2932	19677
APS_PM$_{2.5}$ [Particle #/cm^3]				64	2579	2970	20123	2920	3496
APS_PM$_4$ [Particle #/cm^3]	20497	14639	58.3%	3	174	257	3856	2421	562
APS_PM$_{10}$ [Particle #/cm^3]				1	9	20	491	2376	81
APS_PM$_{20}$ [Particle #/cm^3]				1	1	1	26	310	3
VOC [ppb]	32173	2963	91.6%	0	1871	1871	20030	3194	2098
NO [ppb]					0.1	0.2	20.1	0.2	0.5
NO$_2$ [ppb]					0.8	0.8	12.7	0.7	0.7
NO$_x$ [ppb]	5879	2924	66.7%	0	0.9	1.1	32.8	0.9	1.1
O$_3$ [ppb]					26.8	27.2	51.2	9.7	6.6
SO$_2$ [ppb]					0.7	0.8	230.0	0.3	3.1
H$_2$S [ppb]					0.4	0.4	71.3	0.3	1.3
BC [μg/m^3]	10081	527040	1.9%	0	0.040	0.046	0.21	0.05	0.036

DRX = TSI DRX DustTrak photometer
UFP = TSI 3031 Ultrafine Particle Counter
APS = TSI 3321 Aerosol Particle Sizer
VOC = ppbRAE total volatile organic compounds measure by a photoionization detector
NO$_x$ = Nitrogen oxides by molybdenum converter chemiluminescence
O$_3$ = ground level ozone by UV absorption
SO$_2$ = Sulphur dioxide by UV pulsed fluorescence
H$_2$S = Hydrogen sulphide by oxidation and pulsed florescence
BC = Black carbon via a Thermo 5012 MAAP multi-angle reflectance and transmission instrument
IRQ = Interquartile range i.e., 25 to 75 percentile of the spread of the data

As can be seen from Table 1, there was excellent data completeness for the DRX, UFP, and VOC instruments (> 91.6%). The NO_x, O_3, SO_2 and H_2S had 66.7% data capture, which can be considered as reasonable given access to the island is intermittent and problematic. The APS had a data capture of 58% (due to a pump failure) with the BC instrument only managing 5-days of measurement in 2016 due to a data capture error that went unnoticed. The loss of BC is unfortunate, as it is a good marker for combustion of fossil fuels and wildfire smoke. None of the 'criteria' and regulated air pollutants ($PM_{2.5}$, O_3, SO_2, NO_x) were found to be above Provincial or National Air Quality Guidelines. Indeed, the concentrations are low and reflect the fact that Sable Island is in a relatively clean marine environment.

The 2016 data completeness for temperature, wind direction and wind speed was 96%, 100% and 99% respectively, which can be considered excellent data capture for these meteorological variables. The mean (min : max) temperature and wind speed was found to be 9.04 (-11.4 : 53.8°C), 25.39 km/h (0 : 84 km/h). Obviously, the maximum temperature of 53.8°C seems highly unlikely and suggests there might be a temperature sensor malfunction. It was found that the average wind vector for 2016 was 256°, which is consistent with prevailing winds in the North West (NW) Atlantic.

In terms of offshore oil and gas production activity, Deep Panuke had several extended shutdown periods in 2016 for maintenance, repair and/or seasonal production (Jan 15-26; Mar 20-May 26; May 29-Jun 16; Oct 14-25 and Nov 1-8). ExxonMobil had a planned field-wide maintenance shutdown between September 15 and October 7 2016.

It terms of identifying potential O&G production emissions, there was a spike in H_2S of 6.01 ppbv on 17/07/16. This spike was above an operating threshold value of 3.11 ppbv calculated in collaboration with Encana and ExxonMobil. This threshold is based upon previous years elevated levels and not related to any Provincial or National air quality guidelines, but rather a means to help identify excursions from typical observations from Sable Island. This spike on 17/07/16 is well below the 1-hr Nova Scotia air quality objective of 30 ppbv. This H_2S spike is obviously linked to the elevated SO_2 level of 3.04 ppbv that occurred on the same day, but below the operational spike threshold of 6.0 ppbv calculated in collaboration with Encana and

ExxonMobil, and well below the 1-hr Canada Ambient Air Quality Objectives threshold of 344 ppbv. Scrutiny of the air mass back trajectories for this day showed that airflow passed over both the Deep Panuke and Thebaud platforms preceding and during observations on Sable Island. The spike 'might' be associated with flaring of H_2S on the Deep Panuke platform at the time. On 05/10/16 there was a spike in NO_x concentration of 7.16 ppbv. This happened a few days after the ExxonMobil platform wide maintenance shutdown. The airflow during the spike observations was directly over the Thebaud platform. Therefore, it could be a possible source. However, NO_x level was well below the operational spike threshold of 17 ppbv, and well below the Canada Ambient Air Quality Objective of 213 ppbv.

The USEPA PMF source apportionment model of the size-resolved particle number and mass concentration yielded four factors (*which can be translated into sources of PM*): sea spray (2.2% of total Ultrafine particles (UFP), secondary marine biogenic particles (78.2%), long range transport (4.4%) and island surface dust (15.2%). The strong correlations between UFP (20-30 nm & 30-50 nm) and *chlorophyll a* ($R^2 = 0.815$ and $R^2 = 0.815$), was the most salient feature of this study and provides powerful insight into ocean-atmosphere dynamics that remain high uncertainty in global climate. It was not possible to identify a definite O&G source 'factor' using PMF over the year as the emissions from O&G are extremely low, with intermittent 'spikes' that are dwarfed by continental and oceanic atmospheric gas and particle inputs.

In conclusion, O&G production emissions were negligible over the course of the study (January 1st 2013 - Dec 31st 2016). The chief emissions sources impacting air quality on Sable Island are associated with the long-range transport continental outflow of anthropogenic and biogenic gaseous and particulate matter, marine emissions of VOCs and their associated secondary ultrafine particles, sea salt spray and wind-blown sand.

SOMMAIRE

La pollution atmosphérique peut avoir diverses incidences sur la santé et l'environnement, incidences qui ne se limitent pas au point de rejet, d'où l'importance de déterminer et de quantifier les sources de la pollution atmosphérique, leur devenir et leur transport à l'échelle mondiale. La plupart des études sont effectuées dans les zones urbaines et peu d'études sont menées en mer ou près des installations de production pétrolière et gazière (P&G) extracôtières, ce qui explique la rareté des données recueillies dans ces milieux. Le projet financé par le Fonds pour l'étude de l'environnement (FEE) vise à examiner les différentes sources de la pollution et de la chimie atmosphériques responsables de la qualité de l'air sur l'île de Sable, un site marin éloigné, afin de parvenir à une meilleure compréhension des répercussions des émissions émises à proximité des activités pétrolières et gazières extracôtières, des émissions anthropiques de l'île (p. ex. l'incinération des déchets, les émissions des génératrices au diesel, les émissions des aéronefs et les émissions des navires d'approvisionnement), les émissions issues directement de l'océan (p. ex. les embruns marins, les composés organiques volatils provenant du phytoplancton et d'autres organismes marins) et du transport continental des émissions anthropiques (p. ex. les émissions provenant principalement de la combustion des combustibles fossiles), et les émissions biogéniques (p. ex la fumée provoquée par les incendies de forêt et les émissions provenant des composés organiques volatils végétatifs).

Les données sur la matière gazeuse et la matière particulaire, caractérisées en fonction de leur taille, recueillies sur l'île de Sable du 7 mai au 30 octobre 2013 ont été utilisées pour effectuer une analyse statistique, l'attribution des sources et une analyse météorologique. Nous avons poursuivi la surveillance après la collecte des données préliminaires, ce qui nous a permis de recueillir en tout 541 jours de données. Le projet a pris fin le 31 décembre 2017.

Le modèle Hybrid Single-Particle Lagrangian Integrated Trajectory (HYSPLIT) de la National Oceanic and Atmospheric Administration (NOAA) et le modèle de Factorisation de matrice positive (versions 3.0.2.2 et 5.0) de l'Environmental Protection Agency (USEPA) des États-Unis ont été utilisés pour déterminer et quantifier les sources de la pollution atmosphérique. Les

polluants atmosphériques suivants ont été mesurés : les hydrocarbures non méthaniques, (NMHC), le carbone noir (CN), le sulfure d'hydrogène (H2S), les oxydes d'azote (NOx), l'oxyde d'azote (NO), le dioxyde d'azote (NO2), l'ozone (O3), la matière particulaire dont le diamètre aérodynamique médian est inférieur ou égal à 10/4/2,5/1 microns (PM10/4/2.5/1), les particules caractérisées en fonction de leur taille se situant entre 20 nm et 20 microns divisées par incréments de 58 et le dioxyde de soufre (SO2). Les mesures de NMHC et de carbone noir avaient une résolution temporelle de 5 minutes, les particules ultrafines de 15 minutes avec le restant des données caractérisées en moyenne horaire.

Résultats des données recueillies de mai à octobre 2013

Au Canada, du 7 mai au 30 octobre 2013, la concentration moyenne de O3 (30,4 ppb) était inférieure à sa concentration moyenne annuelle dans l'air ambiant qui était de 33 ppb en 2011 (Environnement Canada, 2013). Toutes les concentrations moyennes et maximales des polluants régis par le *Règlement sur la qualité de l'air* du ministère de l'Environnement de la Nouvelle-Écosse (y compris l'ozone (O3)) étaient inférieures aux seuils maximums admissibles. Les valeurs moyennes (min:max) des NMHC, de CN, PM2.5, SO2, H2S, O3, NO, NOx et de NO2 étaient de 0,034 ppm (0,0 : 1,13), 0,092 µg/m3 (0,0 : 13), 14,1 µg/m3 (0 : 43), 0,168 ppb (0,0 : 3), 0,361 ppb (0,0 : 13,7), 30,4 ppb (8,24 : 61,1), 2,17 ppb (0,0 : 3,5), 1,12 ppb (0,0 : 28,7), 0,998 ppb (0,0 : 14,6). Au cours de cette étude, une nouvelle installation de production gazière a été mise en service le 22 juillet 2013. Des différences considérables (P<0,05) ont été enregistrées entre les concentrations de CN, PM2.5, SO2, H2S, O3, NO, NOx et de NO2 après le 22 juillet 2013. Après cette date, les valeurs moyennes et les percentiles supérieurs de CN, PM2.5, NO et NOx ont diminué alors que celles de SO2, H2S et NO2 ont augmenté. En ce qui a trait aux données préliminaires recueillies entre le 7 mai et le 30 octobre 2013, le modèle Factorisation de matrice positive a identifié quatre sources responsables de la qualité de l'air sur l'île de Sable, notamment le transport à grande distance, les activités gazières et pétrolières extracôtières, les émissions marines et la combustion sur l'île qui constituaient les sources associées à ces quatre facteurs. Cependant, en raison de l'absence d'un ensemble complet d'instruments, attribuable aux nombreuses modifications apportées au contrat visant à remplacer les instruments qui devaient être fournis par les partenaires de recherche ou être retirés de l'île par le ministère de

l'Environnement de la Nouvelle-Écosse, il a été impossible de quantifier les apports de chaque source en raison de l'insuffisance des données sur les aérosols et la spéciation chimique des composés organiques volatils. La perte de ces instruments, les données essentielles qu'ils auraient fournies et l'incapacité de déterminer ces sources étaient contraires aux buts et objectifs de l'étude. Ces données auraient permis de terminer le projet plus tôt ou de fournir un ensemble de données plus vaste qui aurait servi à acquérir une meilleure connaissance de l'origine des sources d'émissions atmosphériques ayant des incidences sur l'île de Sable.

Résultats de l'ensemble des données de 2016

Après l'installation de l'ensemble des instruments à la fin de 2015, la surveillance a été effectuée tout au long de 2016 (et se poursuit encore). Le présent rapport renferme également l'analyse et la modélisation de l'ensemble des données de 2016. Le résumé des statistiques descriptives pour l'ensemble des données de 2016 est présenté dans le tableau 1 ci-dessous.

Tableau 1: Statistiques descriptives de l'ensemble des données de 2016

Variables	N	Données manquantes	Exhaustivité des données	Min	Médiane	Moyenne	Max	Intervalle	Interquartile Écart-type
DRX_PM$_1$ *[mg/m^3]*						0,011	0,087	0,01	0,009
DRX_PM$_{2.5}$ *[mg/m^3]*						0,012	0,093	0,01	0,01
DRX_PM$_4$ *[mg/m^3]*	32866	739	97,75 %	0	0,009	0,011	0,124	0,011	0,010
DRX_PM$_{10}$ *[mg/m^3]*						0,012	0,124	0,011	0,010
DRX PM$_{Total}$ *[mg/m^3]*						0,012	0,127	0,011	0,010
UFP 20-30 nm *[Particule #/cm^3]*					185	328	34766	354	597
UFP 30-50 nm *[Particule #/cm^3]*					214	360	35441	394	595
UFP 50-70 nm *[Particule #/cm^3]*	32502	2634	92,5 %	0	138	227	20213	266	339
UFP 70-100 nm *[Particule #/cm^3]*					129	205	17333	241	286
UFP 100-200 nm *[Particule #/cm^3]*					191	252	32469	261	321
UFP 200-800 nm *[Particule #/cm^3]*					25	43	4261	57	66
APS_PM$_1$ *[Particule #/cm^3]*				1879	18360	21249	79590	2932	19677
APS_PM$_{2.5}$ *[Particule #/cm^3]*				64	2579	2970	20123	2920	3496
APS_PM$_4$ *[Particule #/cm^3]*	20497	14639	58,3 %	3	174	257	3856	2421	562
APS_PM$_{10}$ *[Particule #/cm^3]*				1	9	20	491	2376	81
APS_PM$_{20}$ *[Particule #/cm^3]*				1	1	1	26	310	3
COV *[ppb]*	32173	2963	91,6 %	0	1871	1871	20030	3194	2098
NO *[ppb]*					0,1	0,2	20,1	0,2	0,5
NO$_2$ *[ppb]*					0,8	0,8	12,7	0,7	0,7
NO$_x$ *[ppb]*	5879	2924	66.70%	0	0,9	1,1	32,8	0,9	1,1
O$_3$ *[ppb]*					26,8	27,2	51,2	9,7	6,6
SO$_2$ *[ppb]*					0,7	0,8	230,0	0,3	3,1
H$_2$S *[ppb]*					0,4	0,4	71,3	0,3	1,3
CN *[µg/m^3]*	10081	527040	1,9 %	0	0,040	0,046	0,21	0,05	0,036

DRX =Photomètre DustTrak TSI DRX

UFP = Particule ultrafine TSI 3031

APS = Calibreur des particules d'aérosol TSI 3321

COV = Mesure des composés organiques volatiles totaux d'un pppRAE par un détecteur à photo-ionisation

NO$_x$ = Oxydes d'azote par un convertisseur au molybdène par chimiluminescence

O$_3$ = Ozone au niveau du sol par l'absorption ultraviolette

SO$_2$ = Dioxyde de soufre par fluorescence ultraviolette pulsée

H$_2$S = Sulfure d'hydrogène par oxydation et florescence pulsée

CN = Carbone noir par l'instrument de réflexe et transmission multi-angle Thermo 5012 MAAP

Ainsi qu'il ressort du tableau 1, l'intégralité des données était excellente pour les instruments DRX, UFP et COV (> 91,6 %). Le pourcentage des données saisies pour NOx, O3, SO2 et H2S était de 66,7 %, ce qui peut être considéré comme acceptable étant donné que l'accès à l'île était intermittent et problématique. La capture des données de l'APS était de 58 % (en raison d'une défaillance de la pompe) et l'instrument de mesure du charbon noir a fonctionné que pendant 5 jours en 2016, due à une erreur dans la saisie des données qui était passée inaperçue. La perte des mesures du charbon noir est regrettable, car il est un bon marqueur de la combustion des combustibles fossiles et de la fumée provoquée par les incendies de forêt. Aucun des 'critères' et des polluants atmosphériques règlementés (PM2.5, O3, SO2, NOx) n'a dépassé la limite indiquée dans les lignes directrices provinciales ou nationales visant la qualité de l'air. En effet, les concentrations étaient faibles et témoignaient du fait que l'île de Sable est située dans un milieu marin relativement sain.

L'exhaustivité des données de 2016 sur la température et la direction et la vitesse du vent était respectivement de 96 %, 100 %, et 99 %, ce qu'on peut considérer comme une excellente saisie des données pour ces variables météorologiques. La moyenne (min : max) de température et de la vitesse du vent était de 9,04 (-11,4 : 53,8 °C) et 25,39 km/h (0 : 84 km/h), respectivement. La température maximale de 53,8 °C semble très peu probable et semble indiquer une défaillance du capteur de température. En 2016, le vecteur éolien moyen était de 256°, ce qui est conforme aux vents dominants dans l'Atlantique du Nord-Ouest (NO).

En ce qui a trait aux activités de production gazière et pétrolière extracôtières, Deep Panuke a subi plusieurs périodes d'arrêt prolongées en 2016 liées à l'entretien, la réparation et/ou la saisonnalité de la production. (15-26 janvier; 20 mars-26 mai ; 29 mai-16 juin; 14-25 octobre et 1er-8 novembre). ExxonMobil avait prévu l'arrêt des activités dans l'ensemble du champ, à des fins d'entretien, du 15 septembre au 7 octobre 2016.

Pour ce qui est de la détermination des émissions possibles provenant de la production gazière et pétrolière, un pic de 6,01 ppbv du H2S a été atteint le 17 juillet 2016. Ce pic était supérieur à la valeur du seuil d'exploitation de 3,11 ppbv calculée en collaboration avec Encana et ExxonMobile. Ce seuil est basé sur les niveaux élevés des années antérieures et n'est liée à aucune ligne directrice

provinciale ou nationale sur la qualité de l'air; elle est plutôt un moyen contribuant à déterminer les dépassements observés en général sur l'île de Sable. Ce pic atteint le 17 juillet 2016 est nettement inférieur à l'objectif de 30 ppbv par période d'une heure fixée par la Nouvelle-Écosse pour la qualité de l'air. Ce pic du H2S est manifestement lié au niveau élevé de SO2 de 3,04 ppbv qui a été enregistré le même jour, mais il est inférieur au seuil du pic d'exploitation de 6,0 ppbv calculé en collaboration avec Encana et ExxonMobil et nettement inférieur au seuil de 344 ppbv par période d'une heure fixée par les normes canadiennes de la qualité de l'air ambiant. L'examen des rétrotrajectoires de la masse d'air observées le même jour a révélé que le flux d'air passait sur les plateformes DeepPanuke et Thebaud avant et durant les observations sur l'île de Sable. Le pic « pourrait » être associé au torchage de H2S sur la plateforme Deep Panuke à ce moment-là. Le 10 mai 2016, un pic de 7,16 ppbv a été relevé dans une concentration de NOx quelques jours après que ExxonMobil ait ordonné l'arrêt des activités sur l'ensemble de la plateforme, à des fins d'entretien. Le flux d'air durant les observations du pic est passé directement sur la plateforme Thebaud. Par conséquent, il pourrait être une source possible. Cependant, le niveau du NOx est nettement inférieur au seuil du pic d'exploitation de 17 ppbv et à l'objectif de 213 ppbv fixé pour la qualité de l'air ambiant du Canada.

Le modèle FMP de l'USEPA pour l'attribution des sources de particules caractérisées en fonction de la taille de leur concentration de masse a révélé quatre facteurs (qui peut se traduire en sources de particules dans l'air): les embruns (2,2 % de la totalité des particules ultrafines (PUF), les particules biogéniques marines secondaires (78,2 %), les particules transportées sur une grande distance (4,4 %) et la poussière sur la surface de l'île (15,2 %). Les fortes corrélations des PUF (20-30 nm et 30-50 nm) et du *chlorophylle-a* (R2 = 0,815 et R2 = 0,815), constituent la caractéristique la plus marquante de cette étude et fournissent des informations importantes sur la dynamique de l'atmosphère de l'océan qui demeure une grande incertitude en ce qui a trait au climat mondial. La source principale d'émissions venant des industries pétrolières et gazières n'a pu être déterminé en utilisant le CMR au fil des ans puisque les émissions rejetées par le pétrole et le gaz sont extrêmement faibles avec des « pics » intermittents qui semblent minuscules par rapport aux entrées du gaz et des particules atmosphériques continentales et océaniques.

Pour conclure, les émissions de la production gazière et pétrolière étaient négligeables durant l'étude (du 1er janvier au 31 décembre 2016). Les principales sources d'émissions ayant des répercussions sur la qualité de l'air sur l'île de Sable sont associées à l'écoulement des matières gazeuses et des particules anthropiques et biogéniques et de la matière particulaire transportées sur une grande distance, aux émissions de composés organiques volatils et leurs particules ultrafines secondaires connexes, aux embruns marins et au sable transporté par le vent.

LIST OF ABBREVIATIONS USED

ASO_4 / $(NH_4)_2SO_4$	Ammonium sulphate
APS	TSI aerodynamic particle sizer - model 3321
BC	Black carbon
CCN	Cloud condensation nuclei
CH	Hydrocarbons
CH_4	Methane
Chl a	Chlorophyll a
Cl	Chloride
CMB	Chemical Mass Balance
CNSOPB	Canada-Nova Scotia Offshore Petroleum Board
CO	Carbon monoxide
CO_2	Carbon dioxide
$\delta^{13}C$	Carbon 13
$\delta^{18}O$	Oxygen 18
DMS	Dimethyl sulphide
DRX	TSI DustTrak DRX model 8533
EA	Environmental Assessment
EC	Environment Canada
GPC	Gas-to-particle conversion
H_2	Hydrogen
H_2S	Hydrogen Sulphide
H_2SO_4	Sulphuric acid
HNO_3	Nitric acid
HO_x	Hydroxyl radicals (HO, RO_2 and HO_2)
HYSPLIT	Hybrid Single-Particle Lagrangian Integrated Trajectory
IPCC	Intergovernmental Panel on Climate Change
IQR	Inter Quartile Range
LRT	Long range transport

MODIS	Moderate Resolution Imaging Spectroradiometer
N_2O	Nitrous oxide
Na	Sodium
NASA	National Aeronautics and Space Administration
NE US	Northeast United States
NH_3	Ammonia
Ni	Nickel
NO	Nitrogen oxide
NO_2	Nitrogen dioxide
NO_3	Nitrate
NOAA	National Oceanic and Atmospheric Administration
NO_x	Mono-nitrogen oxides (including NO and NO_2)
NS	Nova Scotia
NSE	Nova Scotia Environment
O&G	Oil and gas
O_3	Ozone
OC	Organic Carbon
OH	Hydroxide
PCA/APCS	Principal Component Analysis/Absolute Principle Component Scores
PM	Particulate matter
PM_{10}	Particulate matter with a mean aerodynamic diameter of less than or equal to 10 μm
$PM_{2.5}$	Particulate matter with a median aerodynamic diameter less than or equal to 2.5 μm
PMF	Positive Matrix Factorization
ppb	Parts per billion
pphm	Parts per hundred million
ppm	Parts per million
RH	Used to denote a hydroxyl radical
Rn	Radon
RO_2	Peroxyl radical
SF_6	Sulphur Hexafluoride
SO_2	Sulphur dioxide

SO_4^{2-}	Sulphate
SOA	Secondary organic aerosols
SOM	Secondary organic matter
TSP	Total suspended particles
UFP	Ultrafine Particle
UFPM	TSI ultrafine particle monitor model 3031
USDA	United States Department of Agriculture
USEPA	United States Environmental Protection Agency
UV	Ultraviolet
V	Vanadium
VIIRS	Visible Infrared Imaging Radiometer Suite
VOC	Volatile organic compound

1 INTRODUCTION

1.1 Structure of the report

There are two results and discussion sections found in the report. Prior to 2016 data information is found in section 4, and 2016 data is found in section 5.

1.2 Rationale and Objectives of the Study

Air pollution can have varied and severe effects on health, ecosystems, and climate. Its impacts are also not limited to the point of release with air quality transcending all scales in the atmosphere from local to global with feedbacks and interactions between all levels (Monks et al., 2009). The World Health Organization estimates that 2.4 million people die each year from causes directly attributable to air pollution (WHO, 2002). It is therefore important to identify and quantify sources of air pollution and their fate and transport globally (Monks et al, 2009). Most studies are conducted in urban areas with few studies taking place at sea or near offshore O&G production facilities. Therefore, there is a paucity of data related to air emissions in marine locations impacted by offshore O&G production (Gibson et al., 2009a, Waugh et al., 2010).

It has been established that further research is needed on the contribution of airborne particulate matter with a mean aerodynamic diameter ≤ 2.5 microns (PM$_{2.5}$) and VOCs to the air quality in environments such as the Atlantic Marine Airshed (Gibson et al., 2009a). The relative isolation of Sable Island from local point sources make it a site that is largely marine influenced and it can be an area transitioning from the polluted continent to a clean marine environment (Duderstadt et al., 1998) making it an ideal location for examining these impacts. Its remote location also makes it an ideal site for looking at the impact of nearby offshore oil and gas activities (Waugh et al., 2010). Sable Island recently became a National Park (Sable island national park reserve: Park establishment, 2012). This new status only increases the need to improve air quality surveillance and our understanding of pollution sources to better protect this fragile ecosystem (Waugh et al., 2010).

The objective of the study is to:

- Apportion the different sources of both gaseous and particulate air pollution affecting the air quality on Sable Island; and
- Investigate the impact of bringing a new O&G platform online through to production.

The results of the study will allow for increased awareness of the main pollution sources and their impacts that can then be used to make informed policy decisions and aid in pollution prevention planning.

The study utilized the different methods outlined below:

- Real time in situ air pollution sampling;
- Statistical analysis; and
- Positive Matrix Factorization (PMF) modelling.

Using the data gathered from these methods, source apportionment; or receptor modelling as it is often called, will be used to accomplish the goal of identifying the various pollution sources impacting Sable Island.

2 BACKGROUND

2.1 Sable Island

Sable Island is located in the Atlantic Ocean approximately 300 km southeast of Halifax, Nova Scotia, Canada. A sand bar approximately 42 km long, it has long been known for its shipwrecks (over 350 recorded) and wild horses (Sable Island: A story of survival, 2001). The establishment of the Sable Island National Park Reserve made Sable Island the 43rd national park in Canada (Sable Island National Park Reserve: Park establishment, 2012). Figure 1 shows the location of Sable Island in reference to Atlantic Canada with inlays showing the distance from Halifax and the size of the Island.

Figure 1 Map showing the location of Sable Island.

Due to its location and relative isolation from local point sources Sable Island is an example of a site that is largely influenced by marine emissions (sea spray). The island can be considered to be in an area transitioning 'air zone', from the polluted continent to a clean marine environment (Duderstadt et al., 1998). As a result, it has been the focus of various air quality related research projects as far back as the 1960's (Waugh et al., 2010). Local sources for the island do however exist and include offshore O&G production, long-range transport (largely from the Great Lakes and US Eastern Seaboard regions), and other localized emissions. Other local emissions include transportation emissions to and from both the island and offshore facilities by aircraft and ships, emissions from passing ships, and localized emissions on the island itself related to electricity generation and waste incineration (Waugh et al., 2010).

Offshore petroleum activities can result in emissions of NO_x, SO_2, VOCs, airborne particulate matter (PM), reduced sulphur compounds, e.g. H_2S, and greenhouse gases such as carbon dioxide (CO_2) and methane (CH_4) (Waugh et al., 2010). Petroleum activities have been ongoing in the area surrounding Sable Island since 1992. The Cohasset-Panuke project ran from 1992-1999 and was operated by Pan Canadian (now Encana) and Lasmo. The Sable Offshore Energy Project began in 1999 and is operated by Exxon Mobil and partners. It consists of five gas production platforms, which can be seen in Figure 2. The Deep Panuke Offshore Gas Development Project is run by Encana Corporation and was brought on-line on July 22nd 2013. It can also be seen in Figure 2 (Offshore Projects, 2013).
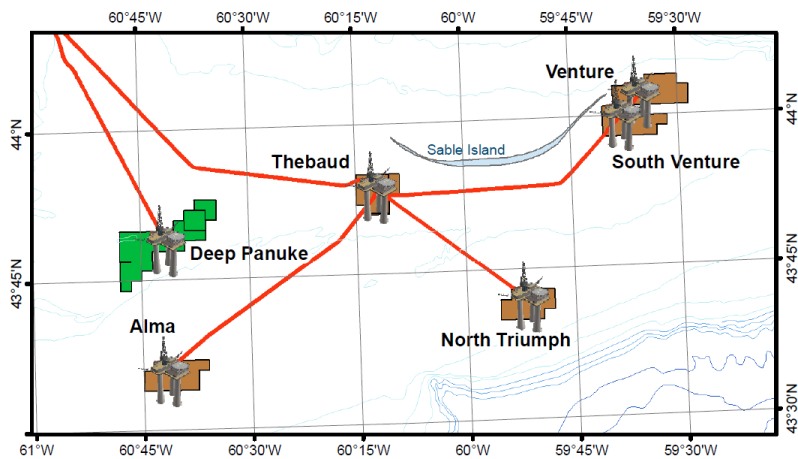
Figure 2 Offshore oil and gas activities near Sable Island (Offshore Projects, 2013)

2.2 Background Literature

A report published by Waugh et al. 2010 summarized the initial set-up and the results from the Sable Island Air Monitoring Station over the first four years of operation. This station was set up as part of the Nova Scotia Ambient Air Quality Monitoring Network. The study consisted of monitoring for NO_x, SO_2, H_2S, and $PM_{2.5}$. Environment Canada used the opportunity provided by the study to also monitor for O_3 as well as greenhouse gases such as carbon monoxide (CO), CO_2, and CH_4. The purpose of the study was to determine the impact of contaminant emissions from petroleum related activities and to report this data to several provincial national, and international monitoring programs. The study concluded that it was hard to determine the impact of local sources (offshore oil and gas activities included) due to the lack of information on specific local emission sources. The lack of speciated sample data and limited use of smoke observation data from the Thebaud offshore platform also posed issues, and it was suggested that additional information from project partners would be needed to determine the impact of local sources on Sable Island's air quality.

A study done by Duderstadt et al., 1998 looked at the instantaneous photochemical production and loss rates of ozone using a numerical photochemical model and three weeks' of summertime surface based chemical and meteorological observations on Sable Island. Meteorological observations included continuous measurements of temperature, relative humidity, UV radiation, wind speed, wind direction, standard meteorological hourly surface observations, and twice daily upper air sonde observations. Chemical measurements included NO, NO_2, total reactive nitrogen, O_3, CO, various hydrocarbons, aerosol measurements, and speciated chlorinated compounds. The study concluded that the background photochemistry of the island was impacted by polluted continental plumes containing NO_x, O_3, non-methane hydrocarbons, as well as solar intensity (which was determined by cloud cover), that had the greatest impact. The model outputs agreed well with the measured values apart from there was intermittent cloud cover, fog, and/or rain present. This showed the influence of cloud processes on the air parcels reaching Sable Island.

2.3 Available Data

Monitoring by Nova Scotia Environment (NSE) on Sable Island has been ongoing since 2003 as part of the Nova Scotia Ambient Air Quality Monitoring Network. NSE used to manage the

measurement for hydrocarbons (CH), CO, CO_2, H_2S, NO_x, NO, NO_2, O_3, $PM_{2.5}$, Radon (Rn), SO_2, weather data, and wind speed (Nova Scotia Ambient Air Quality Monitoring Network, 2010). However, NSE withdrew resources from Sable Island in 2015. Replacement automatic gas analyzers were provided by additional ESRF funds and in-kind from Dr. Gibson (Dalhousie University). Flask sampling for carbon 13 ($d^{13}C$), and delta-O-18 ($d^{18}O$) in CO, CH_4, CO, CO_2, nitrous oxide (N_2O), sulphur hexafluoride (SF_6), and hydrogen (H_2) was previously performed on the Island but ceased before this project started.

2.4   Particulate Matter

Airborne particulates consist of a mixture of both solid and liquid particles and can consist of many different chemical species such as sulphates (SO_4), nitrates (NO_3), chloride (Cl), sodium (Na), BC, organic carbon (OC), elements common to the hydrosphere and lithosphere and trace aliphatic and aromatic organic species, e.g. dodecane and polycyclic hydrocarbons (Gibson et al., 2013). Particulates are classified according to size range (Gibson et al., 2009b). Those with a mean aerodynamic diameter ≤ 10 µm are designated as PM_{10} (Harrison et al., 1997; Gibson et al., 2009b; Gibson et al., 2013).

2.4.1   Environmental Effects

Emissions of sulphur and nitrogen gaseous and particulate matter species, e.g. SO_2, NO_2, nitric acid (HNO_3) and sulphuric acid (H_2SO_4) are known to have a direct negative impact on plant species such as lichen and lichen abundance (Gibson et al., 2013a). NO_2 and SO_2 can impact lichen directly while their secondary products (HNO_3 and H_2SO_4) can acidify and damage tree bark (Will-Wolf and Neitlich, 2010). In this way secondary particulate and liquid phase pollutants formed from SO_2 and NO_2 can have the largest impact on sensitive sentinel species such as lichen (Bell and Treshow, 2003; Conti and Cecchetti, 2001).

Aerosol deposition can cause damage such as dissolving limestone and soiling (soot stains) to buildings and other man made materials (Querol et al., 2004). The deposition of acidified aerosols can rapidly accelerate the degradation of building materials and occurs when deposited particles adsorb or absorb acidic gases from primary pollutants such as SO_2 and NO_2. These acid forming

aerosols limit the lifetime of paints and can cause soiling of both painted surfaces and other building materials (Bhattacharjee, et al., 1999).

Acid deposition can also affect plant life and aquatic environments (Bell, & Treshow, 2003; Bhattacharjee, et al., 1999; Dillon, et al., 1984). One of the biggest issues is that air pollution can be transported long distances, having negative health and environmental impacts on downwind receptors (Gibson et al., 2009b). In Europe it is estimated that approximately half of the air pollution emitted crosses borders and negatively impacts neighbouring countries (Levy, 1993;Gibson et al., 2009b; Querol et al., 2004). Aerosols can cause changes in the chemistry of aquatic environments such as oceans and lakes with the impacts varying depending on the type of pollution and the ecosystem being affected. Some examples of impacts include changes in naturally occurring organic acidity, depletion of base cation reserves from soils, and changes in nitrogen dynamics (Bell, & Treshow., 2003; Bhattacharjee, et al., 1999). Collectively these air pollution impacts can negatively influence native species such as fish populations. Acid deposition can also impact trees and plant life through acidification of soils and altering of the naturally occurring soil chemistry which in turn negatively impacts the soil nutrition and surface water quality (Bhattacharjee, et al., 1999).

Through the scattering and absorption of sunlight aerosols can directly influence climate both positively and negatively (Solomon, et al., 2007). The magnitude of this forcing depends on the size, abundance, and optical properties of the aerosol particles in question as well as the solar zenith angle of the sun (Solomon, et al., 2007). Scattering of light by particles generally causes UV radiation to be reflected away from the planet and results in less radiation reaching Earth's surface. This causes a cooling effect. As particle absorbance increases this effect changes. Some aerosols absorb, e.g. black and brown carbon aerosols, strongly absorb light in the visible and some wavelengths in the IR spectrum, which has a net warming effect on climate (Seinfeld & Pandis, 2006; Solomon, et al., 2007). The threshold where particles change from having a warming or a cooling effect depends on particle size, the albedo of the underlying surface, mixing rates of absorbing and reflective particles in the outmost layer of the particle, and many other factors (Seinfeld & Pandis, 2006).

Aerosols can also indirectly influence climate by causing the formation of cloud condensation nuclei. Cloud condensation nuclei formed from aerosols aid in the formation of clouds that have larger number concentrations of water droplets than normal clouds. These droplets also have

smaller radii, resulting in clouds with a higher albedo. This higher albedo results in the reflection of greater amounts of solar radiation and causes cooling (Senfield & Pandis, 2006).

2.4.2 Health Effects

Air pollution episodes such as the Muesse Valley incident of 1930, Donora Pennsylvania in 1948, and London in December of 1952 undoubtedly showed the cause and effect relationship between air pollution events and mortality/human health. Epidemiological studies followed soon after and can be dated from the London episode (Holgate et al., 1999). Contemporary epidemiological studies such as Dockery et al. (1993), Evans et al. (1984), and Shwartz et al. (1990) have established a direct link between mortality rates and air pollution in US cities as far back as the 1980's.

Dockery et al. (1993) investigated the link between air pollution and mortality rates in six US cities. Previous studies had reported that daily mortality rates could be associated with changes in air quality in London (Schwartz et al., 1990) and other US cities such as Philadelphia (Schwartz et al., 1992). The association between particulate air pollution and mortality rates had been previously established for quite some time through studies such as Evans et al. (1984). However, many of these studies were criticized as they did not correct for cigarette smoking. The study in question looked to estimate the effects of air quality on mortality rates within a well-characterized group of individuals while taking into account smoking status, sex, age, and other risk factors. The study population was obtained from the communities of Watertown, Massachusetts; Harriman, Tennessee (including Kingston); St. Louis; Steubenville, Ohio; Portage, Wisconsin (Wyocena and Pardeeville included); and Topeka, Kansas. The population consisted of 8,111 white individuals between the ages of 25 and 74 who had undergone spirometric testing (a form of lung capacity testing) and completed a standardized questionnaire. The status of each subject was determined annually and the National Death Index checked from 1979 through to 1989. Causes of death were determined from death certificates where possible.

Air quality monitoring was performed at a centrally located site in each community. 24-hour integrated sampling of ambient concentrations for total suspended particulate matter, SO_2, O_3, and suspended sulfates were measured. For total suspended particulate matter, both fine and inhalable particles were monitored. Cox proportional hazards regressions models were then used to assess the effects of air pollution (Dockery et al., 1993). This involved classifying study participants into

age and sex groups as well as applying variables for hazards such as smoking. The effect of air pollution on mortality rates was then looked at in two ways. It was first estimated including hazard variables and compared to mean pollution levels in each city. Next, city specific pollution levels were included as hazard variables in running the Cox regression model.

It was found that smoking, lack of a high school education, and increased body mass index all increased mortality rates, but after adjusting for these variables significant differences between the six cities still existed. Significant associations between mortality and inhalable, fine, or sulfate particles were found, while correlations with total suspended particles, sulphur and NO_2 levels, and the acidity of the aerosol were comparatively weak. Only small differences in ozone levels between the six cities existed, making it impossible to determine the impact on mortality rates. It was found that the effect of air pollution on mortality rates was somewhat stronger within subgroups that had occupational exposure to dust, gases or fumes, but positive associations were noted for all subgroups.

The results of the study performed by Dockery et al., (1993) played a key role in establishing the current U.S. ambient air quality objective for fine particles. Because of this, an independent study was performed to validate the results. The study was done in two parts. Krewski et al., (2005b) looked to validate the original study by replicating the original results and performing a detailed statistical audit. No discrepancies were identified in the original questionnaires and death certificates with the exception of minor differences in those related to occupational exposure to dust. A computer-programming problem was identified that had resulted in the loss of approximately 1% of the reported person-years of follow up. The original six cities study was updated to include this and the results of the study were recreated. The original results were re-produced almost exactly, including the 26% increase in mortality in Steubenville Ohio (the most polluted city). Krewski et al., (2005b) determined that the discrepancies found in the original study by Dockery et al., 1993 were not of epidemiologic importance and the risk estimates and conclusions drawn were still valid.

In the second part of the study, Krewski et al., (2005a) looked to test the results of the original study by Dockery et al., (1993) by conducting a wide range of sensitivity analyses. Alternative risk models and their impact on estimates of risk were performed considering new covariates not included in the original study. This allowed for the identification of covariates that could potentially confound associations between air pollution and mortality. It was found that few

subjects changed their original city of residence, therefore limiting the ability to identify critical exposure time windows. It was also found that the risk of mortality was increased when living in a city with higher levels of air pollution, but that occupational exposure likely played a larger role in this risk. As a result, risk factors generally decreased with higher levels of education (it can be assumed that individuals with higher education tend to perform jobs with lower exposure levels). In the end, it was concluded that the study by Krewski et al., (2005a) supported the results of the original study and showed the robustness of the conclusions when examined using alternative methods.

Since these studies, interest in particulate matter has only continued to grow as the potential health effects associated with exposure have become increasingly apparent. Acute effects for fine particulate matter (PM) associated with air pollution have been established in studies such as Dominici et al. (2006) and chronic effects in studies such as Pope et al. (2002). Acute effects include but are not limited to cardiovascular and respiratory distress (Dominici et al., 2006) as well as impaired vascular function and increased diastolic blood pressure (Brook et al., 2009). Chronic effects can include lung cancer and cardiopulmonary mortality (Pope et al., 2002). Of concern is the impact of $PM_{2.5}$. Due to their small size, they can be transported long distances and can also penetrate deep into the lungs (Harrison et al., 1997). A linear association between airborne concentrations and cardio pulmonary mortality and morbidity has been established in the past by multiple studies (Dockery et al., 2007; Stieb et al., 2002; Donaldson et al., 2001). The findings of the study are especially significant given that there does not appear to be a safe lower limit for negative impacts (Stieb et al., 2008). It must be remembered that the impacts on human health can vary depending on the size fraction, particle counts, and the chemical make-up of the particulates (Mills et al., 2008).

2.4.3   Sources

PM can originate from anthropogenic, biogenic, geogenic, primary and secondary, local, or long range sources (Gibson et al., 2009b). Some primary sources include sea spray, fossil fuel combustion, windblown dust, and dust from road transport (Pilling et al., 2005). It is estimated that 32% of the mass flux in terms of sea salt production comes from the Northern Hemisphere (O'Dowd et al., 2007). Secondary particulate components such as SO_4 and NO_3 are formed from the oxidation and chemical transformation of primary SO_2 and NO_x gaseous emissions (Pilling et

al., 2005). Some of the major sources in nearby Nova Scotia are power generation, both domestic and industrial space heating using both fossil fuels and biomass, construction activities, and ship emissions (Gibson et al., 2013b). Approximately 12,000 wildfires every year in North America impact concentrations of surface level $PM_{2.5}$ at long-distances. For example, a study by Gibson et al., (2013 and 2015) showed that 11% of the total $PM_{2.5}$ mass in Halifax over a 45-day period in the summer of 2011 was from wildfire smoke (Gibson et al., 2013a; Palmer et al., 2013; Franklin et al., 2014).

2.5 Volatile Organic Compounds (VOCs)

VOCs are a group of carbon containing organic chemicals that are known to participate in photochemical reactions that can form secondary gases and $PM_{2.5}$ species such as oxalate and formate (Environment Canada, 2012). Of particular interest is the effect VOCs have on ozone formation and related reactions in the troposphere, but they can also have many negative health impacts (Dohoo et al., 2013). Local and long-range sources, both biogenic and anthropogenic, exist and there are currently substantial gaps in our understanding of these sources and their relative contributions.

2.5.1 Environmental Effects

Ozone production involves complex chemical reactions, many of which are cyclic, therefore making it difficult to quantify the direct impact of VOCs on ozone formation. However, the impact of VOCs on ozone formation generally increases with their abundance and reactivity with OH (Jacob, 1999). The production of O_3 follows the reaction below.

$$O_3 + hv \rightarrow O_2 + O(^1D)$$
$$O(^1D) + M \rightarrow O + M$$
$$H_2O + O(^1D) \rightarrow 2OH$$
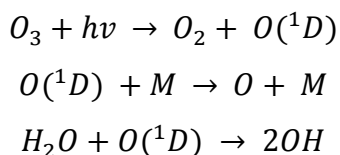
Where M represents any atmospheric species that accepts energy in the form of vibrational energy. After this production of HO_x, the chain is propagated by reaction of OH with hydrocarbons (as represented by RH) in the equation below.

$$RH + OH \xrightarrow{O_2} RO_2 + H_2O$$
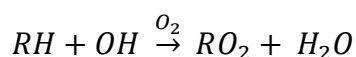
This RO_2 radical can then go on to produce NO_2 by reaction with NO. The next step of the chain is that NO_2 photolyzes in the presence of oxygen and produces O_3. (Gibson et al., 2009a)

$$RO_2 + NO \rightarrow RO + NO_2$$

$$NO_2 + h\nu \xrightarrow{O_2} NO + O_3$$
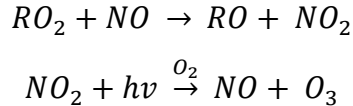
As can be seen, the end result of this set of reactions is that increasing concentrations of VOCs cause an increase in ozone production rates with the impact of individual VOC species depending on their reactivity with OH (Jacob, D.J., 1999; Gibson et al., 2009a).

It has been found through ambient measurements that ozone formation consistently occurs at an increased rate downwind of anthropogenic NO_x and VOC sources but this relationship becomes more complex when the impact of NO_x/VOC concentration ratios on ozone formation is considered. For example, emissions such as those from a power plant that contain low concentrations of VOCs compared to NO_x will initially suppress the formation of O_3 in favor of HNO_3 production. Meanwhile, vehicle emissions (which have higher concentrations of VOCs compared to NO_x) will favor earlier formation of ozone and therefore result in higher concentrations (Ryerson et al., 2003).

Secondary organic aerosols (SOA) can both scatter and absorb solar radiation (Andreae et al., 1997) as well as aid in the formation of cloud condensation nuclei (Novakov et al., 1993). The combined effect can either positively or negatively influence climate (Pierce and Adams, 2009).

VOCs can increase the formation of SOA and therefore increase the formation of cloud condensation nuclei (Pierce and Adams, 2009). The photo-oxidation of isoprene, a VOC produced by many terrestrial and marine plants, has been shown to result in the formation of substantial concentrations of SOA (Claeys et al., 2004; Colomb et al., 2009; Shaw et al., 2010).

2.5.2 Health Impacts

VOCs specifically are known to cause negative health impacts, with examples including the link between VOCs and chronic respiratory illnesses (Ware et al., 1993). Chronic domestic exposure to VOCs has been shown to increase the risk of asthma in children (Rumchev et al., 2004), and acute effects also exist. A study by Yang et al., (1997) concluded that residents living in a petrochemical-polluted area in Taiwan experienced acute irritative symptoms such as eye irritation, nausea, throat irritation, and chemical odor perception resulting from exposure to VOCs.

2.5.3 Sources

Sources specific to VOCs can include both anthropogenic and natural sources with biogenic sources comprising most VOC emissions within the North American continent. Biogenic sources include soil microbes, vegetation, biomass burning, and lightning (Guenther et al. 2000). Examples of VOCs emitted by these biogenic sources include isoprene, monoterpenes, hydrocarbons, and VOCs (Guenther et al. 2000).

The oceans are a source of non-methane hydrocarbons (NMHCs) from photochemical processes in the water column. The production of many NMHCs shows distinct seasonal cycles in surface waters with summer maxima and winter minima (Shaw et al., 2003). In the northwest Atlantic Ocean, massive springtime phytoplankton blooms, dominated by large diatom species (Johnson et al. 2012), occur because of a stabilization of the nutrient-rich water column. Throughout the summer, a phytoplankton assemblage dominated by smaller cells (Johnson et al. 2012) is maintained by regenerated nutrients until a secondary autumn bloom occurs due to nutrients being driven upwards as a result of wind driven mixing (Greenan et al. 2004). During the winter months, the water column is mixed and light levels are low, resulting in phytoplankton abundance minimum (Georges et al., 2014). Although the relative oceanic contribution of NMHC's is considered to be minor compared with other terrestrial sources, it is not well quantified or understood and emissions into the atmosphere are considered to be a major loss of oceanic NMHC production (Reimer et al., 2000). Phytoplankton blooms can be a contributor of atmospheric VOC's (Colomb et al., 2008) that would be of concern on Sable Island, with various phytoplankton species being capable of producing isoprene (Shaw et al., 2003). It was found in a paper by Palmer et al., (2005), that global oceanic emission of isoprene is estimated at 0.1 TgC/yr making the contribution from phytoplankton blooms a source that must be considered. The only known source of this oceanic isoprene flux is phytoplankton blooms (Shaw et al., 2003). The photochemical production of isoprene in phytoplankton is a function of light intensity and temperature and occurs during the growth stage (Shaw et al., 2003). Strong positive correlations between isoprene and bulk chlorophyll concentration, a proxy for phytoplankton biomass, were found in data from surface waters in the East Atlantic and Southern Ocean (Broadgate et al., 1997; Baker et al., 2000). It should be noted that it is possible to measure chlorophyll concentration based on ocean colour. This can be done either in situ or from space using remote sensing techniques (Craig et al., 2012). Ocean colour is directly related to its constituents and many different approaches have been

developed to derive water constituents from measurements of ocean colour (Craig et al., 2012). A major part of this study examined the potential contribution of phytoplankton to NHMC concentrations on Sable Island by way of ocean colour. From prior knowledge of the literature it was anticipated before the start of the project that VOC sources directly from the ocean would dwarf any emissions of VOCs from O&G platforms under normal operating conditions.

Offshore oil and gas activities can have many different sources that result in the release of VOC's into the atmosphere (Beusse et al., 2013) and will be discussed further in Section 2.6. Other than emissions from O&G production, anthropogenic VOC sources include vehicle emissions, solvent based products (particularly cleaning products), paints, and many others. The manufacturing of organic chemicals and rubber has been identified as significant sources of VOC's (Piccot et al., 1992).

2.6   Offshore Oil and Gas Production

The production of offshore O&G on the Scotian Shelf, and the natural gas fields surrounding Sable Island have been active for many years now. Their location was shown previously in Figure 2. With these activities however, is the potential for airborne emissions of pollutants, which can be harmful to human health as well as the environment.

2.6.1   Emissions from Offshore Oil and Gas Activities

Due to concern over potential O&G air pollution emissions in the US, it was recognised that a need existed for a thorough understanding of the impacts associated with these activities (Beusse et al., 2013) Our understanding of emissions from offshore O&G production and their impacts in Canadian waters was not well understood. This gap in knowledge is why this ESRF study was undertaken.

Offshore O&G production activities can result in the emission of greenhouse gases (GHGs), secondary pollutants that act as O_3 precursors, and climate forcing agents such as BC (Zahniser, A., 2007, Beusse et al., 2013). The main GHGs associated with offshore oil and gas emissions are CO_2 and CH_4 (Zahniser, A., 2007). Many pollutants involved in the formation of O_3 are emitted through combustion, vented, and fugitive sources. These include N_2O, VOC's, and NO_x (Zahniser, A., 2007; Beusse et al., 2013). Climate forcing agents include PM, BC, and SO_4. Emissions can also include pollutants with health and environmental concerns such as CO and air toxics such as benzene, toluene, ethylbenzene, xylenes, and H_2S (Beusse et al., 2013).

2.6.1.1   Combustion Sources

Combustion sources are sources associated with the production of oil and gas that include engines, heaters, incinerators, and turbines. Most of these emissions come from the equipment used to obtain the oil or natural gas but flaring is another combustion source (Beusse et al., 2013).

Flaring is the controlled burning of excess natural gas using a flare stack to avoid safety issues associated with its build-up. Flaring is performed on excess gas that cannot be re-injected into hydrocarbon reservoirs to maintain hydrocarbon production, supplied to customers, unburned process gas, vapors that accumulate in the tops of tanks, and gas from process upsets. The main

emissions produced when flaring is performed efficiently are CH_4 and CO_2. Ideally flaring should be minimized and as much value realized from hydrocarbon accumulations as possible (Kearns, J. et al., 2000). Emissions from combustion sources include NO_x, CO, air toxics, VOC's, and methane (Beusse et al., 2013).

2.6.1.2   Vented Sources

Vented sources include pneumatic devices, dehydration processes, gas sweetening processes, chemical injection pumps, compressors, tanks, and well testing, completions, and work overs (Beusse et al., 2013). The gases produced by these sources are either vented directly into the atmosphere or burned off using a flare.

Venting is the controlled release of gases to avoid safety issues associated with their buildup. Vented gases are lighter than air, and for safety reasons, are released at high pressure. For some gases being produced, inert gases in high concentrations will prevent the gas from burning and require that venting be performed over flaring (Kearns, J. et al., 2000). This can result in the direct release of VOCs, air toxics, and methane into the atmosphere (Beusse et al., 2013).

2.6.1.3   Fugitive Sources

Fugitive sources encompass emissions from unplanned sources. These include leaks from valves, connectors, flanges, compressor seals, and other kinds of equipment. It can also include evaporative sources from tanks and other sources of that nature. In an idealized system, these sources would not exist, however, in real world systems they represent a significant contribution of VOCs, air toxics, and CH_4 to the atmosphere (Beusse et al., 2013).

2.6.1.4   Offshore Oil and Gas Activities Monitoring

An environmental assessment (EA) is required to be submitted to the Canada-Nova Scotia Offshore Petroleum Board (CNSOPB) as part of an application for authorization of an activity offshore. EAs are used to assess the impact of proposed projects through the prediction of environmental effects. All EAs for petroleum activities are undertaken in accordance with the Canadian Environmental Assessment Act as the CNSOPB is a federal authority under this act ("A Synopsis of Nova Scotia's Offshore Oil and Gas Environmental Effects Monitoring Programs,"

2011). Some of the predictions are verified using environmental effects monitoring programs. Nova Scotia environmental effects monitoring programs related to the offshore oil and gas activities surrounding Sable Island look to monitor produced water, the water column, sediment chemistry, and seabird life to ensure no undue harm is done the environment by such activities. However, air quality monitoring to ensure airborne emissions from the sites do not cause undue harm is not generally performed ("A Synopsis of Nova Scotia's Offshore Oil and Gas Environmental Effects Monitoring Programs," 2011). As previously discussed, monitoring by Nova Scotia Environment on Sable Island has been ongoing since 2003 as part of the Nova Scotia Ambient Air Quality Monitoring Network. This data gives the best available record of the impact of O&G production activity on the air quality on Sable Island. Monitoring of occupational exposure and facility safety air emissions on the O&G platforms is performed, but this data is not made public.

2.6.2   Deep Panuke

The Nova Scotia offshore area extends from the low water mark on the coast of Nova Scotia to the edges of the continental margin. This area is approximately 400 000 km^2. Exploration first began in the 1950s and since that time 395 km of 2D seismic and 6076 km^2 of 3D seismic surveys have been recorded and 168 wells have been drilled. A total of 21 significant discoveries and 5 commercial discoveries have been made in the Sable Island area ("Technical Summaries of Scotian Shelf Significant and Commercial Discoveries", 2000). A significant discovery is defined as "a discovery indicated by the first well on a geological feature that demonstrates by flow testing the existence of hydrocarbons in that feature and, having regard to geological and engineering factors, suggests the existence of an accumulation of hydrocarbons that has potential for sustained production ("Technical Summaries of Scotian Shelf Significant and Commercial Discoveries", 2000)". A commercial discover is defined as "a discovery of petroleum that has been demonstrated to contain petroleum reserves that justify the investment of capital and effort to bring the discovery to production ("Technical Summaries of Scotian Shelf Significant and Commercial Discoveries", 2000)."

Offshore petroleum activities have been ongoing in the Scotian Shelf since 1992. The Cohasset-Panuke project ran from 1992-1999 and was operated by Pan Canadian (now Encana) and Lasmo.

The Sable Offshore Energy Project began in 1999 and is operated by Exxon Mobil and partners. It consists of five gas production platforms, which were shown, previously in Figure 2. The Deep Panuke Offshore Gas Development Project is run by Encana Corporation and was brought on-line on July 22nd 2013. It can also be seen in Figure 2 ("Offshore projects", 2013).

The Deep Panuke Comprehensive Study Report was approved in 2002 based on a three platform natural gas drilling project with 176 km of pipeline for tie-in with the pre-existing Maritimes and Northeast Pipeline facilities ("Deep Panuke Offshore Gas Development Environmental Assessment Report," 2006).

Final approval for Deep Panuke was given in 2007 ("Deep Panuke Project Newsletter," December 2007) and production was expected to begin in the summer of 2013 ("Deep Panuke gas production 'on track' for June," 2013). The commissioning phase began on July 22nd 2013 with the introduction of gas to the production field center and production commenced shortly after ("Weekly operations report EnCana Deep Panuke production status," 2013).

The positive economic impacts of a project like Deep Panuke are immediately obvious and include jobs for Nova Scotian's and jobs for Canadians from other provinces ("Deep Panuke Canada - Nova Scotia Benefits," 2013). However, there are potential environmental and health impacts of a project such as this. As previously discussed, there is a lack of adequate monitoring and information on the impacts of offshore oil and gas activities on air quality and human health, particularly those associated with the start-up and commissioning phases of operation. Although there is substantial occupational health and safety monitoring (particularly for H$_2$S) of personnel on the production platform itself, this data is kept by the operators and not used to determine the impact of the production platforms on the surrounding air quality.

The Environmental Impact Assessment for Deep Panuke identifies "the only predicted significant adverse effect is the effect on air quality in the unlikely event of a well blowout or piping rupture resulting in the release of large amounts of acid gas" ("Deep Panuke Offshore Gas Development Environmental Assessment Report," 2006). It is stated in the document that atmospheric emissions will comply with the *Air Quality Regulations* (Nova Scotia *Environment Act*) and Ambient Air Quality Objectives (*CEPA*) and that flaring of gas will be performed for acid gas.

2.7 Source Apportionment (Receptor Modelling)

To assess the impact of air pollution, it is important to understand pollution sources and their relative contributions. One way of doing this is through the modelling process known as source apportionment or receptor modelling (Brown et al., 2007; Gibson et al., 2009b; Gibson et al., 2010; Harrison et al., 2011; Gibson et al., 2013). Source apportionment can help establish the major polluters and areas to focus on when creating pollution prevention policies (Gibson et al., 2009b). There are four different source apportionment modelling methods that can be used. They include Principal Component Analysis/Absolute Principal Component Scores (PCA/APCS), USEPA Chemical Mass Balance (CMB) v8.1, USEPA Positive Matrix Factorization (PMF) version 3.0, and Pragmatic Mass Closure (PMC) (Thurston and Spengler, 1985; Watson et al., 1998; Jaeckels et al., 2007).

All applications of source apportionment of VOCs and $PM_{2.5}$ to air quality assessment require ambient sampling of the air that is then analyzed in the laboratory to produce speciated sample data. This data can then be used in the source apportionment/receptor models. The choice of model depends greatly on the study in question, its goals and aims, the sources of interest, and the availability of existing source chemical species profiles, e.g. the USEPA VOC and $PM_{2.5}$ speciate data base (Watson et al., 1998; Ward et al., 2006a; Ward et al., 2006b; Ward and Noonan, 2008). Meteorological data, knowledge of strong local sources and their chemistry, and knowledge of topography are also important parameters to consider when interpreting the source apportionment model results. The receptor model source factors and profiles only go so far in understanding pollution sources and events, expert knowledge of source chemical fingerprints or conservative source chemical markers is needed. Being able to interpret them in meaningful ways is only possible when they are combined with other data and knowledge and analyzed critically.

2.7.1   Principal Component Analysis/Absolute Principal Component Scores

The PCA/APCS method is a multivariate receptor model that predicts sources, their chemical composition, and their contributions to a sample by simultaneously analyzing a set of speciated sample results. It does not require inputs of source profiles (Guo et al, 2004). The source profiles are estimated using linear regression and then compared to known source profiles. Based on similarities between the chemical compositions of these source profiles, it is determined which source they represent (Thurston et al., 1985).

Unlike some other factor analysis methods, which look to identify all underlying factors within a data set, PCA/APCS looks for the principle factors, which explain most the variance within a data matrix. The theory is quite complex, but uses principal component and regression features. The model requires adequate degrees of freedom to produce accurate statistical results. Like all multivariate receptor models, PCA/APCS has difficulty in separating sources that are chemically similar or strongly correlated (Guo et al., 2004).

2.7.2 Positive Matrix Factorization (PMF)

One of the most commonly used source apportionment models is PMF (Harrison et al., 2011). PMF modelling has been used in many studies such as Baumann et al. (2008) performed in Alabama, or Buzcu-Guven et al. (2007), which looked at the apportionment of organic carbon and fine particulate matter across the Midwestern United States. PMF is a form of multivariate least squares statistics used when looking at a given data matrix as related to a specific set of variables to determine spatial relationships or structures within (Hubert et al., 2000). PMF involves a data matrix of observations of a given number of objects over a given number of attributes (Hubert et al., 2000). Entries include some measure of relationship between the attributes. The purpose of PMF is then to simplify the matrix and its relationships to generate a better understanding of the matrix and to draw conclusions about the relationships within (Hubert et al., 2000).

The PMF model requires a matrix of speciated sample data as well as an uncertainty file. The uncertainty file outlines uncertainty values or parameters for calculating uncertainty. Uncertainty values provided should encompass things such as sampling and analytical errors. Uncertainties are estimated based on parameters such as minimum detection limits and error fractions (percent error times 100), or general uncertainty values can be applied to all data. Speciated data consists of samples that have been analyzed for their chemical constituents such as anions, cations, metals, etc. By using multivariate statistics to look for correlations in the data, this data is then broken down into two matrices (factor contributions and factor profiles) (Norris et al., 2008). Factor contributions outline the percent contribution of a source to the overall air quality at a given receptor while source profiles outline the chemical fingerprint of that source. Afterwards, background knowledge of wind direction, emission inventories, and in depth knowledge of source chemical markers is used to determine which sources are represented by these factor

chemical profiles (Norris et al., 2008). Figure 3 below shows an example of the source profiles obtained during the Gibson et al., (2013d) study of the main sources of PM$_{2.5}$ impacting Halifax over a 45-day contiguous period in the summer of 2011. The source profiles outline the different chemical species and the percent they contribute to each factor. From this it can be determined which source each factor represents. For example, a factor containing nickel (Ni) and vanadium (V) are indicative of ship emissions (Gibson et al., 2013d). Figure 4 shows the percent contributions of each source to the overall air quality during the study performed by Gibson et al., (2013d).
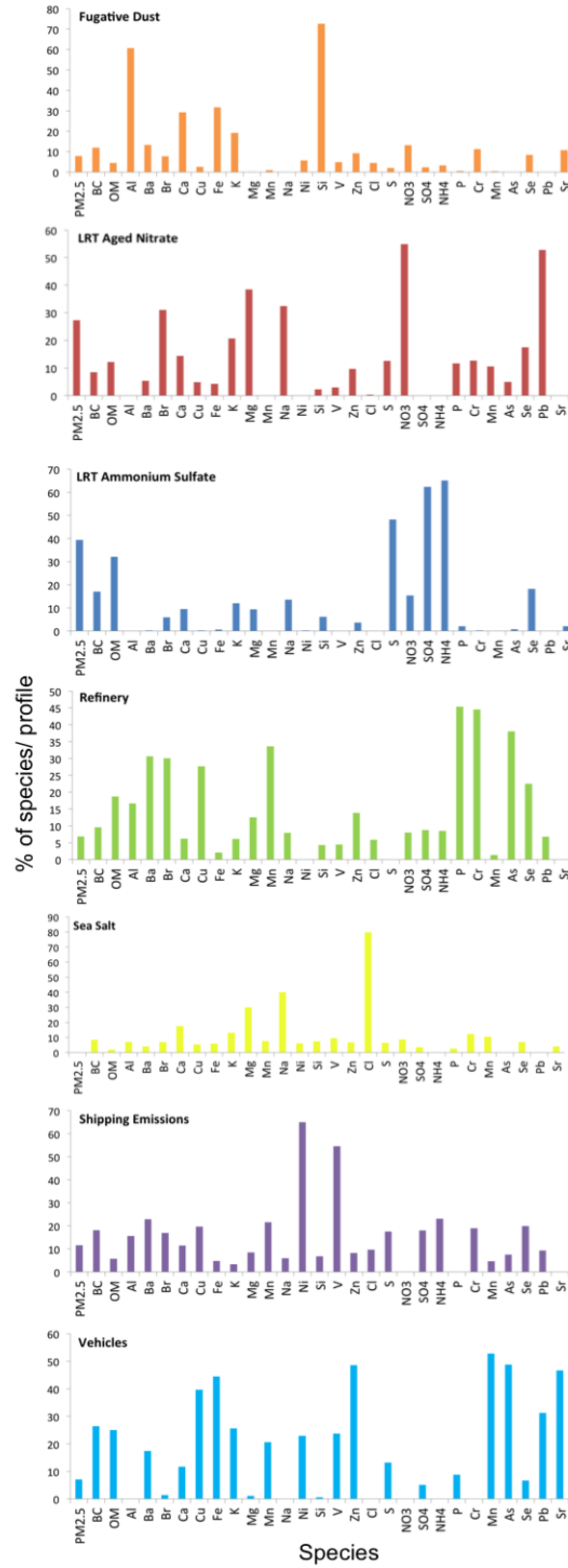
Figure 3 Example of source profile (Gibson et al., 2013d).
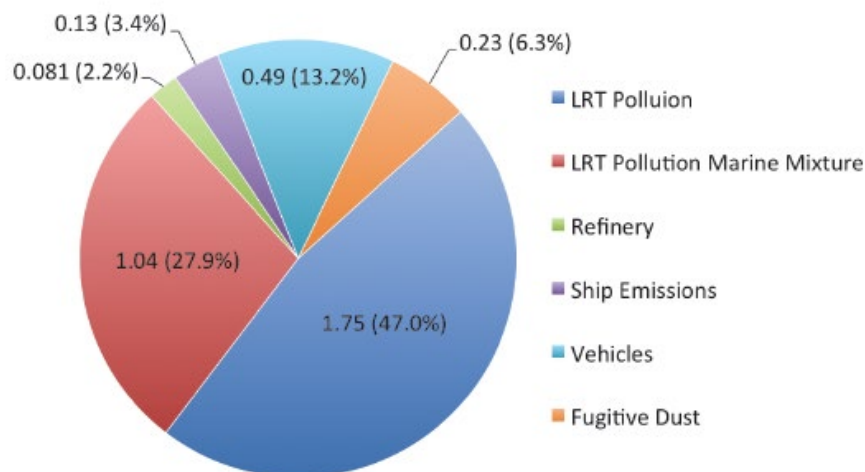
Figure 4 Average mass concentration (μg m^{-3}) of attributed sources and percentage source contributions over the 45 days of sampling (Gibson et al., 2013d).

The result of applying PMF to air quality research is that source factors and their contributions are generated for the air quality at a given receptor, which can then be related to known sources. PMF models do not differentiate between different sources that are chemically similar. For example, the model cannot differentiate between two different coal fired power plants if their fuel types and emissions are similar. The models would include both emissions as one factor as they are not chemically distinct. The contribution of both together could be determined, but not of each individual plant. This would only be possible if one used a different fuel and had a conservative chemical marker related to that fuel and associated emissions and the other power station did not (Paterson et al., 1999). Additionally, only non-negative factors, that is, factors that have positive source contributions, are produced from PMF models (an advantage over other types of models). Error estimates of the data used in the analysis are also included using the uncertainty file (Paterson et al., 1999). PMF was used in this ESRF study.

2.7.3 Chemical Mass Balance (CMB)

CMB is a robust method that can be used for source apportionment (Gibson et al, 2009b). It requires inputs of speciated sample data and information on the chemical composition of sources in the form of source profiles. Source profile chemistry needs to be well understood as these source profiles describe the chemical composition of specific sources (Ward, 2007). One downside of CMB is that it assumes that source chemical compositions do not change and remain constant.

This makes it difficult for the model to properly identify the sources of secondary aerosols formed after emission release (Ward et al, 2006). However, CMB works well when used to apportion primary aerosols (Ward et al, 2006). It may often be necessary to develop source profiles specific to a study as can be seen in Ward et al., 2006. Oil fired heaters and wood stove source profiles were developed by sampling directly from these sources and analyzing their chemical composition for use in the model.

CMB models take speciated sample data and source profiles and then produce a linear sum of products of source fingerprint abundances and contributions by solving a system of linear equations (Ward et al., 2006b). This is achieved by using an effective-variance least squares method. Several sources and species are selected (specific to the study) and the model attempts to reconstruct the sample data using these. This process is repeated with many different combinations until an optimal fit is found. The result is that the sources and their contributions to the air pollution sampled are found (Ward et al., 2012).

CMB modelling has been utilized in many studies over the years. Gibson et al., 2010 used CMB to determine the contribution of residential wood smoke to $PM_{2.5}$ concentrations in the Annapolis Valley. Lee et al. (2007) performed a study that used CMB for the apportionment of fine particulate matter (less than 2.5 µm in diameter) in the southeastern United States. Due to the nature of CMB it can be used anywhere that source profiles are well understood. Studies all over the world have used CMB, including studies in India (Guttikunda, 2012).

2.7.4   Pragmatic Mass Closure

Pragmatic mass closure as used in source apportionment modelling for PM uses multivariate statistics to identify pollution sources from ambient sampling alone. It does not require that source profiles be provided to the model, only speciated sample data (Yin et al., 2005). Pragmatic mass closure attempts to account for all the measured mass of particles through both inferred and measured chemical constituents. Specific measured species are related to other components using coefficients to calculate theoretical values. From this the chemical component masses of the sample can be estimated (Yin et al., 2008). The coefficients used are based on reaction ratios and the interactions between secondary and primary pollutants. These are usually based on

experimental values of previous studies and knowledge of tropospheric chemistry (Yin et al., 2005).

Pragmatic mass closure methods can be used to reconstruct chemical component masses with accurate results. Yin et al., 2005 found very strong correlations between the summed reconstructed chemical component masses and the gravimetric masses with R^2 values from 0.82 to 0.96. Yin et al., 2008 also found strong correlations between the summed reconstructed chemical component masses and the gravimetric masses when pragmatic mass closure was applied to data from 3 different sites, with R^2 values that ranged from 0.69 to 0.98. The same coefficients were used for all 3 sites. Although coefficients used in the model would need to be adjusted if applied to a study area with very different airborne particulate climatology, the method approach is applicable anywhere (Yin et al., 2008).

When combined with meteorological data and concurrent sampling at a number of sites pragmatic mass closure can be very useful in showing how prevailing wind directions can greatly affect the chemical composition of PM_{10} (Gibson et al., 2009b). This illustrates the impact of transport, both localized and long range, on PM chemical compositions and the direct link between emissions and composition at nearby sites. The Gibson et al, 2009b study, performed in West-Central Scotland, showed changes in composition with prevailing wind direction. Sites downwind from urban sources showed primary material associated with high-density urban emissions while those upwind were impacted primarily by marine and long range transport sources.

2.8 Air Mass Back Trajectories

Air mass back trajectories are a useful tool when looking at air pollution. They can be used to compute both air parcel trajectories and dispersion and deposition simulations. A common air mass back trajectory model used is the HYSPLIT (Hybrid Single-Particle Lagrangian Integrated Trajectory) model initially developed jointly by the National Oceanic and Atmospheric Administration (NOAA) Air Resources Laboratory in Silver Spring, Maryland and Australia's Bureau of Meteorology. The model has since been upgraded with contributions from many different parties. The HYSPLIT model is used to identify either backward or forward trajectories based on meteorological parameter inputs and assumes either puff or particle dispersion (HYSPLIT - Hybrid Single Particle Lagrangian Integrated Trajectory Model, 2012). The model

follows a parcel of air as it moves through space and time, as opposed to Eulerian models, which focus on a specific location that the air parcel flows through (Batchelor, 1973). Puff dispersion involves expanding puffs until they exceed the meteorological grid cell size and split into new puffs. Particle dispersion involves a fixed number of particles, which are advected around the model domain by a mean wind field and spread by a turbulent component. Default configurations assume 3-dimensional distribution, both horizontally and vertically (HYSPLIT - Hybrid Single Particle Lagrangian Integrated Trajectory Model, 2012).

The HYSPLIT model has been used in many studies to examine air mass histories, transport, dispersion, and deposition with the goal of mapping pollution sources (Yin et al., 2005; Gibson et al., 2009b; Gibson et al., 2013d). Outputs from the HYSPLIT model can be very useful in interpreting PMF results and identifying sources of pollution events. However, it has been found that errors exist with back trajectory models due to truncation errors, interpolation errors, starting position errors, and amplification of errors. Errors as high as 20% of the distance travelled seem to be typical for trajectories computed from analyzed wind fields (Stohl, 1998). As a result, uncertainties in model outputs need to be considered accordingly when drawing conclusions. However, the uncertainty can be ignored when the VOC and $PM_{2.5}$ species correlate with known upwind source regions, e.g. high concentrations of Na and Cl when air mass trajectories originate from the ocean and high concentrations of $(NH_4)_2SO_4$ when the air mass trajectory originates from the North Eastern United States (Gibson et al., 2013d). Figure 5 shows an example from Gibson et al., (2013d) of air mass back trajectories grouped by major source region.
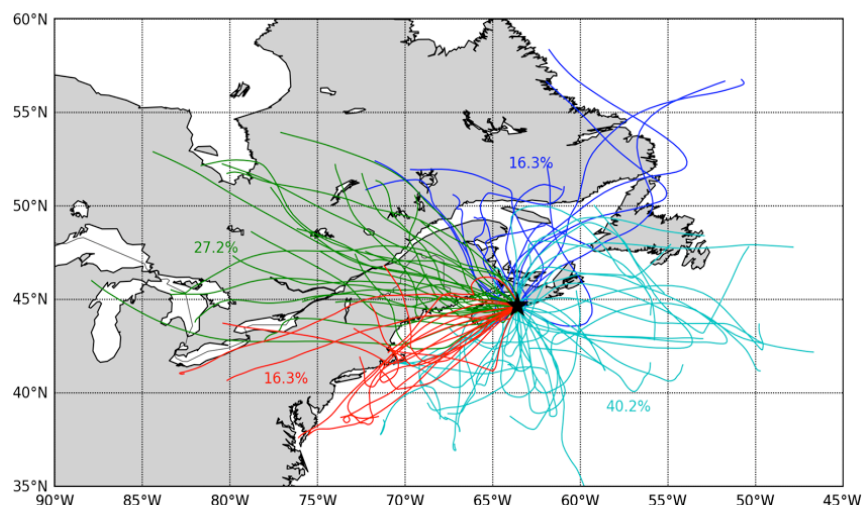
Figure 5 Air mass back trajectories grouped by major source region (Gibson et al., 2013d)

2.9 Meteorological Factors

It is important to measure meteorological conditions in order to be able to properly understand air quality and interpret air quality data. Information on conditions such as temperature, humidity, wind speed and direction, solar radiation, ceiling height, and pressure are all important in understanding how pollution is transported and dispersed as well as the reactions that will occur amongst different pollutants. Meteorological factors can be used to investigate pollutant transport and to establish source-receptor relationships of air pollutants (Stohl, 1998). The link between wind direction and pollution trends can help to link air pollution to a given source. For example, Paterson et al., 1999 linked periods of south and southwesterly flow to long-range transport factors, and Gibson et al., 2009a found that episodes of high concentrations of anthropogenic photochemical ground level ozone in Atlantic Canada coincided with high temperatures and strong solar radiation coupled with a high-pressure system to the southeast. Harrison et al., 1997 found a marked difference between particulate matter concentrations and composition between the summer and winter months, illustrating the impact seasonal changes in meteorological conditions can have.

MATERIALS AND METHODS

2.10 Sable Island Study

During the earlier stages of the study, on Island instrument data was streamed to a live website where it was displayed in an interactive manner. The data display was shut down in 2015 after demonstrating its utility, a lack of funding, but most of all due to a change in data communications, after NSE withdrew their resources consequent to a government policy decision on air quality monitoring priorities, making the use of the data display impossible.

2.11 Site Description

All the equipment for the study was housed in the air chemistry shed located at the Environment/Parks Canada site on Sable Island. The shed is located along the west edge of the site. It can be seen in Figure 6 circled in red and in the center of Figure 7. Modifications were made to the roof and walls of the shed to allow the installation of sampling inlets for the equipment contained inside. Figure 8 and Figure 9 show the sampling inlets installed. Power is supplied from the same diesel generator used to power the rest of the Parks Canada site and a satellite connection allows for data to be transmitted back to the mainland.

Figure 6 Location of the Air Chemistry Shed on Sable Island.

Figure 7 The Air Chemistry Shed on Sable Island.

Figure 8 Sampling inlet for the Thermo Scientific 55i.

Figure 9 Sampling inlet for the Thermo Scientific 5012

2.12 Equipment

The various instruments and analysis methods used are outlined below.

2.12.1 Methane and Total Non-methane Hydrocarbon (VOC) Analyzer - Model 55i

The Model 55i from Thermo Scientific is a back flush gas chromatography system that provides real time measurements of both methane and non-methane hydrocarbons. It can be seen in Figure 10. The Model 55i operates on the basic principles of gas chromatography and utilizes a proprietary column system. An automated batch analyzer collects samples at preset time intervals. A pump is used to draw in the sample air before it is introduced to an 8 port rotary valve that controls the flow of gases through the analyzer and column. Samples are injected into the column along with an inert carrier gas. Here the different chemical constituents contained within the sample are separated based on retention time. Methane exits the column first where it is then measured using a flame ionization detector (FID). The signal generated by the FID can be related to a concentration through comparison with a calibrant gas of known concentration. Once the methane peak has been detected the rotary valve back flushes the remaining sample through the column and to the FID to analyze for the remaining NMHCs (Model 55i Instruction Manual, 2008). For the purpose of this study only NMHC concentrations were used.

Figure 10 Thermo Scientific 55i set up on Sable Island.

2.12.2 Black Carbon Analyzer - Model 5012

The model 5012 multi angle absorption photometer utilizes aerosol light absorption properties to measure black carbon concentrations. It can be seen in Figure 11. In order to measure black carbon, a sample is first drawn into the instrument inlet using a pump. The aerosol sample is deposited onto a glass fiber filter tape that then advances to a detection chamber. A multi angle absorption photometer is used to analyze changes in the radiation fields in the forward and back hemisphere of the filter. This is than related to a concentration of BC using a data inversion algorithm based on a radiative transfer method. This algorithm takes into account multiple scattering processes inside both the deposited aerosol and between the aerosol layer and filter matrix. Along with the air sample volume and multiple reflection intensities, this data is continuously integrated to determine a real-time measurement of BC concentrations (Model 5012 Instruction Manual, 2009).

Figure 11 Thermo Scientific 5012 set up on Sable Island.

2.12.3 Nova Scotia Environment Data

Nova Scotia Environment (NSE) provided measurement data for H_2S, NO_x, NO, NO_2, O_3, $PM_{2.5}$, SO_2, temperature, wind direction, and wind speed. This data comes from various instruments that were already housed in the air chemistry shed as part of the Nova Scotia Ambient Air Quality Monitoring Network which forms part of the Federal Government, National Air Pollution Surveillance (NAPS) network of over approximately 300 stations (James Kuchta, personal communication, February 4th, 2014). NSE air quality data used in the analyses described herein was taken from a Teledyne T101 H_2S analyzer, Teledyne T100 SO_2 analyzer, TECO 49i O_3 analyzer, METOne 1020 beta attenuation monitor ($PM_{2.5}$), and a Teledyne 200E NO_x analyzer (NO, NO_2, NO_x). In 2015, NSE pulled out of Sable Island consequent to a government policy decision on air quality monitoring priorities. These instruments were replaced with further funding from the ESRF. From 2015 these instruments were managed by Dr. Gibson and Mr. Alan Wilson, with data collected by Mr. Alan Wilson (Environment and Climate Change Canada).

2.12.3.1 TSI Aerodynamic Particle Sizer - Model 3321

A TSI Aerodyne Particle Sizer (APS) (shown in Figure 12) was used for measuring real-time dynamic aerosol number concentrations. The range of the measurement is 0.5 - 20μm over 52 channels. A flow rate of 5L/min is used via an internal pump, a laser is used as the light scattering and an avalanche photodetector (APD) as the sensor (TSI, 2012a). The APS is set to export sample data in .txt format automatically at 15-minute intervals. The APS along with its sampling inlet was installed in the Sable Island Air Chemistry shed on Wednesday, September 30, 2015. The inlet was leveled and secured on the roof of the Air Chemistry shed by a tripod, stainless steel mounting brackets were used to hold the feet of the tripod. A 1.25-inch diameter hole was drilled through the roof and ceiling of the shed to accommodate a candy cane inlet for the APS. The indoor end of the inlet is connected to APS with anti-static tubing from TSI. A weather proof rubber flashing was installed around the inlet at the roof opening and sealed with a weather proof roofing tar to prevent water ingress into the shed. Typical household window bug screen was strapped to the inlet entrance to keep bugs, sand, and other debris from entering the equipment.
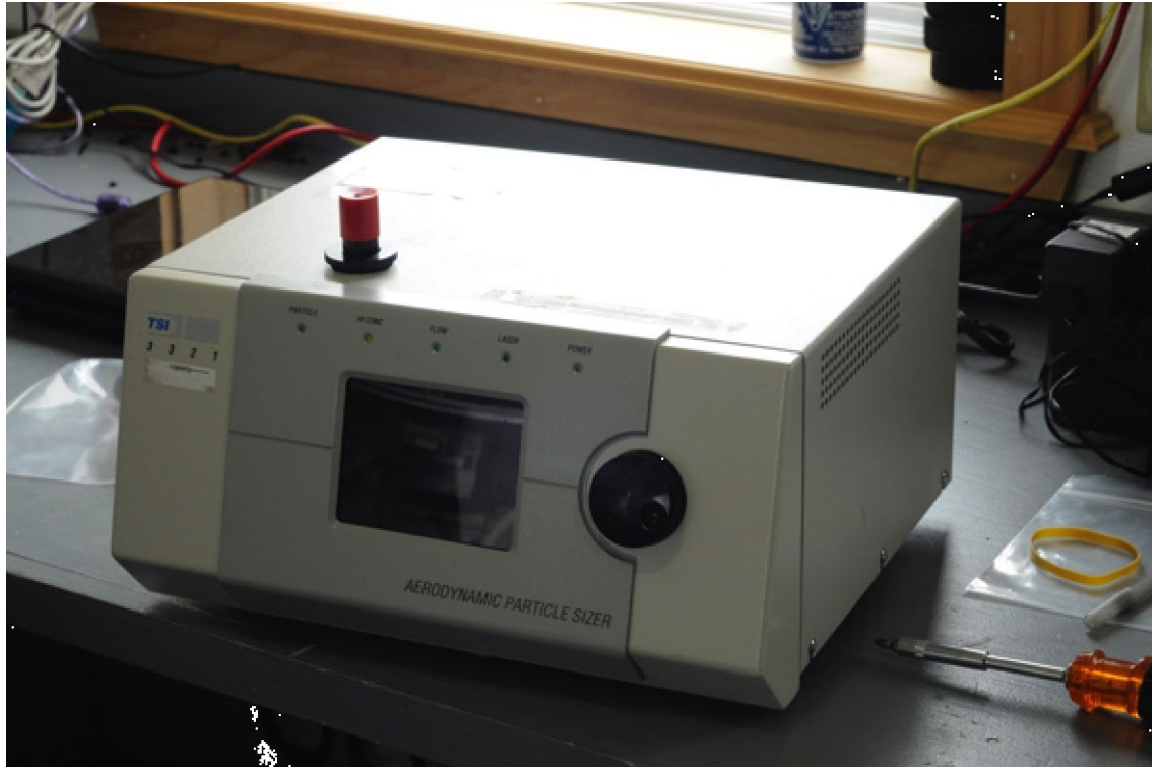
Figure 12 TSI aerodynamic particle sizer (APS) model 3321
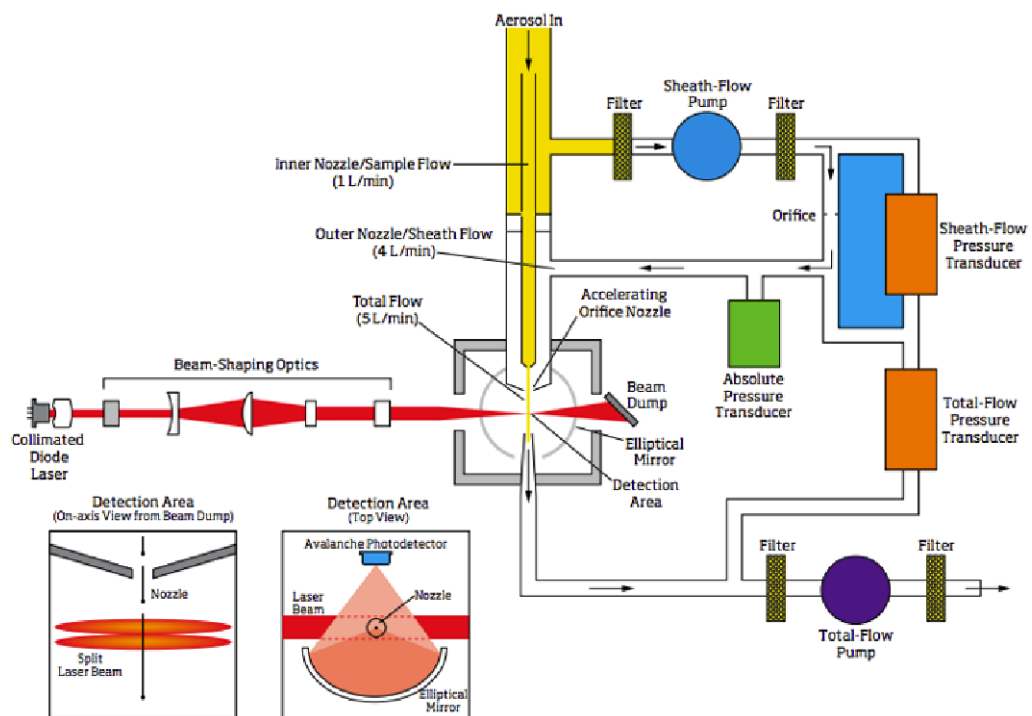
Figure 13 Flow Schematic of APS

As illustrated above in Figure 13, the APS firstly accelerates the aerosol sample flow through an accelerating hole, also known as a critical orifice. The larger particle is accelerated more slowly as it has larger inertia. After particles exit the nozzle, they enter detection area and cross two split laser beams. The laser beam is emitted by a collimated diode laser and reflected by a beam dump so there are two overlapping laser beams. Light will be scattered when each particle cross through laser beams and will be collected by an elliptical mirror. The mirror is placed 90 degrees to the laser beam, the scattered light will be focused onto an avalanche photodetector (APD). The APD then converts the light signal into electrical signal. Each particle will give a single signal with two crests due to the overlapping laser beams. And the time-of-flight (mostly within four nanoseconds) between two peaks will be measured to determine the aerodynamic size of the particle. For the smallest particle (< 0.523 μm), only one crest will be detected due to its small size and high velocity (Palmer et al., 2013).

2.12.3.2 TSI DustTrak DRX Aerosol Monitor model 8533

The TSI DustTrak DRX Aerosol Monitor model 8533 shown below in Figure 14 is a desktop instrument for measuring particle mass concentration. It measures real-time particulate matter mass concentration in the size fractions of PM1, $PM_{2.5}$, PM_4, PM_{10} μm and total suspended particles (TSP). TSP is roughly < 60 μm. The DRX operates at a flow rate of 3L/min. The concentration detection range is between 0.001-150 mg/m^3, the range of particle size detection is 0.1-15μm (TSI, 2012b). Aerosol data can be downloaded by inserting a USB device to the DRX. Data was downloaded every Thursday by ECCC, the flow rate was checked and the DRX should be calibrated before resuming measuring. The DRX was shut down and brought back to the lab in February 2015 due to instrument failure (water ingress).

Figure 14 TSI DustTrak DRX Aerosol Monitor model 8533 (Photo Courtesy of Codey Barnett)

The theory of operation schematic is shown in Figure 15 below. The aerosol is absorbed through the aerosol inlet and goes into two directions continuously by an internal diaphragm pump. Some are split to pass through a HEPA filter before going into the sensing chamber, the rest aerosols. Then the particle will interact with a laser beam, which is emitted from a laser diode. The light first passes through a collimating lens and then a cylindrical lens to give a thin sheet of laser light. The light scattered from particle will be collected by a gold-coated mirror and then focused onto a photodetector. This will cause a voltage difference in photodetector and form photodiode signal.
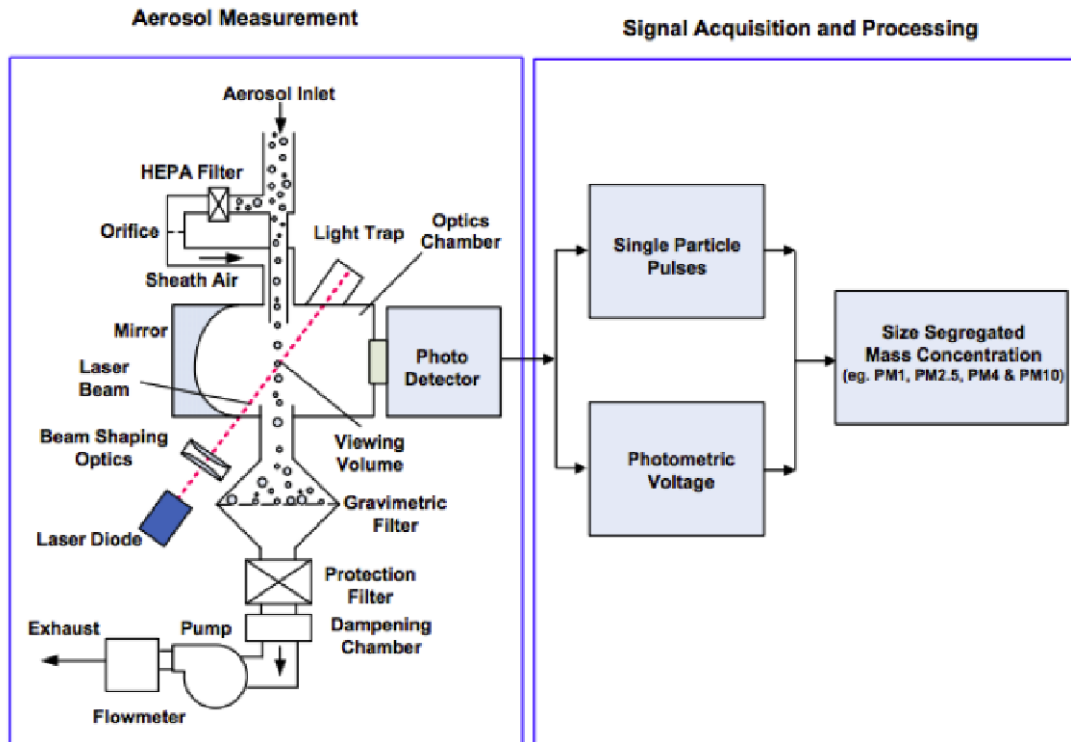
Figure 15 Flow Schematic of DustTrak

2.12.3.3 TSI Ultrafine Particle Monitor - Model 3031

The TSI UFPM (shown in Figure 16) is used for collecting real-time aerosol size-distribution and number concentration data (TSI, 2014). It is designed for aerosols with median aerodynamic diameter between 20 nm to 800 nm. The operation time is set to a 15-min intervals continuously. The UFPM on Sable Island is equipped with TSI 3031200 Environmental Sampling System (ESS) (shown in Figure 17.) that includes a PM_{10} size selective inlet, PM_1 sharp cut cyclone, flow splitter, Nafion dryer, and particle filter (TSI, 2014). A flow rate of 16.67 L/min is achieved using the internal vacuum pump from UFPM 3031 and an external vacuum pump to the left of UFPM for model 3031200 sampling system.

Figure 16 TSI Ultrafine Particle Monitor (UFPM) model 3031

Figure 17 TSI 3031200 Environmental Sampling System (ESS)

The operation schema is shown in Figure 18, steps are (A). to charge the particles (in Corona-Jet charger), (B). classify them by sizes (in Differential Mobility Analyzer, short for "DMA") and (C). quantify the concentrations (Hillemann, Zschoppe, & Caldow, 2007). The aerosols are drawn through the roof-top inlet into the device. Inside the device, the aerosols firstly enter an equalization tank to mix up and smooth out the fluctuations. Then the aerosol flow will be

separated into an 1L/min ion jet flow and a 4L/min aerosol flow. The 1L/min flow will be going through a carbon filter, HEPA filter and an ionizer; the aerosol flow will be going into a mixing chamber to mix with ions delivered by the filtered clean air. Then the aerosols become charged and move to DMA for size classification. The DMA is a metal cylinder with a high-voltage metal cylindrical rod attached in the center (as shown in Figure 18). The aerosols enter from the top of DMA column and flow down, which is maintained at a controlled negative voltage to collect aerosols (shown as orange part in Figure 19). The outer cylinder is electrically grounded so an electric field will be created in the space and attracts positively charged particles to the collector rod. The location that particles will be precipitating along collector rod is determined by the particle electrical mobility, the DMA flow rate, and the DMA inside structure. Particles within a narrow range of electrical mobility exit along the monodisperse air flow through a slit at the end of collector rod. They are transferred to electrometer to determine particle concentration.
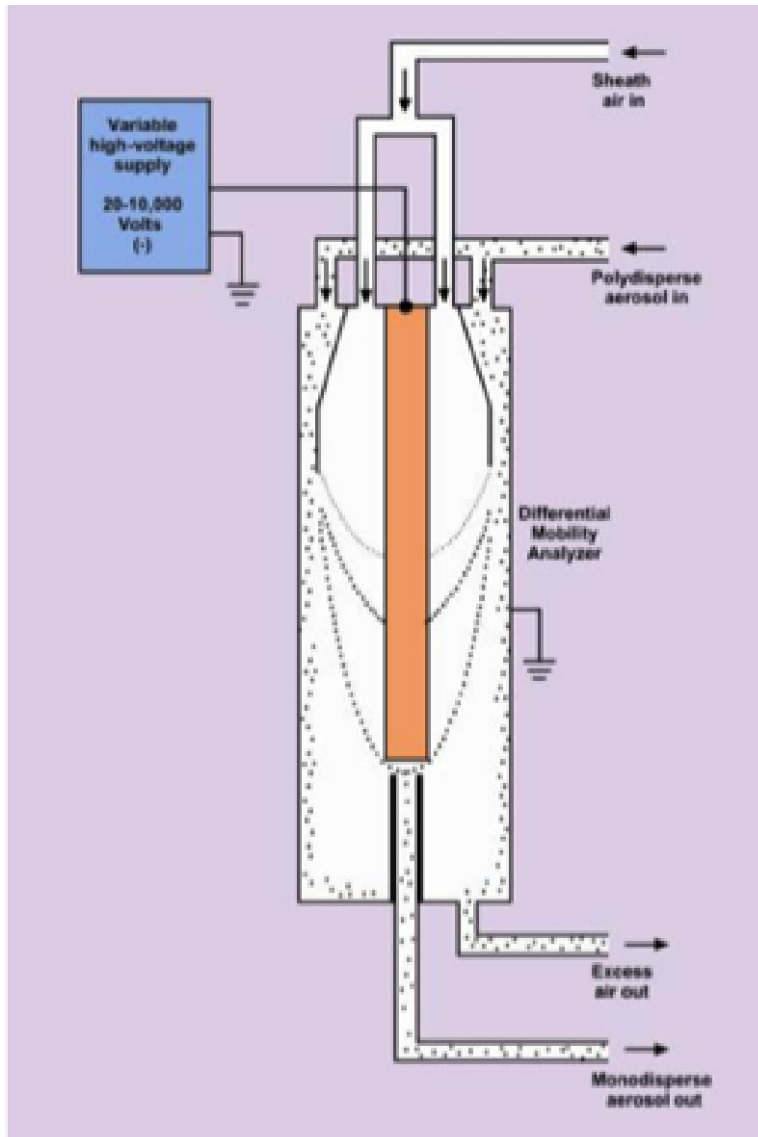
Figure 18 Operation principle of the DMA
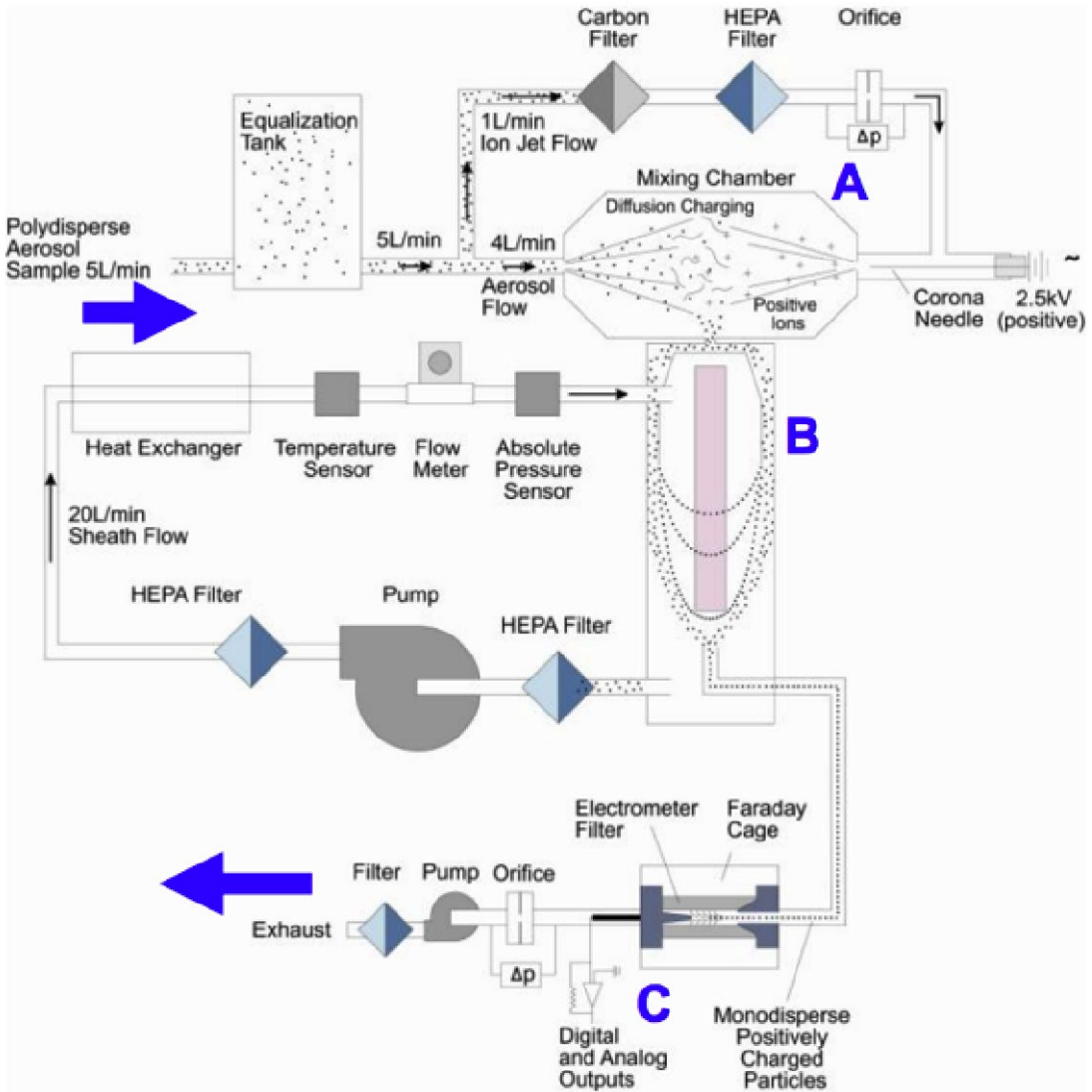
Figure 19 Flow Schematic of UFPM 3031

2.12.4 Equipment Malfunctions

Equipment malfunctions were minimal during the study, but they did occur. This was largely due to the remote nature of the site and the difficulty in performing troubleshooting as a result. The major malfunctions (those that affected daily averages) are summarized in the table below. Reasons for the malfunction are given for equipment run as part of the study, but unfortunately this information was not available for the equipment run by NSE.

Table 2 Equipment Malfunctions over the course of the study

Year	Date	Error / Malfunction	Comments
2016	Jan 7 – 24	APS down	N/A
	Apr 23 – 28	DRX down	N/A
	June 4 – 5	NO_x analyzer down	N/A
	June 22 – July 7	Thermo Scientific 55i was down	Carrier gas pressure too low, tank needed to be changed.
	July 22 – July 25	Thermo Scientific 5012 down	Maintenance and Calibration.
	August 8 – September 1	UFP down	N/A
	August – December 16	APS down	N/A
	September 28 – 30	H_2S analyzer down	N/A
	September 29 – 3	BAM ($PM_{2.5}$) down	N/A
	October 8 – 13	BAM ($PM_{2.5}$) down	N/A
	October 19 – 22	Thermo Scientific 55i down	Carrier gas pressure too low, tank needed to be changed.
	October 5, 6, 8 – 17, 22, 23, 26, 29	H_2S analyzer down	N/A
2017	Fault found on March 2. Removed from the Island March 24.	DRX was found to have stopped working on March 2nd due to water ingress,	Fixed and installed again during the next visit to the Island.
	Fault found on March 28. Removed from the island on April 24.	APS signal dropped due to pump malfunctioning on	Borrowed an APS from U of Calgary. Returned September 2017.

2.13 Statistical Analysis

The data collected from the study instrumentation consisted of data averaged over 5 minute intervals while data obtained from NSE consisted of data averaged over 1 hour intervals. All the data was compiled into a master spreadsheet in excel. The data was filtered and extreme outliers or negative values removed. Extreme outliers were identified when concentrations far exceeded guidelines and regulations. Outliers also consisted of single data points, where true pollution events tended to show elevated concentrations for hours or days. H_2S values experienced sudden spike after which they remained high for approximately a month, spiking once again before dropping. This first spike was from May 16th to June 12th and the second from June 12th to June 21st. The values were reduced (by 1.3 and 2.8 ppb for each spike) so that the lowest reading for each time period was 0 ppm as it was assumed baseline drift which is a feature of auto-gas analyzers. NO, NO_2, and NO_x values also had calibration issues where they consistently reported negative values. The measurements were adjusted so that values were positive. Data were projected onto common hourly and daily time vectors in order to be able to allow comparison and for use in running PMF. Descriptive statistics, time series analysis, box plots, and other statistical tests were generated using Minitab 16 and SigmaPlot (v12.0). The software used for source apportionment was the USEPA PMF model v3.0.2.2 (and version 5 after January 1st 2016) as discussed in more detail in Section 2.8. A pollution rose or the factors obtained from the PMF model was generated using IgorPro v6.2.2.2.

2.14 Meteorological Data

Although wind speed, wind direction, and temperature were monitored by NSE this data contained many gaps due to instrument malfunction. As a result, it was not used in any analyses. Instead, hourly and daily meteorological data for the sampling time frame was obtained from Environment Canada. Historical weather data is available for download from the Environment Canada website, with data available from the Sable Island weather station (http://climate.weather.gc.ca/index_e.html). The data was used to generate pollution roses and to aid with the interpretation of local upwind sources of PM and VOCs.

2.15 Air Mass Back Trajectories

Air mass back trajectories were generated to aid in the source apportionment process. They were generated using the HYSPLIT model available online from the National Oceanic and Atmospheric Administration (http://ready.arl.noaa.gov/HYSPLIT_traj.php). Backward trajectories were run for each day of the sampling period. A modelling time of 120 hours (5 days) was used for the back trajectories and the air mass was modeled to arrive at Sable at 23:00 in order to correspond with the end of a daily sampling period. The default arrival height of 500 m was used in running the model to avoid trajectories impacting the surface before reaching the receptor (Sable Island) (Gibson et al., 2009b).

2.16 Receptor Modelling Software

The USEPA PMF model v 3.0.2.2 was used to conduct source apportionment on the data collected. The model was run using daily averages of the data. In order to run, it requires both a species concentration file and species uncertainty file related to the data set.

A concentration file containing daily averages was generated in Excel and quality controlled for input into the model. The model will not run if null values are present so where they did occur a value of -999 was entered to allow the model to run without errors.

The uncertainty file outlines any uncertainties in the data collected. To be safe, an uncertainty of 10% was applied to all the measurements. The value of 10% was used as information on the NSE instruments was not available. If the percent error for measurements from each instrument were known this would have allowed for better estimates of uncertainty. When null values were encountered, an uncertainty value of half the minimum detection limit was used as recommended by the USEPA (Norris et al., 2008). Minimum detection limits were not available for the NSE data, and so minimum detection limit values available for real time gas monitors used to measure the species in question were used instead. It was assumed that these values would be comparable if not the same as those for the NSE equipment.

The model was run using the USEPA default of 20 base runs with 4 factors (sources) being chosen. Each run starts at a different point in the time series data in an attempt to account for any elevated concentrations within the data set. It tests to determine if each run has converged and at the end selects the run that best fits the data (Norris et al., 2008). The number of factors selected tells the model how many factor profiles/contributions to look for within the data set. The model was run for a range of factors from 3-10. Based on the results, as well as knowledge of the potential sources on Sable Island identified through the literature review and on Island experience, it was decided that 4 factors gave the best representation. Emissions from offshore O&G activities, LRT, and on-site combustion were the main expected sources on Sable. The base runs are the basis for advanced analysis using bootstrapping or Fpeak (Norris et al., 2008).

The bootstrap and Fpeak models were also applied to the data. Both models help to ensure the base model runs provide stable and robust results. Bootstrapping[1] is performed to estimate the stability

---

[1] Bootstrapping is a common model validation method where a sub-set of the data is removed from the whole, the model run on the remaining data, the model is then used to predict the data subset. If the model cannot predict the data subset is not a useful model.

and uncertainty of the solution. The bootstrapping method randomly selects non-overlapping blocks of samples and creates a new input data file for them. The PMF model is then re-run and each bootstrap factor is mapped to the base run factor for comparison. The Fpeak test looks at whether a pair of factor matrices can be transformed to another pair of matrices with the same "Q" value, or in other words, whether they can be rotated. This is done to ensure that there is little rotational ambiguity in a solution (Norris et al., 2008). The bootstrap model was performed on Run 15 with 100 bootstraps and a minimum correlation R-value of 0.6. The seed was random and the block size 6. The Fpeak model was run for one Fpeak with a strength of 0.1.

It should be noted that the PMF model was originally developed for source apportionment of $PM_{2.5}$ using speciated sample data obtained from filter based sampling, but can be run with any kind of speciated sample data (Reff et al., 2007). The sample data obtained during the study contains both mass concentrations of $PM_{2.5}$ and BC along with gaseous measurements. As a result, final source contributions to a total air pollutant cannot be accurately determined. However, the model is capable of identifying source factors and their chemical profiles from the data matrix provided and the correlations contained. As a result, factor contribution outputs from the model will not be used. In the future, VOC speciation data as well as more in depth mass concentration measurements would be beneficial to the broader study taking place on Sable in that they would allow for accurate mass contributions to be determined.

2.17 Visible Satellite images

Satellite observations for Sable Island study are obtained from National Aeronautics and Space Administration (NASA) Ocean Color Web database (http://oceancolor.gsfc.nasa.gov /cgi/browse.pl?sen=am). The database is based on data record taken by Visible Infrared Imaging Radiometer Suite (VIIRS) on board the Suomi NPP satellite and Moderate Resolution Imaging Spectroradiometer (MODIS) on board the Terra and Aqua satellites. MODIS satellites observe every point on Earth's surface every 24-48 hours. The instruments can capture cloud cover status, distribution and size of cloud droplet, aerosol properties, terrestrial, and marine biomass activities (e.g. phytoplankton which live in the upper ocean layer). MODIS satellites also measure chlorophyll fluorescence, which can help with monitoring phytoplankton growth ("MODIS Web", 2017; Tassia Owen, 2017). VIIRS satellite is a successor of the two MODIS satellites, comprising

a scanning radiometer which has almost same capability as MODIS instruments but it provides much better spatial resolution ("Visible Infrared Imaging Radiometer Suite (VIIRS)", 2017).

3 PRIOR TO 2016 – RESULTS AND DISCUSSION

After data was collected and compiled into a master spreadsheet descriptive statistics were performed. Time series graphs and box plots were generated and the non-parametric Mann-Whitney statistical comparison test runs. The data was then used to run Principal Component Analysis followed by USEPA PMF model v5 software. Finally, a pollution rose was generated for the factor profiles obtained through the PMF model. The pollution rose shows the average wind direction and its association with factor contributions from the four factors. Hourly meteorological data from environment Canada was used to obtain daily averages of wind speed and direction for comparison to the PMF factors. The data from the Sable Island instruments was then split into data collected before and after July 22nd to examine the impact of new oil and gas activity, which commenced at approximately this time.

3.1 General Air Quality

3.1.1 Time Series Analysis of 2013 data

The following figures show the time series of each pollutant measured. A visual inspection clearly reveals spikes and correlations between pollutants. Data points are shown in red with connecting lines shown in blue.
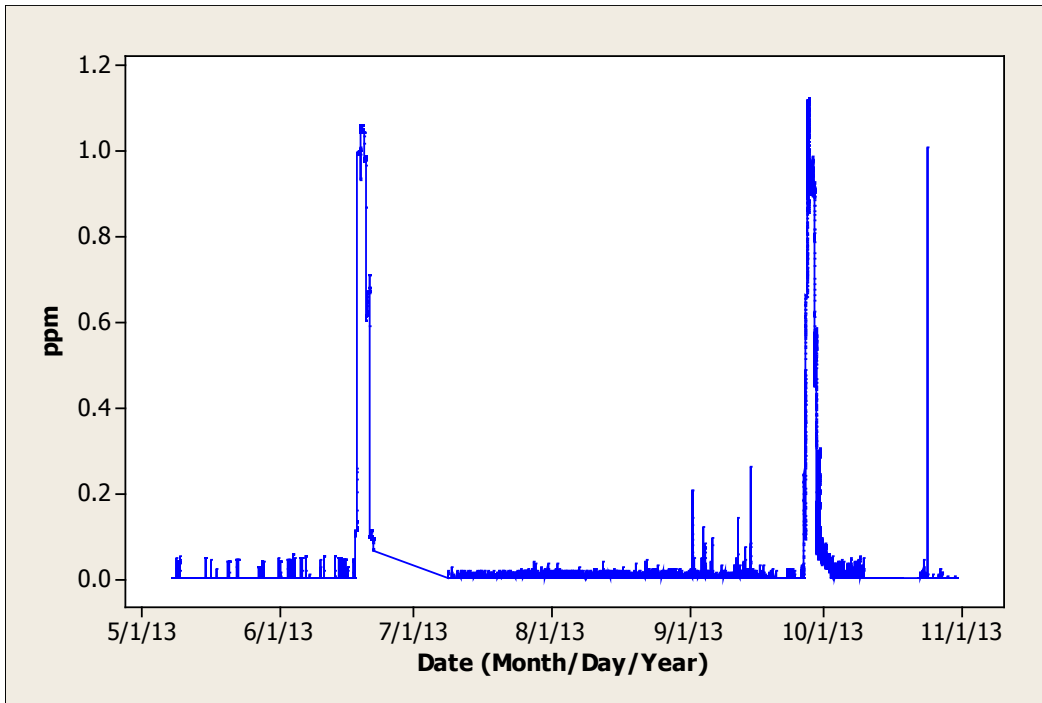
Figure 20 NMHC time series from 05/01/13 to 11/01/13 (m/d/y)
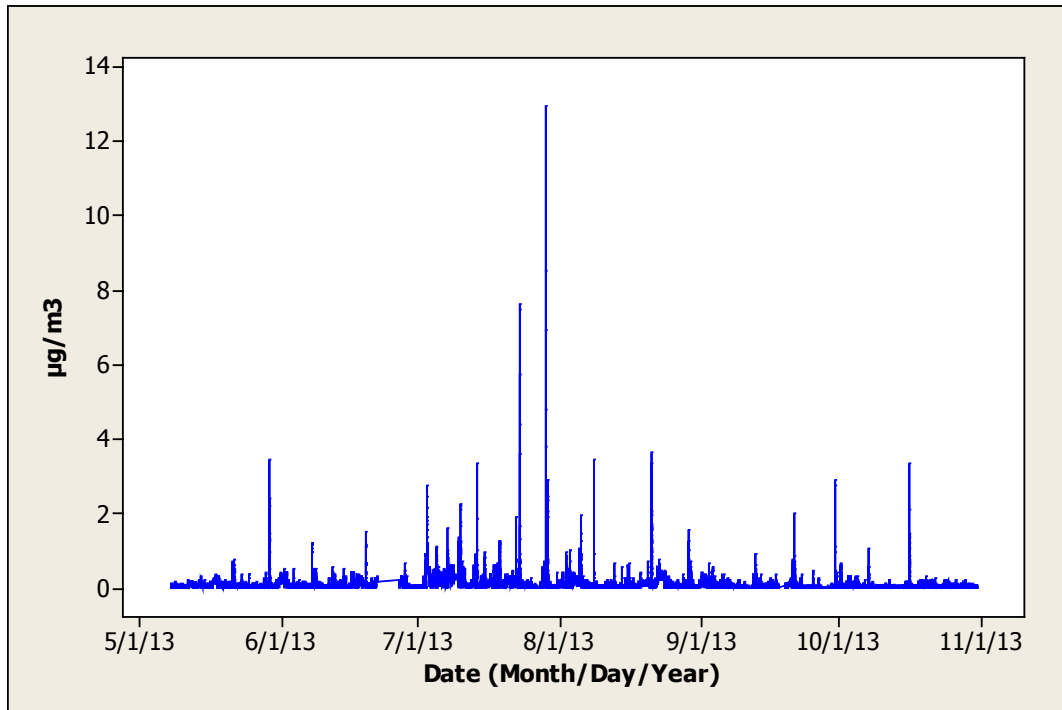
Figure 21 BC time series from 05/01/13 to 11/01/13 (m/d/y)

52
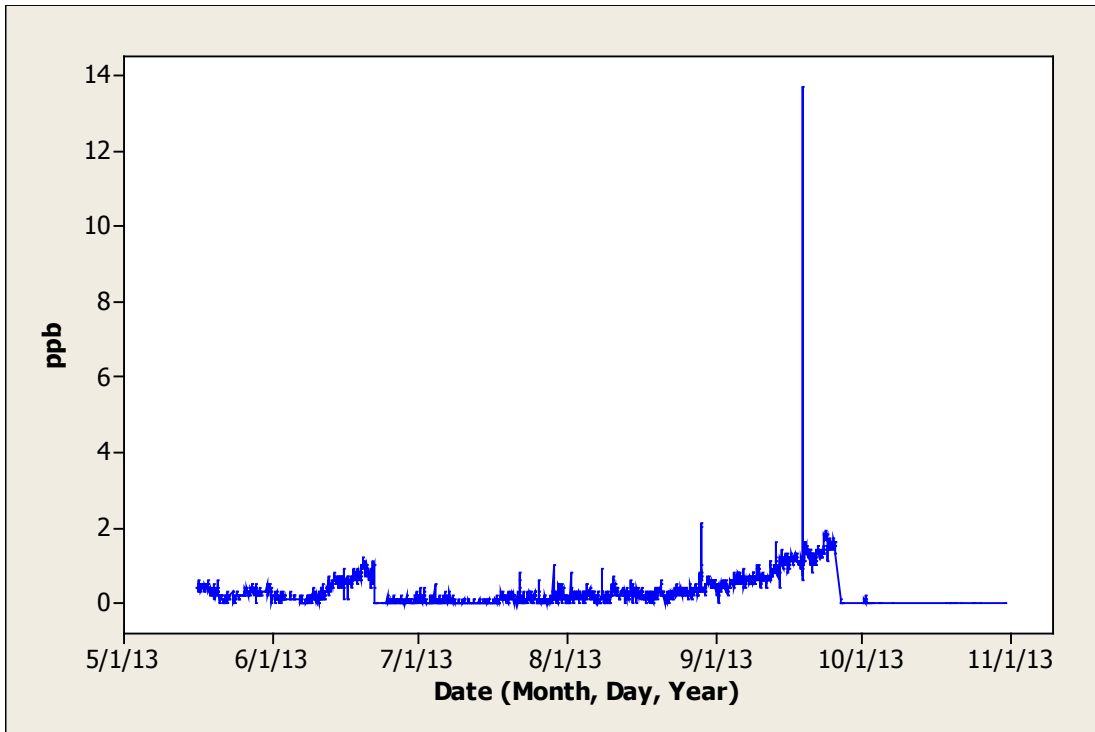
Figure 22 H$_2$S time series from 05/01/13 to 11/01/13 (m/d/y)
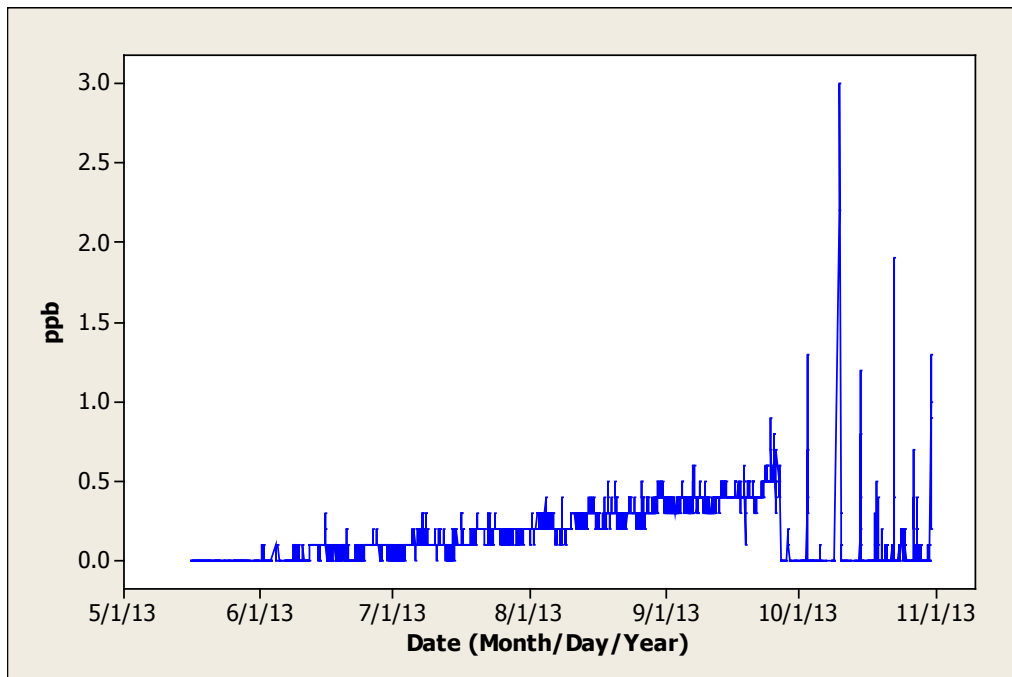
Figure 23 SO$_2$ time series from 05/01/13 to 11/01/13 (m/d/y)
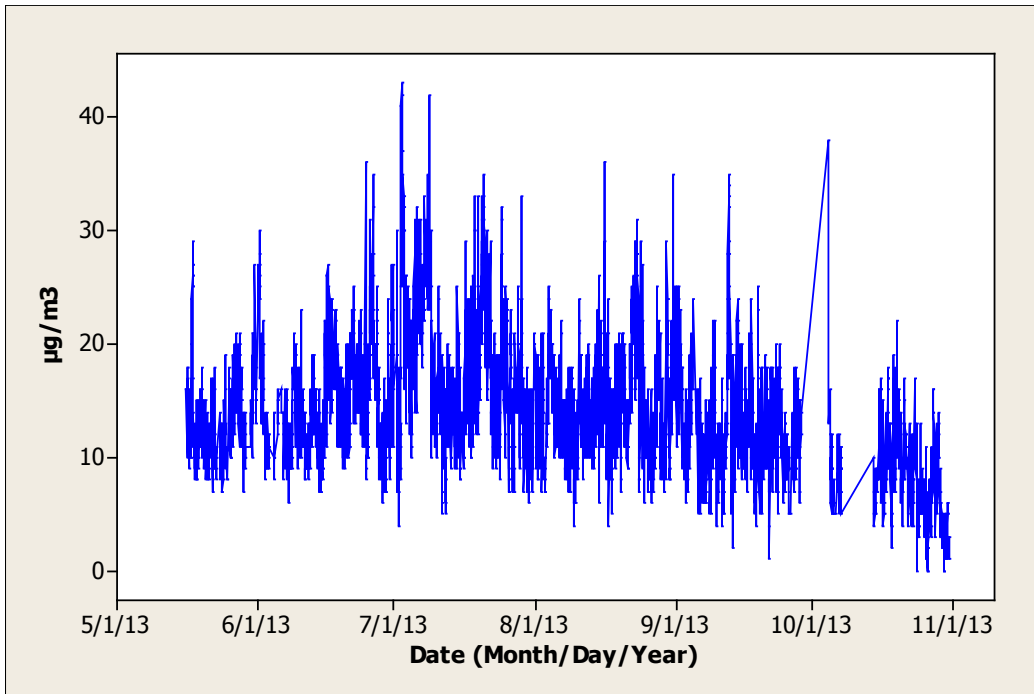
Figure 24 PM$_{2.5}$ time series from 05/01/13 to 11/01/13 (m/d/y)
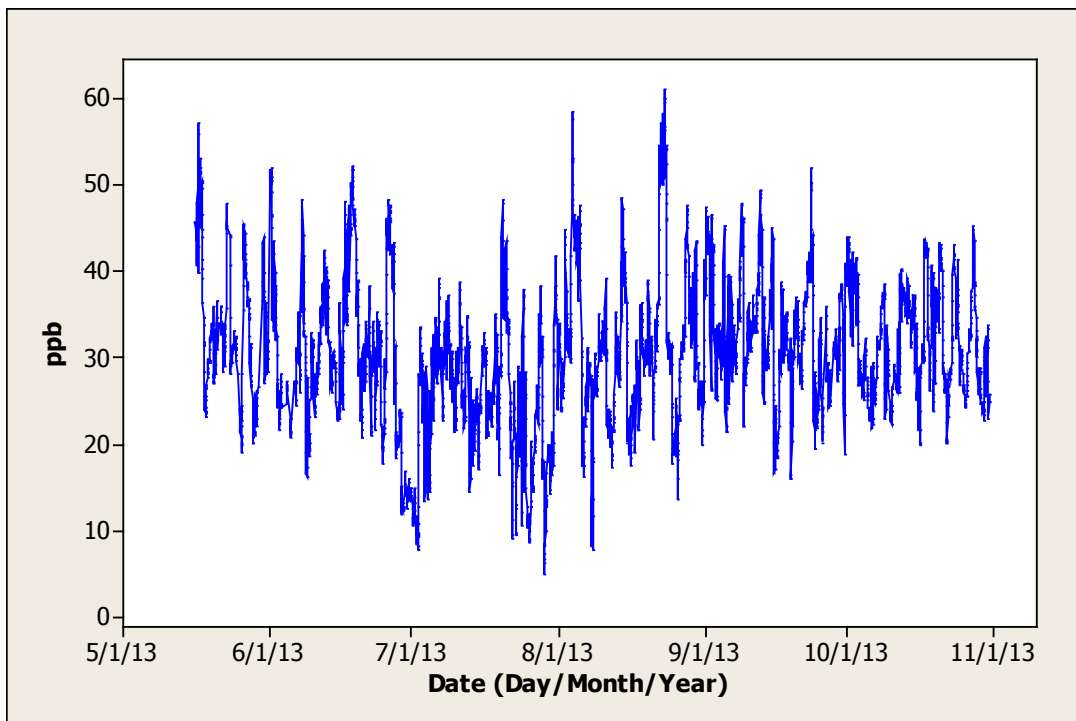
Figure 25 O$_3$ time series from 05/01/13 to 11/01/13 (m/d/y)

54
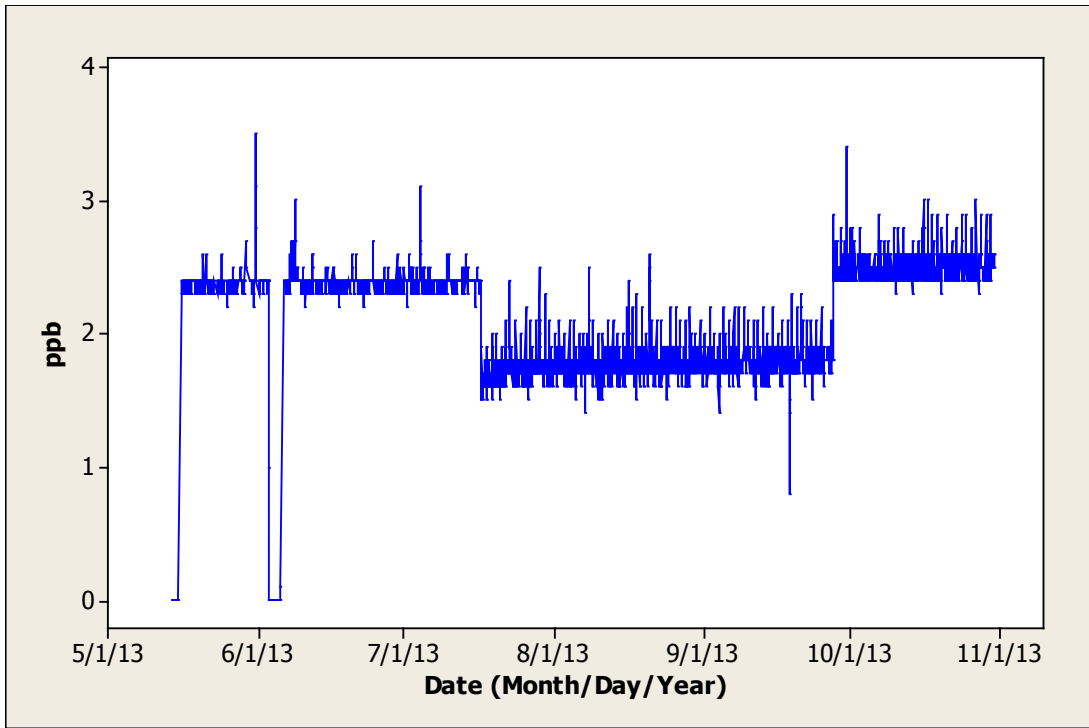
Figure 26 NO time series from 05/01/13 to 11/01/13 (m/d/y)
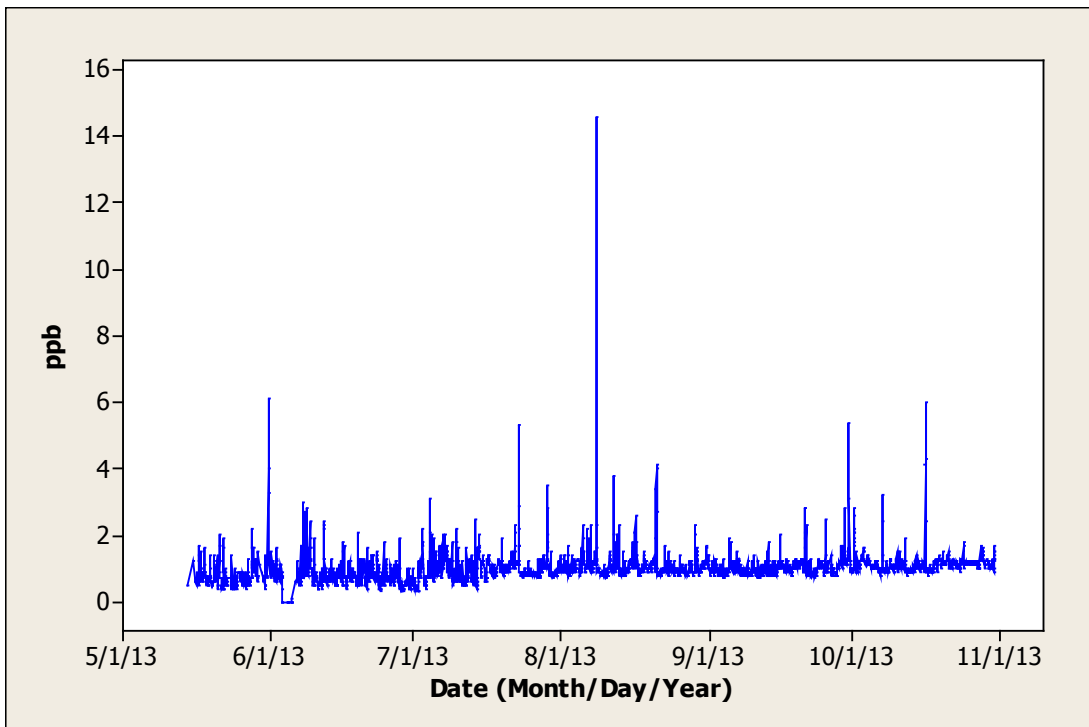
Figure 27 NO$_2$ time series from 05/01/13 to 11/01/13 (m/d/y)
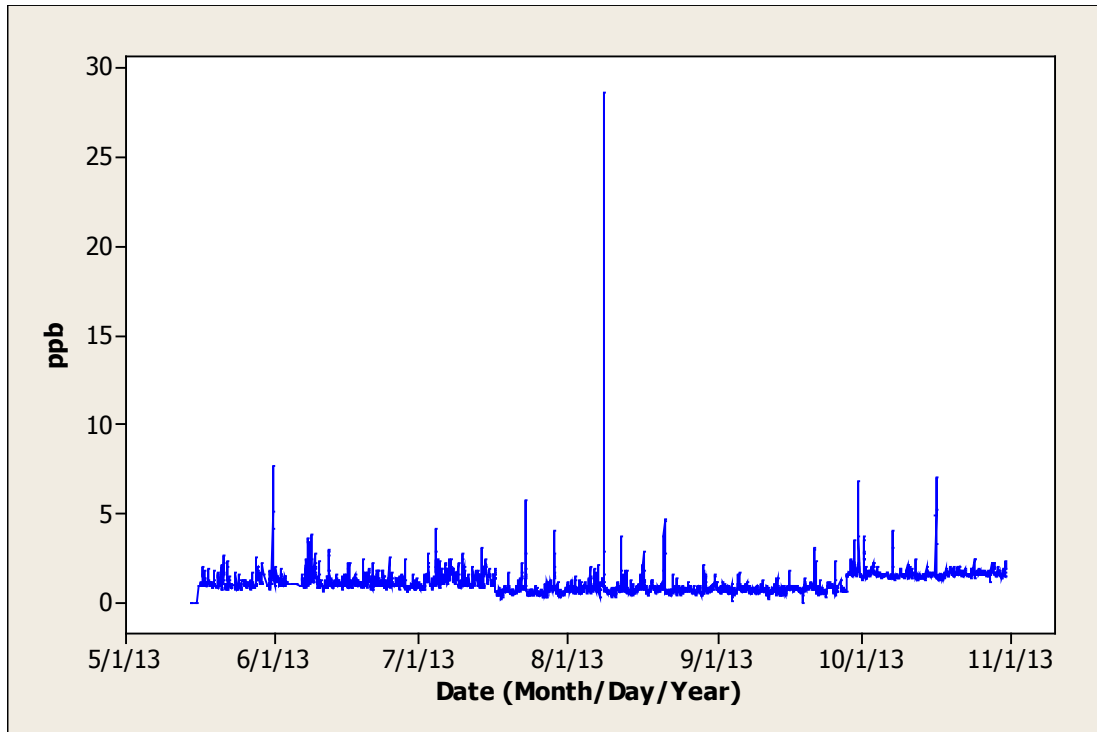
Figure 28 NO$_x$ time series from 05/01/13 to 11/01/13 (m/d/y)

From analyzing the time series plots of the various pollutants certain trends begin to become apparent. For example, it can be seen that NMHC, BC, H$_2$S, and SO$_2$ (Figure 20 to Figure 23) concentrations tend to be generally low (at or around zero readings) with proportionally higher spikes occurring at specific times. These spikes are most likely linked to pollution events, meaning that NMHC, BC, H$_2$S, and SO$_2$ concentrations are likely associated with specific sources with intermittent emissions.

The time series plots for PM$_{2.5}$, O$_3$, NO, NO$_2$, and NO$_x$ (Figure 24 to Figure 28) tend to show more constant concentrations. The conclusion can be drawn that these pollutants are present in the majority of sources impacting the island and in particular those that are more constant in nature, i.e. background pollutants. For example, it is well known that O$_3$ in particular can be considered a "background" air contaminant, while PM$_{2.5}$ can be to a certain extent (through sea salt and LRT) (Gibson et al., 2009a; Gibson et al., 2013d). Specific pollution events are apparent from the time series and they will be discussed further in Section 4.2.2 through the use of HYSPLIT back trajectories and satellite imagery.

56

3.1.2 Descriptive Statistics

Descriptive statistics for the data is summarized below in Table 3. Skewness is a measure of the asymmetry, while kurtosis is a measure of the 'peakedness' of the probability distribution of a real-valued random variable (Novak, 2004). The closer to zero, the closer the data follows a normal distribution (Novak, 2004).

Table 3 Descriptive statistics for all species up to the end of 2013.

Variable	Mean	Standard Deviation	Min	Q1	Median	Q3	Max	IQR	Skewness	Kurtosis
NMHC (ppm)	0.034	0.163	0.00	0.00	0.00	0.00	1.13	0.00	5.29	27.1
BC ($\mu g/m^3$)	0.092	0.170	0.00	0.02	0.05	0.11	13.0	0.09	23.0	1180
$PM_{2.5}$ ($\mu g/m^3$)	14.1	5.71	0.00	10.0	13.0	17.0	43.0	7.00	0.83	1.36
SO_2 (ppb)	0.168	0.173	0.00	0.0	0.10	0.30	3.00	0.30	2.63	28.0
H_2S (ppb)	0.361	0.452	0.00	0.10	0.20	0.50	13.7	0.40	9.49	255
O_3 (ppb)	30.4	8.24	4.90	25.3	30.2	35.0	61.1	9.70	0.18	0.50
NO_x (ppb)	2.17	0.379	0.00	1.80	2.30	2.40	35.0	0.60	-0.92	2.95
NO_2 (ppb)	1.12	0.700	0.00	0.70	1.00	1.50	28.7	0.80	17.0	627
NO (ppb)	0.998	0.434	0.00	0.80	1.00	1.10	14.6	0.30	10.5	269

Scrutiny of the skewness and kurtosis it becomes immediately apparent that the data are not normally distributed, with the exception of O_3 and $PM_{2.5}$. This was unexpected, as environmental data does not usually follow a normal distribution. The normal distributions of O_3 and $PM_{2.5}$ are likely due to their presence as "background" air contaminants present in a number of sources impacting the Island (Gibson et al., 2009a; Gibson et al., 2013d). As a result, the overall data set requires non-parametric statistics to be run. Mean and median concentrations are close to one another, with relatively low standard deviations. However, maximum concentrations tend to be quite a bit higher than mean values, and can be considered as special air pollution episodes or events, e.g. LRT smog or continental wild fire plumes advecting over Sable Island. Unlike outliers that were removed and consisted of single unrealistically large data points, these pollution events

tended to show more realistic concentrations based on maximum permissible guidelines and showed elevated concentrations for hours or even days.

From Table 3 it can be seen that the mean concentration for $PM_{2.5}$ was 14.1 μg/m^3. This is a rather high value considering Sable Island's remote location in the North West Atlantic. Average concentrations for Halifax, Nova Scotia were found by Jeong et al., 2011 to be around 7.1 μg/m^3 for the year and approximately 9.0 μg/m^3 over the summer months. Gibson et.al. (2013d) found the average $PM_{2.5}$ concentration in Halifax during the summer of 2011 to be only 3.9 μg/m^3. These higher than expected concentrations are likely due to sea salt PM generated from wave action.

The mean concentration for NMHCs was 0.034 ppm and for BC was 0.092 μg/m^3. Maximum values are 1.13 ppm and 13.0 μg/m^3 respectively. The mean concentrations for SO_2, H_2S, O_3, NO_x, NO_2, and NO were 0.17 ppb, 0.36 ppb, 30.4 ppb, 2.17 ppb, 1.12 ppb, and 1.0 ppb respectively. The concentration of O_3 is comparable with the annual average concentration of O_3 in ambient air in Canada, which was 33 ppb in 2011 (Environment Canada, 2013).

The Air Quality Regulations from NSE outline maximum permissible ground level concentrations for H_2S, NO_2, O_3, and SO_2 of 3 pphm, 21 pphm, 8.2 pphm, and 34 pphm respectively over a 1-hour averaging period. This equates to concentrations of 30, 210, 82, and 340 ppb respectively. A summary of the applicable Air Quality Regulations can be seen below in Table 4. All of the average and maximum concentrations for pollutants monitored on Sable Island fall below maximum permissible levels.

Table 4 Maximum Permissible Ground Level Concentrations (Nova Scotia Environment: Air Quality Regulations, 2010).

Contaminant	Averaging Period	Maximum Permissible Ground Level Concentrations (ppb)	Maximum concentrations on Sable Island (ppb)
H_2S	1-hour	30	13.7
NO_2	1-hour	210	14.6
O_3	1-hour	82	61.1
SO_2	1-hour	340	3.00

The Canada-Wide Standards (CWS) for $PM_{2.5}$ outline maximum desirable concentrations of 30 μg/m^3 over a 24-hour averaging period and concentrations of 65 ppb over an 8-hour averaging

period for O_3 (Environment Canada, 2013c). The new 2020 Canadian Air Quality Standards for fine particulate matter and ground level ozone will be adjusted to 27 $\mu g/m^3$ for $PM_{2.5}$ over a 24-hour averaging period and 62 ppb for O_3 over an 8-hour averaging period (Environment Canada, 2013b). Mean concentrations of $PM_{2.5}$ and O_3 on Sable Island were below both of these guidelines. The WHO outlines maximum desirable concentrations of 25 $\mu g/m^3$ for $PM_{2.5}$ over a 24-hour averaging period, 105 ppb for NO_2 over a 1-hour averaging period, 7.5 ppb for SO_2 over a 24-hour averaging period, and 50 ppb for O_3 over an 8-hour averaging period (WHO Air quality guidelines for particulate matter, ozone, nitrogen dioxide and sulphur dioxide, 2005). Mean concentrations on Sable Island are below these guidelines. The guidelines are summarized below in Table 5.

Table 5 Canada-Wide Standards, 2020 Canadian Air Quality Standards, and World Health Organization maximum desirable air quality metrics.

Pollutant	Canada-Wide Standards	2020 Canadian Air Quality Standards	World Health Organization	Average concentration on Sable	Maximum concentration on Sable Island
$PM_{2.5}$ ($\mu g/m^3$)	30 (24 hours)	27 (24 hours)	25 (24 hours)	14.1	43.0
O_3 (ppb)	65 (8 hours)	65 (8 hours)	50 (8 hours)	30.4	61.1
NO_2 (ppb)	-	-	105 (1 hour)	0.998	14.6
SO_2 (ppb)	-	-	7.5 (24 hours)	0.168	3.00

There was an interesting bimodal distribution for NO concentrations as seen in Figure 68, possibly due to the impact of 2 separate sources (potentially fresh and aged combustion).

3.1.3 Box Plots

Box plots were generated in order to compare the distribution of the data. Due to the vast number of data points the 5th/95th percentiles were shown instead of outliers.
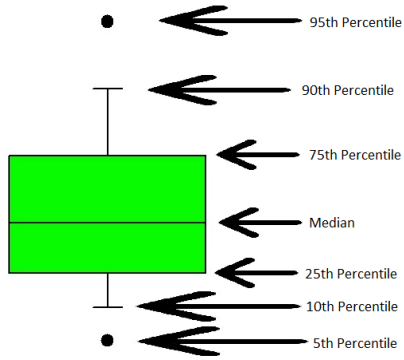
Figure 29 Box plot legend
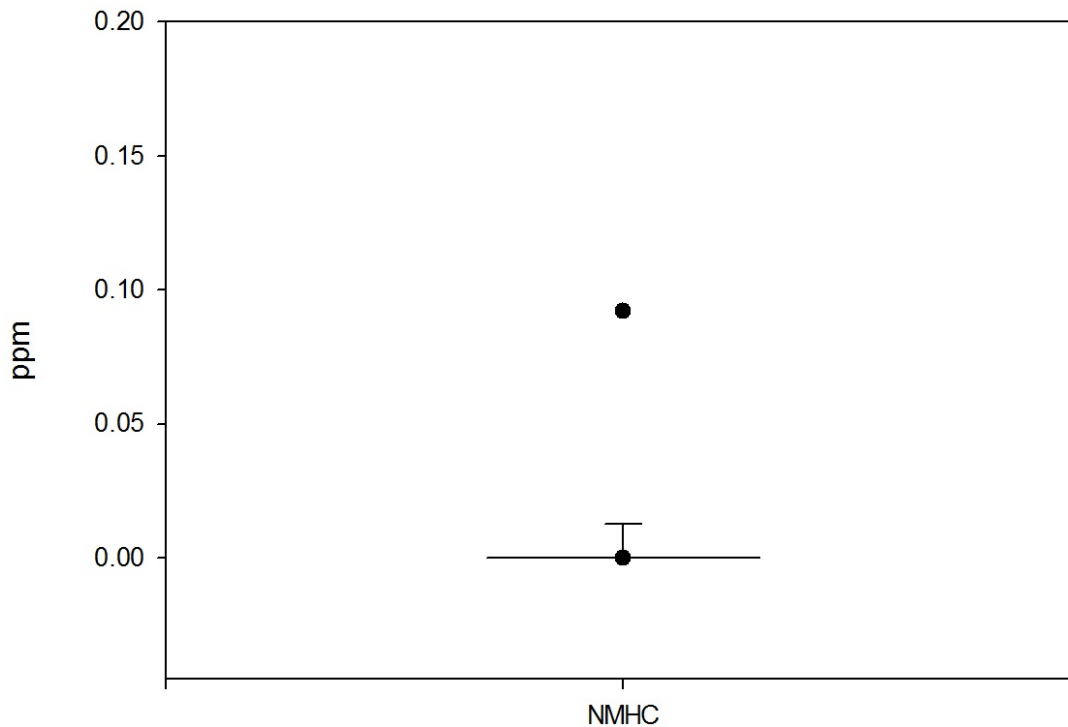
Figure 30 Box plot of NMHCs

From Figure 30 we can see a median value for NMHCs of 0 ppm. This is due to the fact that the majority of readings taken by the Thermo Scientific 55i were zero readings with intermittent spikes. The 95th percentile is just below 0.1 ppm, indicating the relatively small range of data.
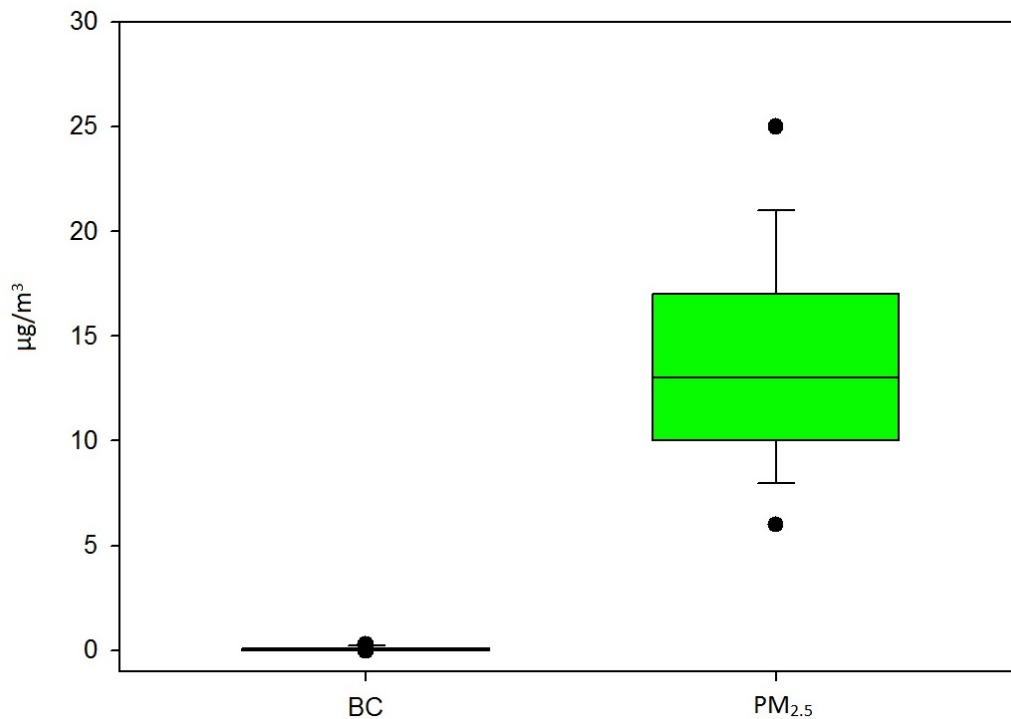
Figure 31 Box plot of Black Carbon (BC) and PM₂.₅

Figure 31 compares BC and PM$_{2.5}$ and shows that median values of PM$_{2.5}$ are considerably higher, which is to be expected as BC is generally a component of PM$_{2.5}$. PM$_{2.5}$ also shows a much greater range of values than BC. This is due to the presence of PM$_{2.5}$ in many sources where BC tends to be associated with a more limited number (Gibson et al., 2013). It should be noted that sea salt is a major contributor to PM$_{2.5}$ (Waugh et al., 2010) and this would likely be part of the reason for higher PM$_{2.5}$ concentrations on a heavily marine influenced location such as Sable Island.
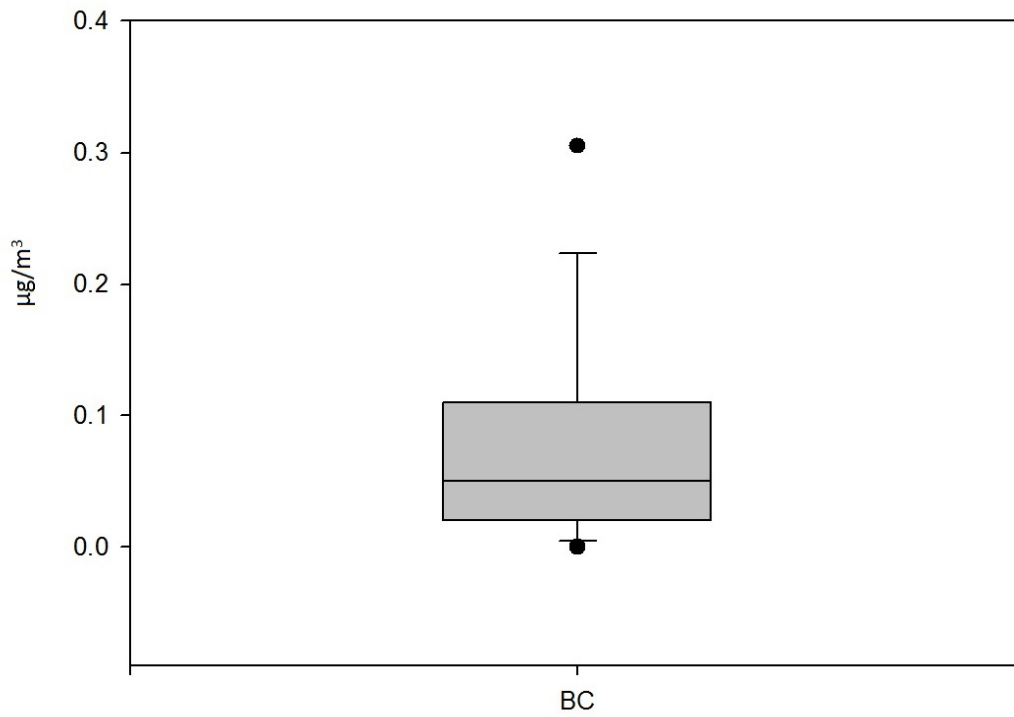
Figure 32 Box plot of Black Carbon (BC)
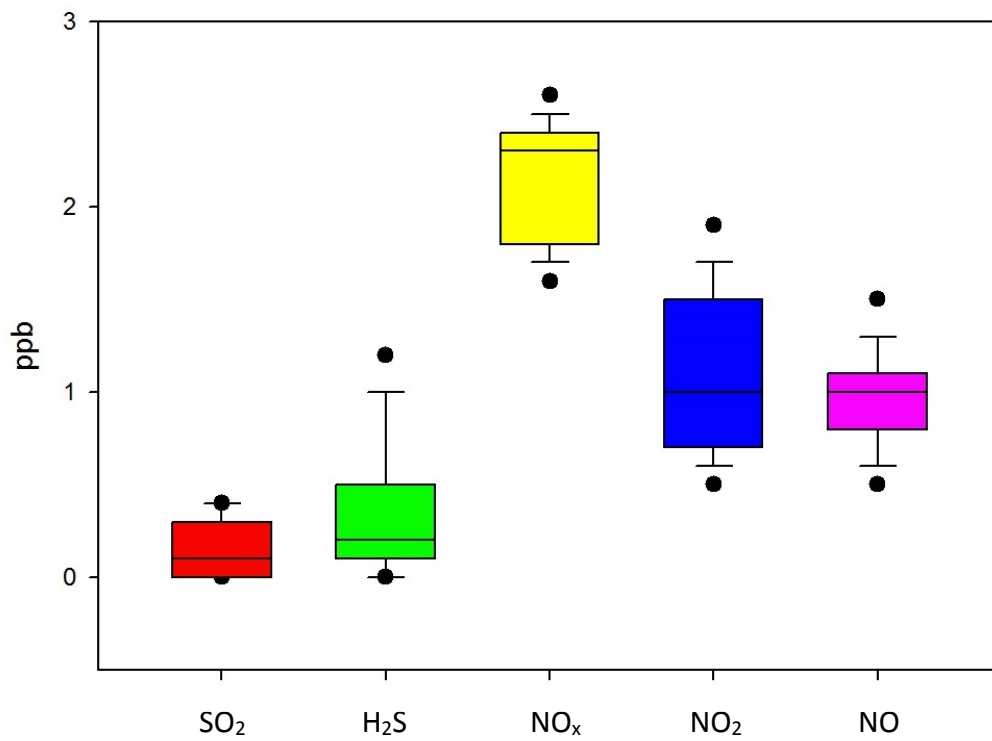
Figure 33 Box plot of SO₂, H₂S, NOₓ, NO₂ and NO

Figure 33 shows the box plots for SO_2, H_2S, NO_x, NO_2, and NO. They show similar ranges and median values with NO_x exhibiting slightly higher values (due to it being the summation of NO2 and NO concentrations). The NOx maybe be influenced from on-site combustion (including the burning of garbage). Trash burning and log fires on the beach were banned soon afterwards due to concerns they may be impacting the NO_x results.

3.2   Source Apportionment

3.2.1   PMF Model Run and Results

The outputs from the USEPA PMF model v5 run will be presented in this section. The model was run using 20 base runs and 4 factors. The bootstrap and Fpeak models were also applied to the data. The bootstrap model was performed on Run 15 with 100 bootstraps and a minimum correlation R-value of 0.6. The seed was random and the block size 6. The Fpeak model was run for one Fpeak with a strength of 0.1. As can be seen from the tables below, all runs converged for Q (Robust) and Q (True) and the Fpeak run also converged. In this section predicted and observed concentrations for the base model run, variability in concentration and percentage of species for the bootstrap runs, Fpeak factor profiles and concentrations, and seasonal contributions are shown. Dates shown in figures are in the format dd/mm/yy.

Table 6 PMF base run summary

Run #	Q(Robust)	Q(True)	Converged	# Steps
1	4129.34	5524.53	Yes	2710
2	4137.42	5445.12	Yes	1593
3	4533.56	6068.03	Yes	2296
4	4533.79	6068.01	Yes	3284
5	4137.18	5445.12	Yes	1935
6	4388.94	6256	Yes	1420
7	4137.82	5444.95	Yes	1772
8	4129.16	5524.38	Yes	2553
9	4110.8	5540.35	Yes	2296
10	4388.98	6256.46	Yes	1645
11	4129.03	5524.31	Yes	2441
12	4128.61	5524.25	Yes	2640
13	4523.98	6134.3	Yes	1086
14	4137.79	5444.94	Yes	1727
15	4109.8	5546.26	Yes	2076
16	4138.46	5445.69	Yes	2290
17	4138.86	5444.88	Yes	2268
18	4128.5	5524.55	Yes	2605
19	4138.17	5444.86	Yes	2026
20	4138.22	5444.93	Yes	1972

It can be seen from

Table 6 that for the base model run Q robust and Q true converged for all runs. This demonstrates the stability of the base model run. Q true was found to vary from Q robust by approximately 24 – 30%. This is a less than ideal situation, but is likely due to the impact of large spikes in concentration of species such as NMHC had on the model run.

Table 7 Bootstrap factors mapped to base factors

	Base Factor 1	Base Factor 2	Base Factor 3	Base Factor 4	Unmapped
Boot Factor 1	70	0	0	2	23
Boot Factor 2	0	38	5	0	52
Boot Factor 3	0	0	88	0	7
Boot Factor 4	0	3	0	86	6

Table 7 shows that out of 380 bootstrap runs, 88 were unmapped. This again demonstrated the impact of spikes in the concentration of certain species on model results. Table 8 provides the PMF Fpeak run summary.

Table 8 Fpeak Run Summary

Fpeak #	Strength	Q(Robust)	Q(True)	Converged	# Steps
1	0.1	4111.5	5545.4	Yes	337

Table 8 demonstrates that the Fpeak run converged, showing little rotational ambiguity in the model results.
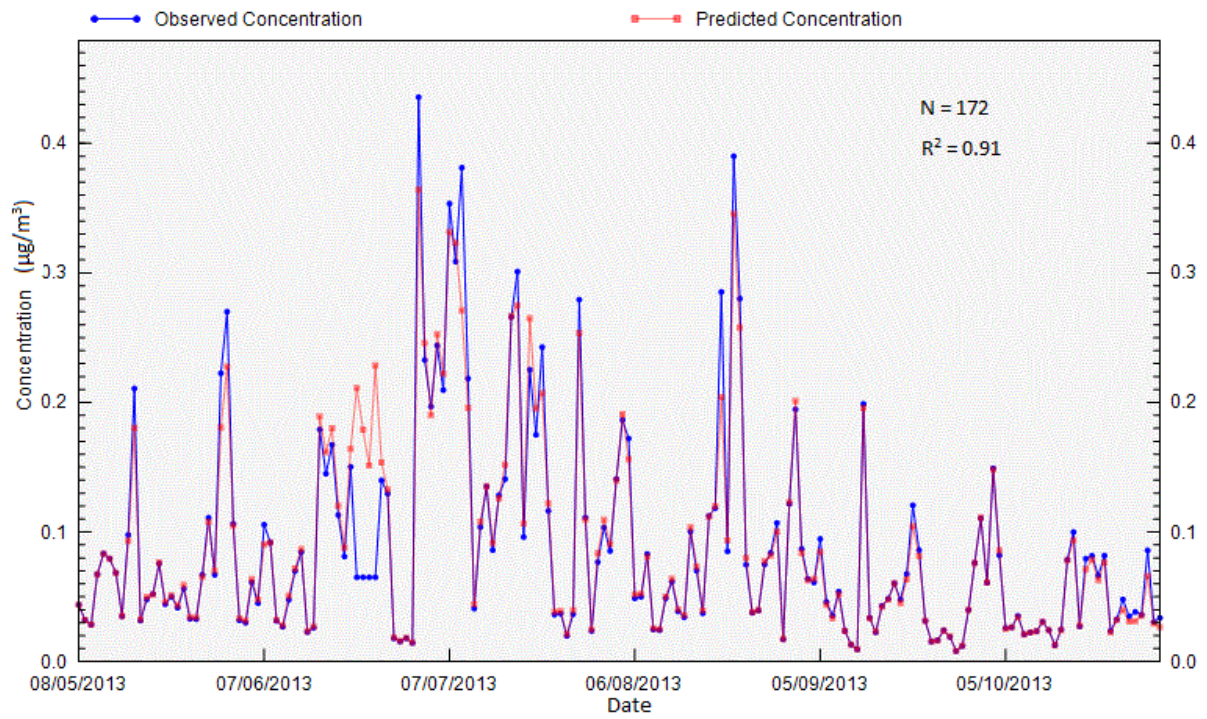
Figure 34 Observed and Model Predicted concentrations of BC
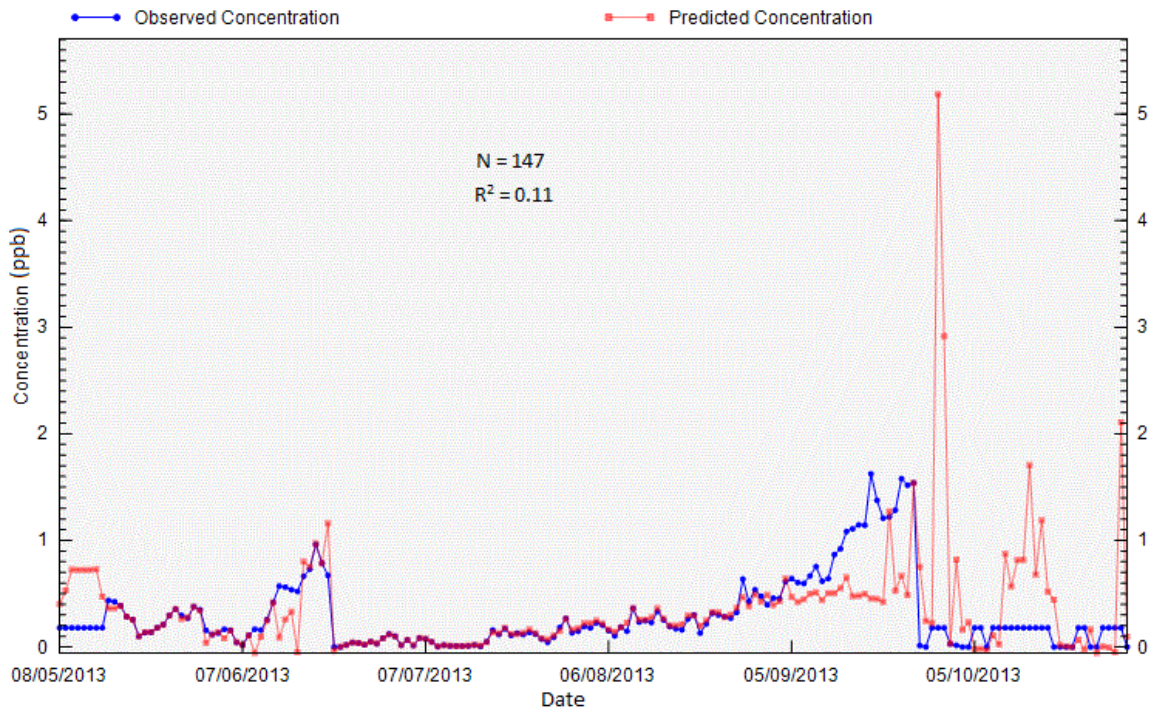
Figure 35 Observed and Model Predicted concentrations of H₂S
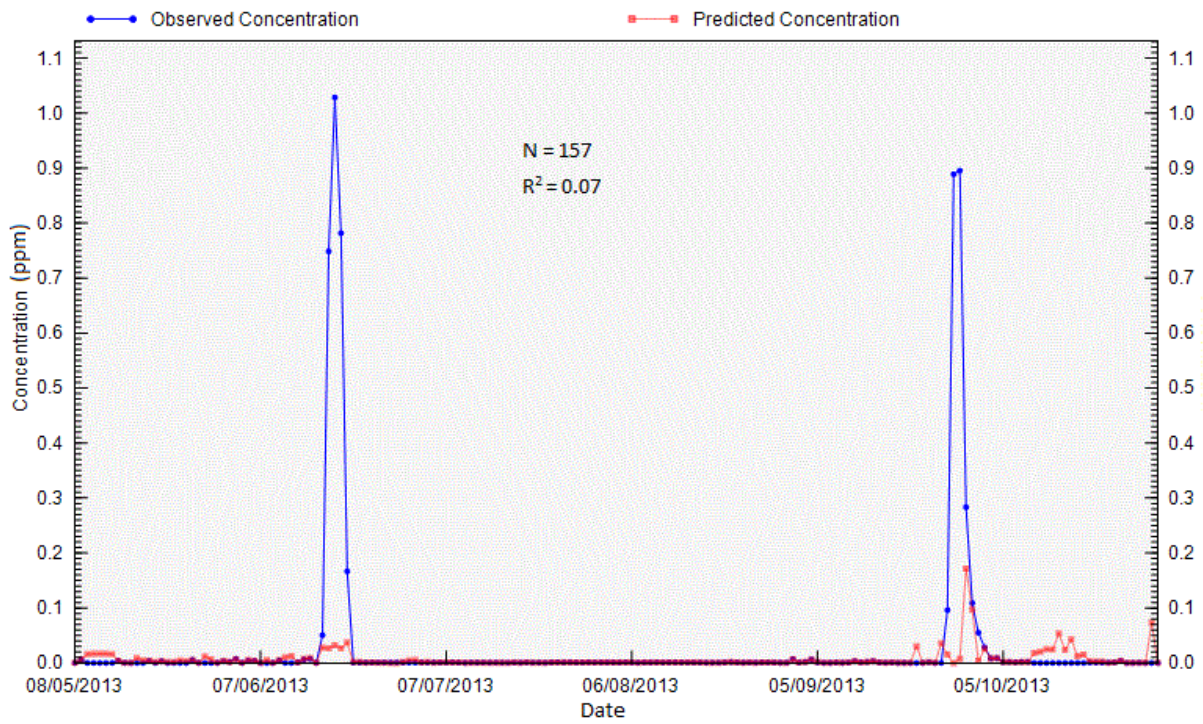
Figure 36 Observed and Model Predicted concentrations of NMHC
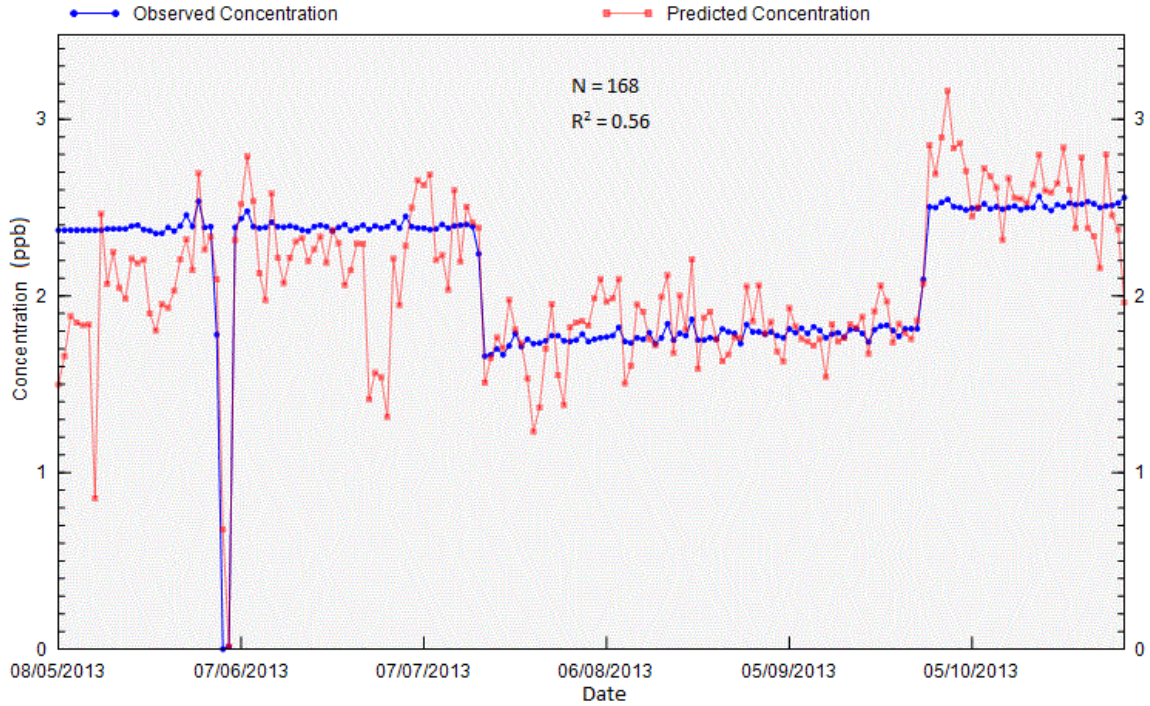
Figure 37 Observed and Model Predicted concentrations of NO
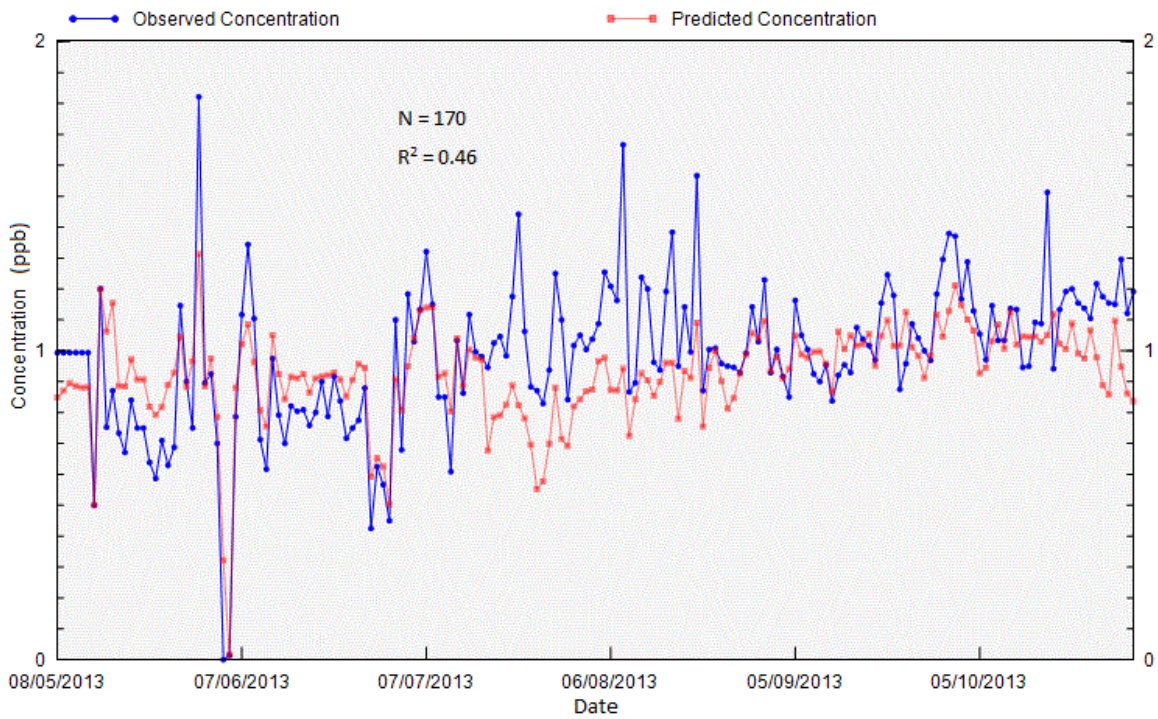
Figure 38 Observed and Model Predicted concentrations of NO₂
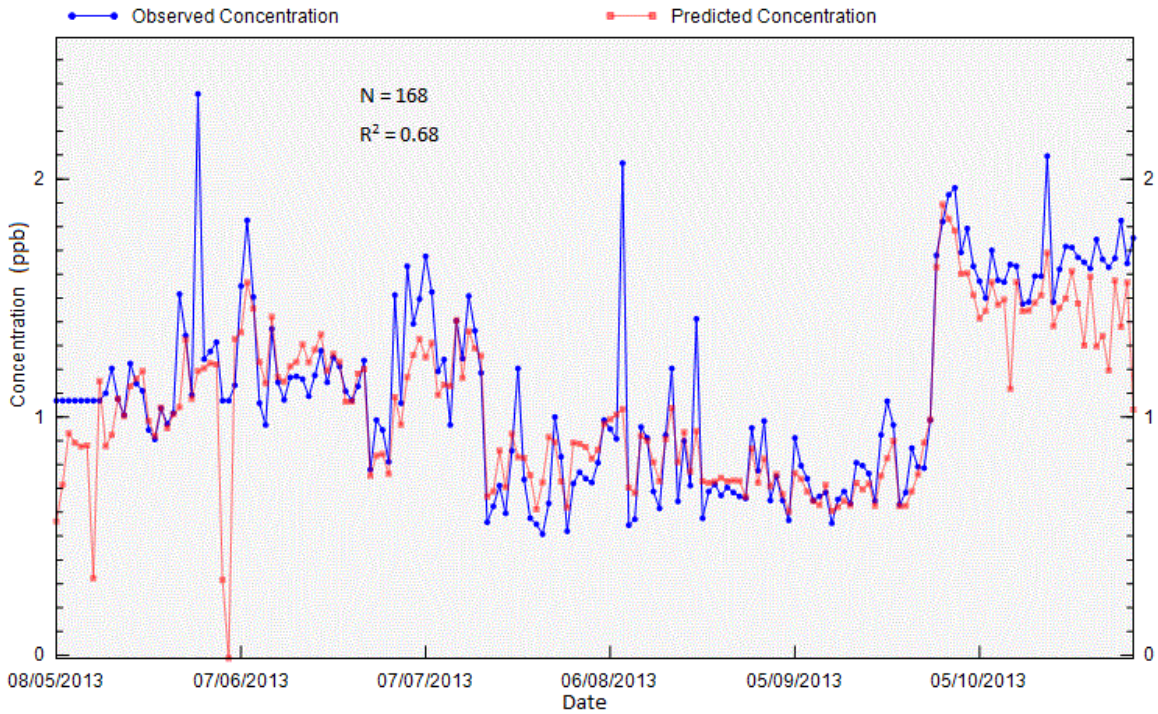
Figure 39 Observed and Model Predicted concentrations of NOₓ
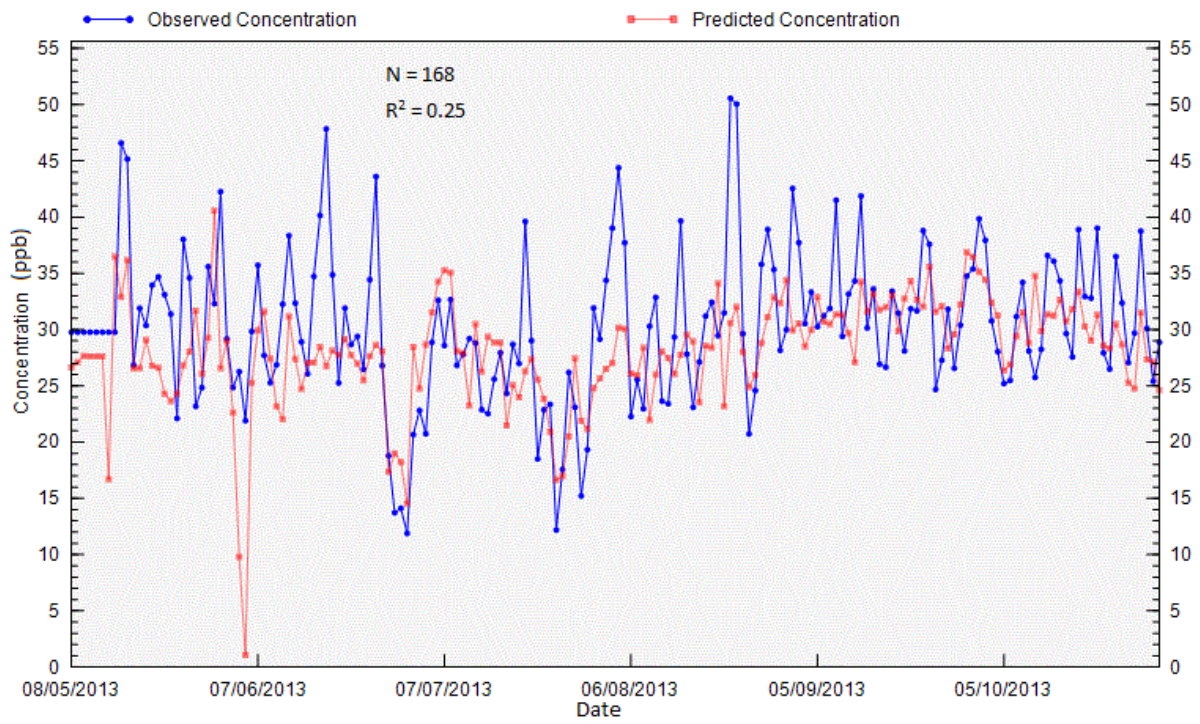
Figure 40 Observed and Model Predicted concentrations of O$_3$
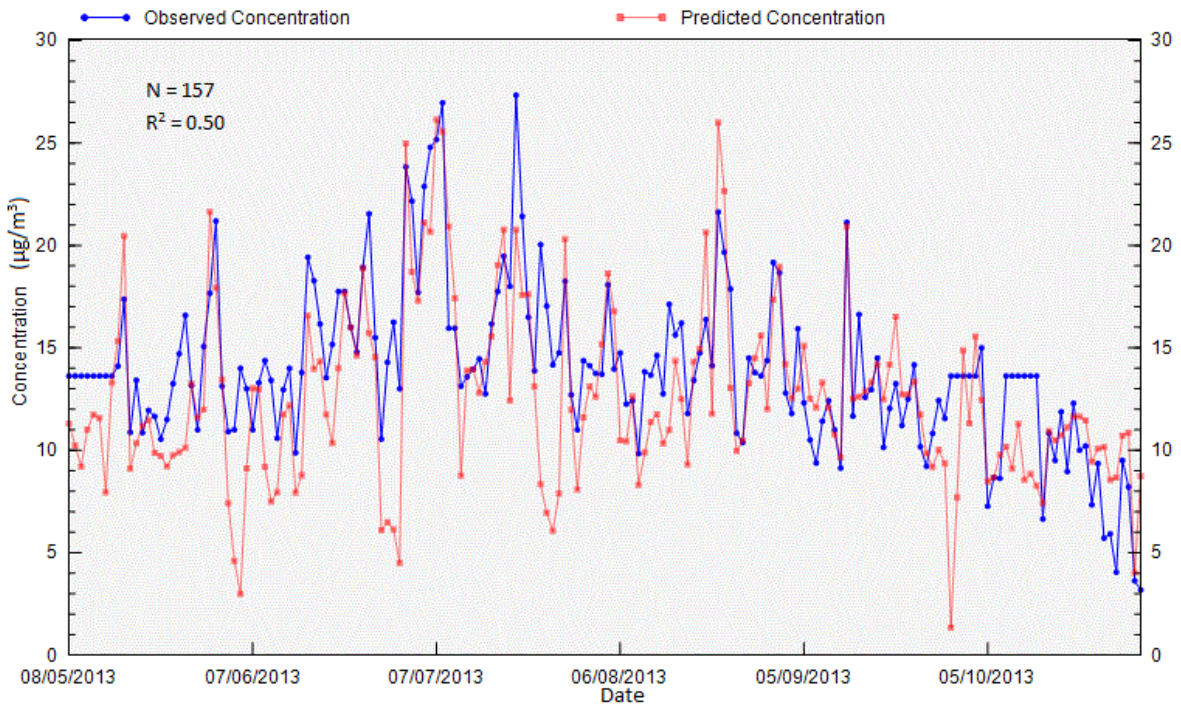
Figure 41 Observed and Model Predicted concentrations of PM$_{2.5}$
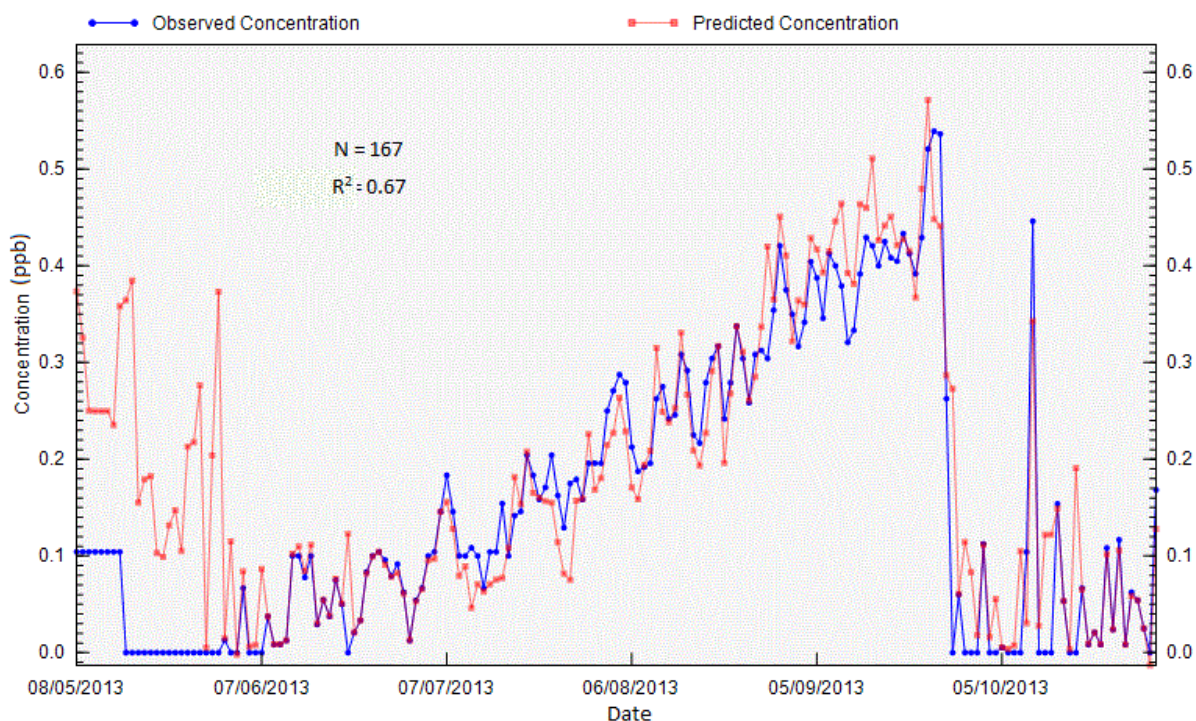
Figure 42 Observed and Model Predicted concentrations of SO₂

When the plots of observed and model predicted concentrations (Figure 34 to Figure 42) are examined, it can be seen that the highest R^2 values exist for BC, SO₂, NOx, NO₂, and NO (>50%) while those for the other species are lower (<50%). The model had the most trouble with species such as NMHC concentrations, which generally were measured at low concentrations but periodically exhibited increased concentration spikes. This reinforces what was found when comparing Q true with Q robust.

The model was initially run for between 3 – 10 factors. When 3 factors were run it was found that the factors representing LRT and on-site combustion were blended together, giving a result with the same chemical characteristics of both factors together. That is to say, a factor with high contributions from PM₂.₅, BC, SO₂, NOx, NO₂, and NO. In reality, and as will be discussed further in the following sections, when split into 2 factors this scenario describes LRT and on-site combustion more satisfactorily. When more than 4 factors were run it was found all factors with the exception of off-gassing were split into smaller and smaller factors with smaller and smaller contributions and virtually the same chemical fingerprint. Consideration of the model outputs, the number of species monitored, and knowledge of the potential sources impacting Sable Island were

70

considered in the decision to optimally run the model for 4 factors (corresponding to 4 major sources).

Factor 1
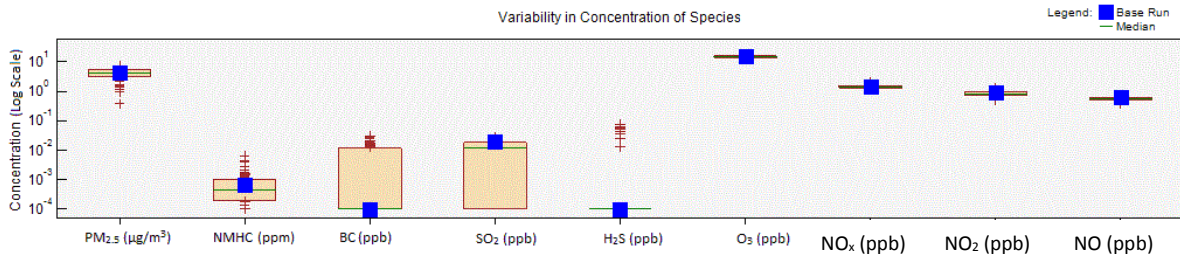
Figure 43 Variability in concentration of species for LRT (Factor 1)
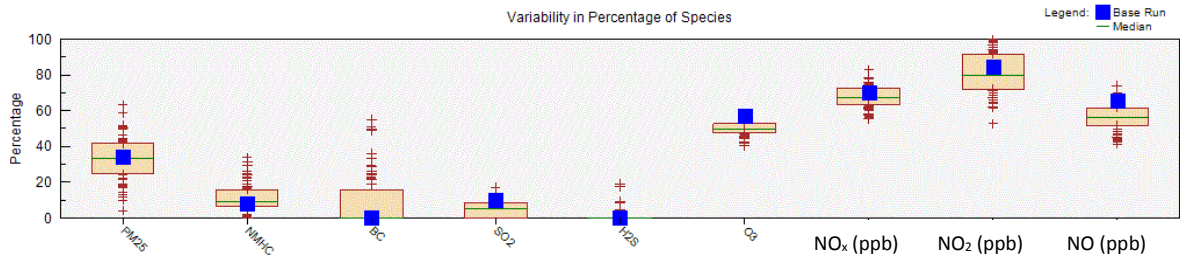
Figure 44 Variability in percentage of species for LRT (Factor 1)
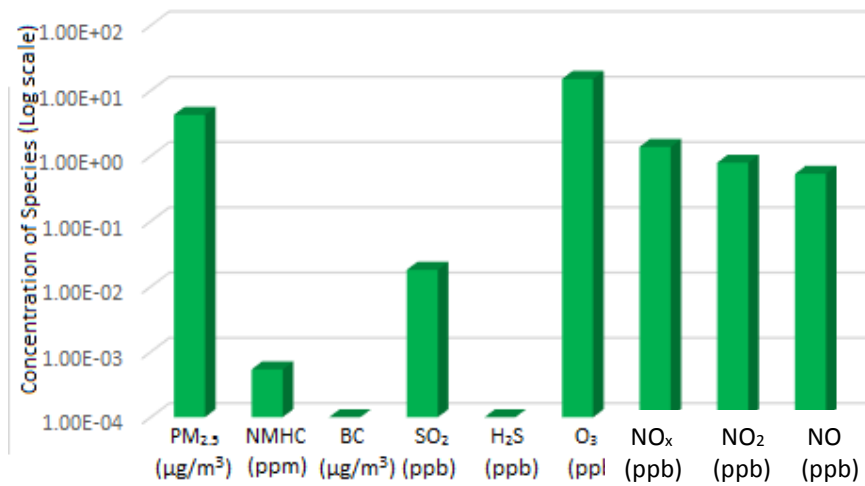
Figure 45 Fpeak Factor Profile for LRT (Factor 1)
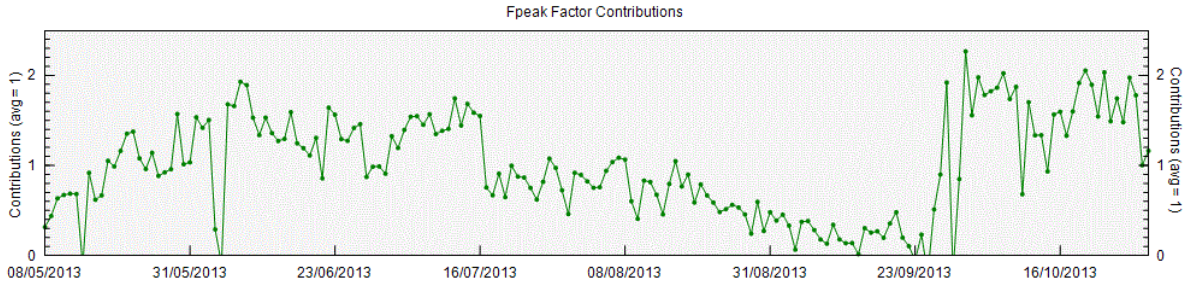
Figure 46 Fpeak Factor Contributions for LRT (Factor 1)
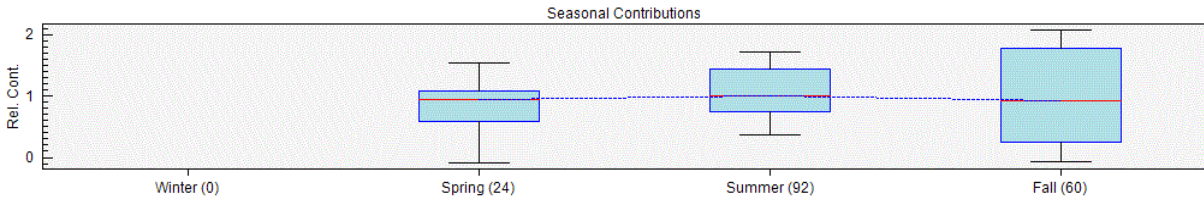
Figure 47 Seasonal contributions for LRT (Factor 1)

Factor 2
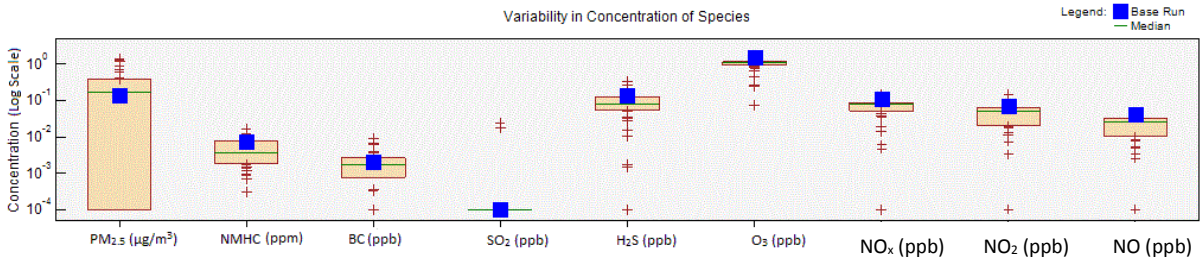
Figure 48 Variability in concentration of species for Off-gassing (Factor 2)
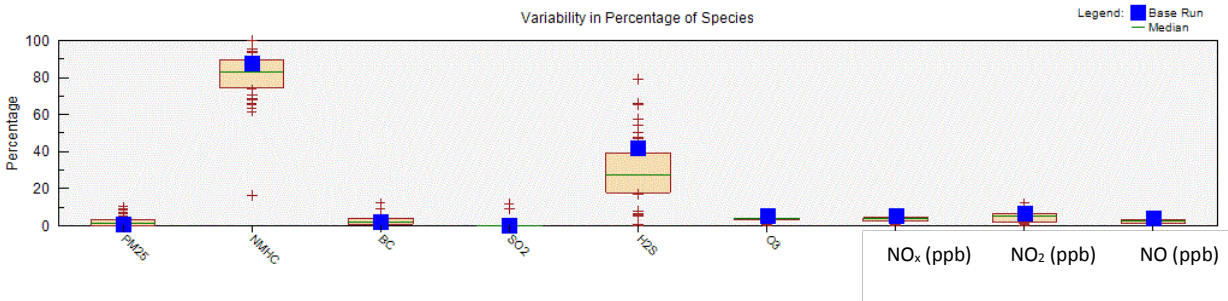
Figure 49 Variability in percentage of species for Off-gassing (Factor 2)
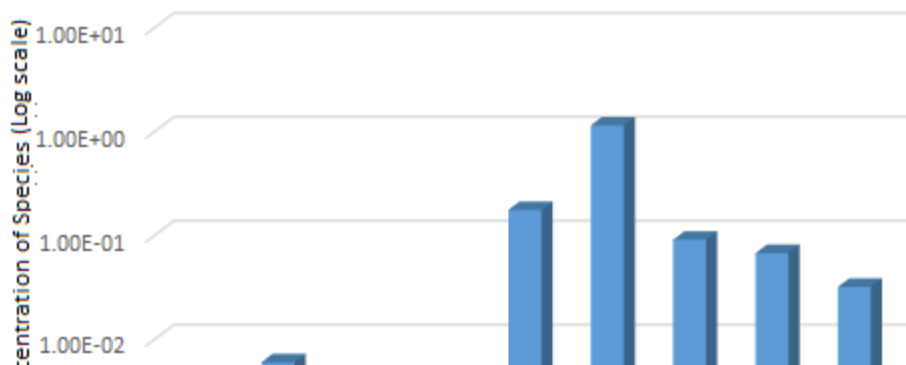
Figure 50 Fpeak Factor Profile for Off-gassing (Factor 2)
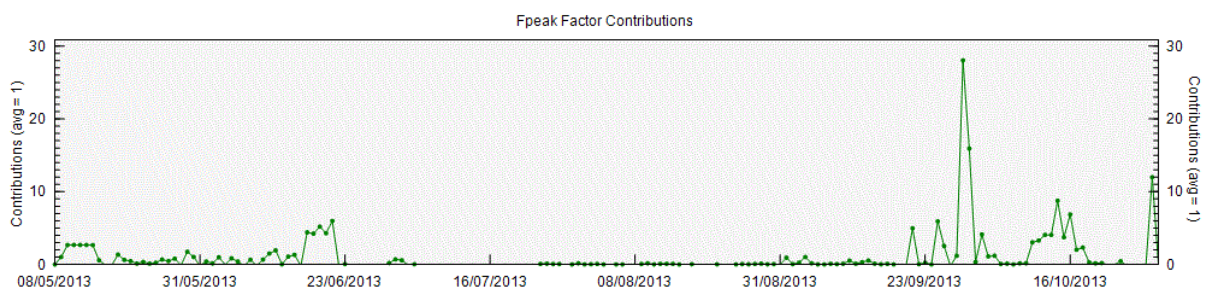
Figure 51 Fpeak Factor Contributions for Off-gassing (Factor 2)
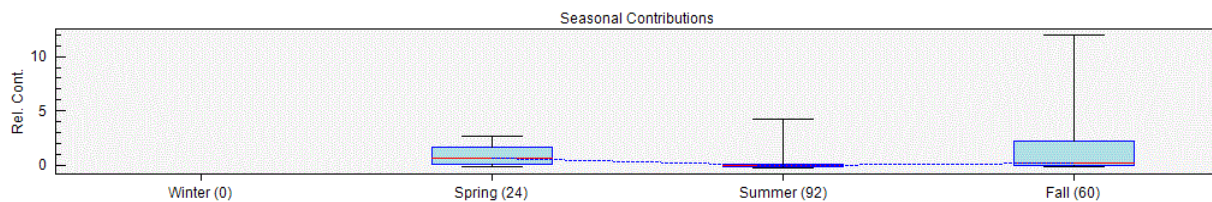
Figure 52 Seasonal contributions for Off-gassing (Factor 2)

Factor 3
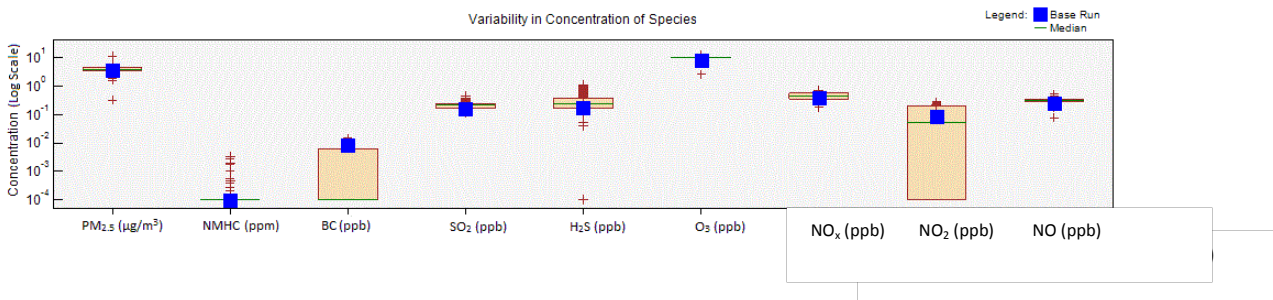
Figure 53 Variability in concentration of species for Flaring (Factor 3)
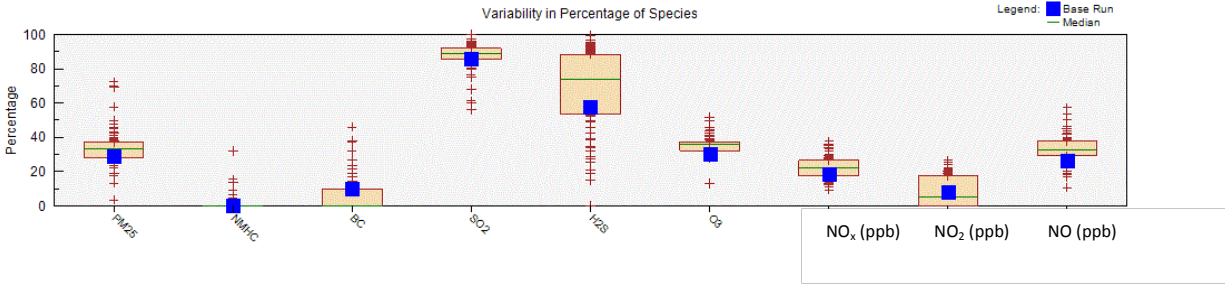
Figure 54 Variability in percentage of species for Flaring (Factor 3)
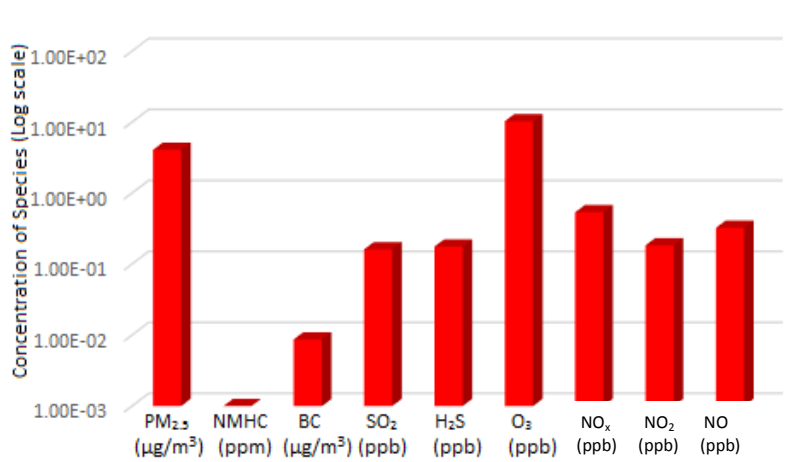
Figure 55 Fpeak Factor Profile for Flaring (Factor 3)
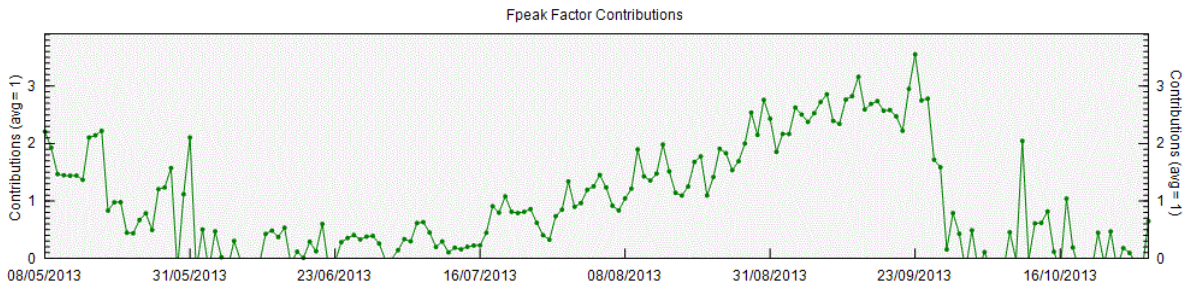
Figure 56 Fpeak Factor Contributions for Flaring (Factor 3)
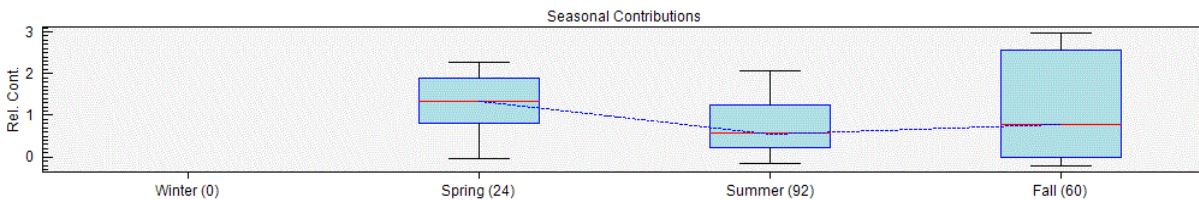
Figure 57 Seasonal contributions for Flaring (Factor 3)
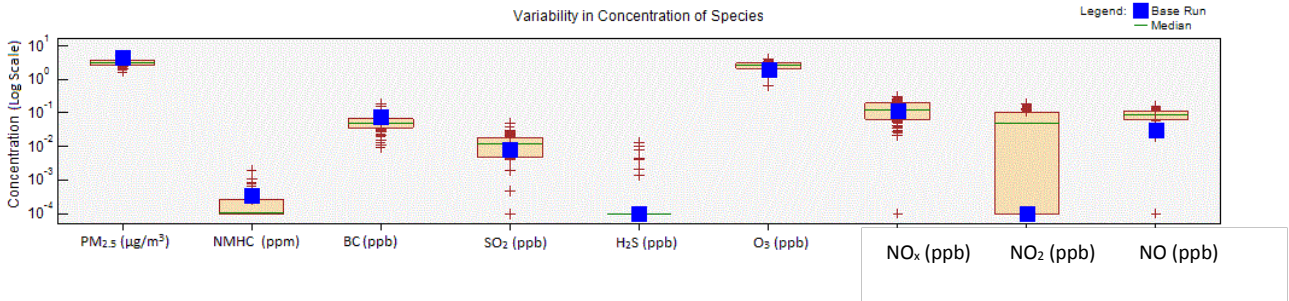
58 Variability in concentration of species for On-site combustion (Factor 4)
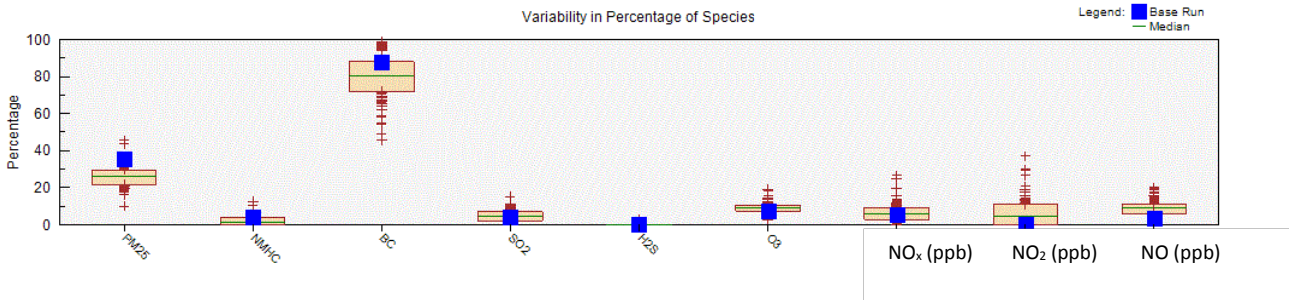
Figure 59 Variability in percentage of species for On-site Combustion (Factor 4)
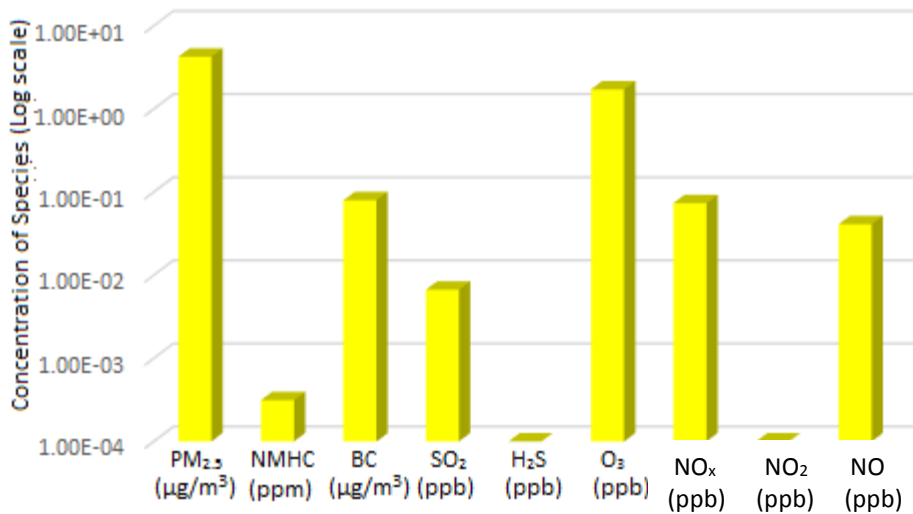
Figure 60 Fpeak Factor Profile for On-site Combustion (Factor 4)
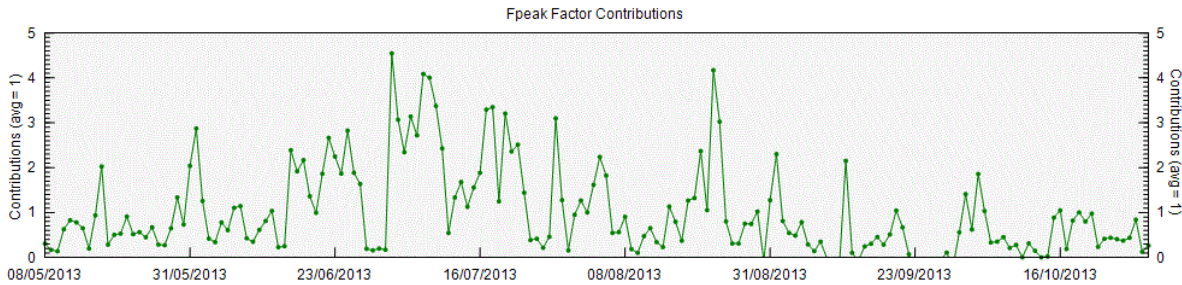
Figure 61 Fpeak Factor Contributions for On-site Combustion (Factor 4)
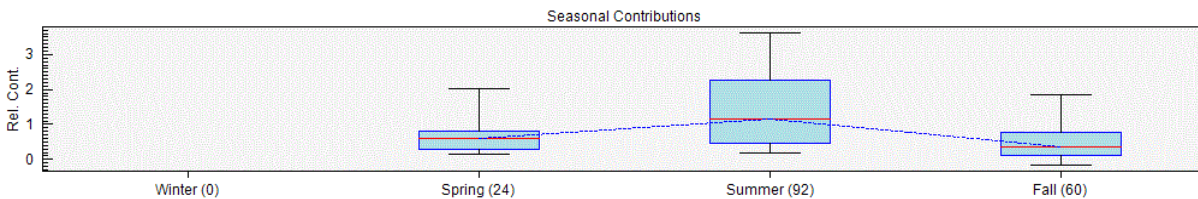
Figure 62 Seasonal contributions for On-site Combustion (Factor 4).

Figure 43 to Figure 47 shows the profile for Factor 1. Factor 1 was determined to be contributions from LRT. Factor 1 had high contributions from $PM_{2.5}$, which is typical of LRT (Ward et al., 2006). The high contribution from O_3 indicated a more aged aerosol where ozone formation reactions have had time to take place, and the SO_2 contribution is low (SO_2 being indicative of a local source). Contributions of NO, NO_x, and NO_2 indicate combustion sources which would fit with LRT transport sources originating from the mainland and consisting of industrial emissions and domestic heating, largely from fossil fuel combustion (Gibson et al., 2009a, Gibson et al., 2013b).

From

Figure 48 to Figure 52, Factor 2 was determined to be off-gassing from offshore O&G activities by the presence of O_3 (a marker for LRT) and the low contributions from $PM_{2.5}$ and BC. The low contributions from $PM_{2.5}$ and BC are indicative of gaseous emissions with relatively large contributions from NMHCs, NO_x, and H_2S (when compared to other sources) indicating offshore oil and gas activity fugitive emissions as the likely source (Beusse et al., 2013). The strong

76

correlation of O_3 with this factor was likely due to the impact of VOCs on its formation (Jacob, D.J., 1999).

It should be noted that emissions of VOCs from phytoplankton blooms also contribute to a percentage of this factor. Analysis of pollution events showed that during certain periods of time, phytoplankton blooms can contribute significantly to NMHC concentrations. Without a GC-MS to perform VOC speciation at the time, it was difficult to apportion the exact VOC contribution from offshore O&G and those VOCs associated with phytoplankton bloom emissions. Although phytoplankton blooms can be a major contributor of VOCs (Colomb et al., 2008) the high contributions from H_2S and NO_x indicate that Factor 2 is still representative of off-gassing from offshore O&G activities (Beusse et al., 2013). A Spearman rank order correlation was run in SigmaPlot and found that NMHC and H_2S concentrations were significantly correlated (correlation coefficient = 0.107, P = 0.000000045), supporting that Factor 2 is representative of off-gassing. From the figures it is shown that contributions from Factor 2 can be seen to increase after July 22nd 2013, which would fit well with off-gassing emissions associated with bringing new oil and gas activity online. However, the study was run mainly over the summer months, therefore likely missing the spring and some of the autumn phytoplankton blooms (Georges et al., 2014; Craig et al., 2011). Therefore, this section can be considered as giving tentative insight into the possible sources of VOCs impacting Sable Island. Section 5 includes air sample analysis results generated by a GC-MS to better apportion the VOC emissions from phytoplankton and VOC emissions from the O&G facility operations.

Figure 53 to Figure 57 shows the profile for Factor 3. Factor 3 was determined to represent Flaring from offshore oil and gas activity. Profile contributions from $PM_{2.5}$, and BC are indicative of combustion while H_2S, SO_2, and NO_x are characteristic of flaring from offshore oil and gas activity (Beusse et al., 2013). H_2S is a strong indicator in this study of offshore oil and gas activity, only contributing to the factors associated with it. NMHC concentrations are minimal, which is likely due to the fact that they would be burned off during flaring. It can be seen from Figure 56 that factor contributions for Factor 3 increase drastically after July 22nd correlating with increased

flaring from new offshore O&G activity. All of these observations together support that Factor 3 represents flaring from offshore O&G activity.

58 to Figure 62 shows the profile for Factor 4. Factor 4 was determined to be on-site combustion. On-site combustion would include local emissions such as transportation emissions to and from both the island and offshore facilities by aircraft and ships, emissions from passing ships, and most importantly, localized emissions on the island itself related to electricity generation (diesel generator) and waste incineration. The latter would likely contribute the largest portion to factor 4. High contributions from $PM_{2.5}$ and BC indicate incomplete combustion from sources such as the diesel generator used for power generation or localized ship emissions (Gibson et al., 2013). Contributions from SO_2, NO, and NO_2 also indicate the diesel generator and transportation sources (Harrison et al., 1997). Figure 61 shows that the Fpeak factor contributions for on-site combustion decrease during the warmer summer months when less electricity is needed for heating purposes. All of this information provides support for factor 4 being representative of on-site combustion.

3.2.2 Examination of Pollution Events

Pollution events for NMHCs and $PM_{2.5}$ were examined using HYSPLIT back trajectories. Instances where NMHC concentrations exceeded 0.1 ppm and where $PM_{2.5}$ concentrations exceeded 30 $\mu g/m^3$ were considered to be pollution events. For NMHCs the direction of the air mass back trajectory source was examined in order to correlate emissions with the production platforms. Additionally, 8-day averages of chlorophyll concentration were examined to ascertain if they could be contributing to NMHC pollution events. These were obtained from the National Aeronautics and Space Administration (NASA) Giovanni website (http://gdata1.sci.gsfc.nasa.gov/daac- bin/G3/gui.cgi?instance_id=ocean_8day). Generated using MODIS Aqua satellite imagery, the 8-day composites of chlorophyll concentrations helped to compensate for cloudy periods that cause patchy coverage and can be found in Figure 63 - Figure 67. For $PM_{2.5}$ pollution events the area of the North American continent from which the air parcels originated was examined to determine if LRT was the cause. Maps of Canadian fire hotspots

obtained from Natural Resources Canada were examined to determine if forest fires may have contributed to these PM$_{2.5}$ pollution events (http://cwfis.cfs.nrcan.gc.ca/maps/fm3?type=fwih&year=2013&mo nth=10&day=31). Instances of fires on the Eastern Seaboard of the US were also examined. They were obtained from the United States Department of Agriculture (USDA) Active Fire Mapping Program (http://firemapper.sc.egov.usda.gov/index.php).

From the time series for NMHCs pollution events were identified as having occurred on June 18th – 20th, September 1st, 4th, 5th, 11th, 13th, and 14th, 27th – 30th, and October 24th 2013. For the pollution events occurring on June 18th – 20th, the air parcels originated to the SW as well as to the N from Nova Scotia and the mainland on June 20th. Offshore O&G activities take place to the SW of Sable Island as can be seen in Figure 2. Figure 63 shows an 8-day composite of chlorophyll concentrations for June 18th and it can be seen that concentrations around Sable Island are in the 0.7 – 1 mg/m^3 range with concentrations around Nova Scotia and the Eastern Seaboard of the US as high as 10-30 mg/m^3 in small isolated pockets.
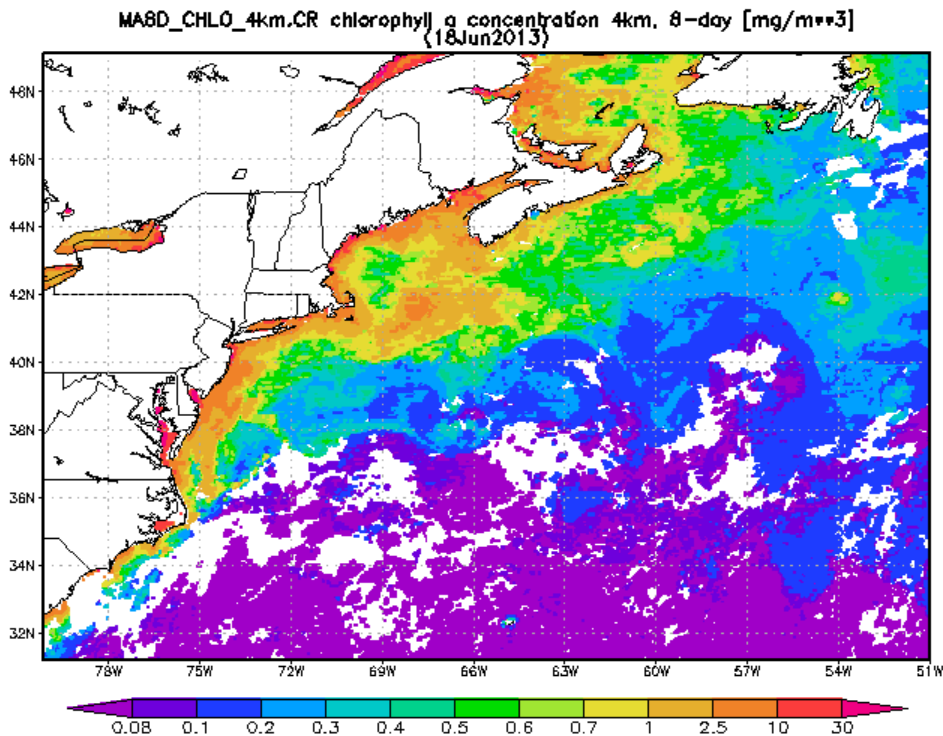
Figure 63 8-day composite of Chlorophyll concentrations for June 18th 2013 obtained from the NASA Giovanni website

For the pollution events on September 1st, 4th, 5th, and 11th the air parcels originated to the SW. On the 11th the air parcel impacting Sable also passed over Nova Scotia. For the air pollution event on September 13th-14th the air parcels originated from the S. Offshore O&G activities take place to the S and SW as shown in Figure 2. Figure 64 shows chlorophyll concentrations for August 21st – September 14th and it can be observed that concentrations S and SW of Sable Island are in the 0.7 – 1 mg/m^3 range with concentrations in small areas around Nova Scotia and the Eastern Seaboard of the US as high as 10 - 30 mg/m^3.
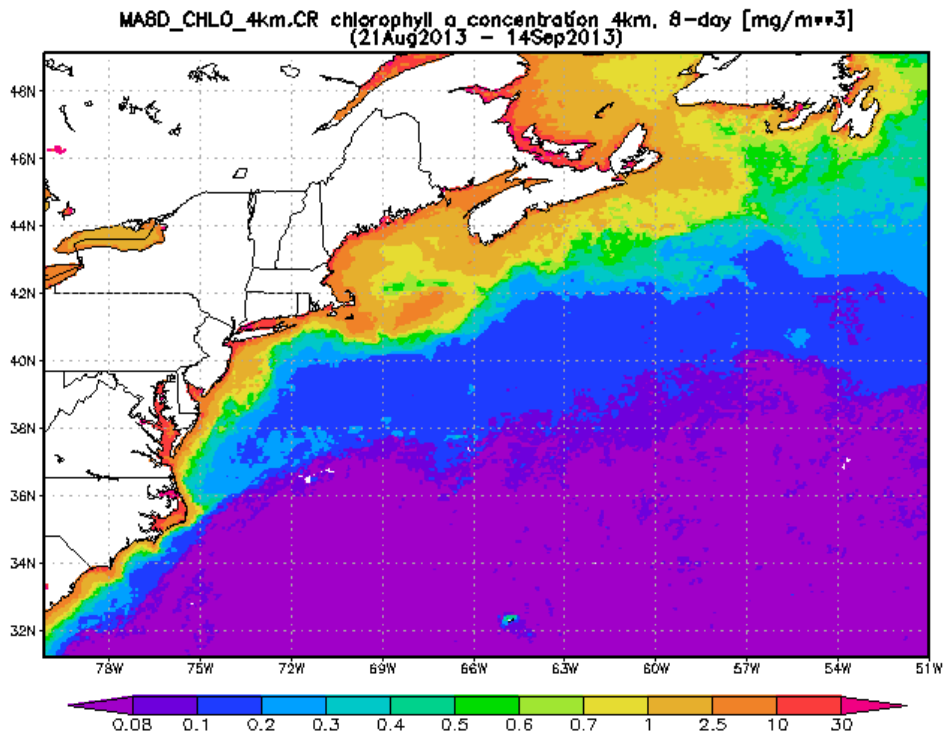
Figure 64 8-day composite of Chlorophyll concentrations for August 21st – September 14th 2013 obtained from the NASA Giovanni website

For the pollutions event from September 27th – 30th the air parcel originated from the N, N, W, and SE with the air parcels having passed over or near the coast of Nova Scotia. Offshore O&G activity is located to the SE of Sable. Figure 65 shows chlorophyll concentrations for September 22nd – September 30th. It can be seen that concentrations around Sable Island are as high as 2.5 – 10 mg/m^3 and near the coast of Nova Scotia as high as 10 - 30 mg/m^3.
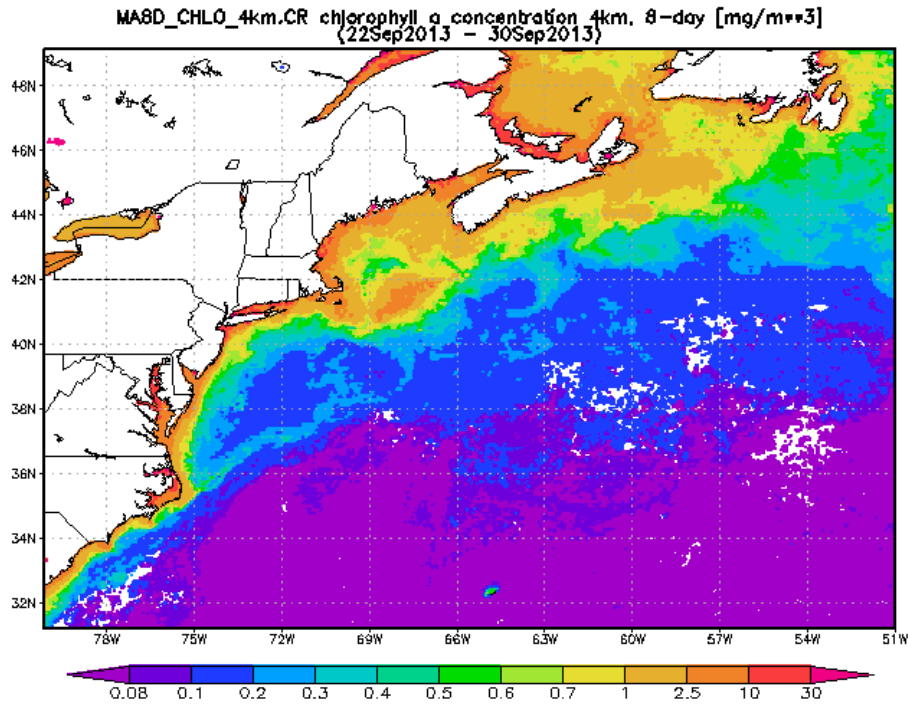
Figure 65 8-day composite of Chlorophyll concentrations for September 22nd – September 30th 2013 obtained from the NASA Giovanni website

On October 24th the wind direction was from the SSW and the air parcel at one point passed over the SW tip of Nova Scotia. Offshore O&G activities are located to the SSW of Sable Island as can be seen in Figure 2. Figure 66 shows chlorophyll concentrations for October 16th – October 24th and it can be seen that elevated concentrations exist around Sable and the throughout the Scotian Shelf with concentrations in many areas reaching the 10 – 30 mg/m^3 range.
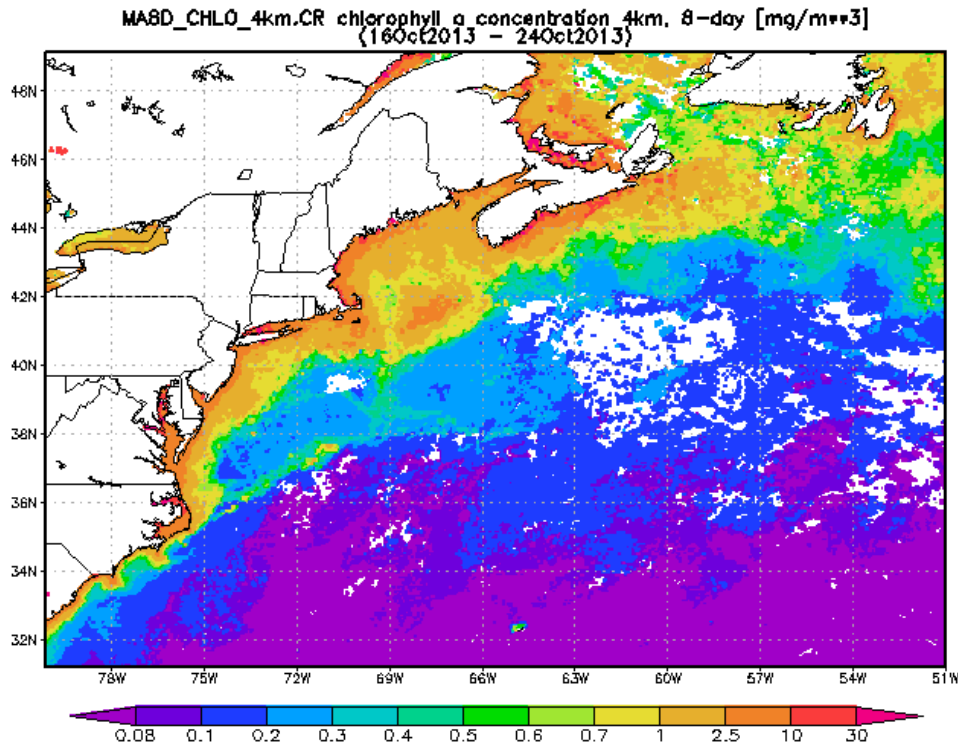
Figure 66 8-day composite of Chlorophyll concentrations for October 16th – October 24th 2013 obtained from the NASA Giovanni website

All of the back trajectory directions correlate with the direction of offshore O&G activities as can be seen from Figure 2 in the literature review. Figure 67 shows 8-day composites of chlorophyll concentrations for July 28th – August 5th. This was done for comparison as this period of time exhibited low concentrations of NMHCs on Sable Island. The concentrations seem to be higher than in June, but similar to those in August and September, however a notable increase into October appears to take place that may correspond to the beginning of an autumnal bloom.
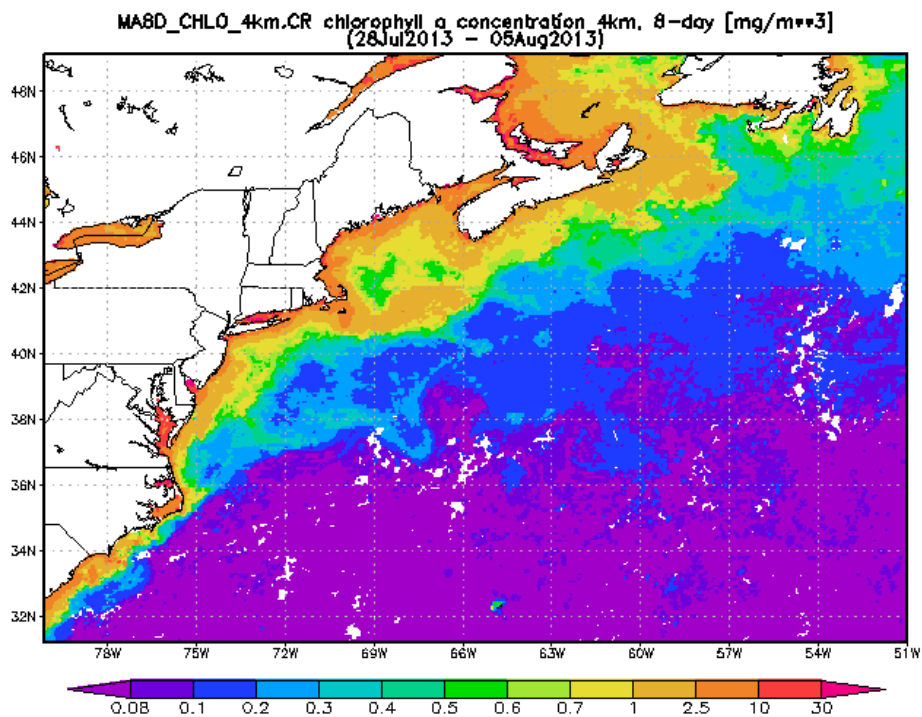
Figure 67 8-day composite of Chlorophyll concentrations for July 28th – August 5th 2013 obtained from the NASA Giovanni website

From this examination, it appears that phytoplankton blooms may have impacted the events in late August and September and likely impacted the events in October. The results of examining HYSPLIT back trajectories when coupled with this enforce the conclusion that off-gassing and flaring from the production platforms is likely the major source of NMHCs on Sable Island with phytoplankton blooms likely contributing. It should be noted that there is a caveat to using standard ocean colour chlorophyll products in coastal regions. The Nova Scotian current influences the ocean waters surrounding Sable Island, and receives waters from the Gulf of St. Lawrence (Hannah et al., 2001), which may contain coloured dissolved organic matter (CDOM) that can confound the algorithms that are used to estimate chlorophyll from ocean colour (Carder et al., 1989). However, broad seasonal patterns were well reproduced in the NASA GIOVANNI satellite estimates of chlorophyll. For the qualitative purpose of this study, the use of the 8-day composites was acceptable

PM$_{2.5}$ pollution events were identified as having occurred on June 24th, 26th, July 2nd, 8th, 18th – 20th, 28th, August 16th, 31st, September 12th, and October 4th 2013. For June 24th and 26th the air parcel originated over the Eastern Seaboard of the US. Figure 68 and Figure 69 show the fire activity detected by the MODIS satellite for June 24th and 26th as obtained from the USDA Active

83

Fire Mapping Program. It can be seen that fire activity was detected in the 6 days prior to the pollution event and likely contributed.
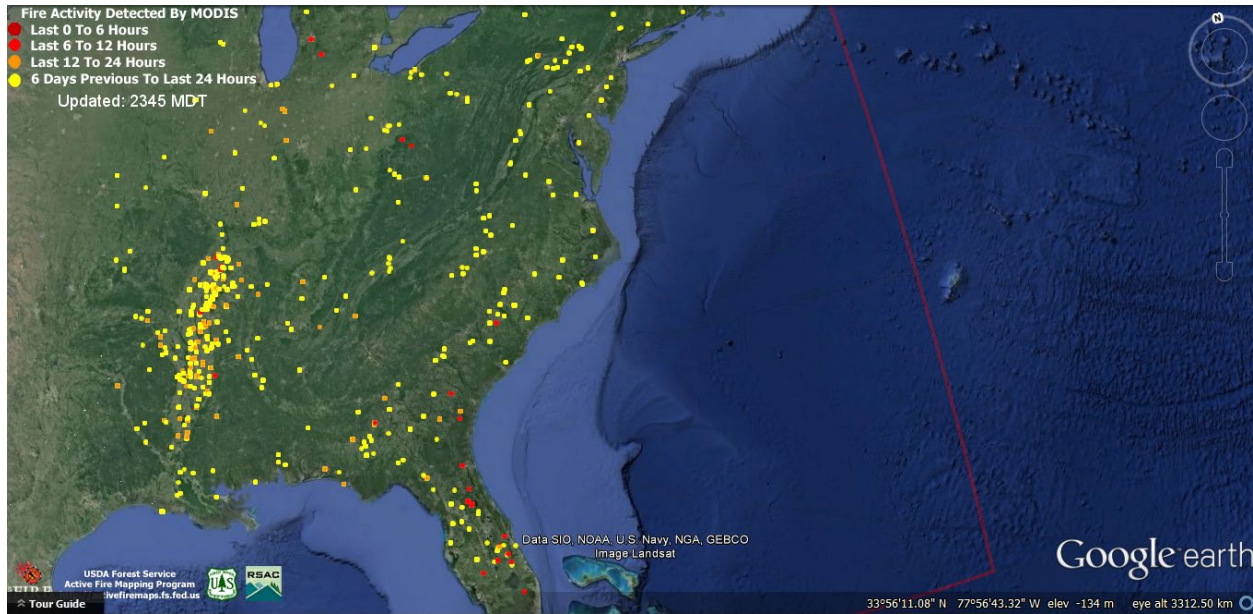
Figure 68 Fire activity detected by the MODIS satellite for June 24th 2013 as obtained from the USDA Active Fire Mapping Program
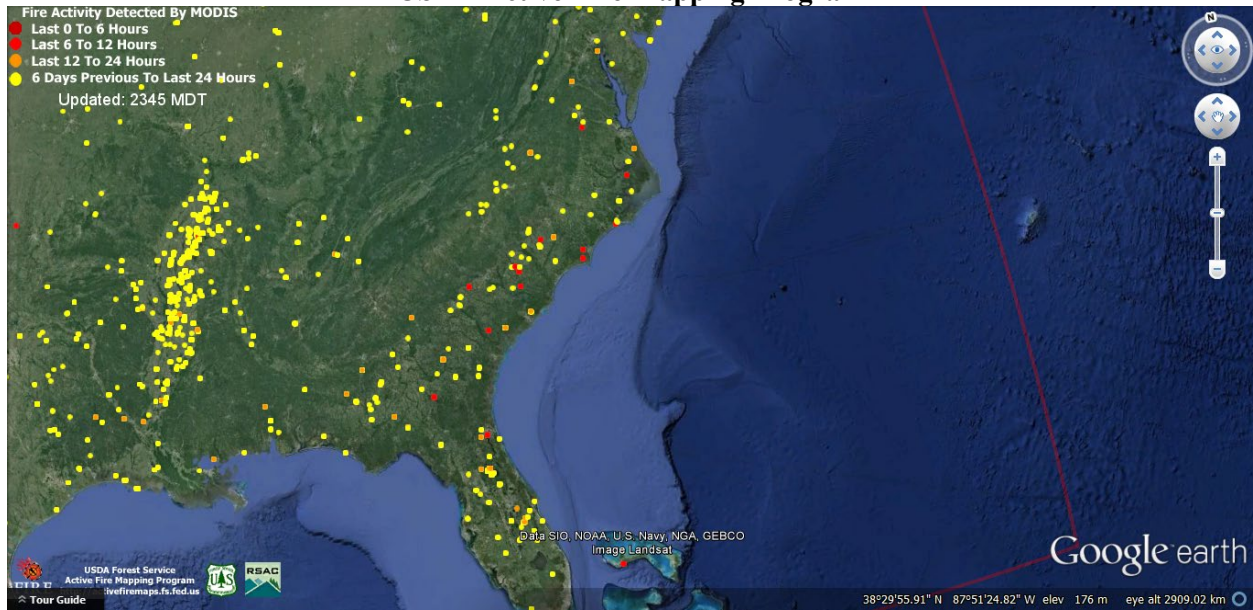
Figure 69 Fire activity detected by the MODIS satellite for June 26th 2013 as obtained from the USDA Active Fire Mapping Program

For July 2nd the air parcel originated over Quebec and Nova Scotia before arriving at Sable Island. Forest fire activity does not appear to have been particularly active preceding this event. For July 8th the parcel passed over the eastern US, Ontario, and Nova Scotia. A map of Canadian fire

hotspots obtained from Natural Resources Canada for July 6th shows a fire index greater than 30 over the area the air parcel impacting Sable Island would have passed over at this time, indicating that forest fires happening in the Quebec and Ontario region likely contributed to this $PM_{2.5}$ pollution event. The map can be seen below in Figure 70.
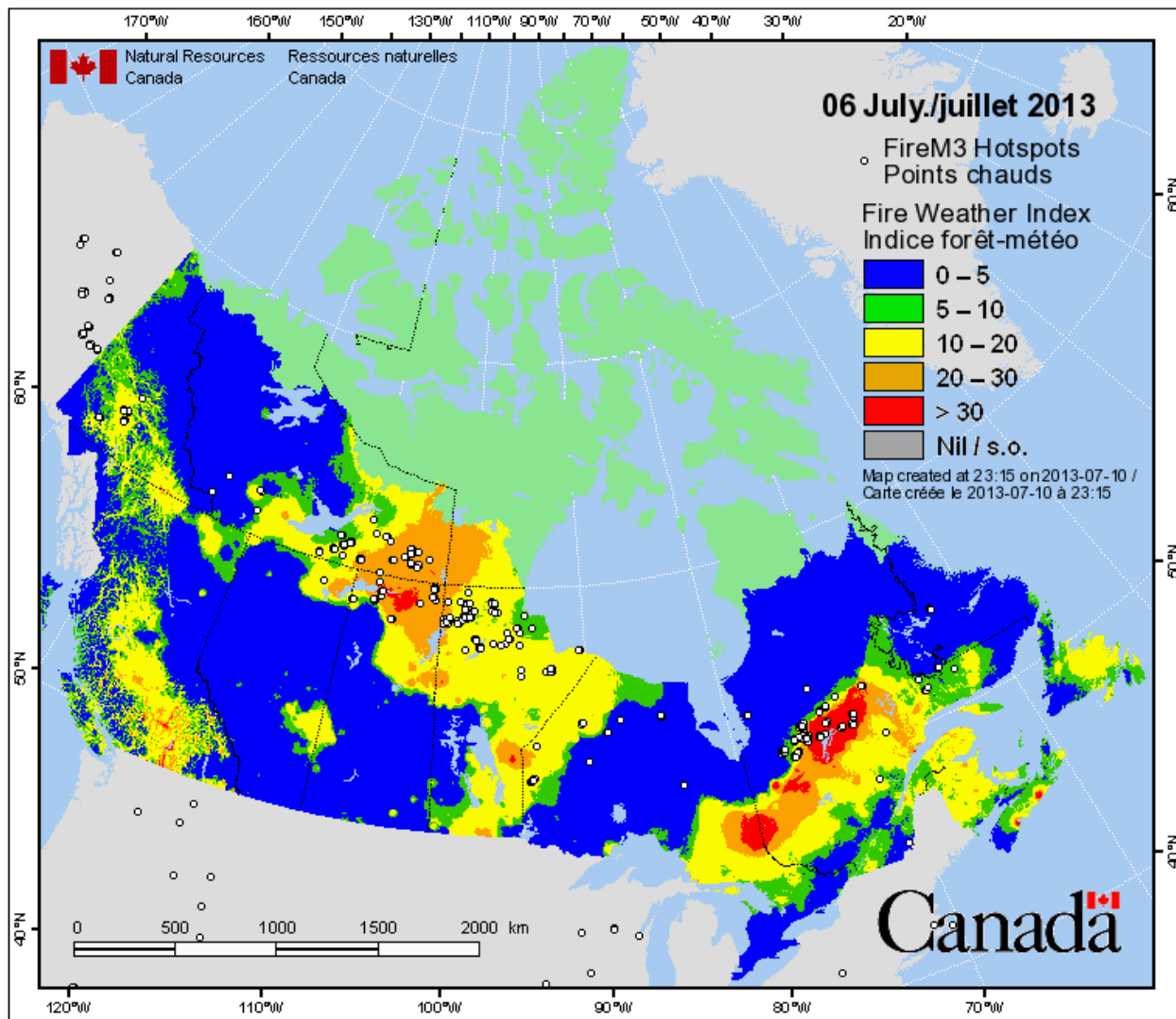
**Figure 70 Fire hotspots for July 6th 2013 obtained from the
Canadian Wildland Fire Information System**

Figure 71 shows fire activity detected by the MODIS satellite for July 8th as obtained from the USDA Active Fire Mapping Program. It can be seen that forest fires were active in the eastern US, with very recent activity near the great lakes.
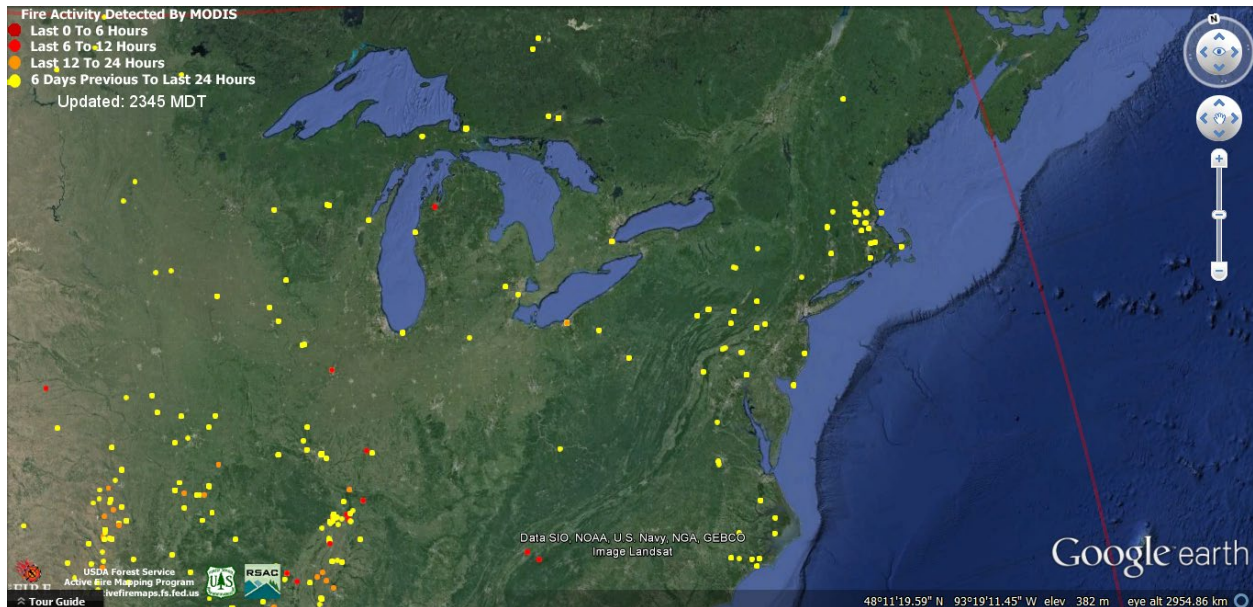
Figure 71 Fire activity detected by the MODIS satellite for July 8th 2013 as obtained from the USDA Active Fire Mapping Program

For the event from July 18th – 20th the parcel originated on the eastern seaboard of the US and passed over Ontario, Quebec, and Nova Scotia. A map of Canadian fire hotspots obtained from Natural Resources Canada for July 16-18th shows a high fire index over the area the air parcel impacting Sable Island would have passed over at this time. Fire index values ranging from 10 to greater than 30 can be seen, indicating that forest fires happening in the Quebec, Ontario, and Nova Scotia region likely contributed to this $PM_{2.5}$ pollution event. The maps can be seen below in Figure 72 - Figure 83. Figure 75 shows fire activity on the eastern seaboard of the US in the 6 days preceding July 20th as well.
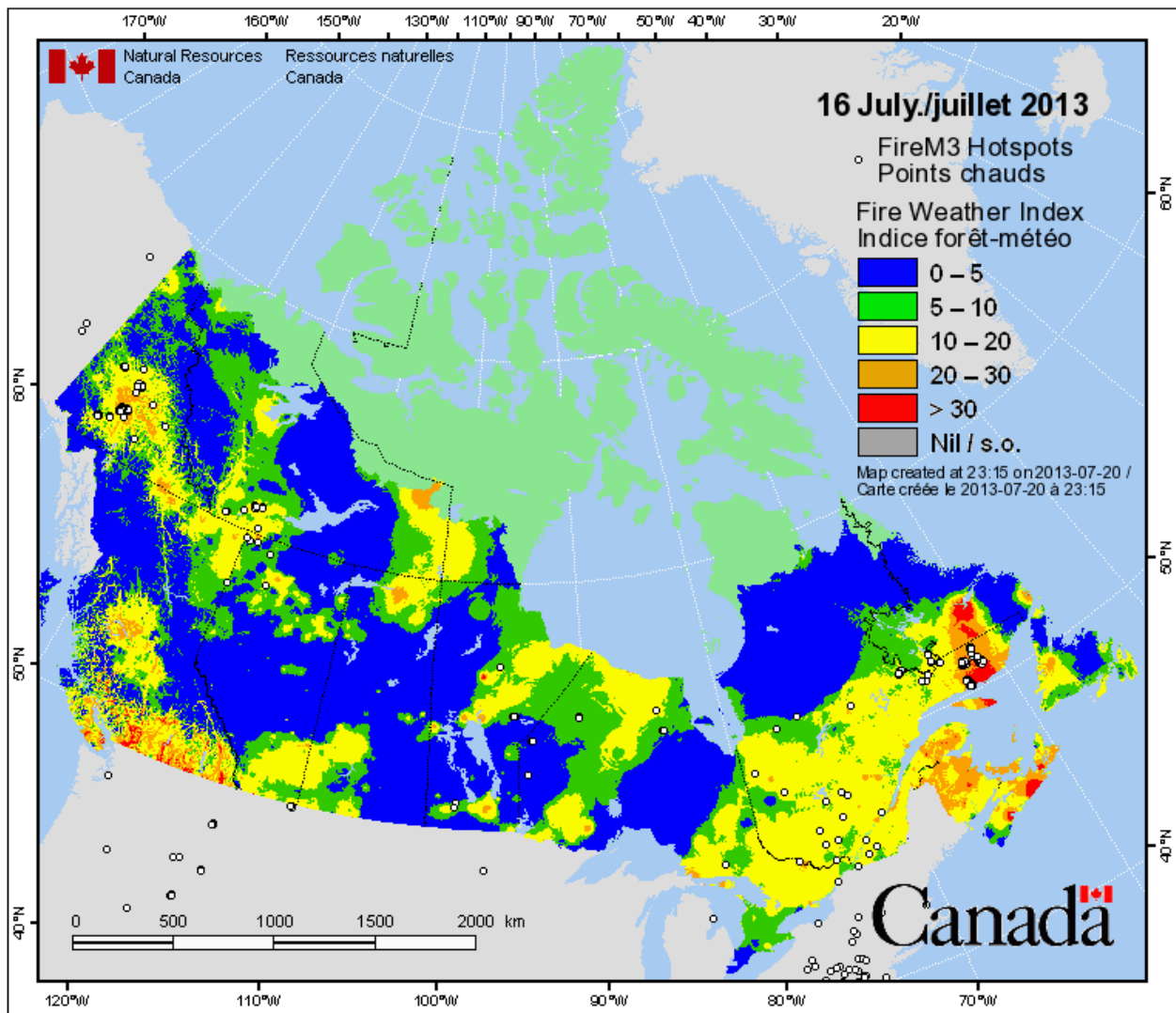
**Figure 72 Fire hotspots for July 16th 2013obtained from the
Canadian Wildland Fire Information System**
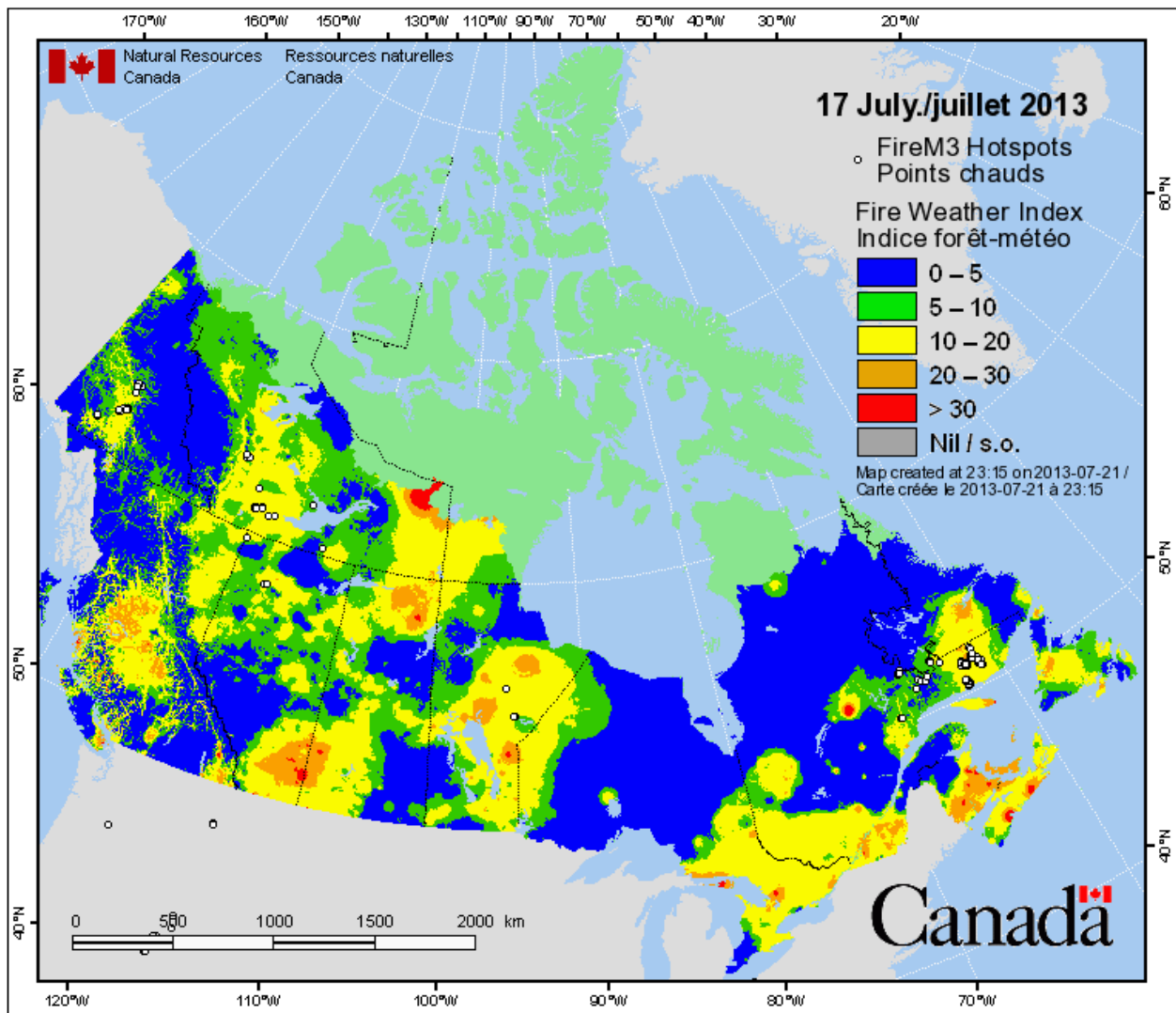
**Figure 73 Fire hotspots for July 17th 2013
obtained from the Canadian Wildland Fire Information System**
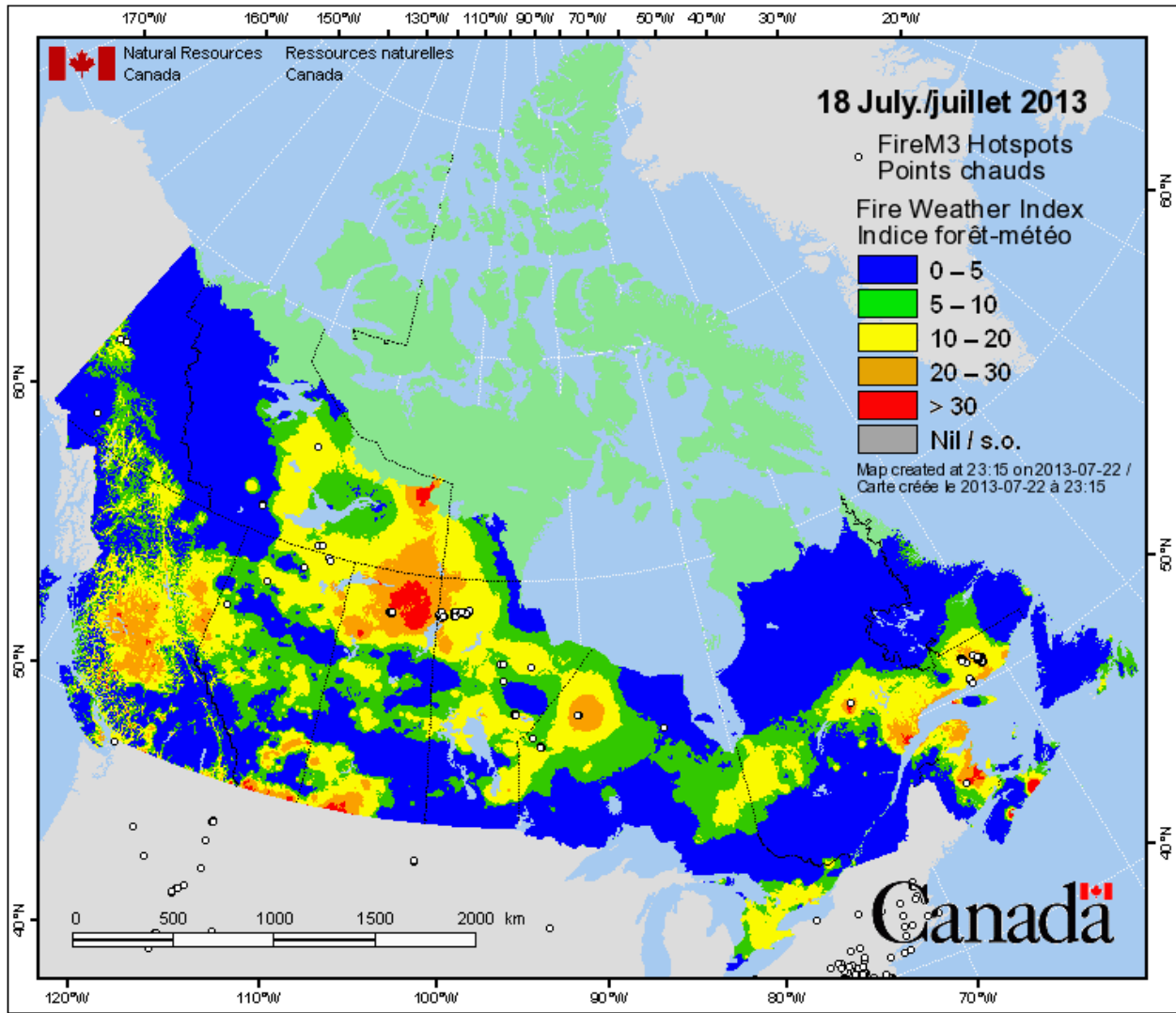
Figure 74 Fire hotspots for July 18th 2013
obtained from the Canadian Wildland Fire Information System
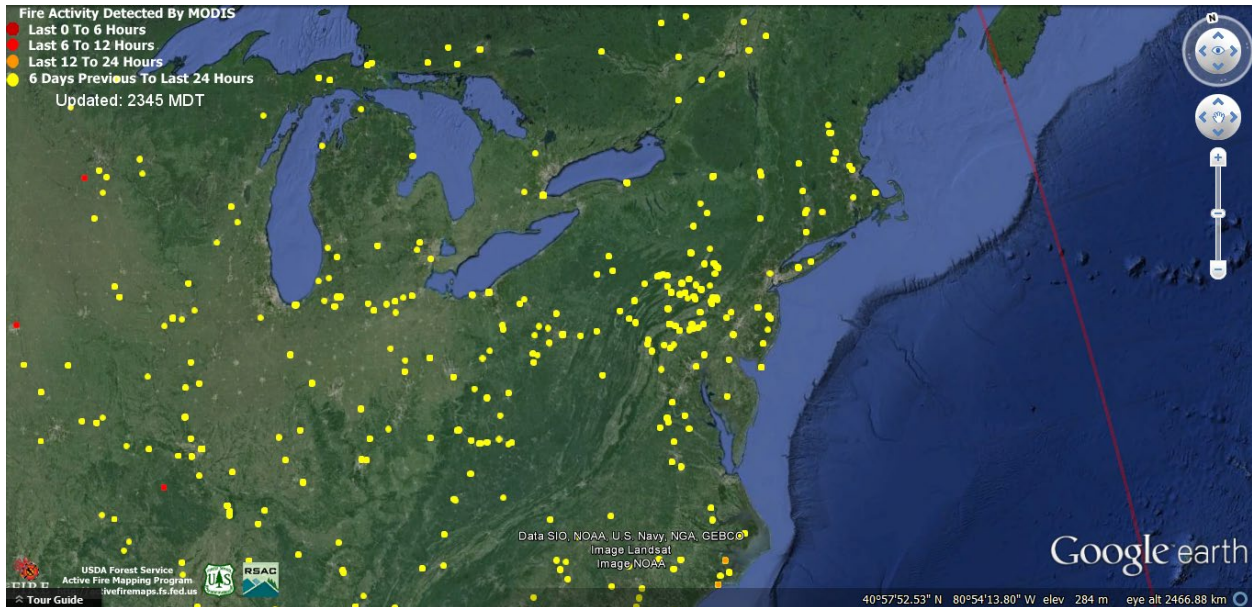
**Figure 75 Fire activity detected by the MODIS satellite for July 20th 2013
as obtained from the USDA Active Fire Mapping Program**

The air parcel on July 28th came from Quebec, New Brunswick, and Nova Scotia. A map of Canadian fire hotspots obtained from Natural Resources Canada for July 27-28th shows a fire index greater than 30 over an area of Nova Scotia that the air parcel impacting Sable Island would have passed over, indicating that forest fires may have contributed to this PM$_{2.5}$ pollution event. The maps can be seen in Figure 76 and Figure 77 below.
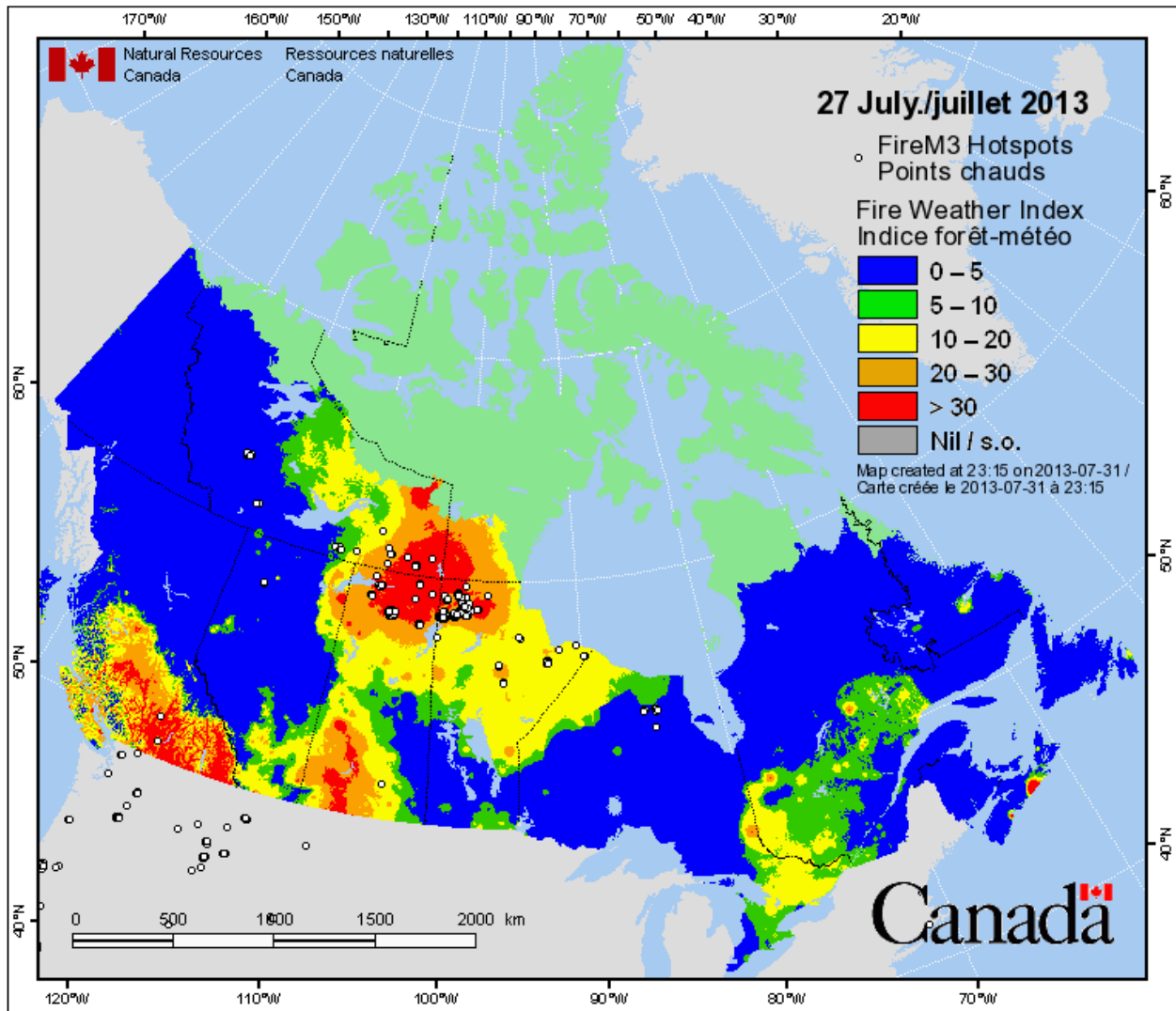
Figure 76 Fire hotspots for July 27th 2013
obtained from the Canadian Wildland Fire Information System
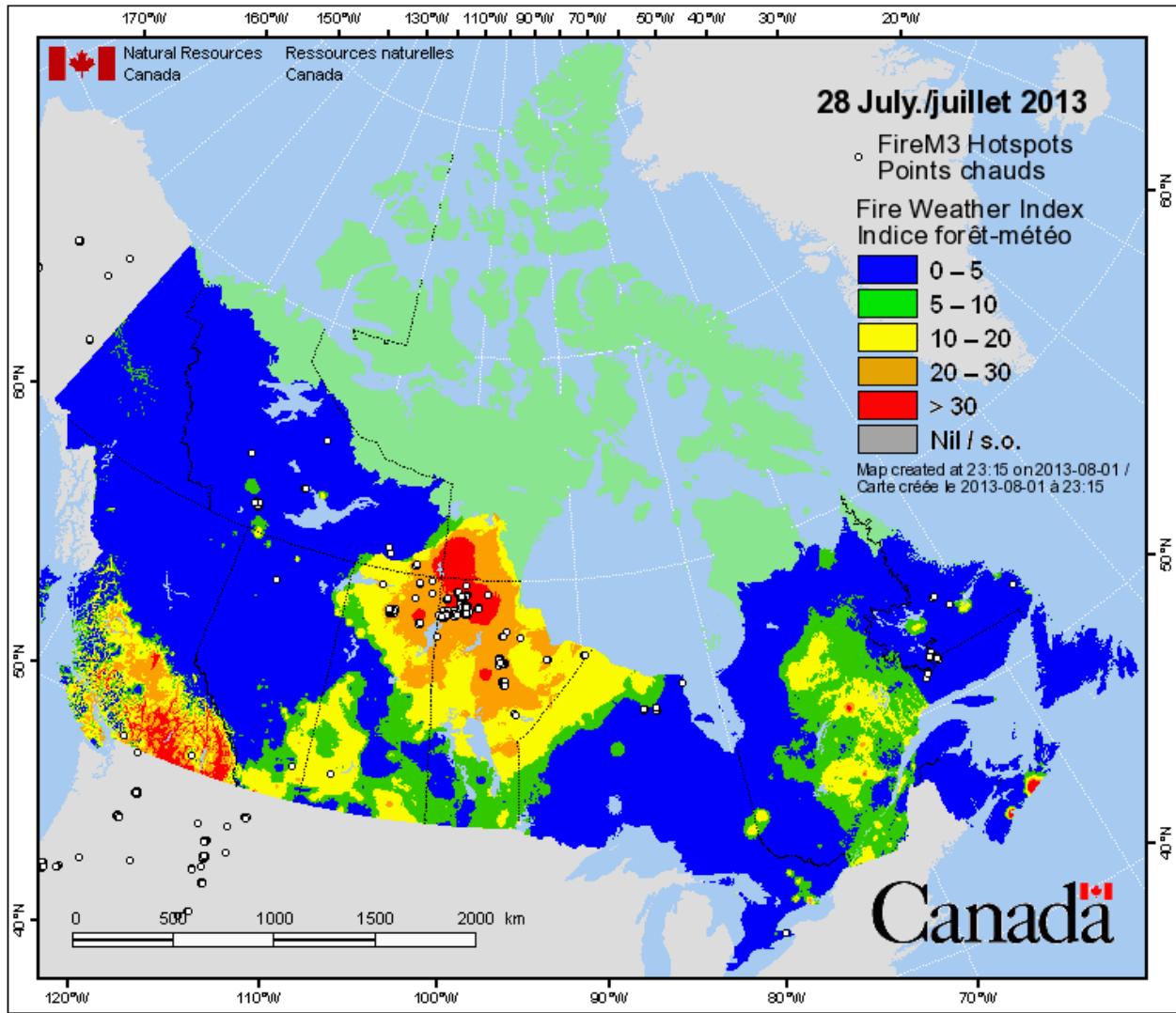
Figure 77 Fire hotspots for July 28th 2013
obtained from the Canadian Wildland Fire Information System

For August 16th the air parcel originated on the eastern seaboard of the US and passed over Ontario and Quebec. Figure 78 shows fire activity on the eastern seaboard of the US area that may have contributed. On August 31st, it originated from the eastern seaboard of the US as well as Quebec. Figure 79 shows fire activity on the eastern seaboard of the US preceding this date that may have contributed. On September 12th, it originated from the eastern seaboard of the US. Figure 80 shows fire activity on the eastern seaboard of the US preceding this date.
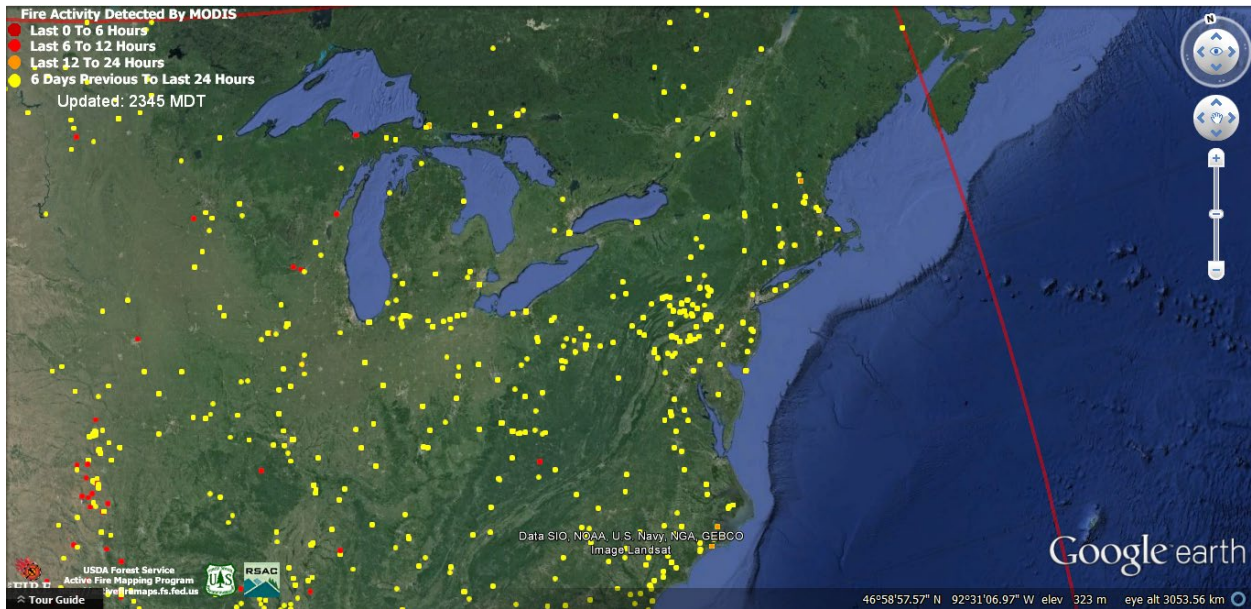
**Figure 78 Fire activity detected by the MODIS satellite for August 16ᵗʰ 2013
as obtained from the USDA Active Fire Mapping Program**
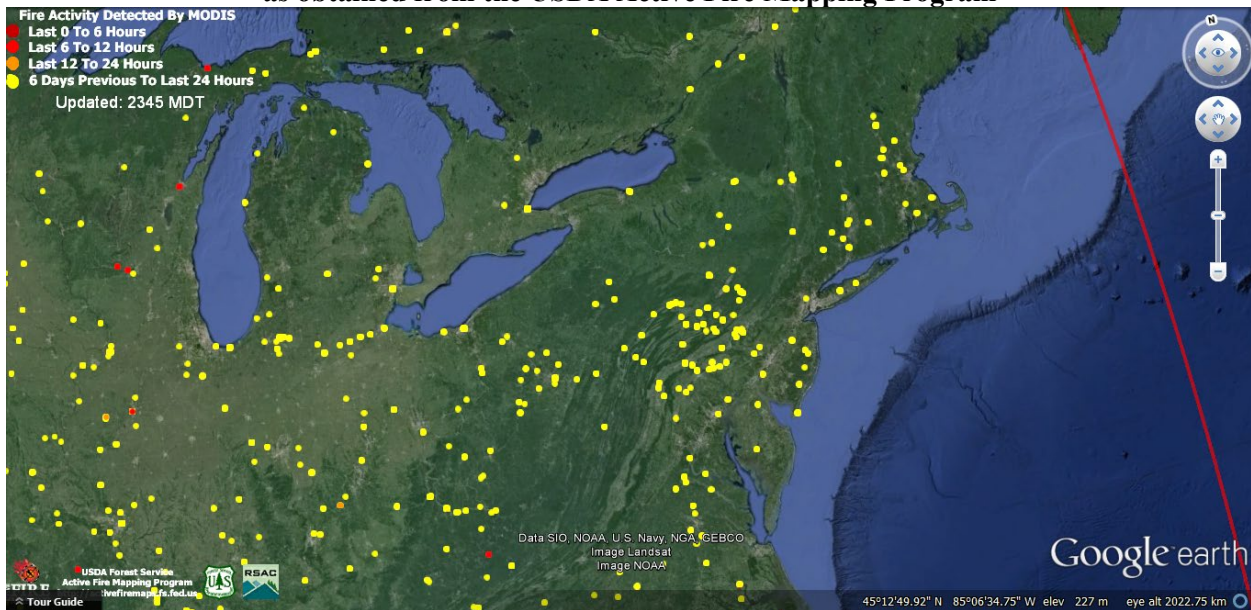
**Figure 79 Fire activity detected by the MODIS satellite for August 31ˢᵗ 2013
as obtained from the USDA Active Fire Mapping Program**
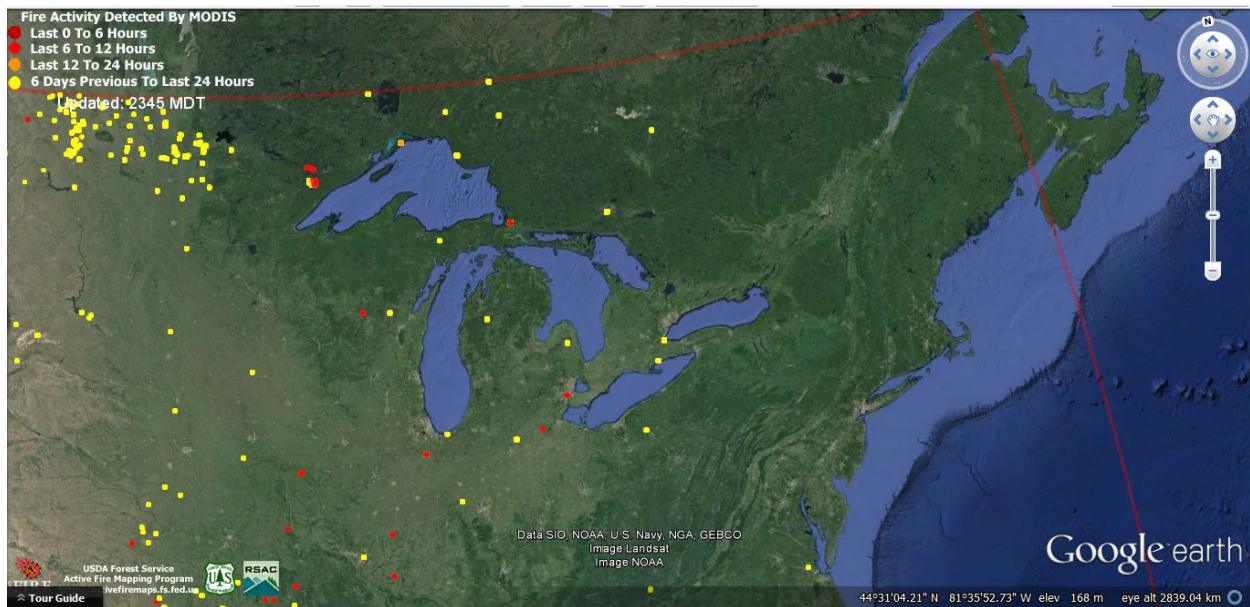
Figure 80 Fire activity detected by the MODIS satellite for September 12th 2013 as obtained from the USDA Active Fire Mapping Program

Finally, the air parcel impacting Sable Island on October 4th brought pollution from Newfoundland, Quebec, New Brunswick, and Nova Scotia. A map of Canadian fire hotspots obtained from Natural Resources Canada for October 4th shows a medium fire index (10-20) over an area in New Brunswick that the air parcel impacting Sable Island would have passed over, indicating that forest fires likely contributed to this $PM_{2.5}$ pollution event. The map can be seen below in Figure 81.
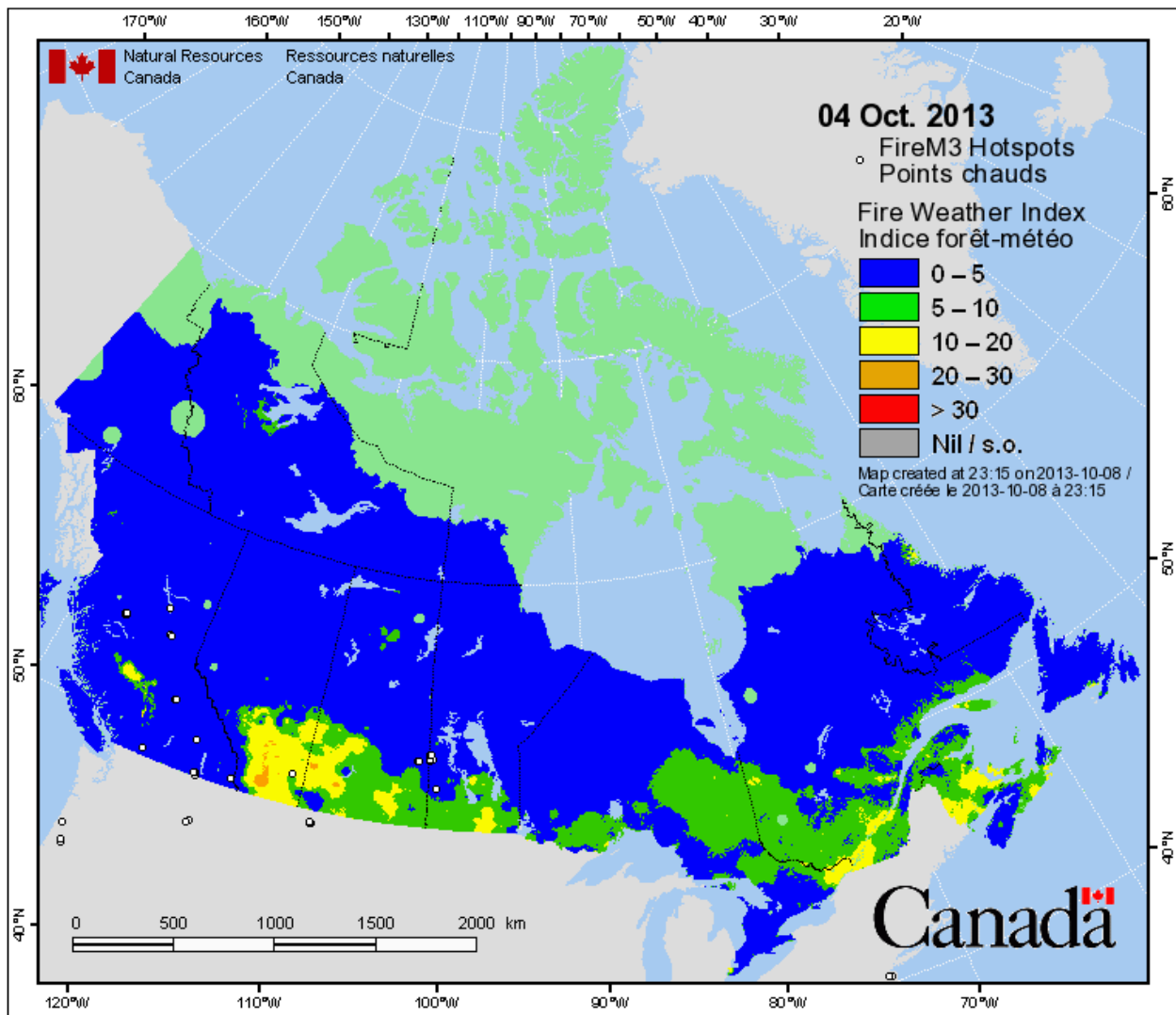
Figure 81 Fire hotspots for October 4th 2013
obtained from the Canadian Wildland Fire Information System

It was hoped that MODIS-Terra satellite imagery obtained from the Active Fire Mapping Program of the USDA (http://firemapper.sc.egov.usda.gov/index.php) could be used to confirm the impact of smoke from forest fires on $PM_{2.5}$ measured on Sable Island on the dates in question. However, cloud cover precluded this on all the dates in question and allowed limited visibility of the Island. The results of examining pollution events through HYSPLIT back trajectories reinforce the sources identified through PMF modelling. It was found that the O&G production facilities were most likely the main contributor to pollution events involving NMHCs but that the impact of phytoplankton blooms during certain periods was likely significant. Meanwhile LRT (backed by the associated ozone concentrations) from the eastern United States and Canada that included

contributions from forest fire events was most likely the main cause of PM$_{2.5}$ pollution events. The pollution events analyzed can be seen below in Table 9. The examination of both oceanographic and terrestrial sources in concert with back trajectory models when examining pollution events is a novel approach that yielded positive results.

Table 9 Summary of PM$_{2.5}$ and NMHC pollution events

Date	Description	Source
June 18th – 20th	NMHC event	Possible offshore O&G activities
June 24th	PM$_{2.5}$ event	LRT (forest fires likely contributed)
June 26th	PM$_{2.5}$ event	LRT (forest fires likely contributed)
July 2nd	PM$_{2.5}$ event	LRT
July 8th	PM$_{2.5}$ event	LRT (forest fires likely contributed)
July 18th – 20th	PM$_{2.5}$ event	LRT (forest fires likely contributed)
July 28th	PM$_{2.5}$ event	LRT (forest fires likely contributed)
August 16th	PM$_{2.5}$ event	LRT (forest fires likely contributed)
August 31st	PM$_{2.5}$ event	LRT (forest fires likely contributed)
September 1st	NMHC event	Possible offshore O&G activities
September 4th	NMHC event	Possible offshore O&G activities
September 5th	NMHC event	Possible offshore O&G activities
September 11th	NMHC event	Possible offshore O&G activities
September 12th	PM$_{2.5}$ event	LRT
September 13th	NMHC event	Possible offshore O&G activities
September 14th	NMHC event	Possible offshore O&G activities
September 27th – 30th	NMHC event	Likely phytoplankton blooms
October 4th	PM$_{2.5}$ event	LRT (forest fires likely contributed)
October 24th	NMHC event	Likely phytoplankton blooms with contributions from offshore O&G activities

3.2.3 Pollution Rose

A Pollution rose was generated using the statistical analysis program Igor to show the association between factor contributions and the predominant wind direction. Daily factor contributions were plotted against the average wind direction for each corresponding day for the entire sampling period. The pollution rose can be seen in Figure 82. The factor contributions of LRT, off-gassing, flaring, and on-site combustion were mapped.
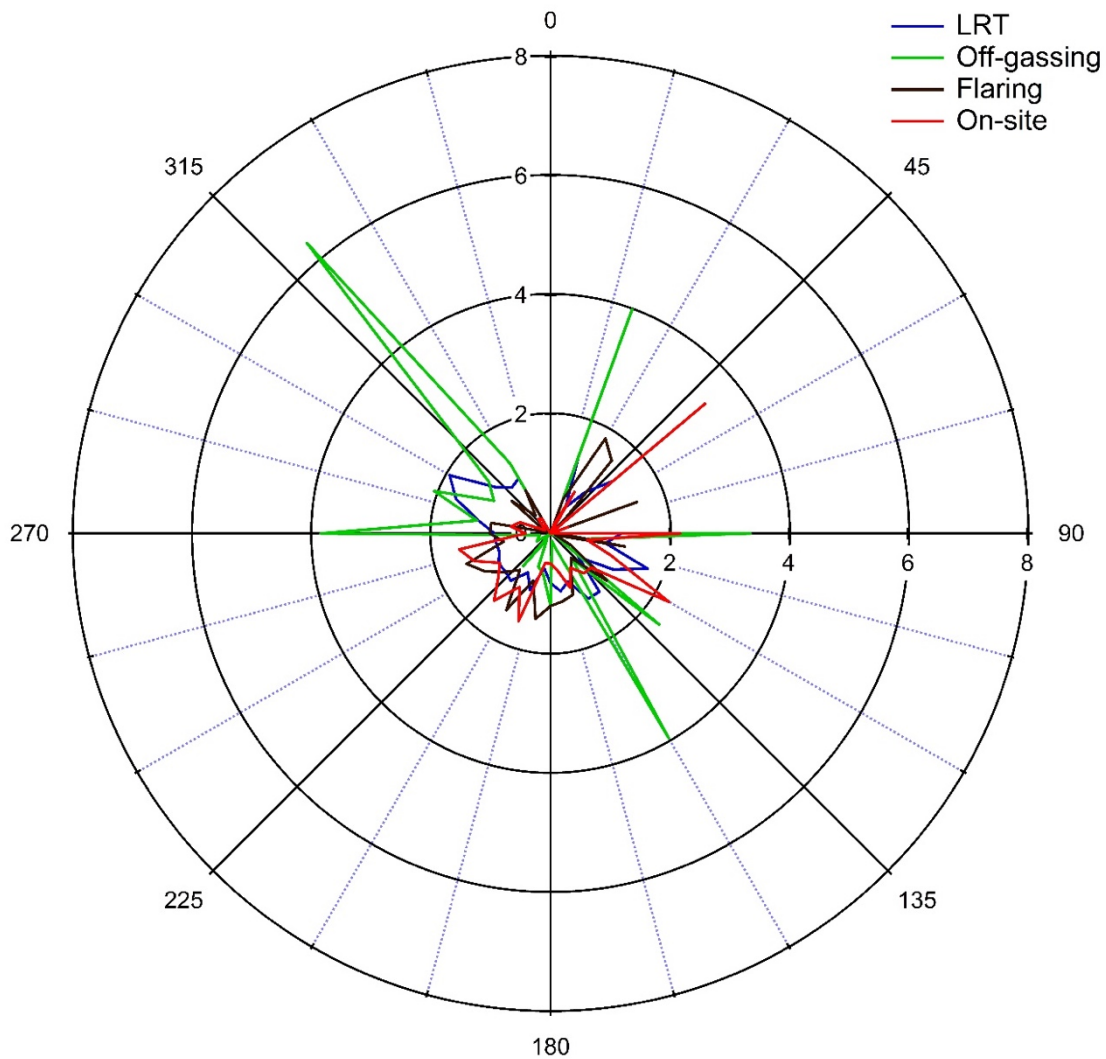
Figure 82 Pollution rose showing association of factor contributions with wind direction

It can be seen from Figure 82 that wind direction is quite variable and does not come from a predominant direction. This is reinforced by the descriptive statistics of wind speed and direction used in generating the pollution roses. The average wind direction is from 206.5 degrees (SSW) but the data exhibits a large deviations in wind direction. The predominant direction for LRT contributions appears to be to the NW, aligning with the Eastern Seaboard of the United States. For off-gassing, the predominant directions appear to be to the NW, NNE, E, SE, and W. Contributions from NW and NNE are likely a result of contributions from phytoplankton while offshore oil and gas activity is located E, S, and SE of Sable Island as can be seen from Figure 2. HYSPLIT back trajectories reinforce that the O&G production platforms are likely the main

contributors to NMHC concentrations on Sable Island with phytoplankton blooms perhaps contributing significantly during certain time periods (Spring and Fall phytoplankton bloom period). Contributions from flaring come predominantly from the SE to W directions, again fitting with the location of O&G production activities. On-site emissions come mainly from the SE to SW. The diesel generator as well as garbage burning takes place in this direction, again correlating well with the predominant wind direction that factor contributions originate from. Contributions coming from other directions attributed to on-site combustion could be due to localized transport in the form of ships, aircraft, and vehicles on the island.

3.3 Impact of New Offshore O&G Production

As outlined previously, the data was split to look for potential differences before and after the start up and commissioning of a new oil and gas platform just off the Coast of Sable Island. The data was split around the date of July 22nd 2013. This was the date when the hook-up and commissioning phase for the new oil and gas activity was initiated (Canada – Nova Scotia Offshore Petroleum Board, 2013). The non-parametric Mann-Whitney statistical test was run in Miniplot. This test was chosen as the data sets contained different numbers of data points. Box plots were generated in SigmaPlot in order to compare the different distributions of the two data sets. A Mann-Whitney statistical test revealed significant differences between the pre and post split data subsets for concentrations of BC, $PM_{2.5}$, SO_2, H_2S, O_3, NO, NO_x, and NO_2. After adjusting for ties all p-values were < 0.05. NMHC was the only pollutant that showed no statistically significant difference with a p-value of 0.2019 after adjusting for ties. Descriptive statistics and box plots were generated and are presented in .

Table 10.

Table 10. Descriptive Statistics for all species before and after July 22nd 2013

Variable	Mean	Standard Deviation	Minimum	Q1	Median	Q3	Maximum
NMHC before (ppm)	0.050	0.203	0.00	0.00	0.00	0.00	1.06
BC before ($\mu g/m^3$)	0.115	0.151	0.00	0.03	0.067	0.155	3.47
$PM_{2.5}$ before ($\mu g/m^3$)	16.0	5.82	4.00	12.0	15.0	19.0	43.0
SO_2 before (ppb)	0.062	0.067	0.00	0.00	0.10	0.10	0.30
H_2S before (ppb)	0.215	0.244	0.00	0.00	0.10	0.30	1.20
O_3 before (ppb)	29.7	8.59	7.80	24.1	29.5	34.1	57.1

NO$_x$ before (ppb)	2.30	0.339	0.00	2.40	2.40	2.40	3.50
NO$_2$ before (ppb)	1.18	0.472	0.00	0.90	1.10	1.325	7.70
NO before (ppb)	0.863	0.402	0.00	0.60	0.80	1.00	6.10
NMHC after (ppm)	0.025	0.134	0.00	0.00	0.00	0.00	1.13
BC after (μg/m^3)	0.075	0.181	0.00	0.017	0.04	0.087	13.0
PM$_{2.5}$ after (μg/m^3)	12.7	5.22	0.00	9.00	12.0	16.0	38.0
SO$_2$ after (ppb)	0.238	0.186	0.00	0.10	0.30	0.40	3.00
H$_2$S after (ppb)	0.485	0.542	0.00	0.20	0.30	0.70	13.7
O$_3$ after (ppb)	30.9	7.99	4.90	26.0	30.7	35.6	61.1
NO$_x$ after (ppb)	2.02	0.363	0.80	1.70	1.80	2.50	3.40
NO$_2$ after (ppb)	1.08	0.807	0.00	0.60	0.80	1.60	28.7
NO after (ppb)	1.08	0.432	0.70	0.90	1.00	1.20	14.6
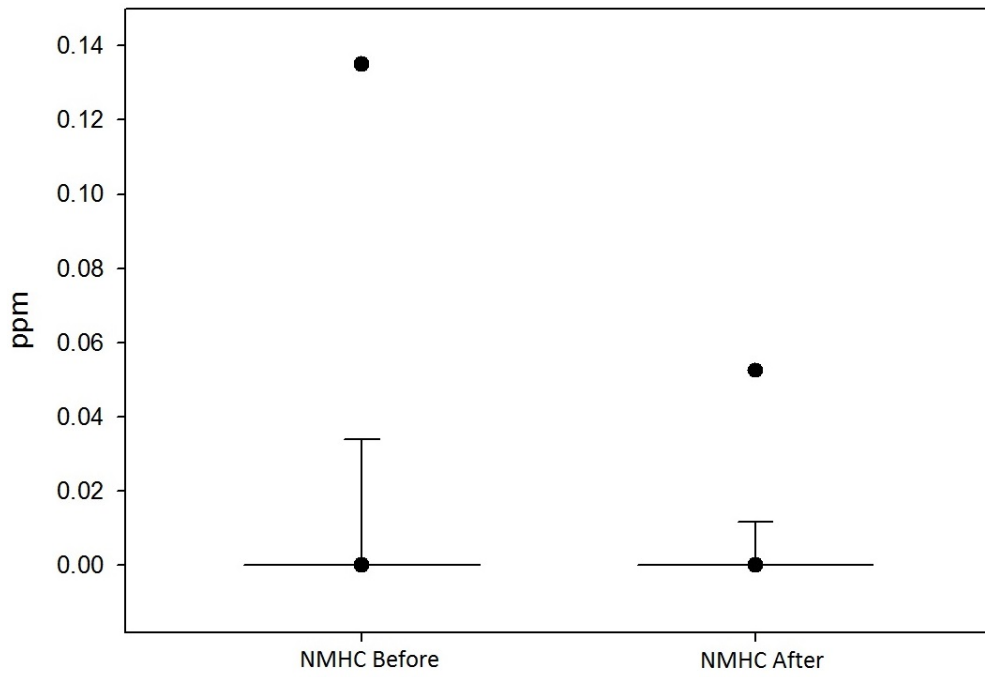
Figure 83 Box plot of NMHC concentrations before and after July 22nd
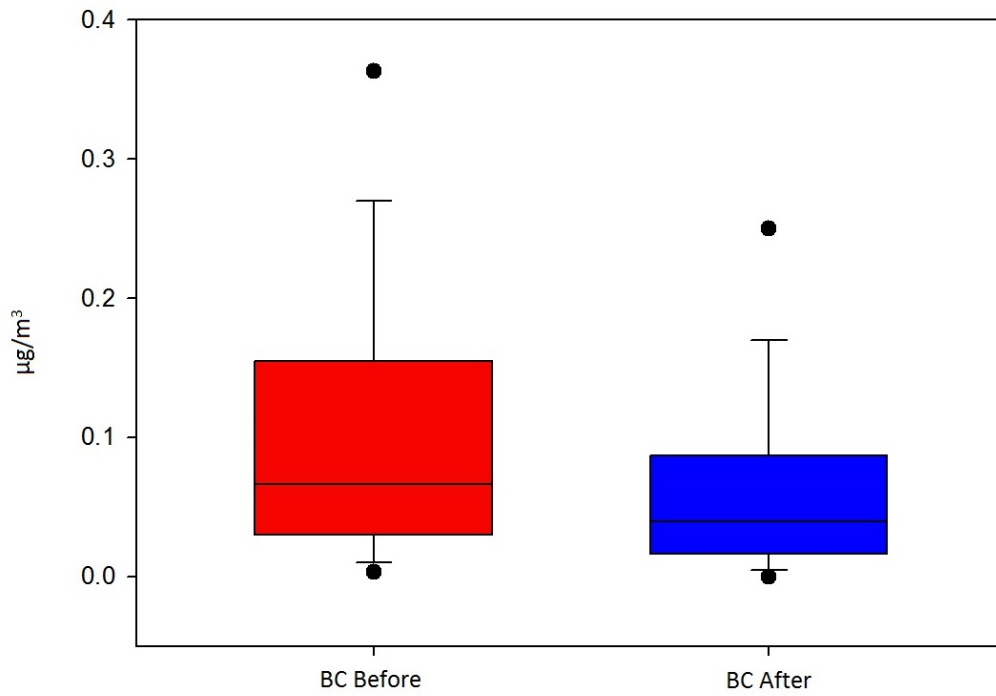
Figure 84 Box plot of BC concentrations before and after July 22nd
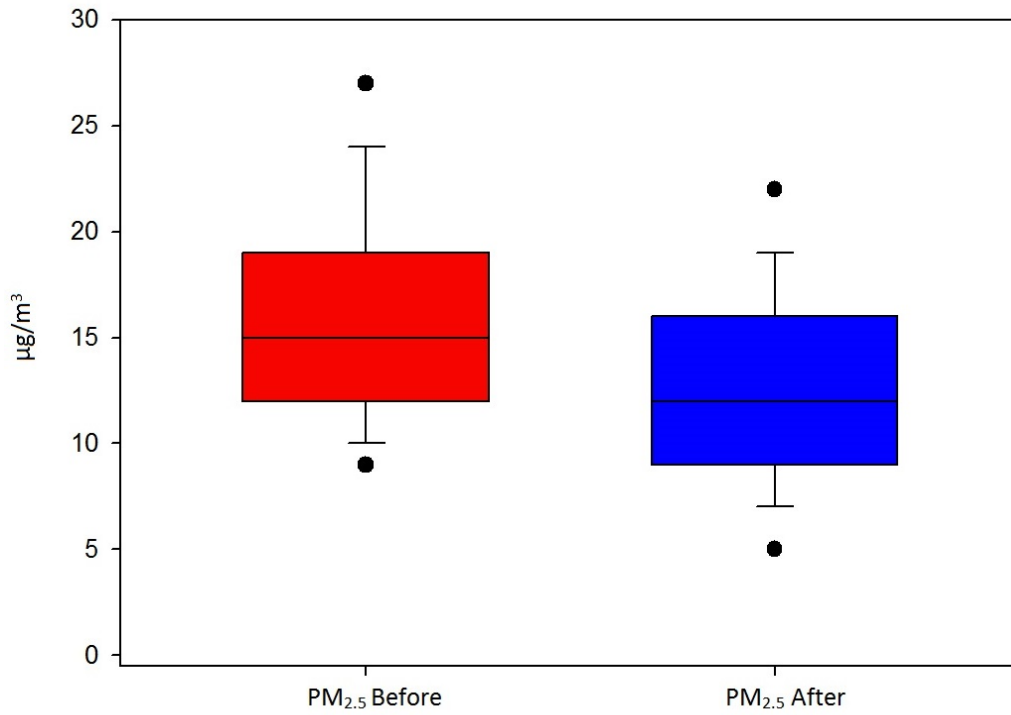
Figure 85 Box plot of PM$_{2.5}$ concentrations before and after July 22nd
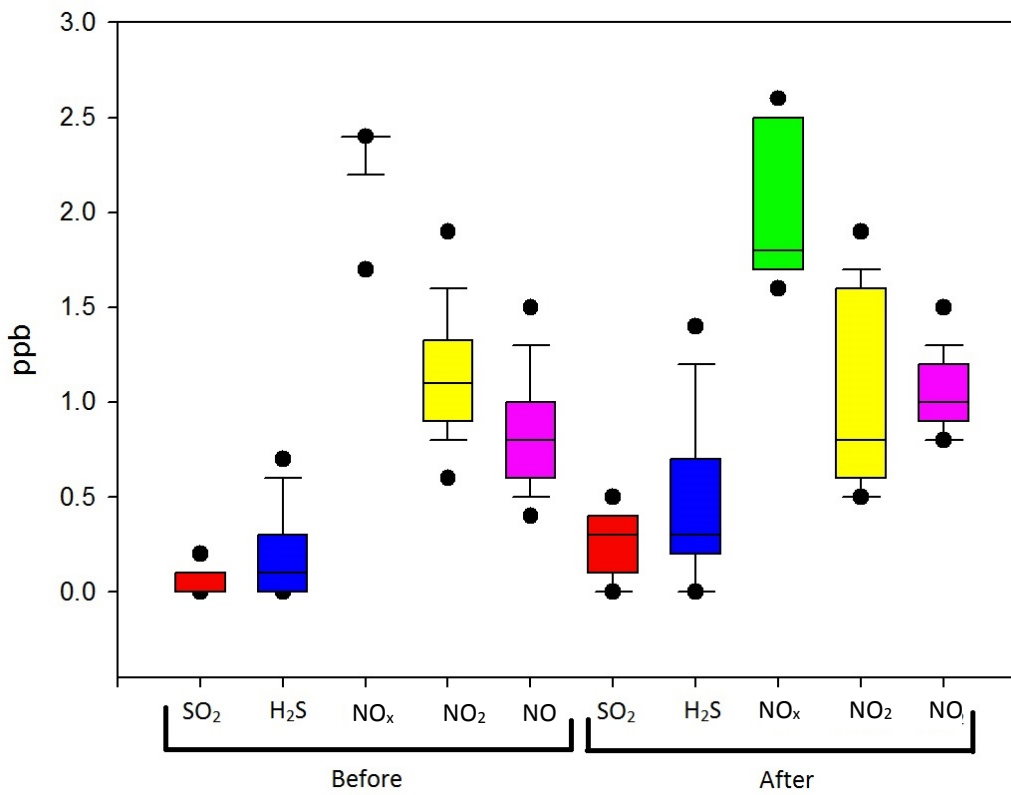
Figure 86 Box plot of SO$_2$, H$_2$S, NO$_x$, NO$_2$, and NO concentrations before and after July 22nd

From looking at the various box plots before and after July 22nd (Figure 83 –

Figure 86) it is reinforced that NMHC concentrations show no significant change before and after July 22nd; the median value remains the same while the 95th and 90th percentile change slightly. All of the other pollutants show a significant change. The median values and upper percentiles for BC, PM$_{2.5}$, NO$_x$, and NO$_2$ show decreases after July 22nd, while those for SO$_2$, H$_2$S, and NO show increases.

The descriptive statistics in Table 3 show that mean concentrations for SO$_2$ increased from 0.062 ppb before July 22nd to 0.24 ppb after. Mean concentrations of H$_2$S increased from 0.21 ppb to 0.48 ppb. This is an increase of 218% for SO$_2$ and 125% for H$_2$S. When considered with the previous factor profiles, found through the PMF model results, it can be seen that SO$_2$ and H$_2$S are the main components of flaring, which would likely increase with bringing new O&G activity online. BC, PM$_{2.5}$, NO, and NO$_x$ are more strongly associated with on-site combustion and LRT. Source contributions from these factors likely decreased in the summer months, as the on-site power needs were less (mainly due to a decreased need for heating). LRT contributions from the mainland were also likely lower for the same reason

4   2016 STUDY – RESULTS AND DISCUSSION

4.1   Meteorology Results

Temperature, wind direction and wind speed were measured hourly on Sable Island during 2016. Comprehensive descriptive statistics of these parameters are provided below in Table 11.

Table 11 Descriptive statistics of temperature, wind direction and wind speed on Sable Island for 2016.

	Temp. (°C)	Wind Direction (°)	Wind Speed (km/hr)
n	8414	8414	8535
n missing	370	343	249
Completeness (%)	95.79	96.10	97.17
Mean	9.43	256	25.36
Std. Deviation	7.35		12.79
Minimum	-9.7		0
25th Percentile	3.8		17
Median	9.4		24
75th Percentile	15.2		34
Maximum	53.8		91
I.Q.R	11.4		17

4.1.1   Temperature

The mean annual temperature for 2016 on Sable Island was 9.43°C ± 7.35°C. January, March and February were the coldest months respectively while August, September and July were the warmest months, respectively. Mean monthly temperatures are shown in

Table 12 contains the mean and standard deviation of monthly temperature with a visual representation of the data in Figure 87.

Table 12 Mean monthly temperatures in °C on Sable Island for 2016

Month	Temperature (°C)	Standard Deviation (±°C)
January	1.64	3.03
February	2.12	4.01
March	1.75	3.40
April	11.06	12.92
May	8.35	2.23
June	11.76	2.29
July	15.99	2.05
August	18.94	1.81
September	17.66	2.76
October	12.94	3.19
November	9.09	2.72
December	2.66	3.90
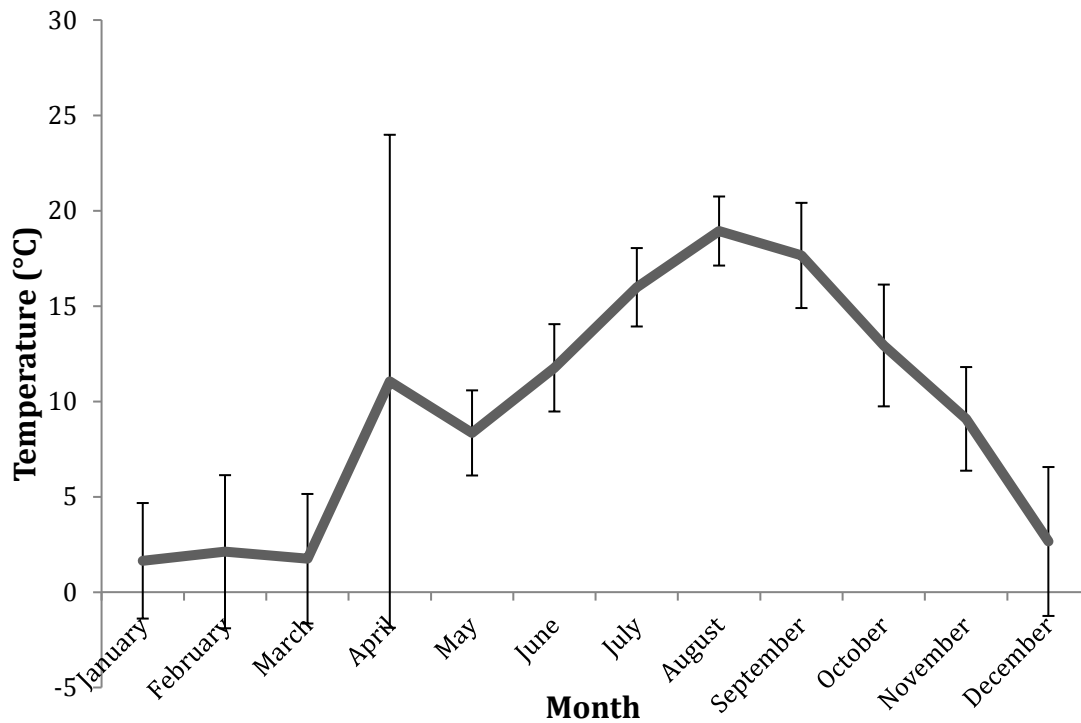
Figure 87 Mean monthly temperature (°C) on Sable Island for 2016. Error bars represent 95% confidence intervals

As expected, winter was the coldest season of the year, followed by autumn, spring and summer respectively (Table 13, Figure 88).

Table 13 Mean seasonal temperatures in °C on Sable Island for 2016

Season	Temperature (°C)	Standard Deviation (±°C)
Summer	17.53	1.21
Autumn	8.23	3.69
Winter	1.84	3.48
Spring	10.39	5.82
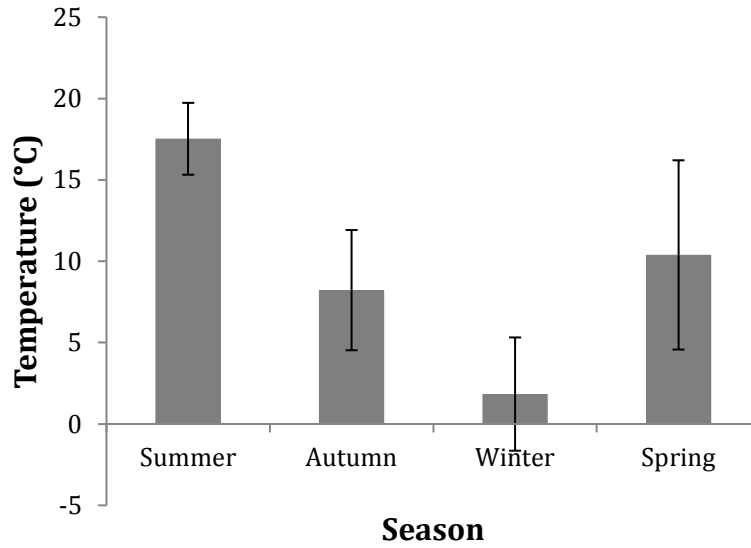
**Figure 88 Mean seasonal temperature (°C) on Sable Island for 2016.
Error bars represent 95% confidence intervals**

4.1.2 Wind

The 2016 mean annual wind speed measured on Sable Island were 25.36 ± 12.79 km/hr respectively. Wind-rose analyses show a mean annual wind direction of 256°, translating to a predominantly WSW wind blowing into the island (Figure 89, Figure 90).
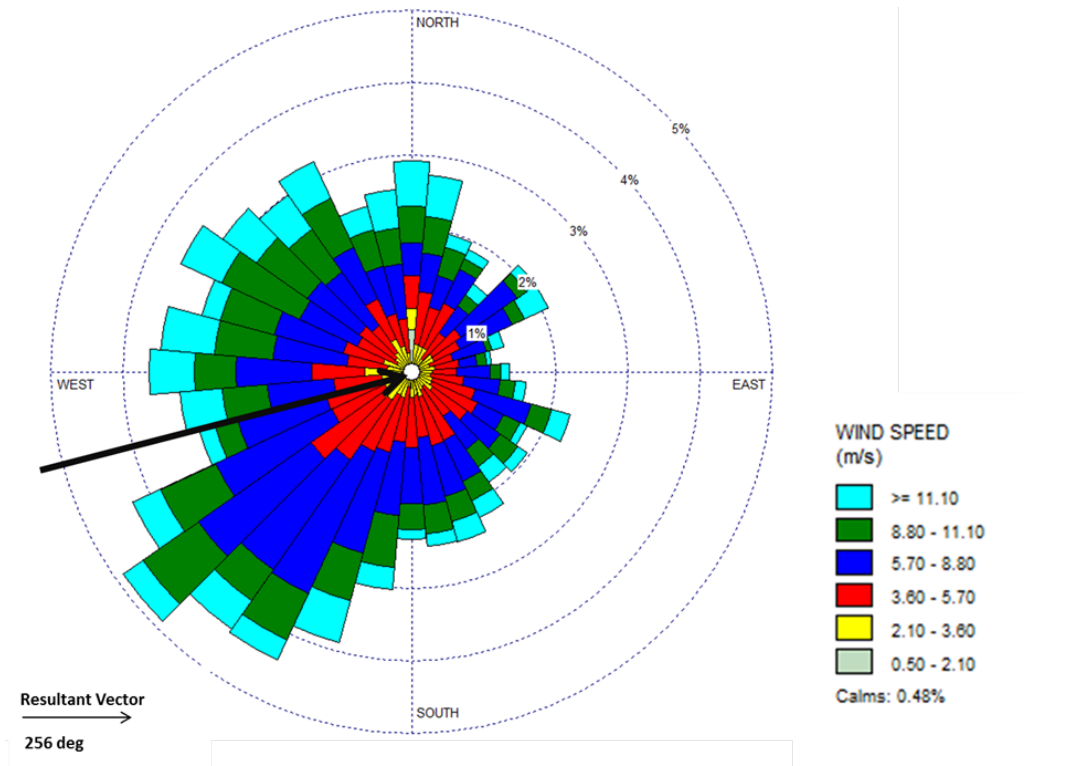
Figure 89 Wind rose plot of mean annual wind directions and speeds blowing into Sable Island for 2016

Figure 90 Google map image of Sable Island with a superimposed wind rose diagram

4.2 Total Volatile Organic Compounds (VOCs)

Total VOC concentrations were measured in 15 minute intervals during 2016. Overall, the summer season had the highest VOC concentrations, followed by spring, autumn and winter respectively (Table 15, Figure 91).

Table 14 Descriptive statistics of Total VOC concentrations (ppb) on Sable Island for 2016

	Total VOC (ppb)
n	32173
n missing	2963
Completeness (%)	91.57
Mean	1871
Std. Deviation	2097.97
Minimum	0
25th Percentile	200
Median	1871
75th Percentile	3394
Maximum	20030
I.Q.R	3194

Table 15 Mean seasonal VOC concentrations (ppb) on Sable Island for 2016

Season	Mean Total VOC Concentration (ppb)	Standard Deviation (± ppb)
Summer	3918.20	1455.81
Autumn	349.49	322.05
Winter	170.36	44.03
Spring	2921.27	1104.02
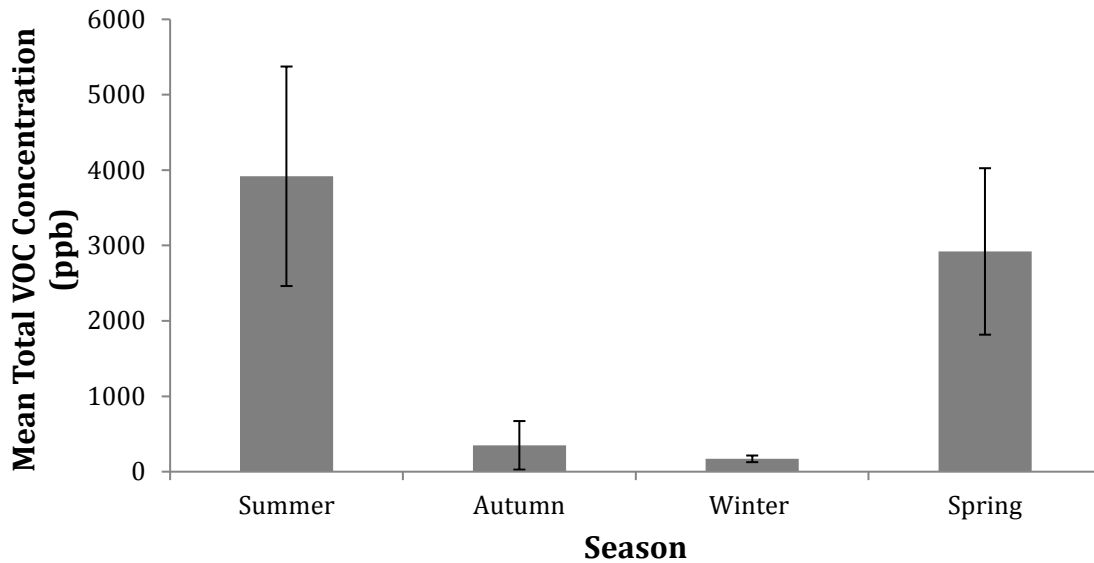
Figure 91 Mean seasonal VOC concentrations (ppb) on Sable Island for 2016

As predicted, monthly mean VOC concentrations also followed the seasonal trends. January and December had the lowest mean VOC concentrations of 6.6 ppb ± 30.47 ppb and 7.28ppb ± 53.41 ppb respectively while July and August had the highest concentrations of 4060.95 ppb ± 845.09 ppb and 5384.58 ppb ± 2385.15 ppb respectively (Table 16, Figure 92 & Figure 93).

Table 16 Mean monthly VOC concentrations (ppb) on Sable Island for 2016

Month	Total VOC (ppb)	Standard Deviation (± ppb)
January	6.60	30.47
February	202.21	48.84
March	302.28	52.79
April	1257.42	1049.19
May	3849.52	1421.98
June	3656.88	840.90
July	4060.95	845.09
August	5384.58	2385.15
September	2309.06	1137.19
October	684.02	565.34
November	357.19	347.38
December	7.28	53.41
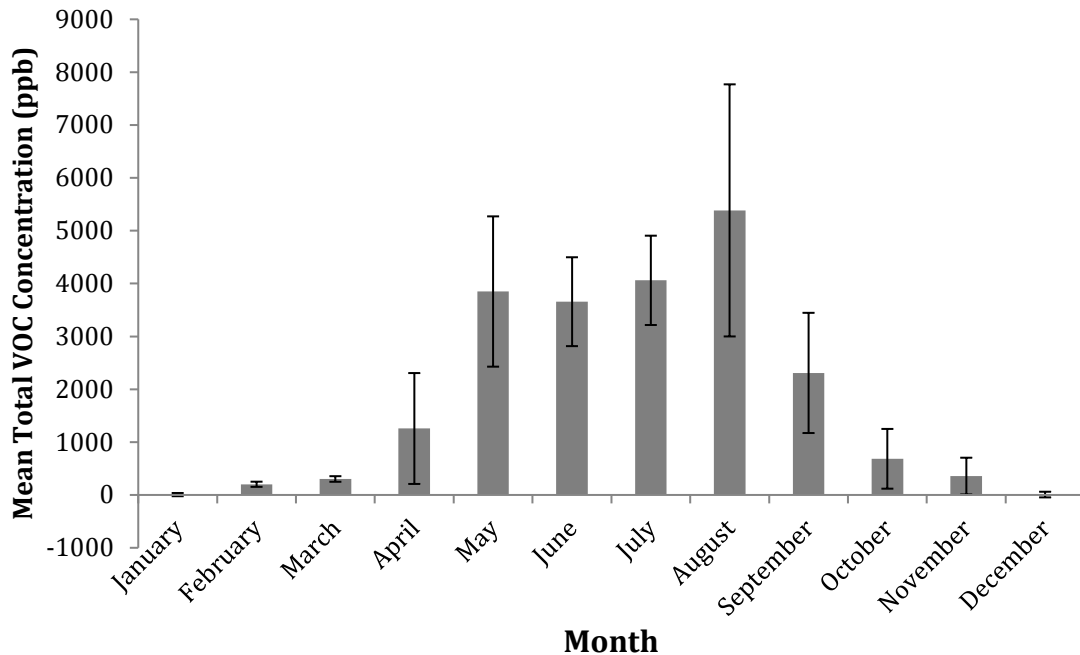
Figure 92 Mean monthly VOC concentrations (ppb) on Sable Island for 2016
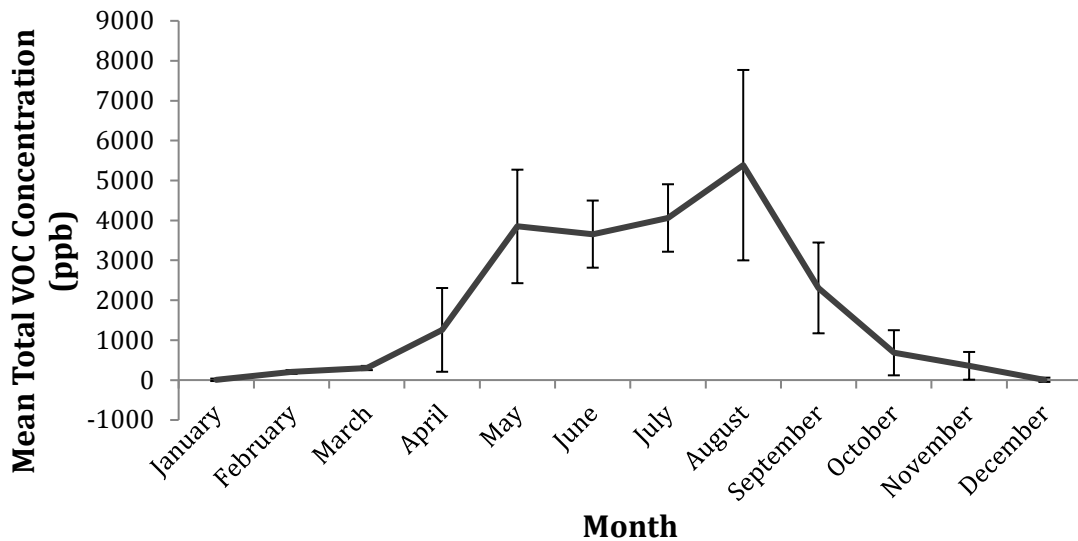
Figure 93 A moving average trend-line of mean monthly VOC concentrations (ppb) on Sable Island for 2016

Diurnal / time-dependent changes in VOC concentrations were also observed in several months throughout 2016. January, February, March, April and December did not have noticeable changes in VOC concentrations (Figure 94, Figure 95, & Figure 97) and September showed a relatively small diurnal change (Figure 96). May, June, July, August, October and November showed the most time-dependent variation in VOCs, with concentrations peaking around mid-day/early

112

afternoon (Figure 95, Figure 97, & Figure 97). Table 17 provides times at which VOC concentrations begin to noticeably increase, reach peak concentrations and then start to tail off.

Table 17 Mean time of day (hh:mm) during which VOC concentrations begin to increase, reach a peak and decline for every month during 2016 on Sable Island

Month	Start Time (hh:mm)	Highest Peak Time (hh:mm)	End Time (hh:mm)
January	-	-	-
February	-	-	-
March	-	-	-
April	-	-	-
May	08:30	14:00	17:15
June	08:30	13:15	16:45
July	09:15	12:45	18:00
August	09:15	13:00	17:45
September	10:00	13:45	17:00
October	10:45	14:30	22:15
November	11:15	16:15	20:00
December	-	-	-
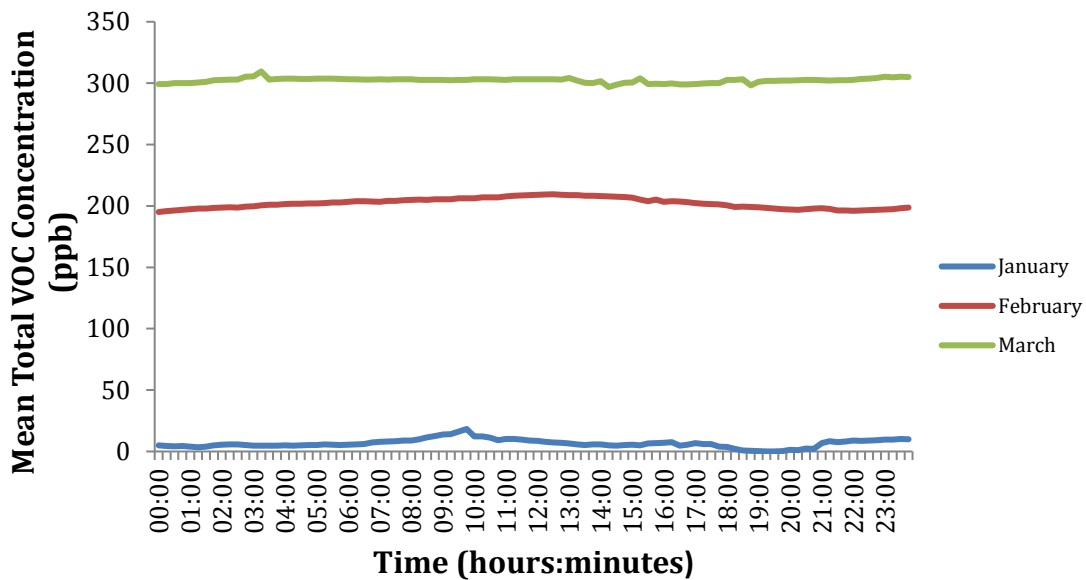
Figure 94 Hourly mean VOC concentrations (ppb) for January, February and March, 2016 on Sable Island
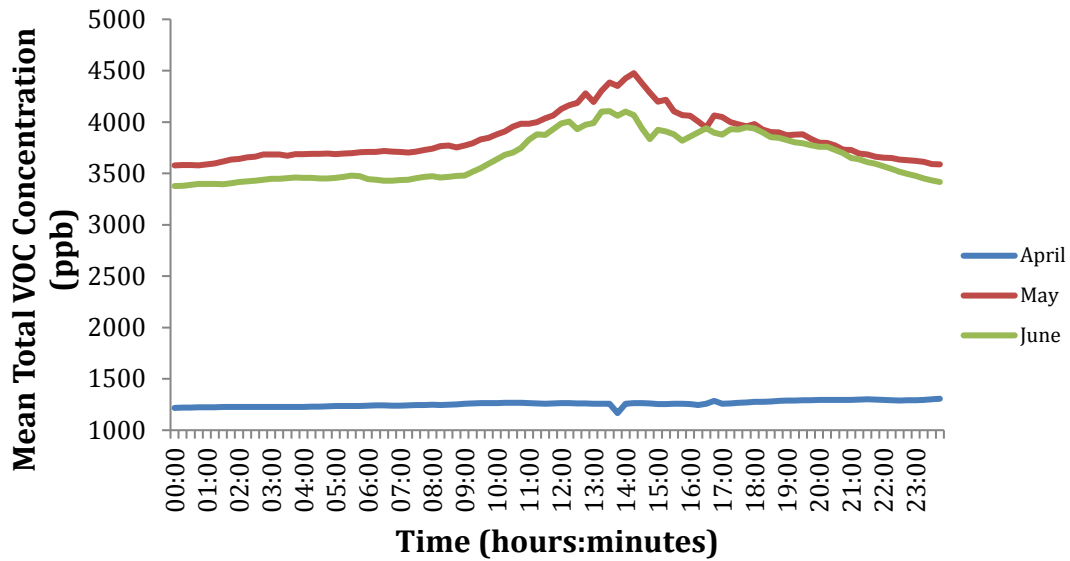
Figure 95 Hourly mean VOC concentrations (ppb) for April, May and June, 2016 on Sable Island
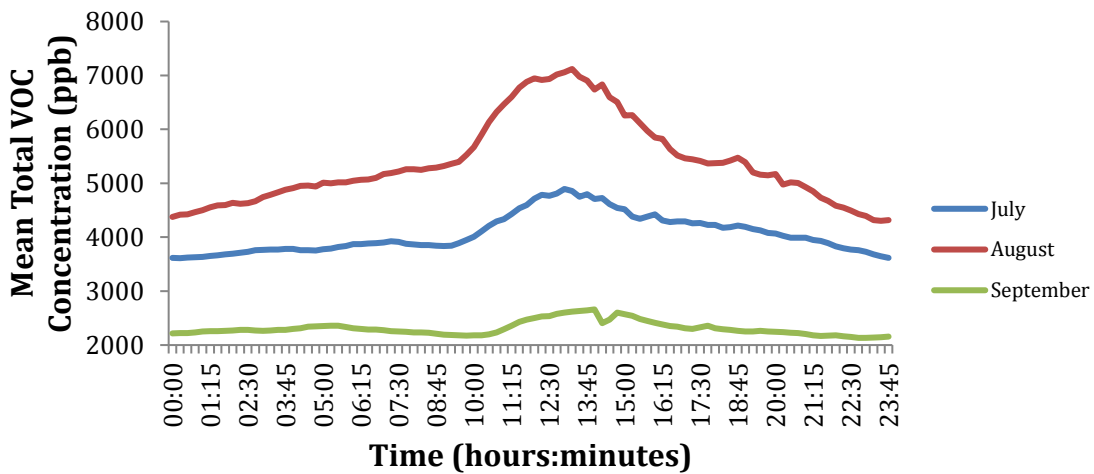
Figure 96 Hourly mean VOC concentrations (ppb) for July, August and September, 2016 on Sable Island
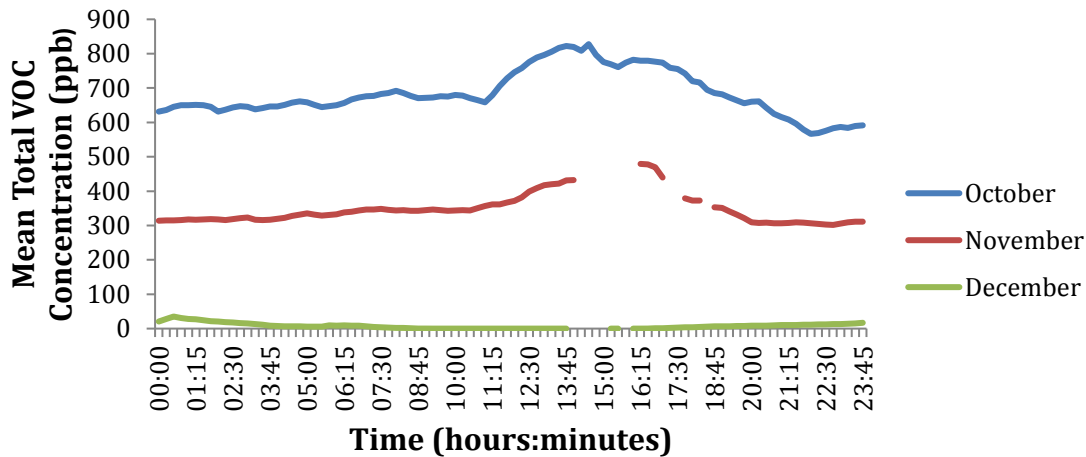
Figure 97 Hourly mean VOC concentrations (ppb) for October, November and December, 2016 on Sable Island

Even though monthly and seasonal trends were observed when VOC concentrations were analyzed for the entire year at once, 'spikes' in concentrations were found throughout the entire year (Figure 98). Table 18 also provides the time at which the highest concentration in each observed spike was measured.
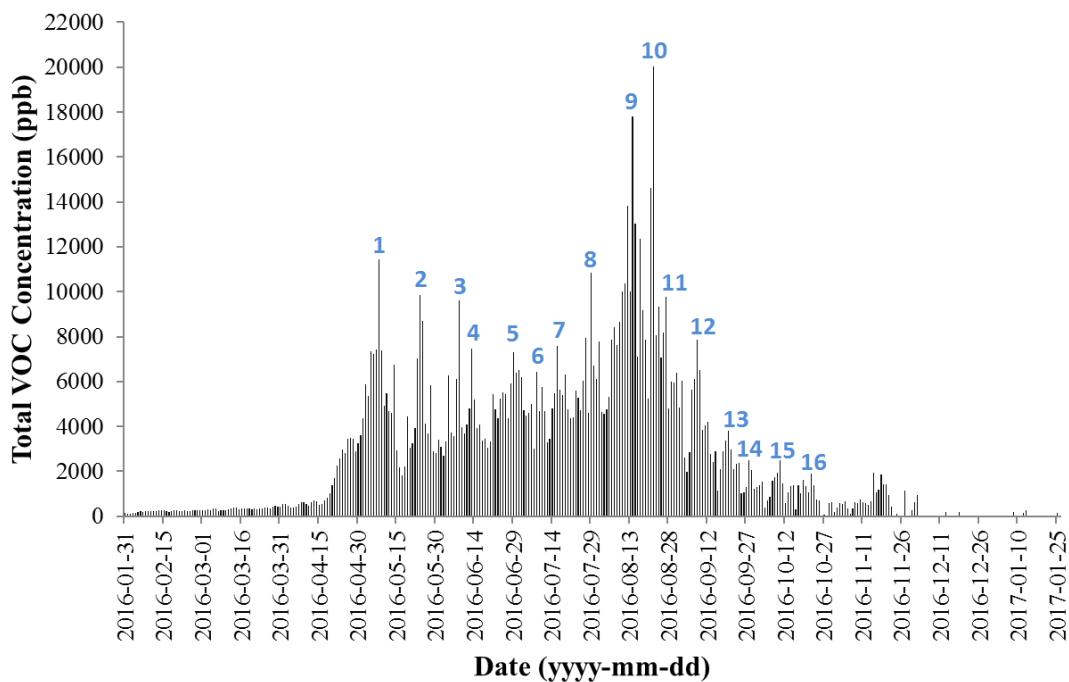
Figure 98 Total VOC concentrations (ppb) measured every 15 minutes in 2016 on Sable Island (Numbers represent spikes in VOC concentrations that were analyzed in detail)

Table 18 Date, Peak Time, and Total VOC concentration for each of the observed spikes found in Figure 98

Spike	Date (yyyy-mm-dd)	Peak Time (hh:mm)	Total VOC (ppb)
1	2016-05-08	14:15	11455
2	2016-05-24	13:45	9843
3	2016-06-08	13:15	9623
4	2016-06-13	14:00	7461
5	2016-06-29	12:00	7285
6	2016-07-08	21:00	6416
7	2016-07-16	14:15	7568
8	2016-07-29	13:00	10849
9	2016-08-14	19:00	17786
10	2016-08-22	13:45	20029
11	2016-08-27	14:00	9787
12	2016-09-08	14:00	7850
13	2016-09-20	13:30	3811
14	2016-09-28	13:45	2608
15	2016-10-10	14:00	2464
16	2016-10-22	16:00	1914

4.3 Long-range and local airflow over Sable Island using the NOAA HYSPLIT Model

Analysis of long-range and local air flow impacting Sable Island from far and near source regions was conducted using five-day air mass back trajectories (NOAA, HYSPLIT) performed twice a day (ending at 00:00 and ending at 12:00) for the entirety of 2016. The trajectory was then categorized into four different zones, Marine, South West, North West and North as shown below (

Figure 99).
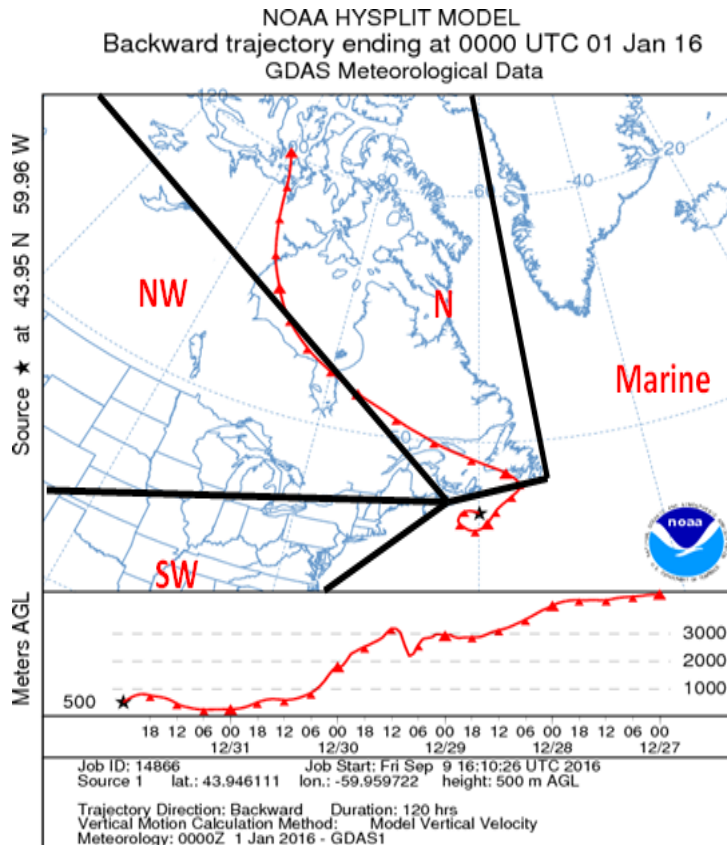
Figure 99 Example of HYSPLIT model output showing the four characterization zones. SW = South West, NW = North West, N = North. This example shows a 5-day air mass back trajectory that would be classified as associated with Northerly airflow

Over all in 2016, air masses travelled mostly from the North (31.64%) and North West (28.9%) to Sable Island and approximately one quarter of the time from marine regions (26.03%). Air masses travelled from the South West direction least frequently (13.42%), as shown in Figure 100.
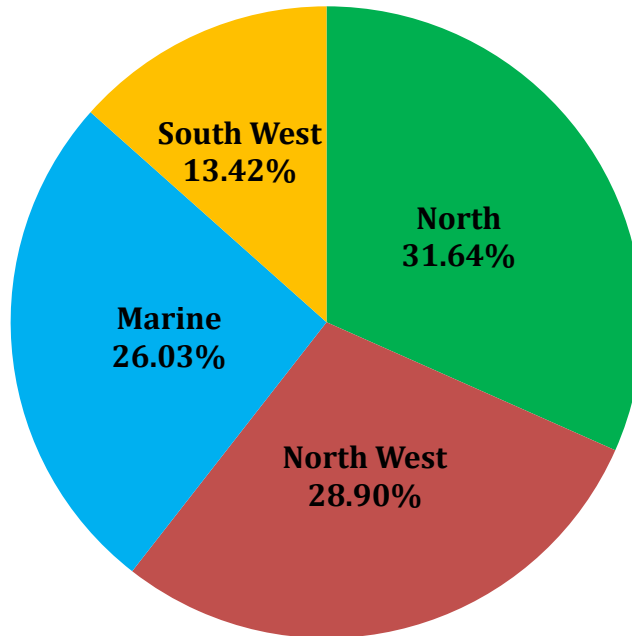
Figure 100 Frequency (percentage) of air mass sources into Sable Island for 2016, derived from HYSPLIT analyses

Seasonal analysis of HYSPLIT showed that winter and autumn were dominated by North and North West wind trajectories (winter: 32% N, 33% NW; autumn: 40% N, 34% NW). Spring and summer seasons were dominated by marine trajectories, with the North being the second most frequent trajectory in the spring and North West for the summer (spring: 35% Marine, 32% N; Summer: 36% Marine, 29% NW). Except for the winter season, the South West trajectory was the least frequent in all seasons. Figure 101 provides a breakdown of the trajectory frequencies during all four seasons.
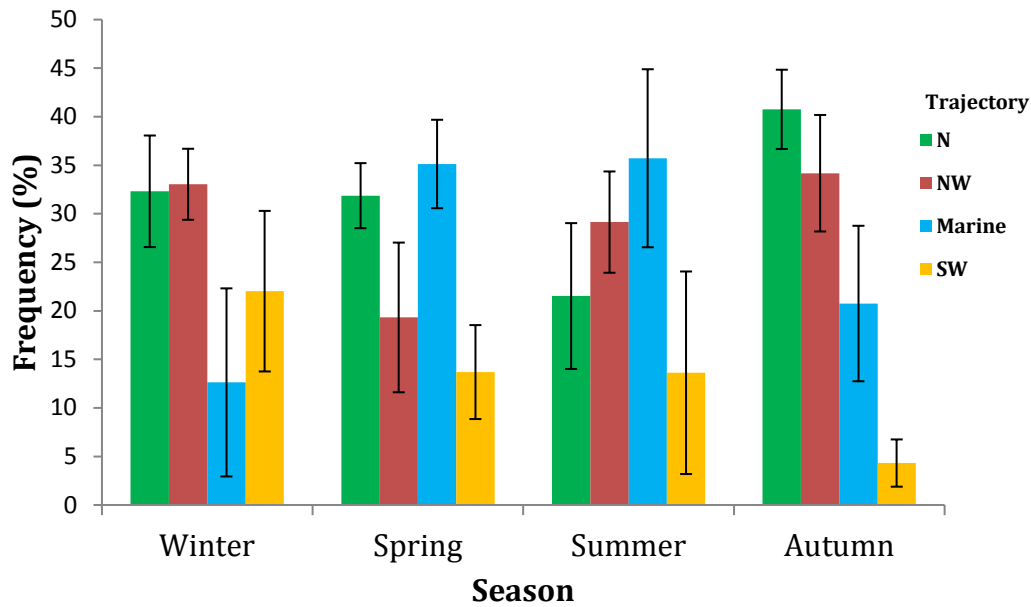
Figure 101 Seasonal analysis of air mass sources to Sable Island in 2016. SW = South West, NW = North West, N = North

Monthly analysis of the HYSPLIT air mass back trajectories showed that October had the highest source of Northern air masses followed by November and January respectively, while July had the smallest sources of Northern air masses, followed by August and September respectively. NW air masses were most frequent in December, followed by February and October respectively, and least frequent in May, followed by June and September respectively. Marine sources were most frequent in September, followed by May and April respectively, and least frequent in January, followed by October and December respectively. South West sources were most frequent in January, followed by February and July respectively, and least frequent in November, followed by September and October respectively. Figure 102 shows a percentage breakdown for each of the four sources for every month in 2016.
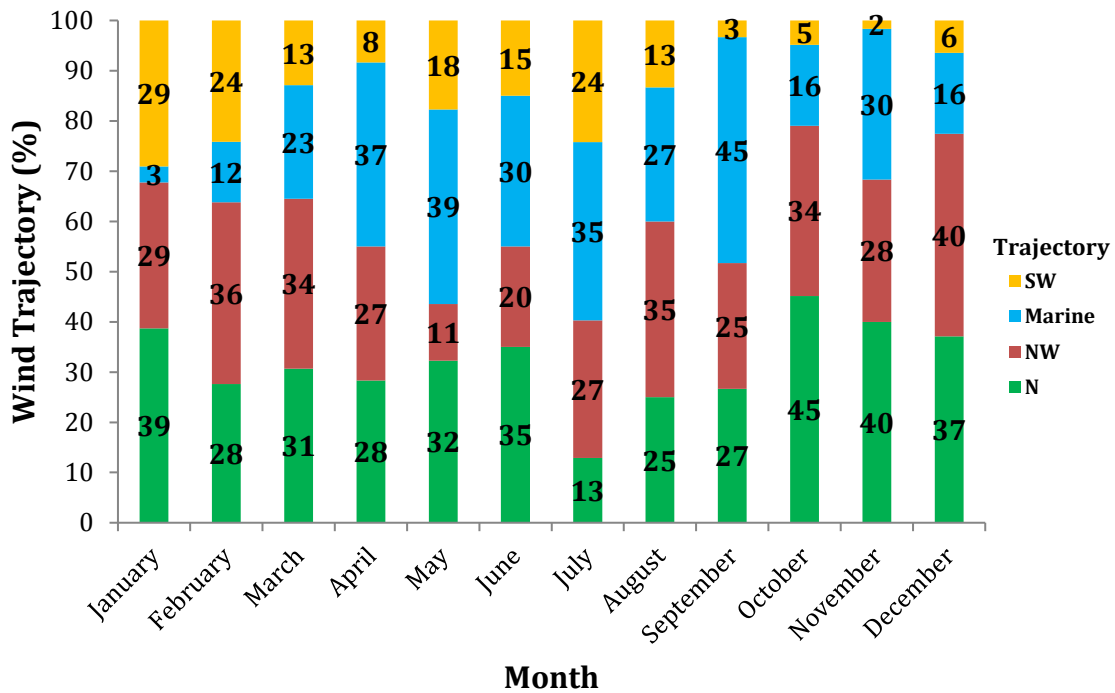
Figure 102 Monthly analysis of air mass sources to Sable Island in 2016. SW = South West, NW = North West, N = North

4.3.1 HYSPLIT Analysis for Select VOC Spikes

16 distinct "spikes" in total VOC concentrations were observed in 2016 (Figure 98).

Table 19 provides the dates during which these spikes were observed, the HYSPLIT trajectory for each spike as well as the "source". To categorize the source, each trajectory's path was examined, and if the trajectory passed over a populated area (i.e. city or industrial zone), it was considered to be industrial, if it passed over forest/areas of low population, it was considered terrestrial, and if it was a marine trajectory, the source was considered marine.

Table 19 Source sectoring of air-mass back trajectories on Sable Island for select days during 2016. HYSPLIT = Trajectories following zones in Figure 98. Source = Trajectories characterized by population density/industrial activity. SW = South West, NW = North West, N = North

Spike	Date (yyyy-mm-dd)	HYSPLIT	Source
1	2016-05-08	Marine	Marine
2	2016-05-24	Marine	Marine
3	2016-06-08	SW	Anthropogenic
4	2016-06-13	NW	Terrestrial
5	2016-06-29	Marine	Marine
6	2016-07-08	Marine	Marine
7	2016-07-16	SW	Anthropogenic
8	2016-07-29	NW	Terrestrial
9	2016-08-14	N	Anthropogenic
10	2016-08-22	Marine	Marine
11	2016-08-27	Marine	Marine
12	2016-09-08	Marine	Marine
13	2016-09-20	Marine	Marine
14	2016-09-28	Marine	Marine
15	2016-10-10	Marine	Marine
16	2016-10-22	Marine	Marine

Overall, the spikes in total VOC concentration were mostly associated with marine sources (68.75%), followed by anthropogenic (18.75%) and terrestrial (12.5%) sources respectively (Figure 103).
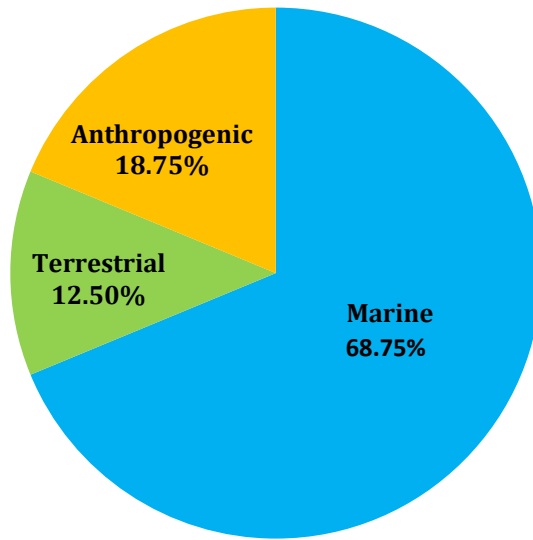
Figure 103 Sources of air mass back trajectories on Sable Island for select days with spikes in VOC concentrations in 2016

Identical HYSPLIT analyses were conducted for the time period during which VOC species were measured (April 15th, 2016 - May 9th, and August 13th - 14th 2016). During that period, marine sources were most common (44.44%) followed by terrestrial (25.93%) and anthropogenic (29.63%) sources respectively (Figure 104).
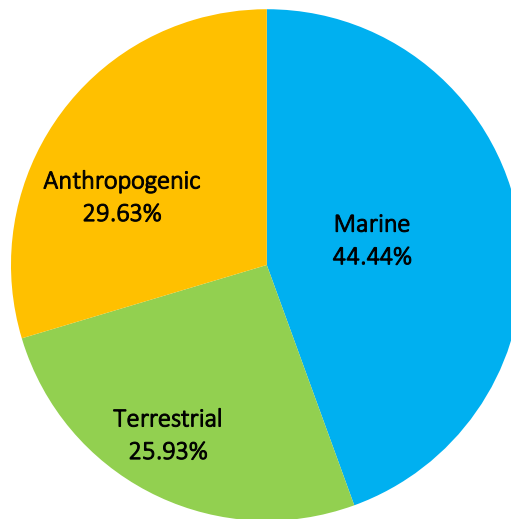
Figure 104 Sources of air mass back trajectories on Sable Island for days during which VOC species measurements were conducted

4.3.2 VOC Species Meta-Analysis

TD-GC-MS was used to identify VOC species through m/*z* ratio, retention time, NIST libraries and standards. Figure 105 to Figure 108 provide examples of sample runs, including a control showing no VOCs, an internal standard run showing deuterated 1,4-dichlorobenzene, and two sample runs showing dimethyl disulfide and bromomethane. TDTs were analyzed for the period of April, 15th, 2016 – May 9th, 2016 as well as August 13th and 14th, 2016.
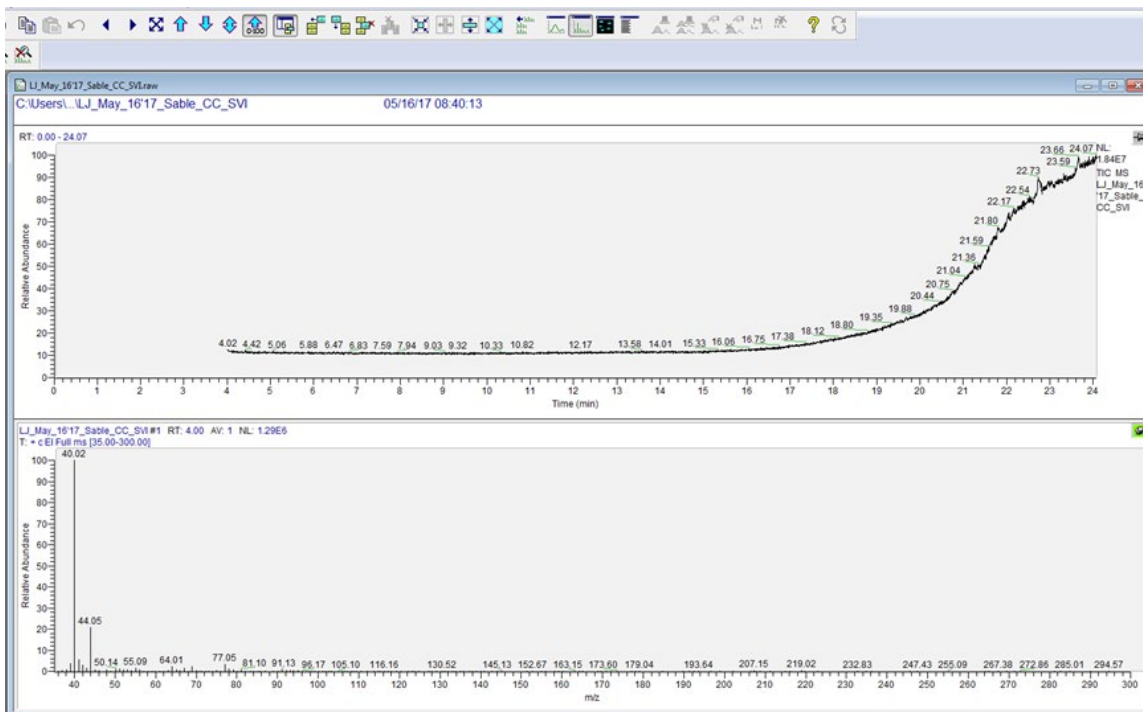
Figure 105 A sample run of a control TDT, containing no VOCs
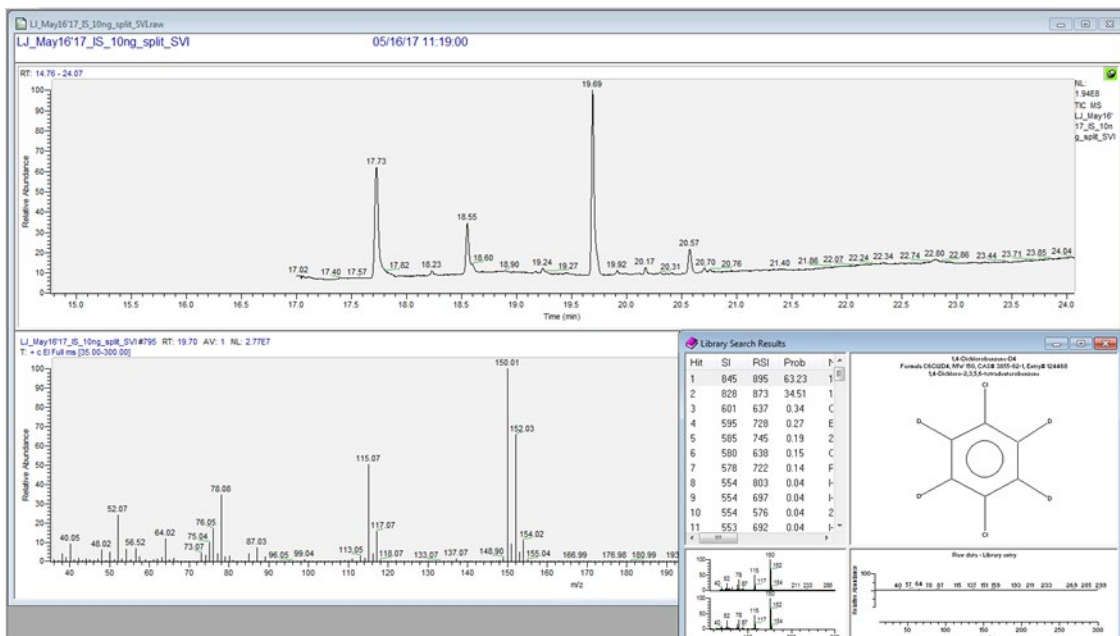
Figure 106 Mass spectra of an internal standard run, showing deuterated 1-4 dichlorobenzene
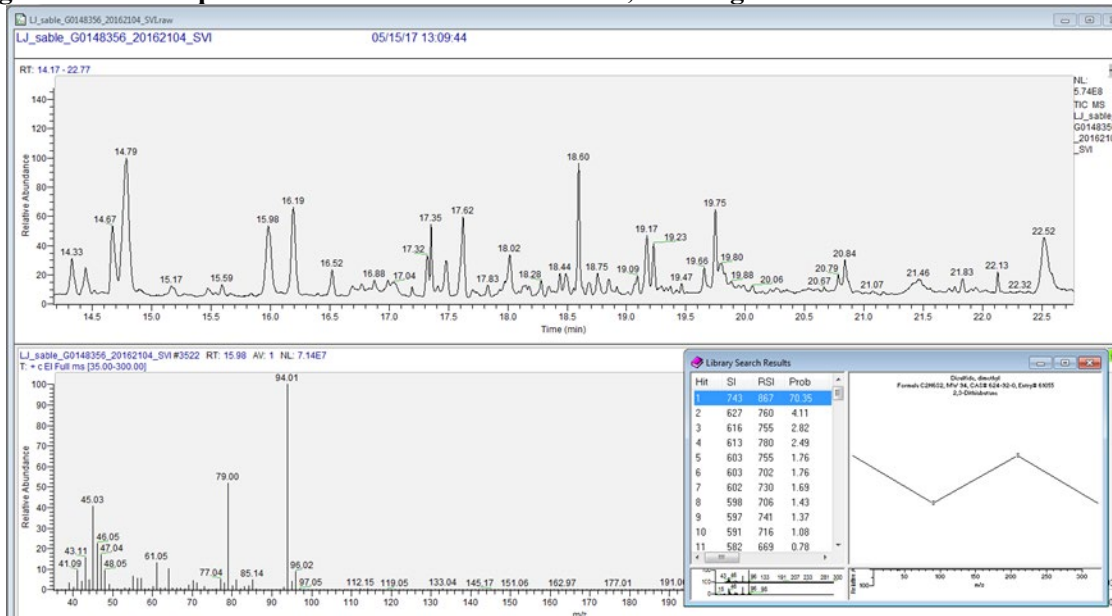
Figure 107 Mass spectra of a full sample run, showing dimethyl disulfide
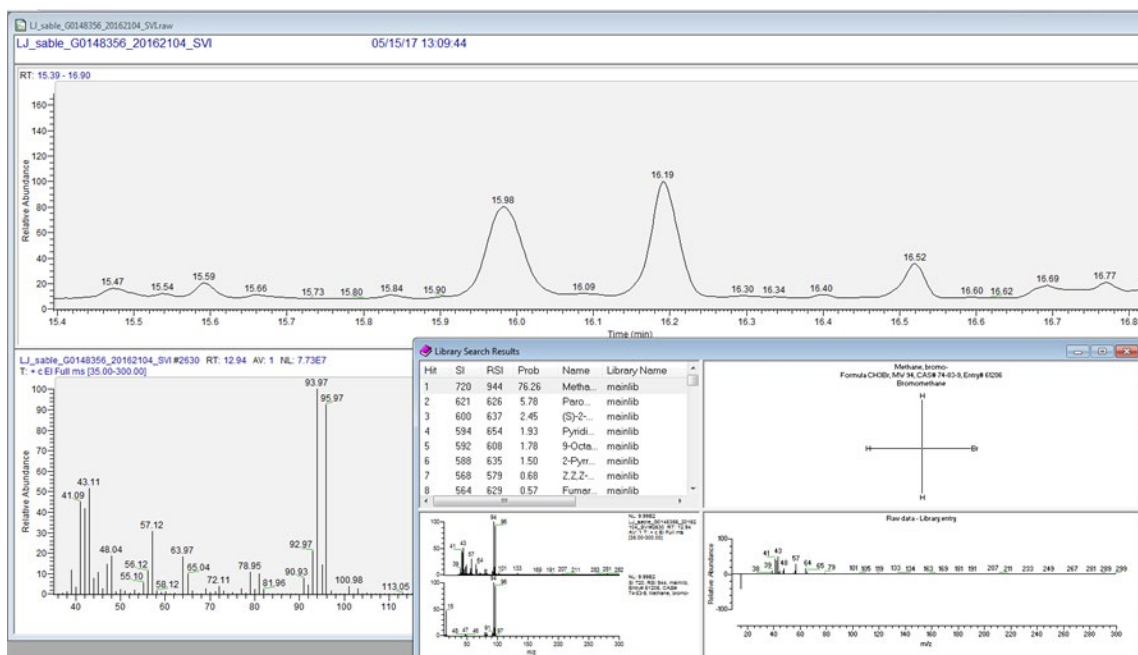
Figure 108 Enlarged mass spectra of a full sample run, showing bromomethane

The most commonly detected VOCs are listed alphabetically in Table 20 and assigned to one or more likely sources; marine, anthropogenic, or terrestrial, based on previously published literature. A "(?)" was used to indicate the best possible source based on chemical composition when the literature survey was insufficient in determining the source.

Table 20 Possible Sources of the most commonly detected compounds on Sable Island. A =
Anthropogenic, M = Marine, T = Terrestrial, (?) = Most likely source.

VOC	Source	Citation
1,2-Dichlorobenzene	A/M	(Colomb et al., 2008; Howard, 1990)
1-Hexanol	M / T	(Evans, 1994; Holopainen, 2004)
1-Trichlorotrifuoroethane	A	(Walker et al., 2000)
2-Bromoheptane	M (?)	N.A
2-Bromooctadecanal	A	(Kaska et al., 1991; Yang et al., 2015)
2-Chlorooctane	M	(Sabolis, 2010)
3-Chlorobenzotrifluoride	M (?)	N.A
4-Chloroheptane	M (?)	N.A
a-methylstyrene	A	(Miller et al., 1994)
a-pinene	M / T	(Palani et al., 2011; Sabolis, 2010)
Benzene	A	(Wallace, 1990)
Benzene-1-chloro-4-trifluoromethyl	A	(Lee et al., 2015)
Bromodichloromethane	M	(Goodwin et al., 1997)
Bromomethane	M	(Kladi et al., 2004; Moore and Tokarczyk, 1993)
Camphene	M / T	(Meskhidze et al., 2015; Sabolis, 2010)
Carbon disulfide	M	(Kim and Andreae, 1987).
Cumene	A	(Harrison et al., 1975)
Decane	A	(Harrison et al., 1975)
Dichloromethane	M	(Kladi et al., 2004; Moore and Tokarczyk, 1993)
Dimethyl disulfide	T/ M (?)	(Trabue et al., 2008)
Dimethyl trisulfide	T/ M (?)	(Trabue et al., 2008)
Ethylbenzene	A	(Liu et al., 2005)
Heptanal	T/ M (?)	(Dąbrowska et al., 2014)
Hexanal	M / T	(Evans, 1994; Holopainen and Gershenzon, 2010)
m-xylene	A	(Liu et al., 2005)
Naphthalene	A	(Harrison et al., 1975)
Nonane	A	(Harrison et al., 1975)
Octanal	T	(Holopainen, 2004)
p-cymene	T	(Holopainen, 2004)
Styrene	A/ M	(Jüttner et al., 1986; Miller et al., 1994)
Tetrachloroethene	M	(Colomb et al., 2008; Meskhidze et al., 2015; Sabolis, 2010)
Tetrachloromethane	A	(Walker et al., 2000)
Thiophene	A	(Sumpter, 1944)
Toluene	A	(Gelencsér et al., 1997; Liu et al., 2005; White et al., 2009)
Trichloroethene	M	(Abrahamsson et al., 1995)
Tricyclene	T/ M (?)	(Jüttner et al., 1986; Spanke et al., 2001)

From the probable emission sources listed above, it was found that marine emissions contributed the most to the VOC species (41%) on Sable Island, followed by anthropogenic and terrestrial sources respectively (Figure 109).
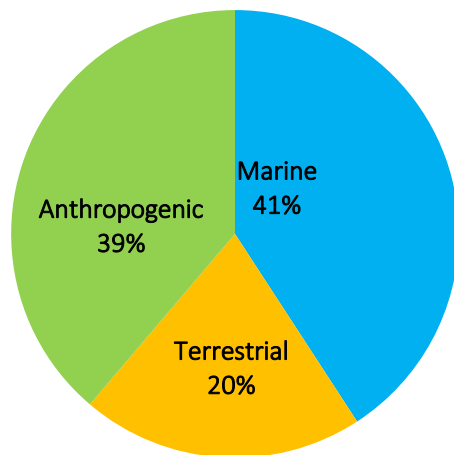
Figure 109 Percent contribution per category of VOC species based solely on literature survey of known emission sources

When literature-based source emissions were combined with HYSPLIT air mass back trajectories, the contribution of both marine and anthropogenic sources were equivalent at 38% each, while terrestrial sources contributed to 24% of all measured VOC species (Figure 110).
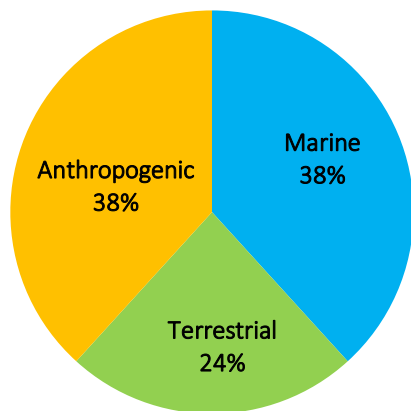
Figure 110 Percent contribution per category of VOC species, based on literature survey of emission sources combined with HYSPLIT air mass back trajectories

HYSPLIT air mass back trajectory analyses were also conducted along with VOC species source emissions to calculate the percent contribution of each source to every VOC species (Figure 111). 48% of all emissions were attributed to marine sources, 40% to terrestrial sources and 11% to anthropogenic sources.
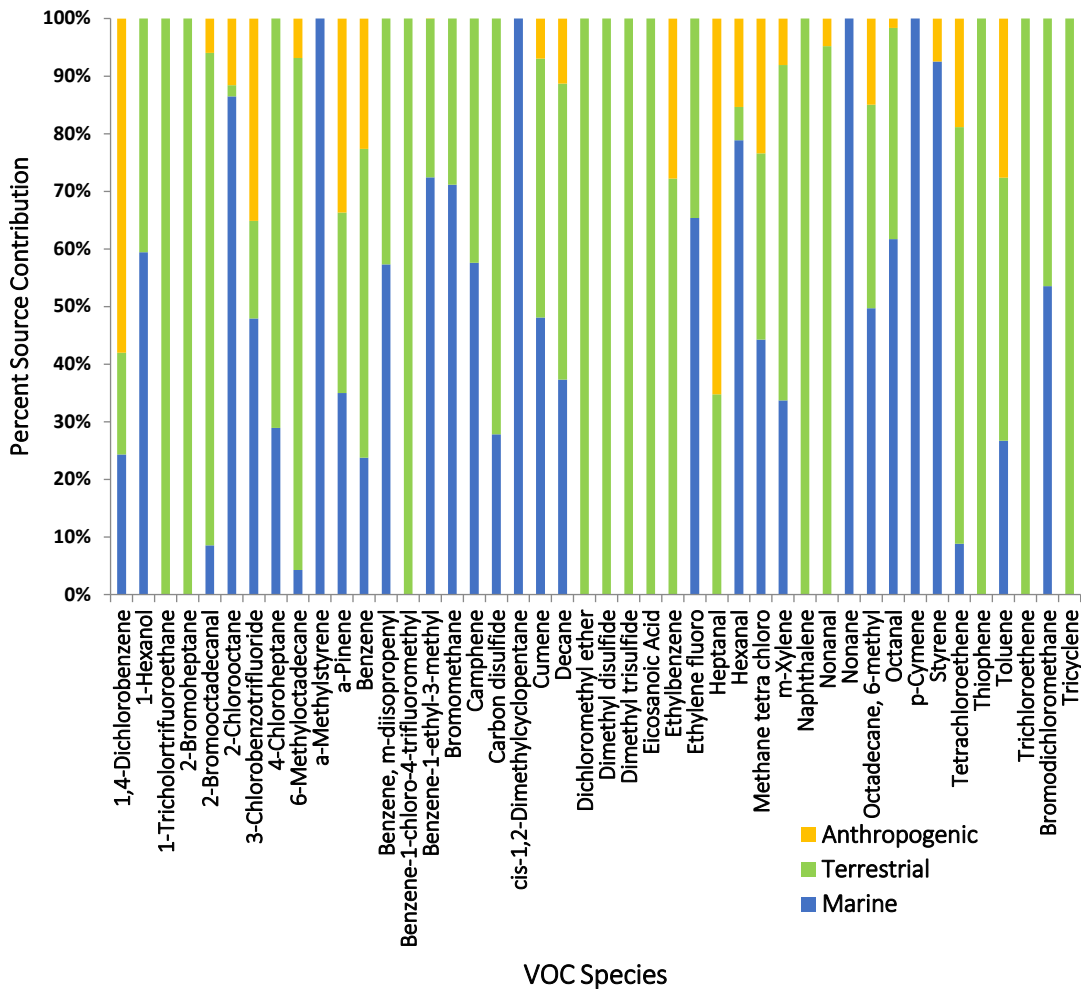
Figure 111 Percent contribution of the three sources to each VOC species analyzed

Additionally, total VOC concentrations (units ranging from ng/m^3 to μg/m^3) were calculated for each VOC species analyzed, and attributed to one or more of the three sources depending on its air mass back trajectory and possible emission sources (Figure 112 & Figure 113).
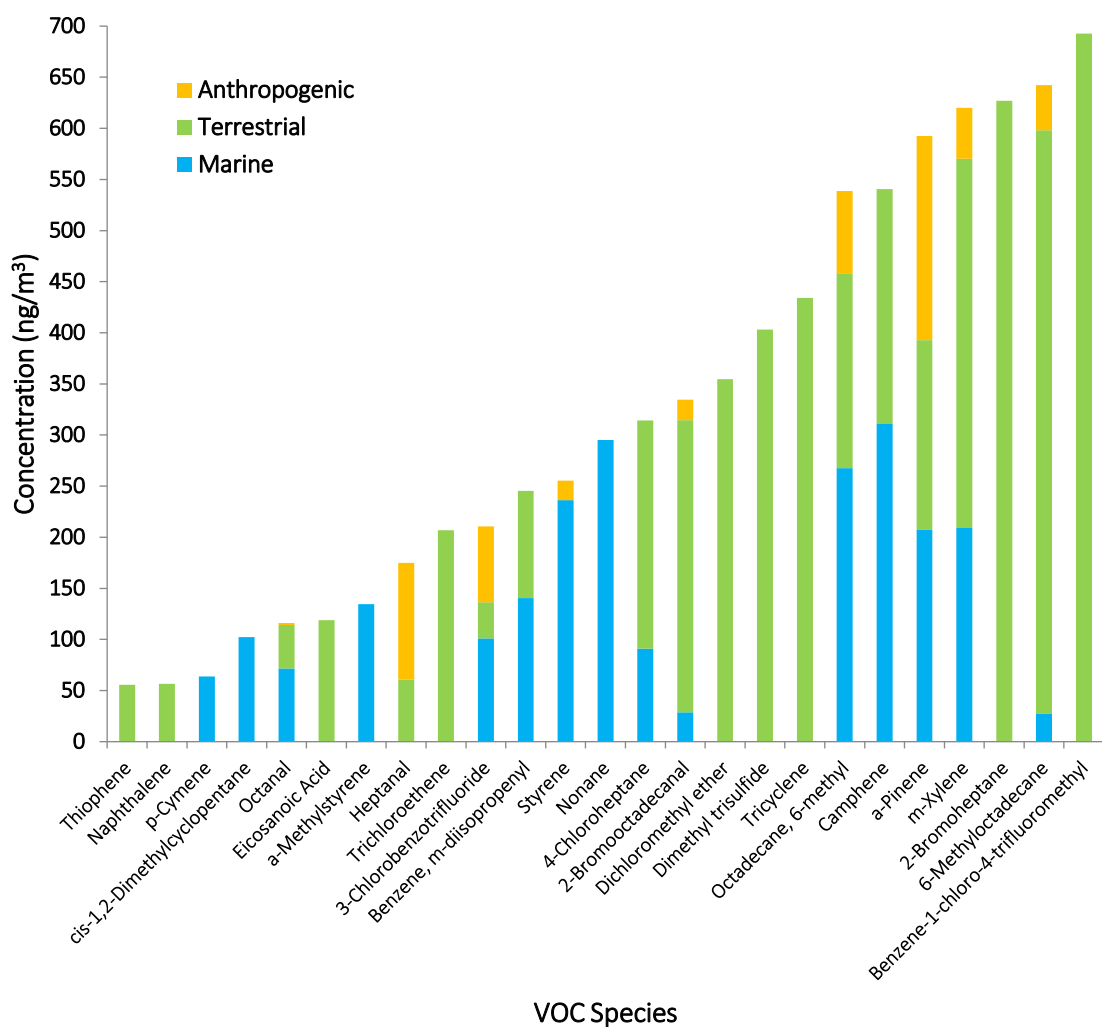
Figure 112 VOC source contributions to ng/m³ concentrations of Thiophene, Naphthalene, p-Cymene, cis-1,2-Dimethylcyclopentane, Octanal, Eicosanoic Acid, a-Methylstyrene, Heptanal, Trichloroethene, 3-Chlorobenzotrifluoride, Benzene- m-diisopropenyl, Styrene, Nonane, 4-Chloroheptane, 2-Bromooctadecanal, Dichloromethyl ether, Dimethyl trisulfide, Tricyclene, Octadecane, 6-methyl, Camphene, a-Pinene, m-Xylene, 2-Bromoheptane, 6-Methyloctadecane and Benzene-1-chloro-4-trifluoromethyl
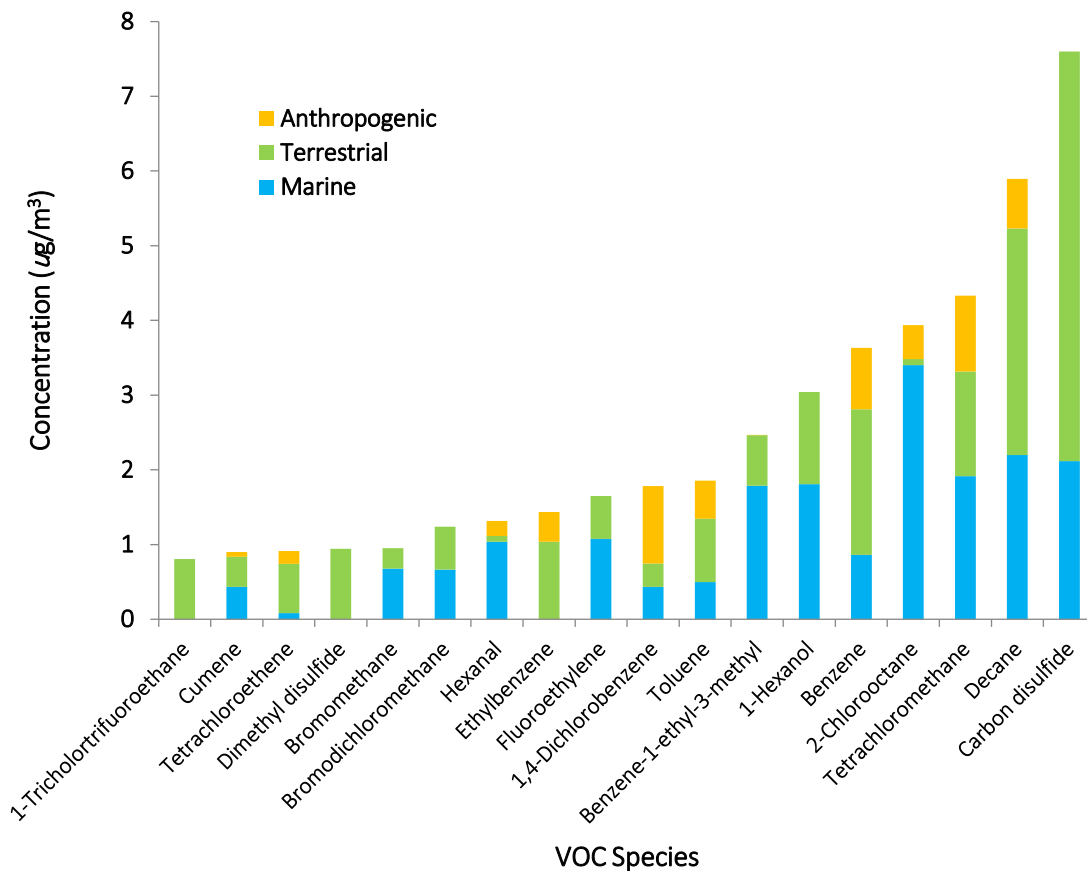
Figure 113 VOC source contributions to *μ*g/m³ concentrations of 1-Tricholortrifuoroethane, Cumene, Tetrachloroethene, Dimethyl disulfide, Bromomethane, Bromodichloromethane, Hexanal, Ethylbenzene, Fluoroethylene, 1,4-Dichlorobenzene, Toluene, Benzene-1-ethyl-3-methyl, 1-Hexanol, Benzene, 2-Chlorooctane, Tetrachloromethane, Decane and Carbon disulfide

4.4 Remote Sensing

The images below capture chl-*a* fluorescence around Sable Island, corresponding to spikes in VOC concentrations measured on Sable Island. Warmer colors (yellows, oranges and reds) signify high photosynthetic activity, while colder colors (blues and violets) represent low photosynthetic activity (Figure 114).

2016-05-12 (Spike 1)
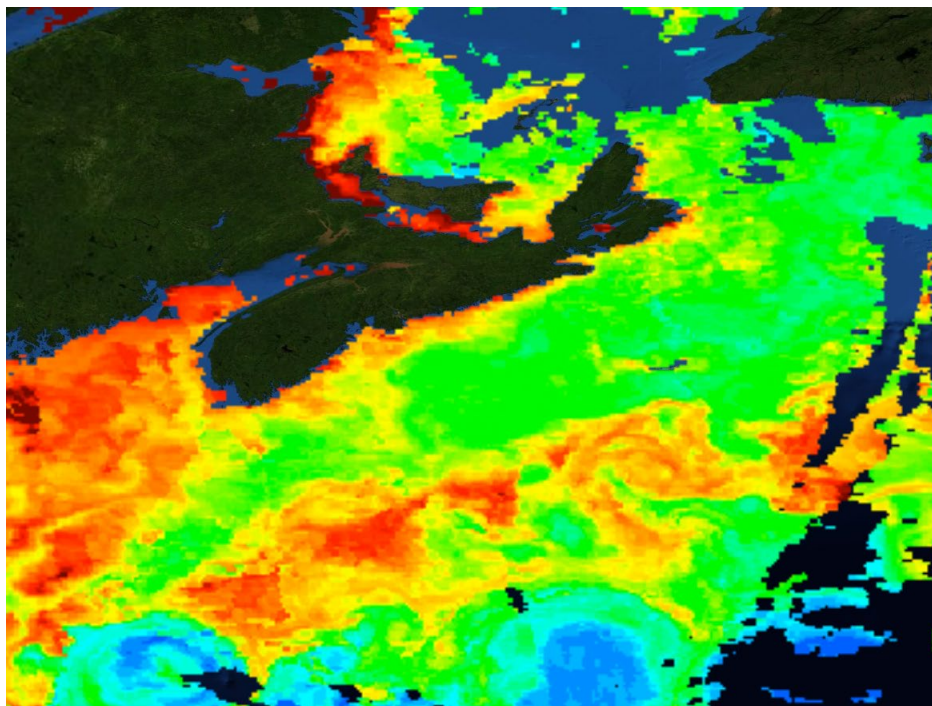
2016-05-23 (Spike 2)
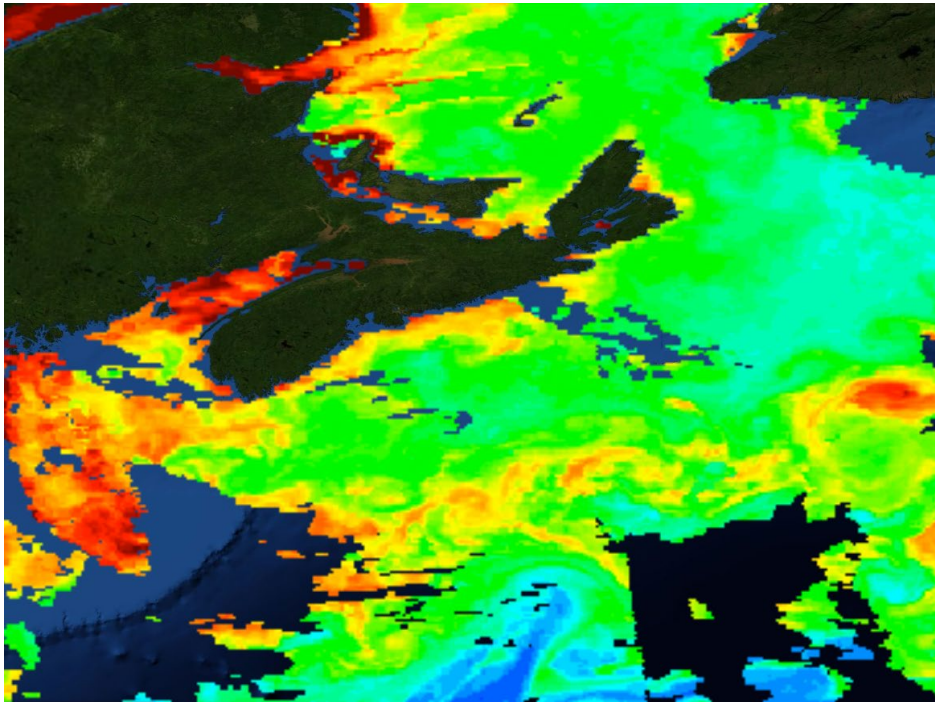
2016-06-03 (Spike 3)
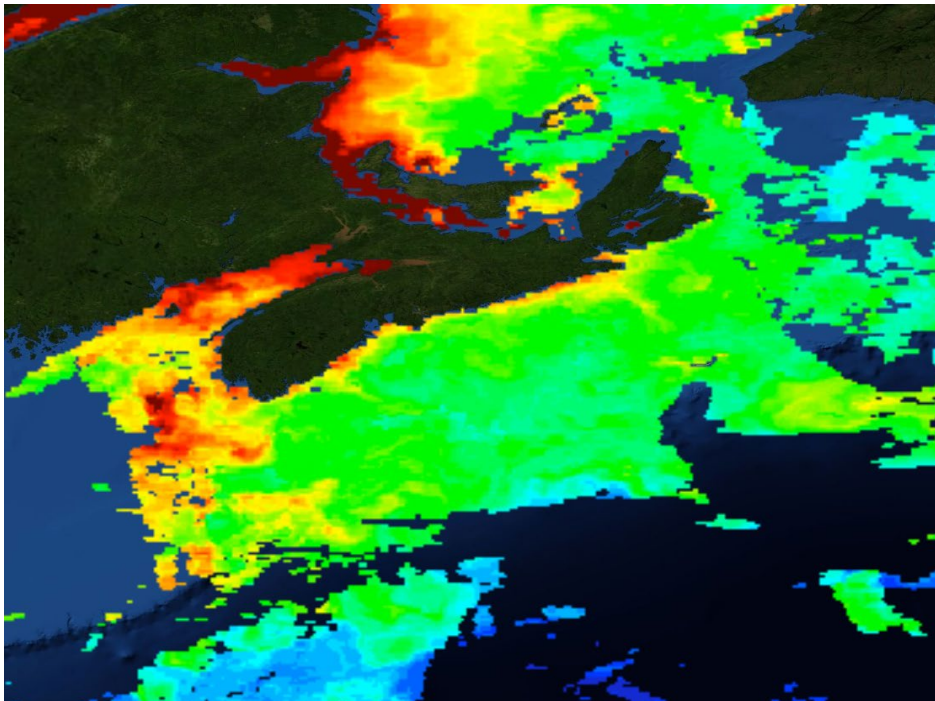
2016-06-18 (Spike 4)
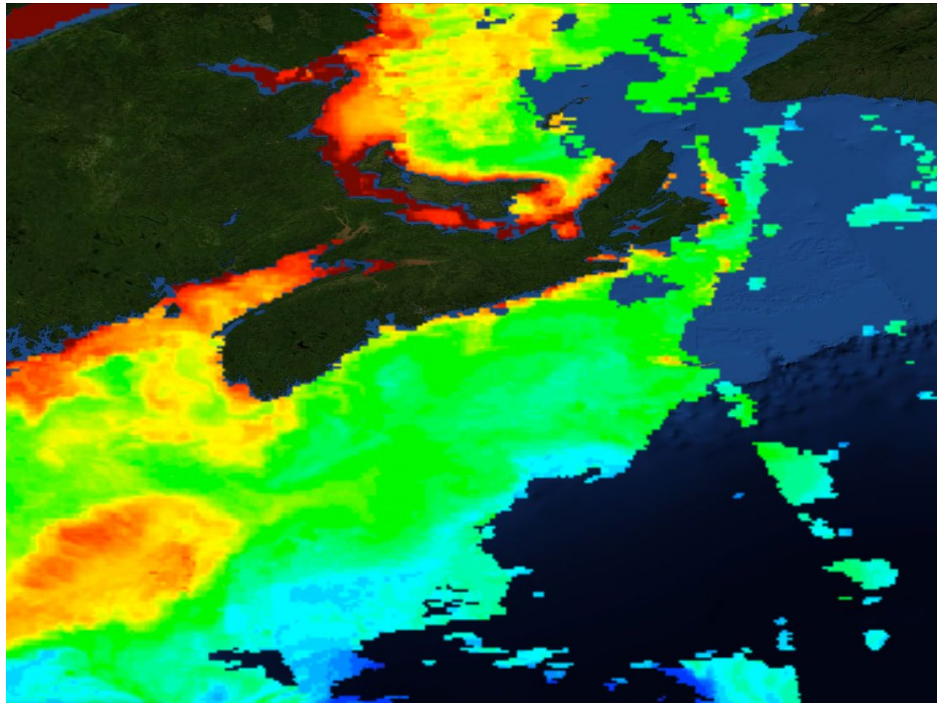
2016-07-01 (Spike 5)
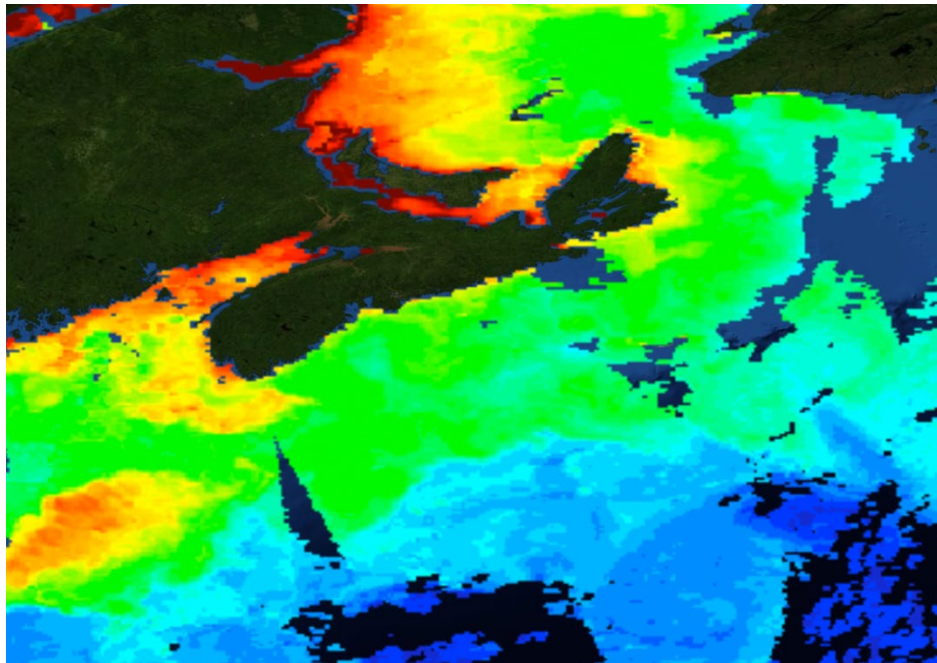
2016-07-13 (Spike 6)
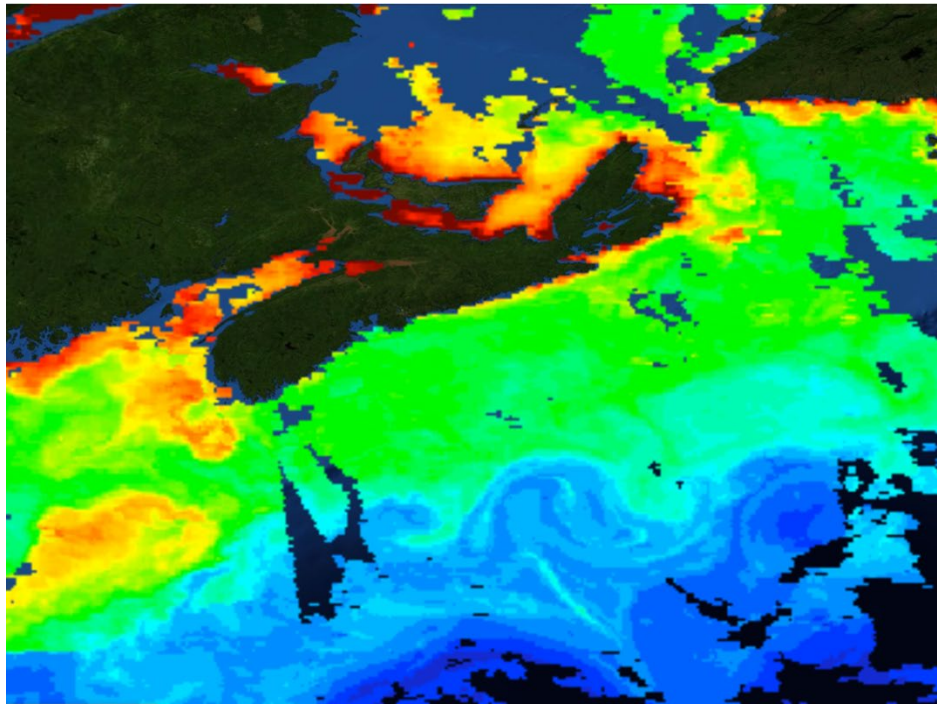
2016-07-16 (Spike 7)
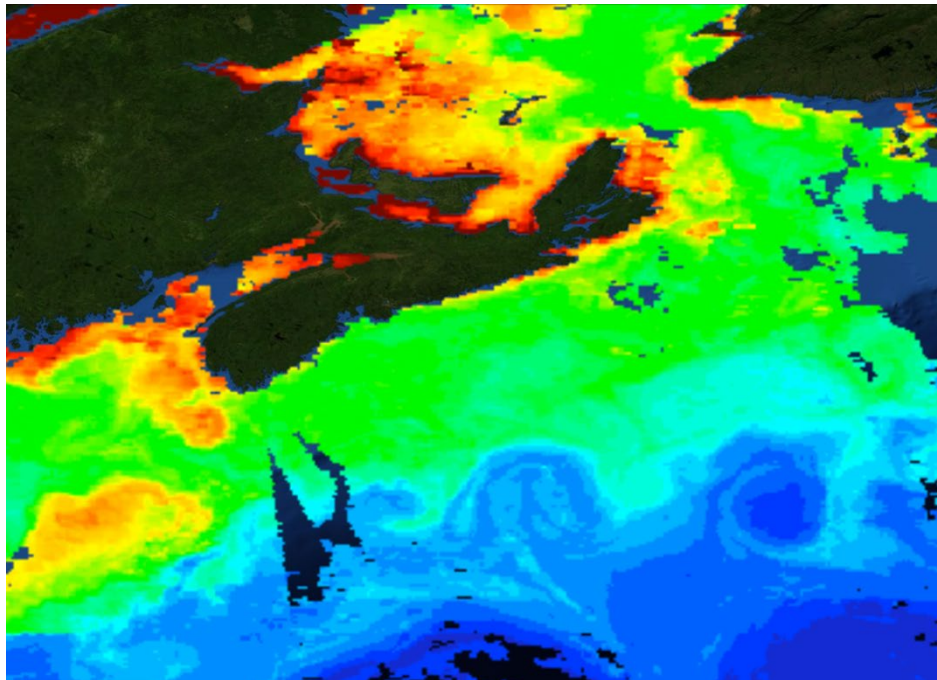
2016-07-25 (Spike 8)
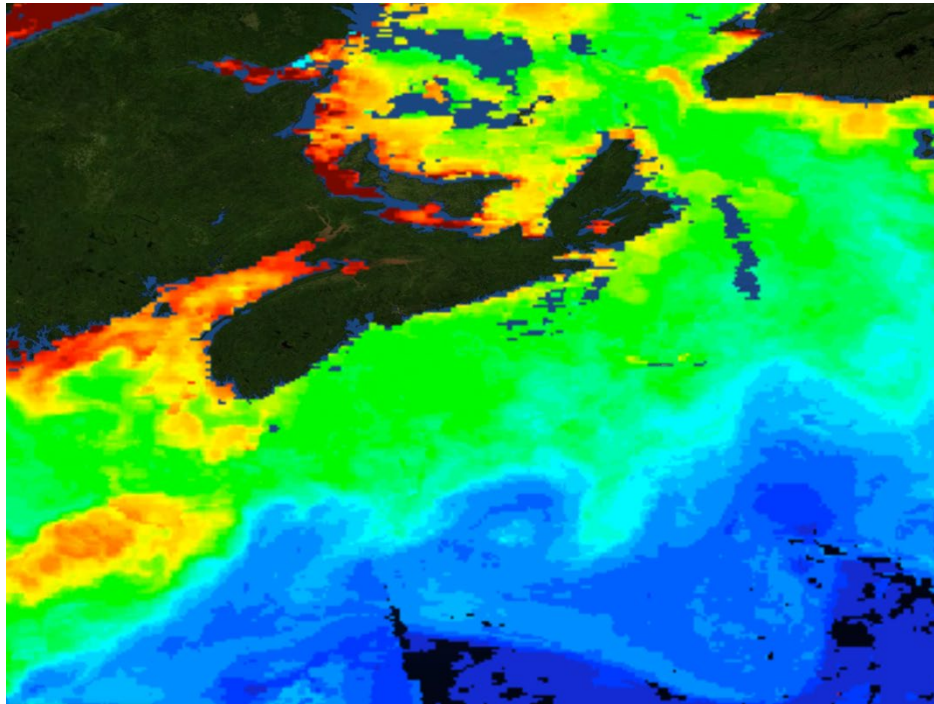
2016-08-11 (Spike 9)
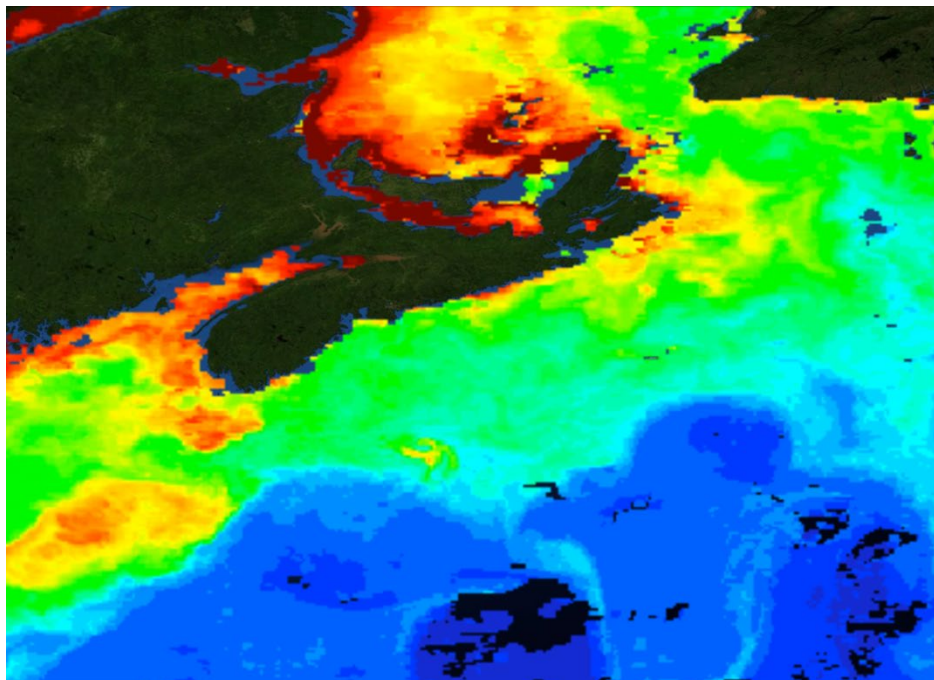
2016-08-24 (Spike 10)
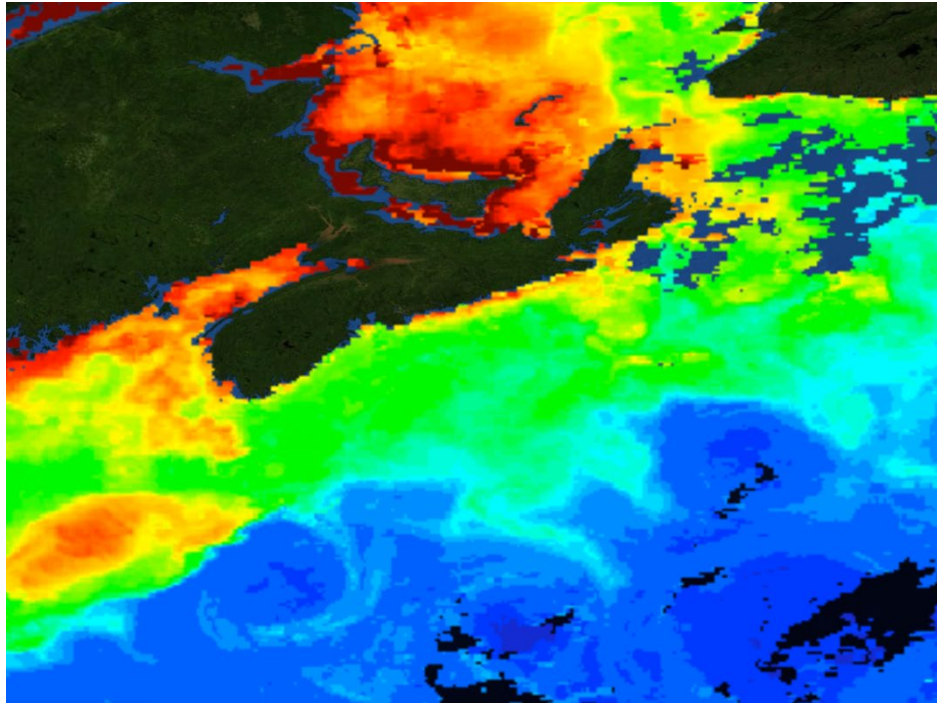
2016-08-27 (Spike 11)
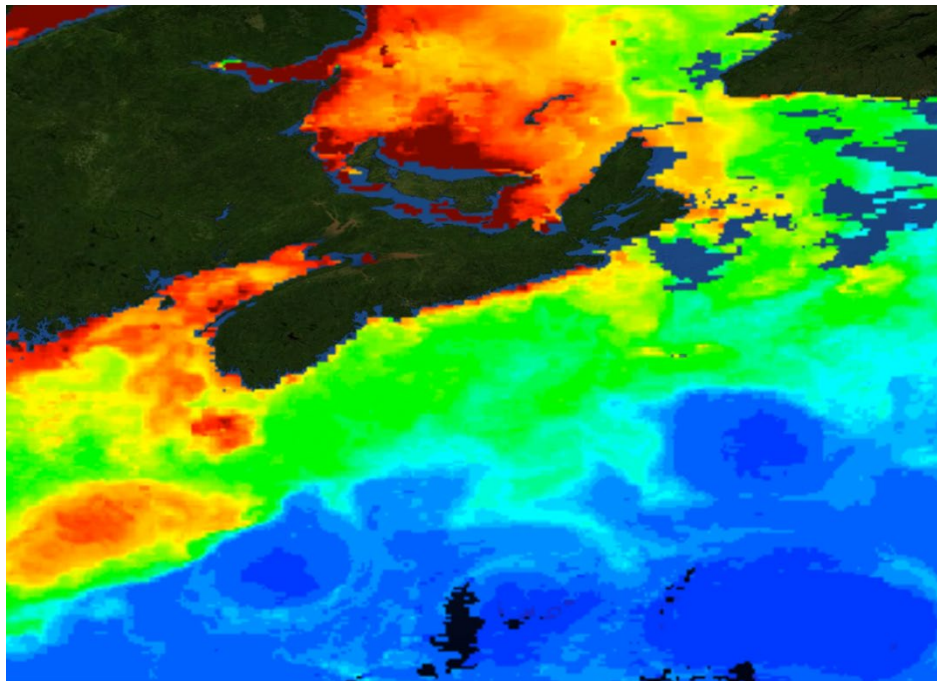
2016-09-12 (Spike 12)
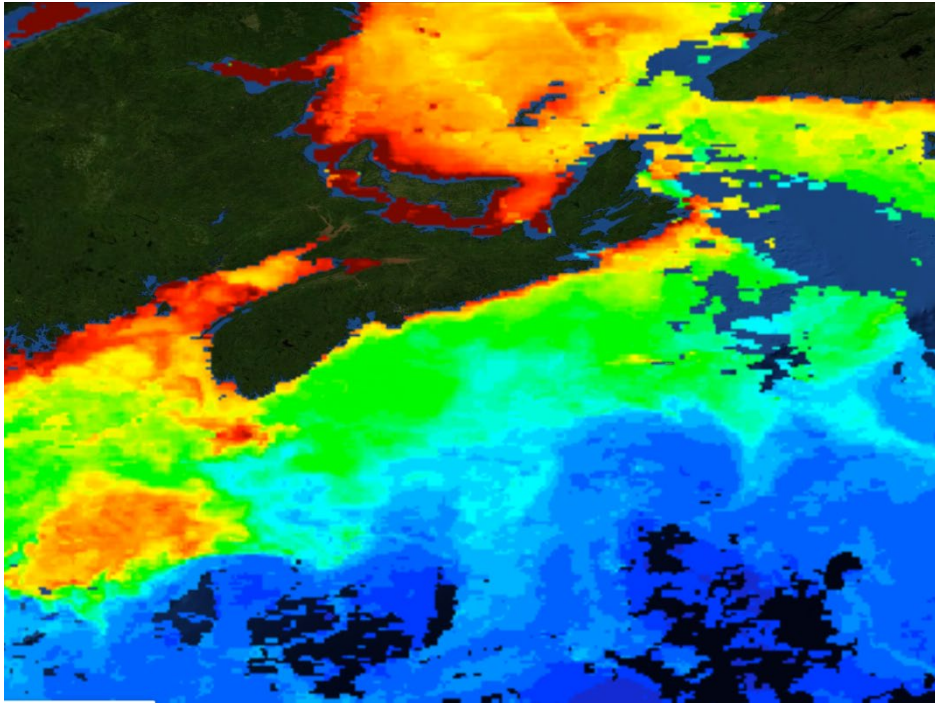
2016-09-18 (Spike 13)
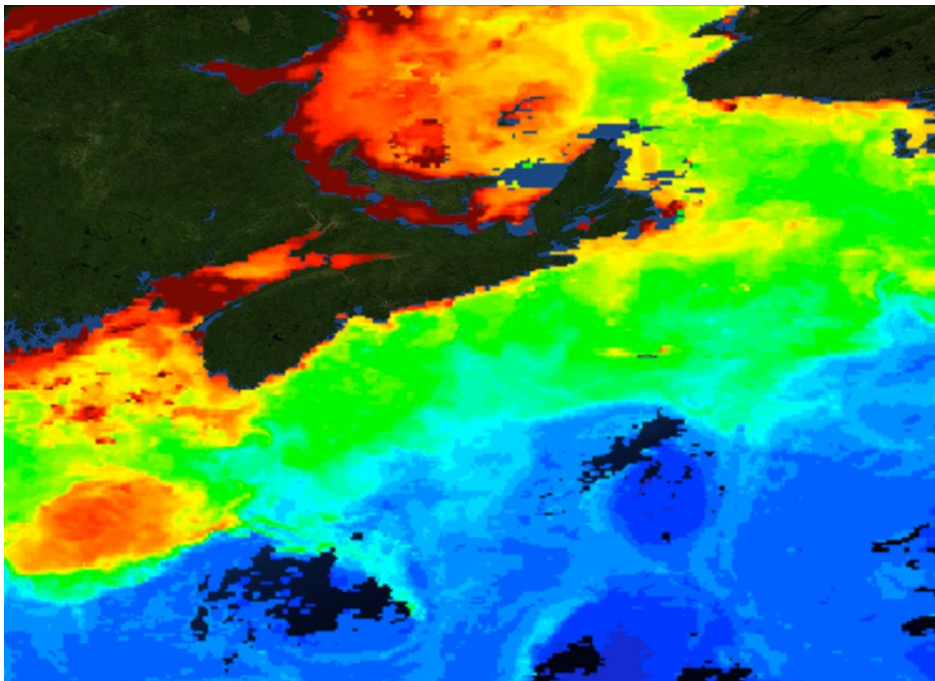
2016-09-26 (Spike 14)
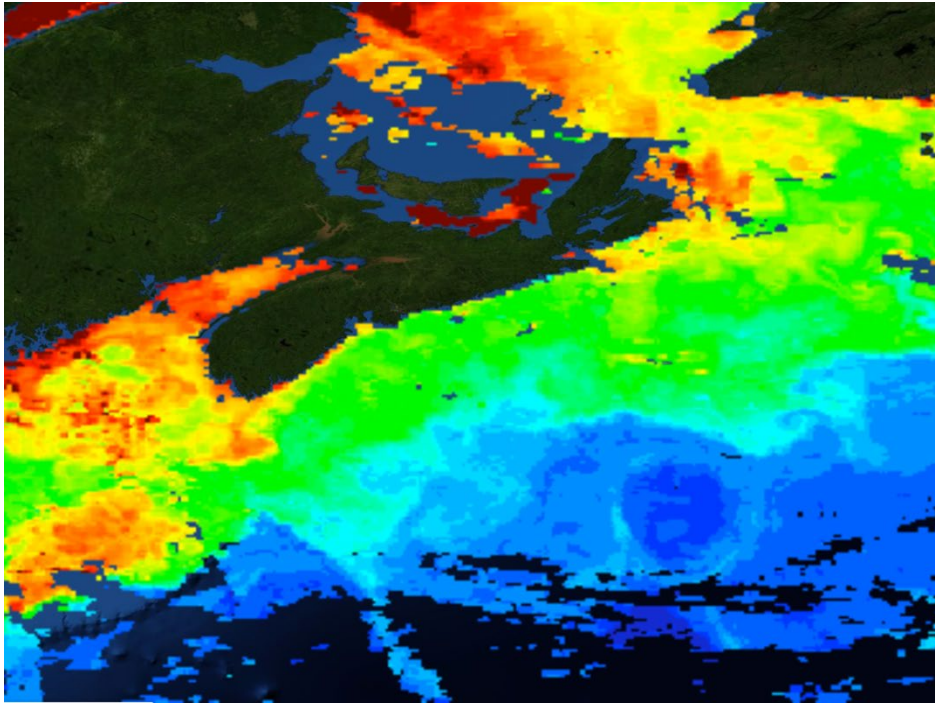
2016-10-10 (Spike 15)
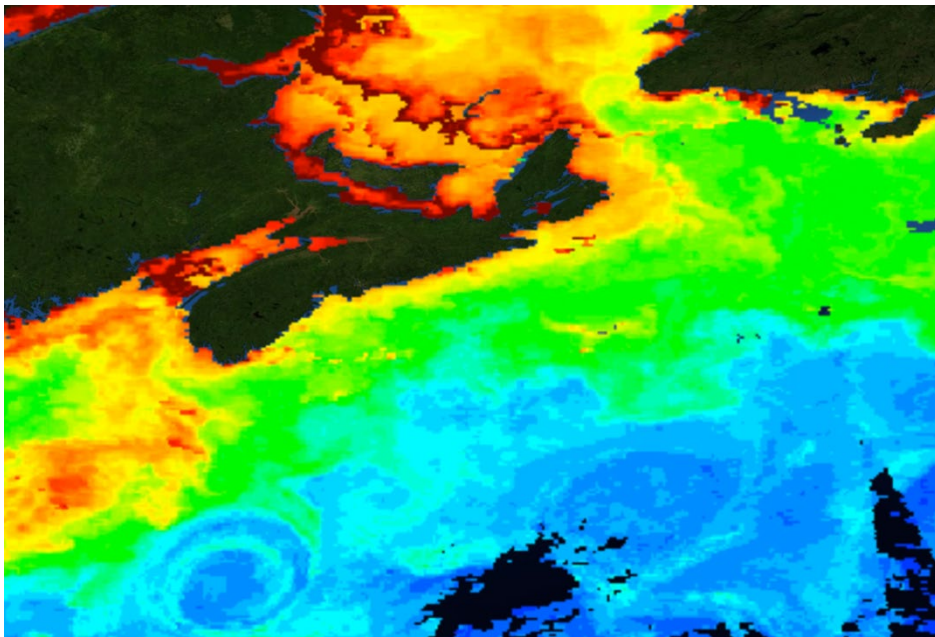
2016-10-22 (Spike 16)
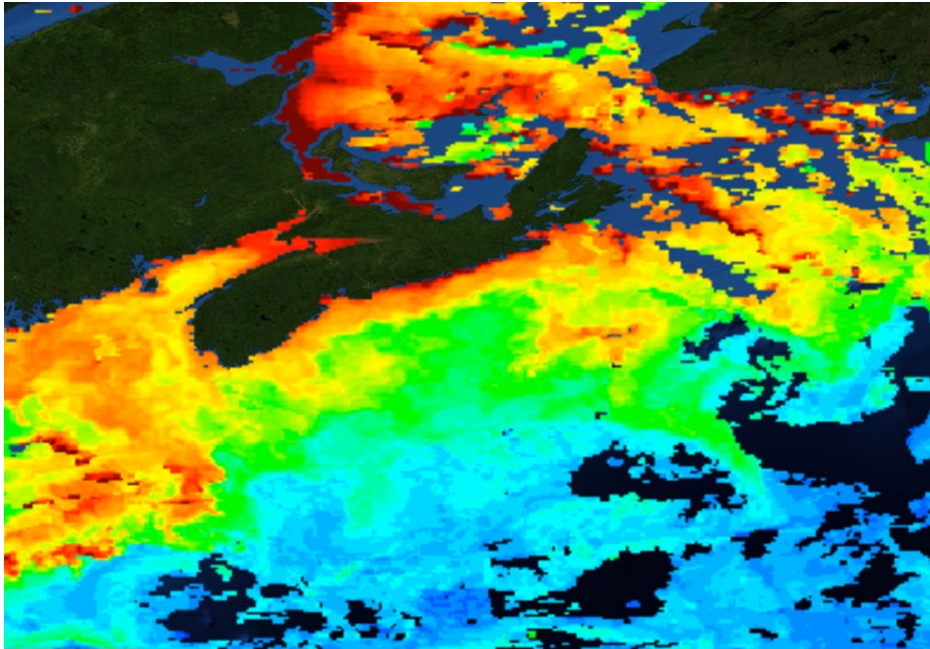
Figure 114 16 separate MODIS- Aqua chl-*a* fluorescence images around Sable Island for periods corresponding to spikes in VOCs

4.5 Discussion of VOC results

The purpose of this part of the ESRF study was to analyze long-term temporal trends in total marine VOC emissions on Sable Island and to use an amalgamation of scientific tools to identify and separate VOC species into their appropriate emission sources.

4.5.1 Meteorology

The temperature profile on Sable Island was relatively mild during winter months considering its Northern Atlantic location (

Table 12). This is in part due to the island's proximity to the Gulf Stream, which exposes the island to warmer waters and wind (Taylor and Stephens, 1998). A similar temperature trend was also observed in 2015 (Qadoumi, 2016), except the mean annual temperature in 2016 (9.43 °C) was 0.4 °C warmer than in the 2015 study.

Interestingly, the seemingly unnatural maximum temperature of 53.8 °C also appeared in 2015, and a review of online weather data sources confirmed this unusual value. With that said, an instrument malfunction is a probable cause to this error (Forbes, 2017- personal communication), and outliers were taken into consideration during data analysis.

As expected, local air flow on Sable Island was from a WSW direction (Figure 89), consistently with previous wind patterns experienced on Sable Island and the Maritimes (Barnett, 2016; Qadoumi, 2016; Waugh et al., 2010). This is also confirmed with the HYSPLIT model for long range wind direction, showing that local wind often blew from a WSW direction, regardless of the previous pathway taken. Wind speed was not fully examined in this study; however, it may be beneficial to inspect the relationship between wind and marine emissions as higher wind speeds can cause an increased rate of wave breaks, contributing to a higher release of VOC from the ocean's surface (Turner et al., 1996).

4.5.2   Temporal Patterns in VOC Concentrations

To our knowledge, this is the first study to examine long-term temporal trends of total VOC emissions in a marine setting. Distinct seasonal variations were measured where spring and summer had significantly higher VOC concentrations than autumn and winter. The increase in VOCs during the spring coincides with the annual NW Atlantic phytoplankton spring bloom, which has been observed for many years (Craig et al., 2014; Mahadevan et al., 2012; Siegel et al., 2002). Remote sensing data also show a substantial amount of chl-*a* around Sable Island on May 12th, 2016 (Figure 115), signifying high phytoplankton activity. This occurs around the same time period during which the first sharp increase in VOC concentrations was observed (Figure 98). Additionally, laboratory and mesocosm studies show that increases in phytoplankton populations carry with them a rise in physiological and chemical reactions (Turner et al., 1996), further supporting the relationship between total VOCs and phytoplankton activity observed in this study.
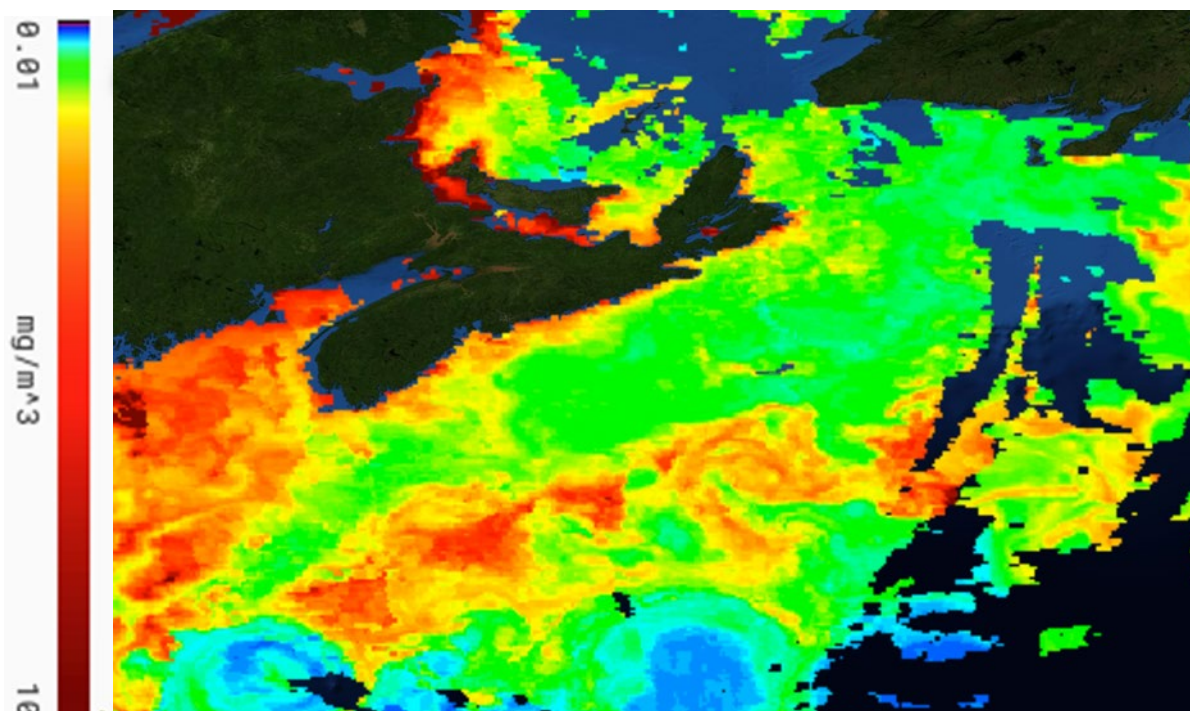
Figure 115 MODIS-Aqua Chl-*a* fluorescence concentrations showing substantial phytoplankton activity around Sable Island on May 12th, 2016

Following the spring season, summer had the largest spikes and highest VOC concentrations of all seasons, with the highest concentration peaking off at 20,029 ppb on August 22nd, 2017.

Interestingly however, remote sensing data show a marked decrease in chl-*a* fluorescence during this period (Figure 114), prompting the belief that phytoplankton activity is reduced. This can be further supported by the increase in ocean stratification as a result of warming, reducing the amount of nutrients available for phytoplankton consumption (Capotondi et al., 2012). Nevertheless, *in situ* measurements showed a large bloom of dinoflagellates on the Scotian Shelf peaking around the end of August, which can contribute immensely to the VOC concentrations measured here (Craig et al., 2014). The lack of remote sensing evidence of chl-*a* fluorescence in this study can be explained by the photo-acclimation of phytoplankton to high irradiance during the summer by reducing intracellular chlorophyll (MacIntyre et al., 2002; Moore et al., 2006). This was also indirectly observed by Craig et al., (2014) and is a common phenomenon exhibited by other terrestrial plants when exposed to strong sunlight (Østrem et al., 2015).

Strong diurnal fluctuations of total VOCs were most apparent during summer months, with concentrations peaking around mid-day and early afternoon (Figure 116). This can be explained by phytoplankton's dependence on light and their increased photosynthetic activity with light availability. However, a large portion of phytoplankton emissions are not released by regular metabolic activity, but instead when cells are under physical, chemical or biological stress (Meskhidze et al., 2015). Tamburic et al. found that phytoplankton exhibit photosystem damage around mid-day due to intense sunlight and temperatures, better explaining the diurnal spikes in VOC concentrations seen in this study (Tamburic et al., 2014). Furthermore, a somewhat puzzling "bump" was consistently observed later in the afternoon in diurnal total VOC plots (Figure 116). These spikes coincide with periods of high physiological activity by phytoplankton and increased cell death, which can cause phytoplankton to release more VOC compounds (Berges and Falkowski, 1998; Veldhuis et al., 2001).
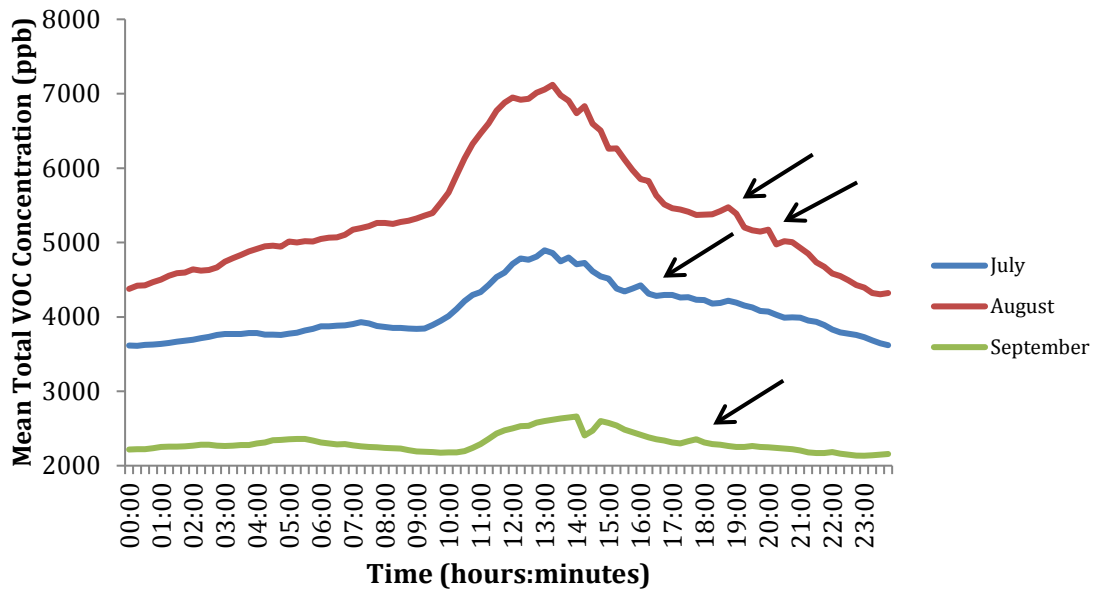
Figure 116 Example of VOC "bumps" in the later afternoon hours in July, August and September

Further evidence of phytoplankton emission of VOCs is seen in the close relationship between temporal variations in temperature and changes in total VOC concentrations (Figure 117). This is further supported by the positive correlation between phytoplankton concentration and temperature shown by Craig et al. (2014) and the increased rate of gas emissions in warmer water (Wiebe and Gaddy, 1940).
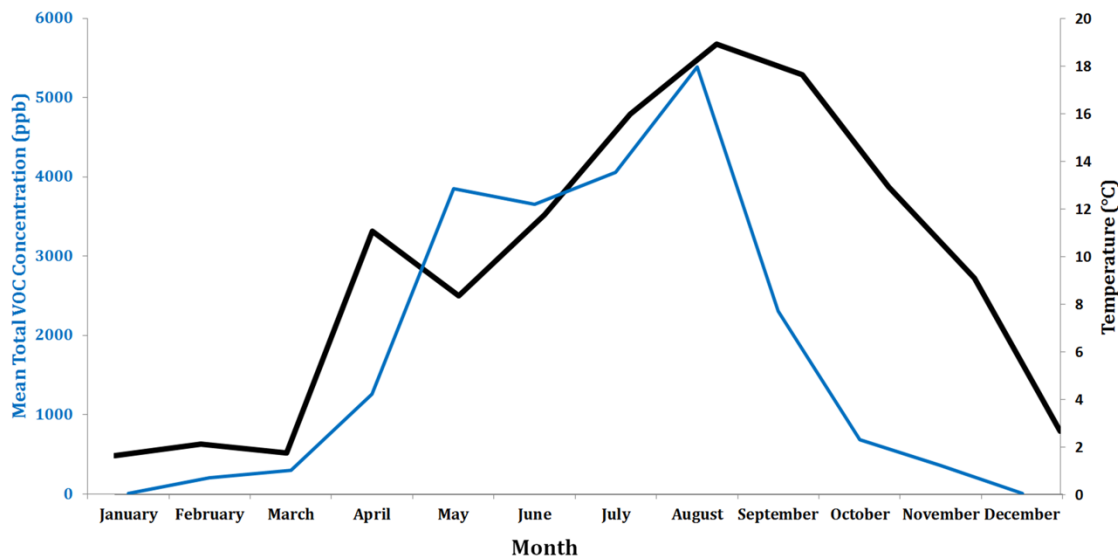
Figure 117 Temperature (°C) and total VOC concentration (ppb) in 2016 plotted against a common timeline (month)

Nevertheless, increases in temperature during the spring and summer seasons also bring with them a rise in terrestrial biogenic emissions (Seco et al., 2011), forest fires and anthropogenic activity; all of which can be sources of VOCs on Sable Island. Further inspection of VOCs and source sector analysis is therefore clearly needed.

4.5.3   Source Sector Analysis

A twice-daily 5-day air mass back trajectory (HYSPLIT) model showed that only 26.03 % of air trajectories pass solely over marine environments before reaching Sable Island in 2016 (Figure 100), with the rest of the trajectories passing over terrestrial and anthropogenic sources of VOCs; however, spring and summer seasons had significantly higher marine trajectories (~35%) than the other seasons. When total VOC spikes were cross-examined with HYSPLIT analyses, it was shown that they were mostly associated with marine sources (68.75%), followed by anthropogenic (18.75%) and terrestrial (12.5%) sources respectively. When HYSPLIT air mass back trajectories were cross-examined with specific VOC species identified using GC-MS, it was found that marine and anthropogenic sources contributed to 38% each to the total emissions and terrestrial sources contributed to 24%. This apparent discrepancy can be due to several reasons.

 The presence of offshore oil and gas platforms around Sable Island is likely to contribute to the total VOC concentrations measured in this study. Platforms Deep Panuke, Alma and Thebaud are located upwind of the island (based on wind patterns discussed previously) and would be

considered as 'Marine' sources using HYSPLIT analysis. Nonetheless, crude oil and refined fuel related compounds such as 2-bromooctadecanal, cumene and thiophene do not have natural marine sources, and it would therefore be incorrect to consider them as marine emissions.

Many VOC species also have several sources of emission and complex chemistry. For example, *a*-pinene is a compound produced widely by coniferous trees, has been shown to be emitted by marine algae (Sabolis, 2010); and 1-hexanol, a compound known for its "freshly cut grass" scent, can be produced by terrestrial and marine photosynthetic organisms (Evans, 1994); with air mass back trajectories showing both *a*-pinene and 1-hexanol to originate mostly from marine and mainland sources. While all of these sources are viable, both of the compounds have relatively short atmospheric lifetimes (Montenegro et al., 2012), which greatly reduces the possibility of this compound reaching Sable Island from far terrestrial sources and increasing the likelihood of them being local emissions. Additionally, 1-hexanol may be released from damaged grass on the island due to grazing by horses or local insects (Scala et al., 2013), and some sulfur containing compounds including dimethyl disulfide may be emitted by horse feces; especially considering the regular close proximity of horses to the instruments used in this study (Garner et al., 2007). With that said, it is difficult to determine the true sources of compounds without considering all possible emitters, keeping in mind that all of air mass back trajectories pass over at least 290 km of marine environments before reaching Sable Island, regardless of their original source.

Figure 118 Sable Island horses only meters away from the air chemistry building and air measurement instruments

Marine biogenic VOCs are also notoriously difficult to analyze. Not only are they difficult to collect (i.e. chloromethane), many of them undergo rapid and complex chemical reactions when released into the atmosphere. For example, carbon disulfide, identified in this study as a mostly terrestrial VOC with substantial marine emissions, has been found in north Atlantic marine environments but has presented challenges in its identification and separation from dimethylsulphide (DMS) since it was first detected in 1971 (Kim and Andreae, 1987) - DMS was not detected in this study, but its presence is synonymous with phytoplankton blooms.

There is noteworthy phytoplankton activity in the winter months in the north Atlantic due to the uptake of nutrients in deep-ocean mixing (Behrenfeld, 2010; Eppley, 1972; Mahadevan et al., 2012). However, VOCs from these populations were not detected by our instruments. In addition to the relatively small phytoplankton concentration in winter, this can be explained by the less frequent calibration and maintenance trips during the winter because of bad weather, and several malfunctions of the instrument in December and January. Continuous, real-time identification and quantification of VOC species would help resolve these discrepancies, but due to logistical and technical issues and of the limitations of funding, it was impossible to install an appropriate instruments on Sable Island for this study.

4.6 Size-Resolved Particulate Matter Number and Mass Concentration

This section covers the size-resolved particulate matter number and mass concentration results from January 1st, 2016 to December 31st, 2016. Comprehensive year-long daily, monthly, and seasonal plots, comparison, and correlation plots will also be displayed. All daily plots were generated from daily data calculated based on an average of 15-interval measurement.

All measurements taken from Sable Island in 2016 were in UTC, only meteorological data was used in local time, time zone difference can be seen in Figure 119. Seasons were defined as follows: Spring: April, May, and June; Summer: July, August and September; Fall: October, November and December; Winter: January, February and March.

Figure 119 UTC and local time converter regarding daylight saving time in 2016

4.6.1 PM Mass Concentration

Mass concentration of particulate matter with a median aerodynamic diameter between 1-10 µm were measured at a temporal resolution of 15 minutes continuously using a TSI DustTrak DRX model 8533. The descriptive statistics for $PM_{1/2.5/4/10/TSP}$ are shown in Table 21.

Table 21 Descriptive Statistics for PM$_{1/2.5/4/10/TSP}$

Variables	PM_1 [mg/m³]	$PM_{2.5}$ [mg/m³]	PM_4 [mg/m³]	PM_{10} [mg/m³]	TSP* [mg/m³]
n	32866	32866	32866	32866	32866
n missing	739	739	739	739	739
Completeness	97.75%	97.75%	97.75%	97.75%	97.75%
Min	0	0	0	0	0
25th Percentile	0.005	0.006	0.006	0.006	0.006
Median	0.009	0.009	0.009	0.009	0.010
Mean	0.011	0.012	0.011	0.012	0.012
75th Percentile	0.014	0.015	0.015	0.015	0.015
Max	0.087	0.093	0.124	0.124	0.127
IQR	0.010	0.010	0.011	0.011	0.011
Standard Deviation	0.009	0.01	0.010	0.010	0.010

* TSP = PM with diameters below ~60 µm

From Table 21, the data completeness for all PM mass concentrations was 97.75%. The mean (min:max *units*) for PM_1 = 0.011 (0:0.087 *mg/m³*), $PM_{2.5}$ = 0.012 (0:0.093 *mg/m³*), PM_4 = 0.011 (0:0.124 *mg/m³*), PM_{10} = 0.012 (0:0.124 *mg/m³*) and PM_{TSP} = 0.012 (0:0.127 *mg/m³*).

Figure 120 below a time series of $PM_{1/2.5/4/10/TSP}$ mass concentration at a temporal resolution of 15 minutes.
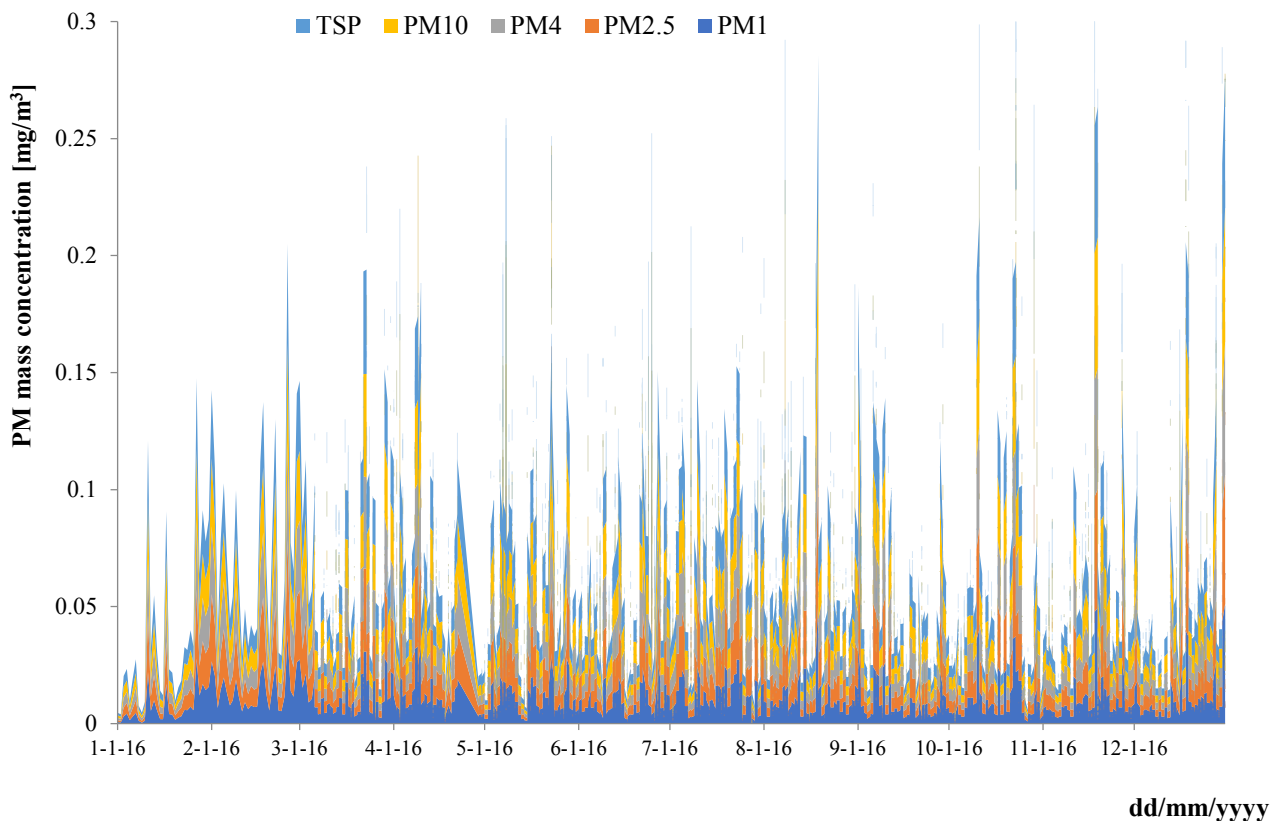
Figure 120 Annual cycle of PM$_{1/2.5/4/10/TSP}$ mass concentration (mg/m³) measured every 15 minutes on Sable Island in 2016

As can be seen in Figure 120, TSP and PM$_{2.5}$ accounts for most of PM mass concentration. Two salient features of the time series plot are the elevated PM mass concentrations on September 14th and December 31st.

Figure 121 below provides the monthly mean PM$_{1/2.5/4/10/TSP}$ mass concentration (mg/m^3) on Sable Island.
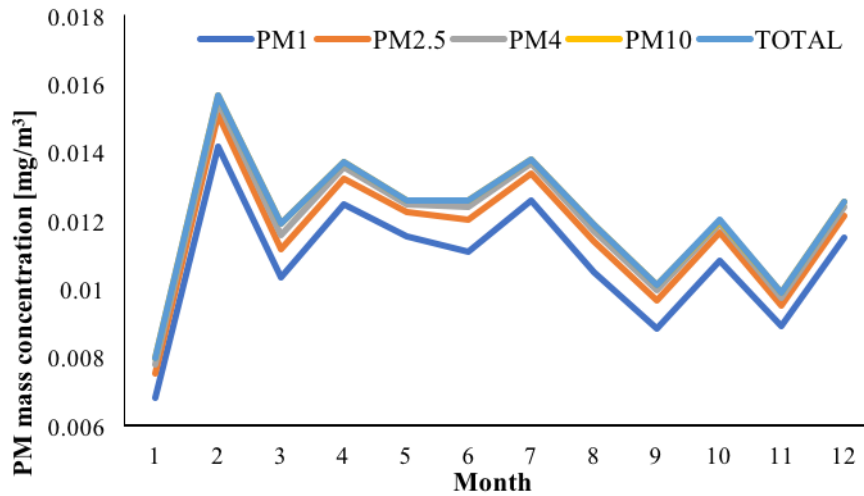
Figure 121 Mean monthly PM$_{1/2.5/4/10/TSP}$ mass concentration (mg/m^3) on Sable Island in 2016.

As can be observed in Figure 121, the mean PM concentration reaches its highest concentration in February, with September and November having the lowest PM mass concentrations.

4.6.2 PM Number Concentration

The number concentrations of particulate matter on Sable Island were measured continuously at a temporal resolution of 15 minutes using the TSI APS model 3321. Particle number concentrations were counted in each of 52 size fractions, also known as 'channels'. For ease of analysis, and data visualization purposes, these 52 size fractions were averaged into the same five size fractions that correspond to the PM mass concentration size fractions presented above, e.g. 1, 2.5, 4, 10 and 20 μm. Table 22 below shows descriptive statistics number concentration of $PM_{1/2.5/4/10/20}$.

Table 22 Descriptive statistics for $PM_{1/2.5/4/10/20}$ number concentration

	PM_1 [Particle #/cm^3]	$PM_{2.5}$ [Particle #/cm^3]	PM_4 [Particle #/cm^3]	PM_{10} [Particle #/cm^3]	PM_{20} [Particle #/cm^3]
n	35136	35136	35136	35136	35136
n missing	14639	14639	14639	14639	14639
Completeness	58.3%	58.3%	58.3%	58.3%	58.3%
Min.	1879	64	3	1	1
1st Percentile	11480	1565	90	5	1
Median	18360	2578	174	9	1
Mean	21249	2970	257	20	1
3rd Percentile	27580	3842	323	20	1
Max	79590	20123	3856	491	26
IQR	2932.5	2920.5	2421	486	310
Standard Deviation	19676.6	3496	562	81	3

As been shown in Table 22, the data completeness for PM number was 58.3%. There are several gaps in annual time series plot due to the APS malfunctioning. The first data gap occurred on January 7th at 14:45, the instrument was running but stopped recording, it started recoding again on January 24th 00:00. The instrument was removed from the island in August for repair and was installed again on August 31st but failed to function. A replacement instrument was loaned from the University of Calgary and installed on December 16th.

The mean (min:max *units*) for $PM_{1/2.5/4/10/20}$ is $PM_1 = 21249$ ($1879 : 79590$ *#/cm³*), $PM_{2.5} = 20122.8$ ($64.0 : 20122.8$ *#/cm³*), $PM_4 = 257.4$ ($3.26 : 3856.33$ *#/cm³*), $PM_{10} = 19.6$ ($1.3 : 490.8$ *#/cm³*) and $PM_{20} = 1.5$ ($1.0 : 25.5$ *#/cm³*).

Annual temporal analysis (Figure 122) investigated the peaks and troughs in the $PM_{1/2.5/4/10/TSP}$ mass concentration to aid in the determination of their sources.
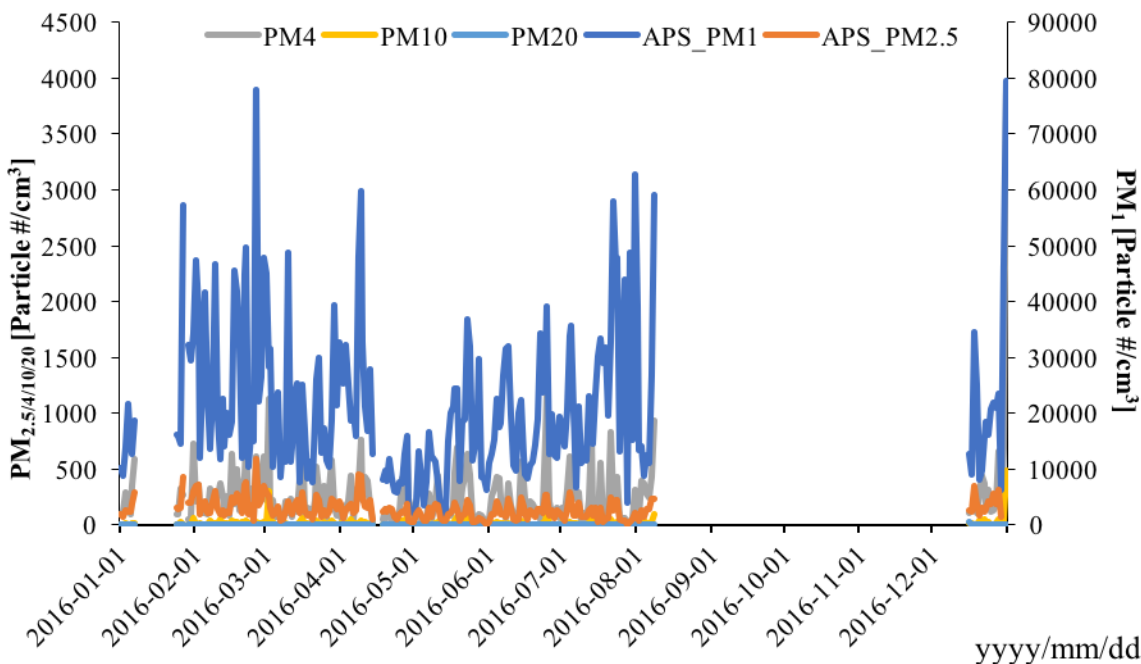
Figure 122 $PM_{1/2.5/4/10/20}$ number concentration (particle #/cm³) measured every 15 minutes on Sable Island in 2016

As can be seen in Figure 122, PM_1 has the highest number concentration among the PM size fractions, which is as expected since fresh combustion particles and particles formed by gas-to-particle conversion are the most numerous within a typical particle size distribution (Hinds, W.C., 2012). PM_{20} has the lowest number concentration as expected as this size mode settles out quickly and also easily washed out of the atmosphere (Gibson et al., 2009). On December 31st, PM_1 reached the maximum value (79590 /cm³); the second highest number concentration for PM_1 was observed on February 26th, reaching a value of 77879 /cm³. The highest PM1 spike also coincides with the NW Atlantic spring phytoplankton bloom, a source of PM_1 pre-cursor gases.

153
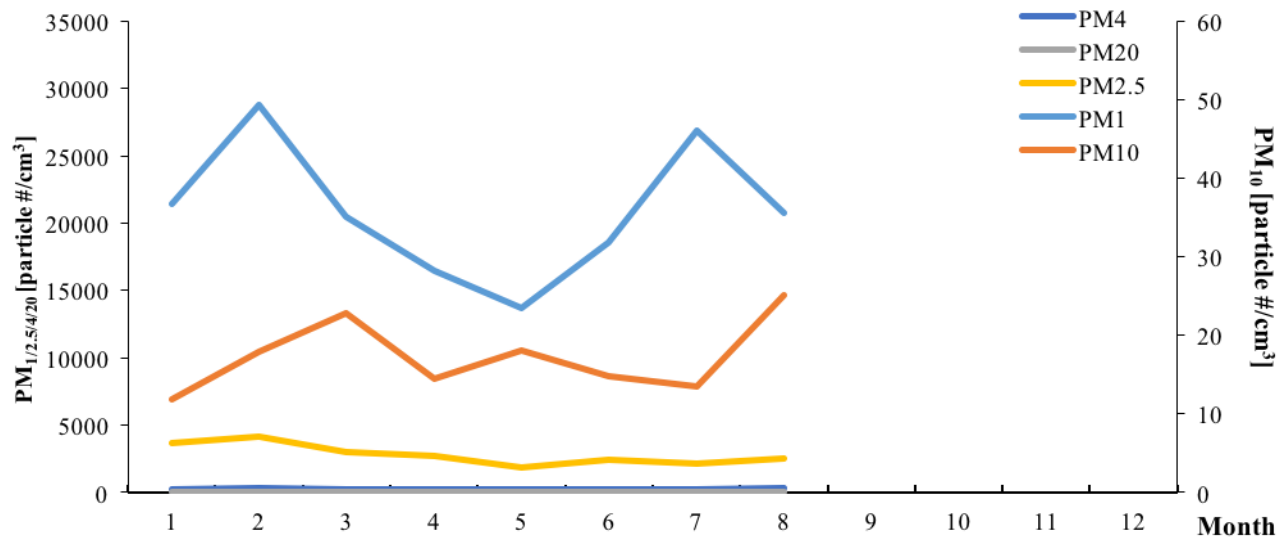
Figure 123 Mean monthly PM$_{1/2.5/4/10/20}$ number concentration (particle #/cm^3) on Sable Island in 2016

From Figure 123, it can be observed that PM$_1$ number concentration (particle #/cm^3) reached maximum monthly mean in February. With July coming in the second place, which is similar to mass concentration trends.

From annual and monthly mean PM number concentrations (Figure 120, Figure 121, Figure 122 & Figure 123), peak dates (Jan. 27th, Feb. 26th and Apr. 9th) have been compared with HYSPLIT air mass back trajectories and satellite images for helping to identify and apportionment upwind sources of PM.

4.6.3 Ultrafine Particle Number Concentration

Number concentrations of Ultrafine Particle number concentration (UFP) on Sable Island were measured continuously at 15-minute intervals via a TSI UFP monitor model 3031 in 2016. Table 23 below provides the descriptive statistics from the UFP instrument. The UFP counts particles in 6 size bins ranging from 20 – 800 nm.

Table 23 Ultrafine particle descriptive statistics

Variables	20-30 nm *[Particle #/cm³]*	30-50 nm *[Particle #/cm³]*	50-70 nm *[Particle #/cm³]*	70-100 nm *[Particle #/cm³]*	100-200 nm *[Particle #/cm³]*	200-800 nm *[Particle #/cm³]*
n	35136	35136	35136	35136	35136	35136
n missing	2634	2634	2634	2634	2634	2634
Completeness	92.50%	92.50%	92.50%	92.50%	92.50%	92.50%
Min	0	0	0	0	0	0
25th Percentile	34	69	42	42	76	2
Median	185	214	138	129	191	25
Mean	328	360	227	205	252	43
75th Percentile	388	463	308	283	337	59
Max	34766	35441	20213	17333	32469	4261
IQR	354	393	266	241	261	57
Standard Deviation	597	595	339	286	321	66

From Table 23, the data completeness for the UFP particles number was 92.50%. The mean (min:max *units*) for UFP in terms of size fractions are (hereafter e.g. UFP 20-30 nm): 20-30 nm = 328 (0:34766 *#/cm³*), 30-50 nm = 360 (0:35441 *#/cm³*), 50-70 nm = 227 (0:20213 *#/cm³*), 70-100 nm = 205 (0:17333 *#/cm³*) , 100-200 nm = 252 (0:32469 *#/cm³*) and 200-800 nm = 43 (0:4261 *#/cm³*).

Figure 124 below shows the annual temporal trend of UFP number concentration measured at a temporal resolution of 15-minutes. The missing data was due to the UFP instrument being removed from the Island for service.
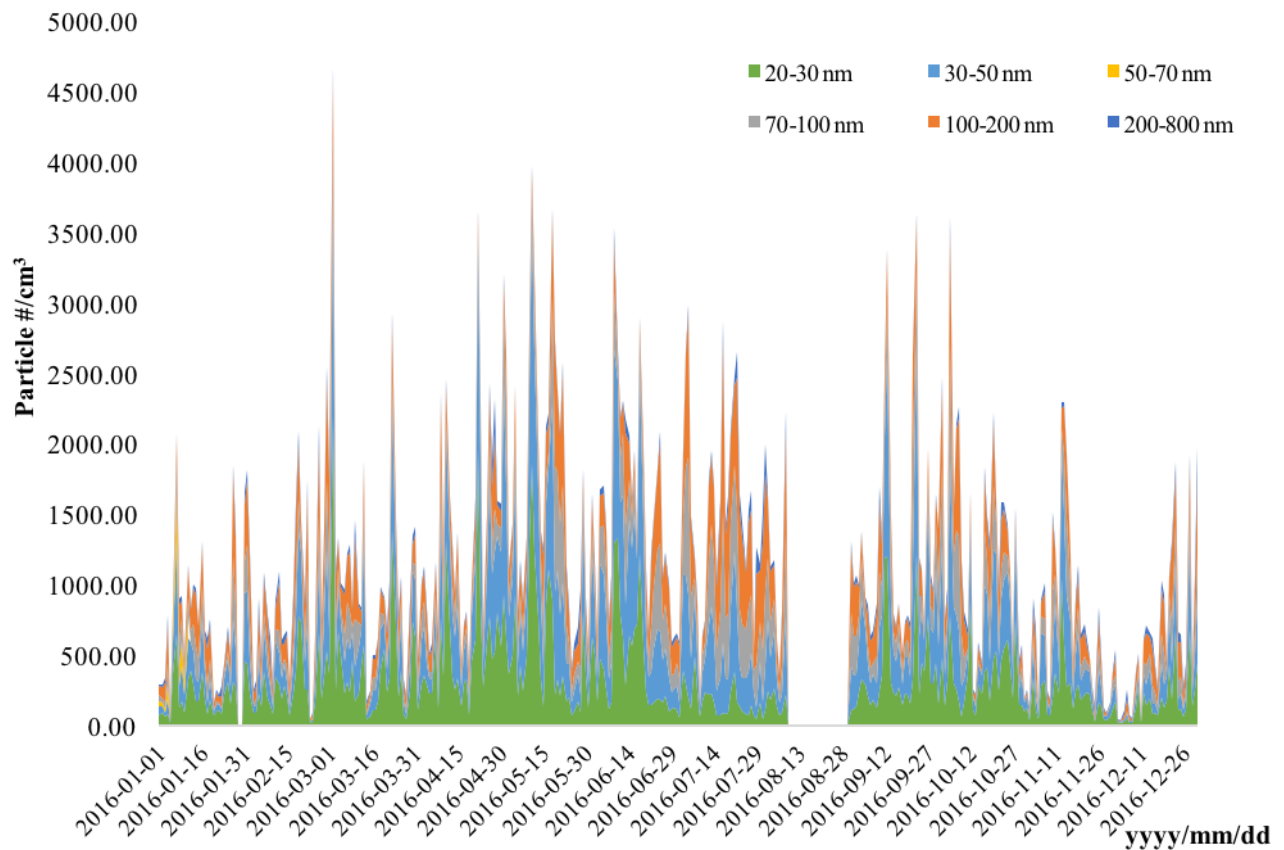
Figure 124 Annual cycle of UFP number concentration (particle #/cm^3) on Sable Island in 2016

It is noticeable from descriptive statistics in Table 23 and the annual cycle plot in Figure 124 that the 20-30 nm and 30-50 nm size fractions account for most of UFP measurements, whereas 200-800 nm accounts for the least. Also interestingly, the 20-30 nm and 30-50 nm UFP have negative correlation with 100 – 200 nm and 200-800 nm UFP, e.g. 20-50 nm UFP tend to have spikes in May and October, troughs in July, while 100-800 nm UFP tend to have troughs in May and a spike in July; in the meantime, 200-800 nm size fraction also has a distinct spike in December, which is consistent with a study conducted in East Atlantic coast in Ireland (Yoon et al., 2007). UFP 20-30 nm and UFP 30-50 nm reached their first peak in May and the second peak in October, which was also reported by Barnett (Barnett, 2016). These two peaks correspond with

the NW Atlantic spring and fall phytoplankton blooms and associated with chlorophyll-a peaks also observed in Craig et al., (2015) (see Chapter 5.1). Monthly mean variance of UFP number counts are shown below in Figure 125.
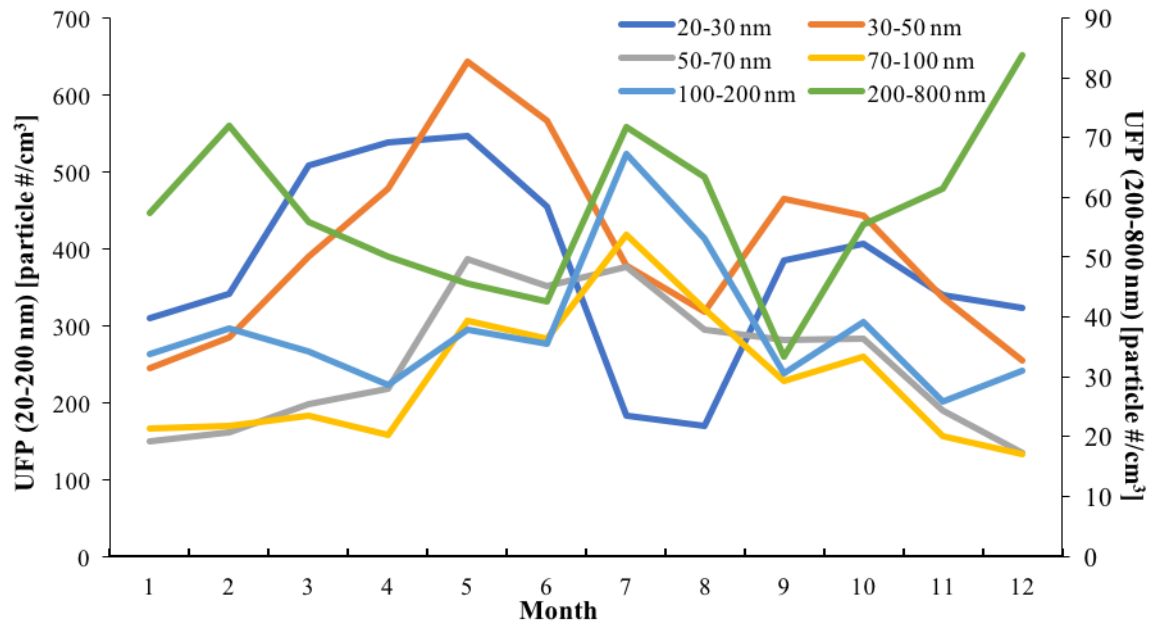
Figure 125 Mean monthly UFP number concentration (particle #/cm^3) on Sable Island in 2016

It can be seen in Figure 125, UFP 20-30 nm and 30-50 nm reached their maximum in May and second peak came in October; UFP 50-70 nm reached its maximum in May as well and then began to decrease; UFP 70-100 nm 200-200 nm reached its maximum in July and then began decrease. UFP 200-800 nm reached its maximum in July, and then began to increase again in October till December it reached another peak, it has three peak through the year: February, July and December.

Closer scrutiny of the two spikes appearing in May and October monthly value is shown in **Figure** 126 & **Figure** 127.
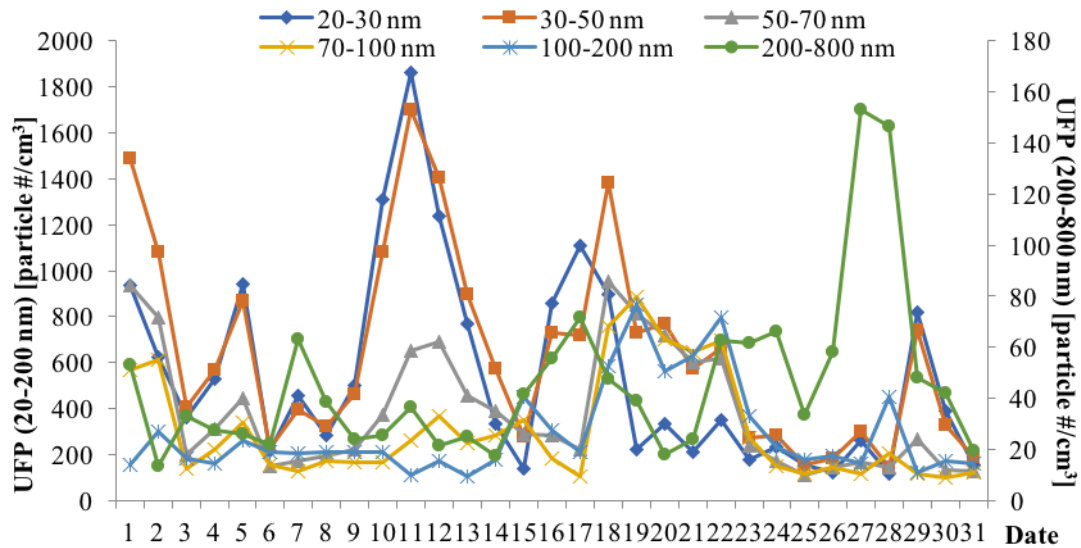
Figure 126 Daily mean UFP number concentration (particle #/cm^3) in May 2016
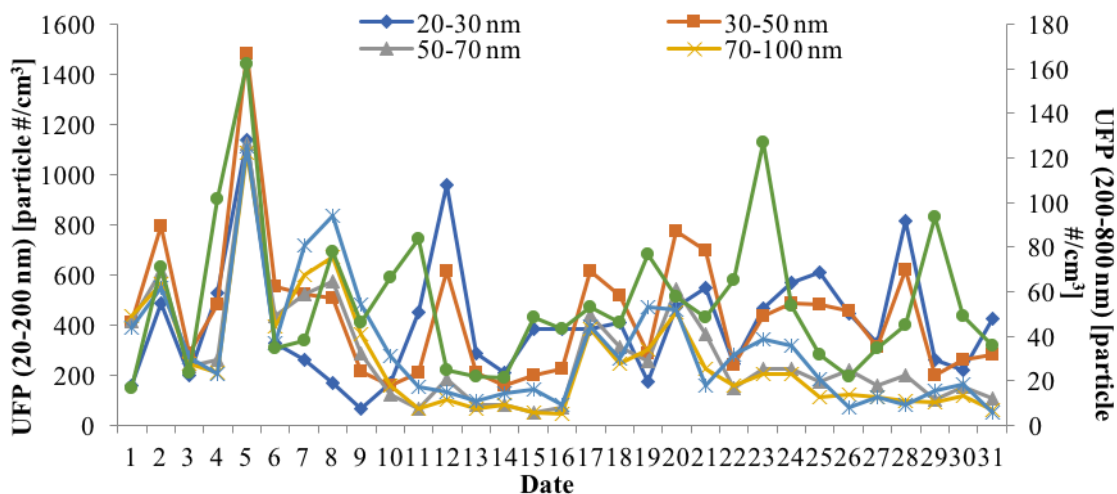
Figure 127 Daily mean UFP number concentration (particle #/cm^3) in October 2016

From Figure 126, spike dates of May can be determined: 1st, 11th, 12th,17th, and18[th]. According to earlier study on phytoplankton and PM studies, May spike is likely to be caused by Atlantic phytoplankton spring bloom (Collins et al., 2017; Craig et al., 2015). As can be seen in Figure 127, 2nd and 5th were two spike days in October. As May spike, October spike is likely to be caused by phytoplankton fall spike. Detailed PM source apportioment analysis would be presented in later sections.

Annual diel average and seasonal diel average will be shown below in Figure 128. Diel time-dependent variations of UFP are also assessed in UTC.
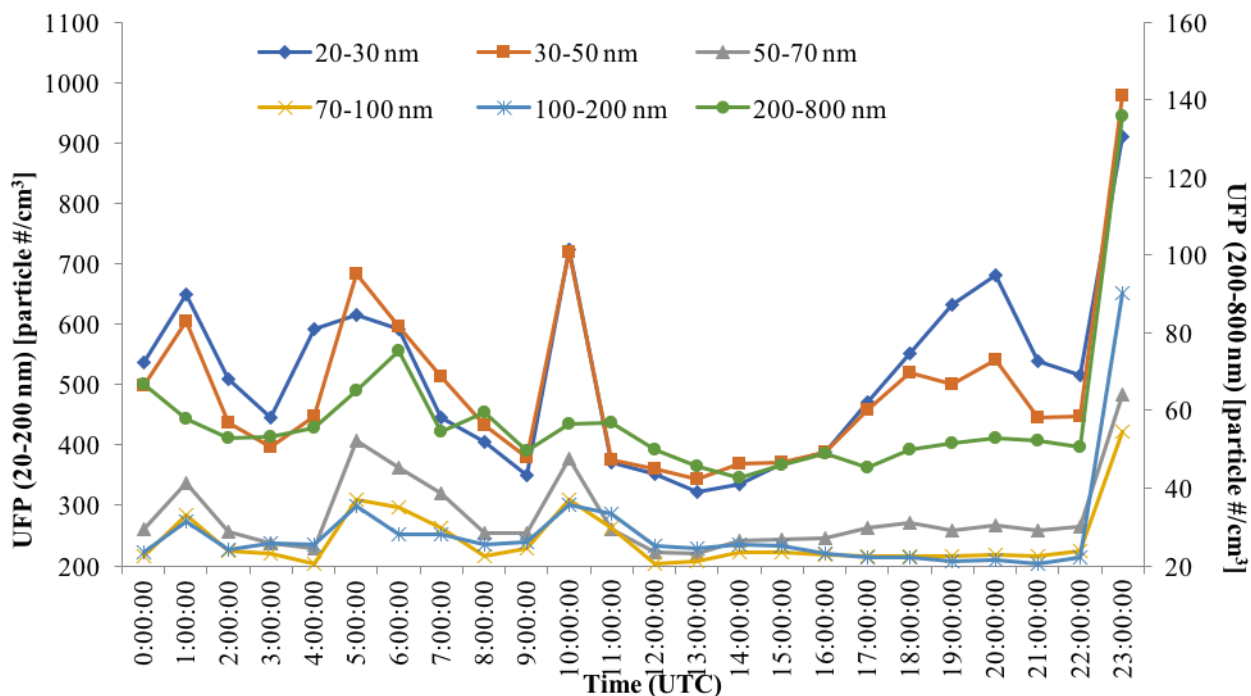
Figure 128 Diel average of UFP number concentration (particle #/cm³) on Sable Island in 2016

From Figure 128, three spikes can be seen for 20-30 nm and 30-50 nm UFP, which occur at 05:00, 10:00, 20:00 and 23:00 UTC and 02:00, 07:00, 17:00 and 20:00 in local time. UFP began to increase at 3 am and 9 am respectively, and reach the first and second peaks at 6 am and 11 am; then they begin to increase at 5 pm and reach the third peak at 8 pm. Among six size fractions, 20-30 nm and 30-50 nm UFP have the largest number concentration.

Figure 129 provides the diel UFP number concentrations averaged according to seasons.
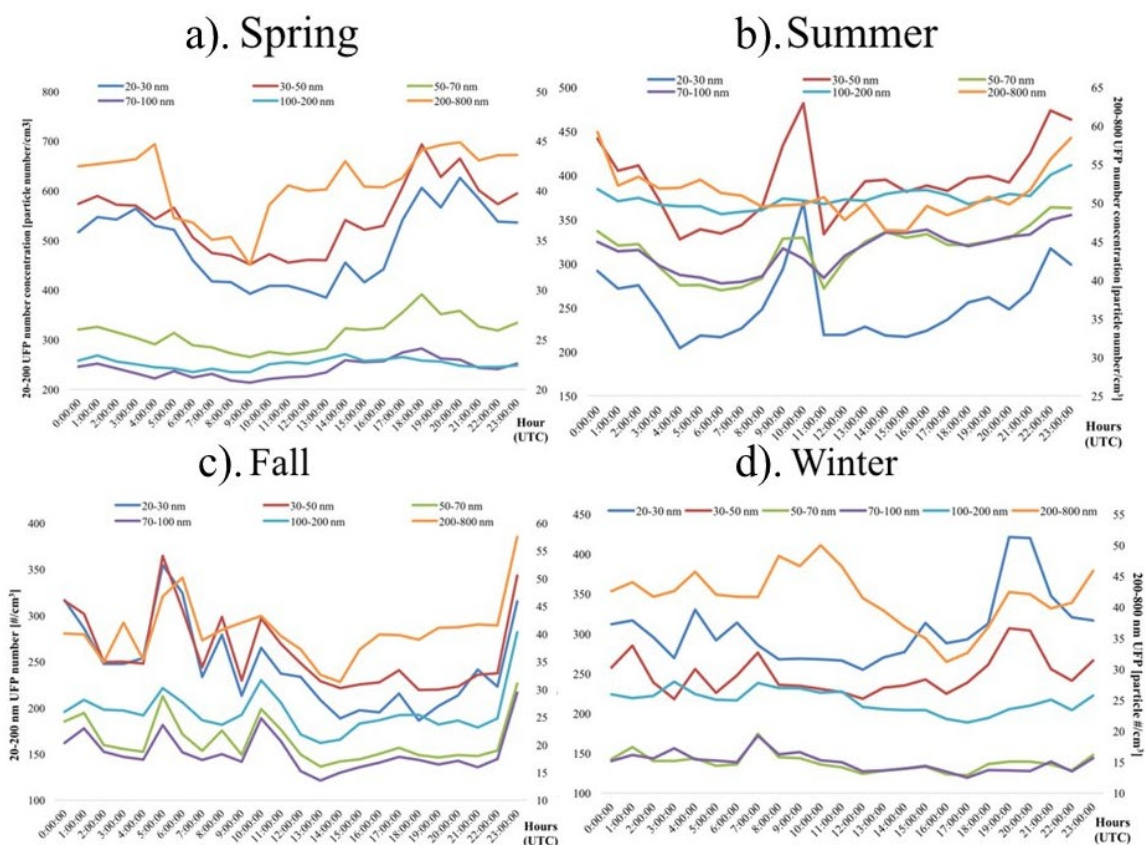
Figure 129 Provides four figures of the diel seasonal average of UFP number concentration (particle #/cm³) on Sable Island in 2016, a) Spring b) Summer c) Fall and d) Winter

From Figure 129, it can be observed that in the spring (panel a), the 20-30 nm and 30-50 nm UFP number began to increase at 4 pm. They began to decrease at 3 am and increase at 1 pm. 200-800 nm UFP number concentration increased at 8 am, right after the 20-50 nm UFP peak, which can be assumed that 200 -800 nm UFP were formed from coagulation of 20-50 nm UFP. In the winter, 20-30 nm and 30-50 nm UFP number reached a twin peak during 3-8 am, and a second peak at 7 pm. 200-800 nm UFP number concentration increases at 8 am, right after the 20-50 nm UFP peak, which can be assumed that 200-800 nm UFP are formed from coagulation of 20-50 nm UFP.

It is likely the spikes in 20-30 nm and 30-50 nm UFP during the day are associated with secondary UFP formed from photochemical induced phytoplankton VOC emissions. Based on a study conducted by Kulmala et al., 2001, an increase of small UFP (<10 nm) concentration was observed during late morning in April; after that they tended to grow into the size fractions associated with the Aitken model and accumulation mode (20-100 nm and 0.1-2.5 μm) particles throughout the afternoon and into evening, which matches the UFP tend in Figure 129 (Hinds,

160

1999). Also, in a study investigated by Coe et al., 2000, in a coastal area in England (North East Atlantic Ocean), UFP in accumulation mode (<50 nm) tended to steadily increase in the afternoon and diminish through the evening. In Kulmala's study, it was also mentioned that particle number reached a spike around noon. In diurnal plots for this study, in spring season, it reached a spike at 14:00 UTC which is 11:00 in local time (Coe et al., 2000; Kulmala et al., 2001). Furthermore, in Coe's study, the 20 nm particles did not increase until around 10:00 in the morning, 2 hours later than the increase in the 5 nm size (Coe et al., 2000).

4.7 UFP and PM Source Apportionment Analyses and Results

4.7.1 Satellite Observations to Aid Source Apportionment

Spikes from PM and UFP annual cycle plots were investigated with the aid of satellite images and air mass back trajectory. NOAA HYSPLIT air mass back trajectory at spike time on spike day was generated to find potential sources for $PM_{1/2.5/4/10/TSP}$ and UFP. Time-averaged maps for selected spikes in UFP annual cycle were generated to identify chlorophyll-a concentration in regions around Sable Island. Giovanni chlorophyll-a concentration maps were blended with air mass back trajectories in Google Earth Pro; graphs were created to aid in identifying potential source regions of UFP on "peak/spike" days. Air mass back trajectories were produced five days before spike day; hourly timestamps were also used to help with identifying potential anthropogenic or natural sources for the formation of UFP.

Figure 130 below is monthly HYSPLIT 5-day air mass back trajectory integrated into Google Earth. Each color represents back trajectory for 17th of each month, which is the middle of each month. It can be seen that half of them were coming from the North (which is a clean source); four were from NE US (known for industry, coal combustion, and agriculture) (Gibson et al., 2013; Jeong et al., 2011), and three originated from marine (mostly sea spray, or marine biomass activities if there is phytoplankton bloom detected from satellite).
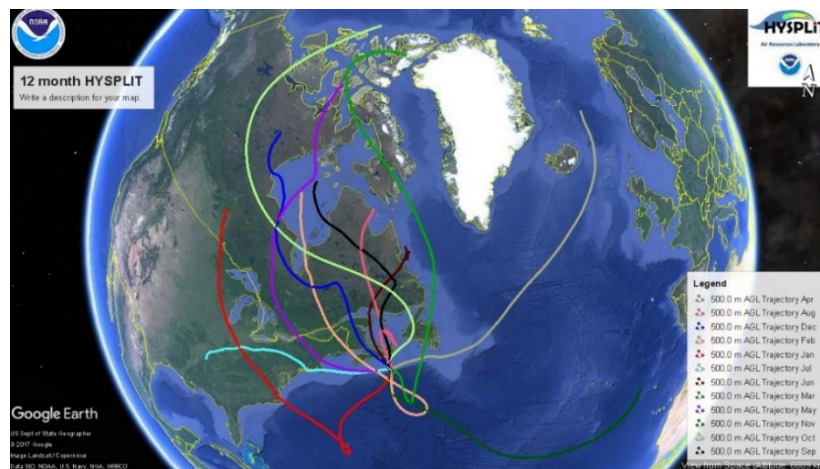
Figure 130 Annual cycle HYSPLIT overview

Annual time averaged map for chlorophyll-a concentration (mg/m^3) from the marine region around Sable Island was also generated and shown in Figure 131. As indicated in the legend, the color represents the concentration of chlorophyll-a, from light blue (lowest) to pink purple (median) to yellow (highest).
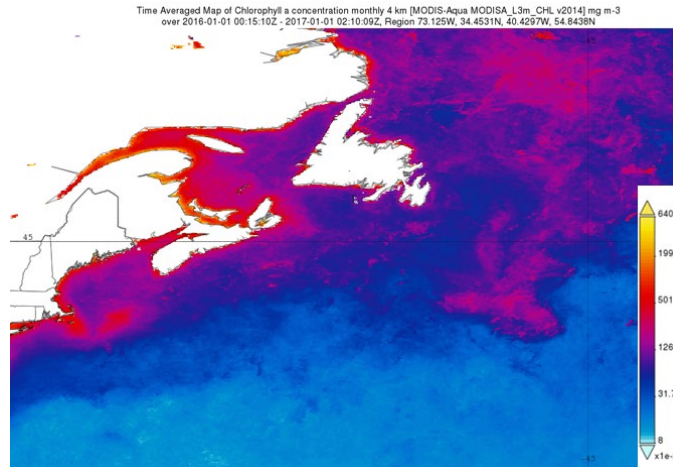
Figure 131 Annual mean *chl a* concentration map around Sable Island in 2016 retrieved from the NASA, Giovanni data system

4.7.2 Potential Sources and Sinks determination - Principle Component Analysis

Principle component analysis looks for covariance between the underlying latent variables that exist between data in eigen space that cannot be seen in the typical two-dimensional correlation analysis. PCA also allows the identification of the main factors that explain the percentage and primary drivers of the variance within a particular data set. PCA provides columns of correlation values against a certain metric. If the correlation value is above 0.3 or below -0.3 then it has an influence upon that 'factor'. In atmospheric chemistry the 'factor' is the source of an atmospheric component, in our case particle number counts found in a particular size fraction associated with a specific source. Principle Component Analysis on total PM (0.02-20 µm) number measurement has been investigated and shown in Table 24.

Table 24 Partial summary of PCA on PM$_{0.02\text{-}20}$ result

Variable	Long Range Transport (LRT)	Sea spray	Wind Blown Sand	Coagulation Particles	Freshly formed UFP	Unclassified
20-30 nm					0.801	
30-50 nm					0.645	
50-70 nm				0.917		
70-100 nm				0.942		
100-200 nm				0.869		
200-800 nm						-0.641
1.286 µm	0.964					
5.829 µm		-0.957				
15.96 µm			-0.989			
Variance	20.31	17.22	6.458	4.001	2.195	2.638
% var	0.369	0.313	0.117	0.073	0.04	0.048

In Table 24, PCA was run on the six size fractions between PM$_{0.02\text{-}20}$, their corresponding factor correlations are displayed. From **Table** 24 it can be seen that PCA revealed 6 factors that accounted for 96% of the variance. Six possible source categories were identified with the knowledge of PM sources and formation (Gibson et al., 2015). The first factor accounted for 36.9% of the variance and had significant factor loadings in the PM$_{1.286}$ size fraction, which is

absolutely typical of 'aged' long range transport (LRT) particles. The second factor has significant negative loadings on $PM_{5.829}$, which is within the coarse particle mode; this size fraction is likely to be associated with wind-blown sand, it has significant negative correlation with sea spray. The third factor has the most negative loading in 15.96 μm, which is comparatively large in size and is likely associated with larger surficial dust and debris. The fourth factor has high loadings in 50-200 nm, which are in accumulation mode formed by coagulation of freshly formed UFP. The fifth factor has significant loadings in 20-50 nm UFP, accounting for 4% of the variance. UFP in the range of 20-200 nm are typical freshly formed combustion particles or from gas-to-particle conversion. Over these long time scales, the most probable source of the 20-50 nm size fractions being phytoplankton generated VOCs reacting in the atmosphere to form these UFP. Factor 6, in 200-800 nm size range is unknown and needs to be investigated further. However, the 200-800 nm size range is likely related to coagulation of aged aerosol, either local or distant.

4.7.3   Potential Sources determination - Positive Matrix Factorization Analysis

The output from EPA PMF model v.5.0.14.21735 run will be presented in this section. The model was run using 20 base runs and 4 factors, with factors representing the source of the PM number counts. The bootstrap and fpeak were also conducted to check the robustness of the PMF model. The fpeak modelling with bootstrapping was performed on Base Run_#20 with Fpeak Runs = 0.5, Bootstraps # = 100, minimum R^2 = 0.6 and block size = 9. As can be seen in Table 25 and Table 26, all runs were converged for Q (Robust) and Q (True), the Fpeak run was also converged. Factor contributions, factor variability in the concentration of species, factor time series and pie charts will be provided in this section.

Table 25 PMF base run summary

Run Number	Q (Robust)	Q (True)	Converged
1	12177.9	12515.3	Yes
2	12177.9	12515.3	Yes
3	12177.9	12515.3	Yes
4	12177.9	12515.3	Yes
5	12177.9	12515.3	Yes
6	12177.9	12515.3	Yes
7	12177.9	12515.3	Yes
8	12177.9	12515.3	Yes
9	12177.9	12515.3	Yes
10	12177.9	12515.3	Yes
11	12177.9	12515.3	Yes
12	12177.9	12515.3	Yes
13	12177.9	12515.3	Yes
14	12177.9	12515.3	Yes
15	12177.9	12515.3	Yes
16	12177.9	12515.3	Yes
17	12177.9	12515.3	Yes
18	12177.9	12515.3	Yes
19	12177.9	12515.3	Yes
20	12177.9	12515.3	Yes

Table 26 Fpeak Model Run Summary

Strength	dQ (Robust)	Q (Robust)	% dQ (Robust)	Q (Aux)	Q (True)	Converged
0.5	45.8	12223.7	0.37	44.3	12516.9	Yes

Q robust and Q true converged for all base runs can be seen in Table 25, which demonstrates the stability of the base model run. As described previously, Q value is determined by the total running times, for this study, 218-day data was used and the number of variables = 59, which gives 12862, which is the ideal value for Q (True). The Q value generated from the PMF model was 12516.9, which is close enough to the ideal value, and it is a proof of the stability of this test. In Figure 132 below (top panel), the orange and grey boxes represent the % of that species, from the total species found in the entire data set, associated with this factor (source of PM). The grey boxes are the base model run, and the orange boxes are the fpeak model robustness check. As can be seen, they agree with which provides confidence in the PMF model's performance. The grey bars and green bars represent the concentration of the species associated with this factor (source of PM). Again, the base model and fpeak robustness check agree. The bottom panel

shows the concentration of this PM source over the sampling period. The figure panel legend and format descriptions are the same for the remaining three factors (Figure 134, and Figure 139).
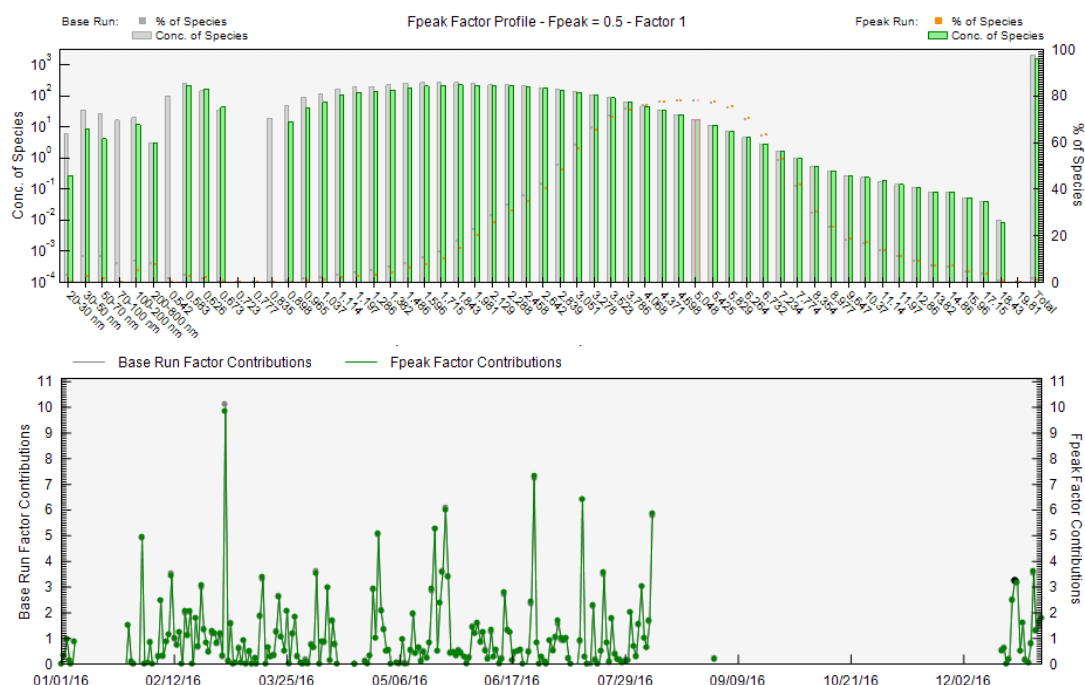
Figure 132 Factor 1 source profile (top panel) and mass contribution plot (bottom panel)

With knowledge of the potential sources and of aerosol theory, Factor 1 was identified as sea spray. In Figure 132 percentage profile (top panel), it can be seen that more than 40% of $PM_{2.5-8}$ were found within Factor 1. The source of coarse particles are normally from the break-up of large solids or droplets such as sea spray and mechanical disruptions (Fuzzi et al., 2015; Wilson & Suh, 1997). From factor contribution, four spikes were investigated to help with determining the source. HYSPLIT 5-day air mass back trajectories for spike days (2nd March, 25th June, 13th July, and 23rd May) were generated and shown in Figure 133. Three of them originated from the North, which has few anthropogenic sources. Coarse particles do not have a long residence time in the atmosphere, as they are either washed out by precipitation or deposit quickly by gravity due to their relatively large mass compared to fine particles and UFP. Because of this, LRT can be excluded from Factor 1 as this aerosol is typically found below 2.5 μm. For 23rd May air mass back trajectory, the air mass spent its entire 5-day lifetime over the ocean, which leaves sea spray to be the probable source.
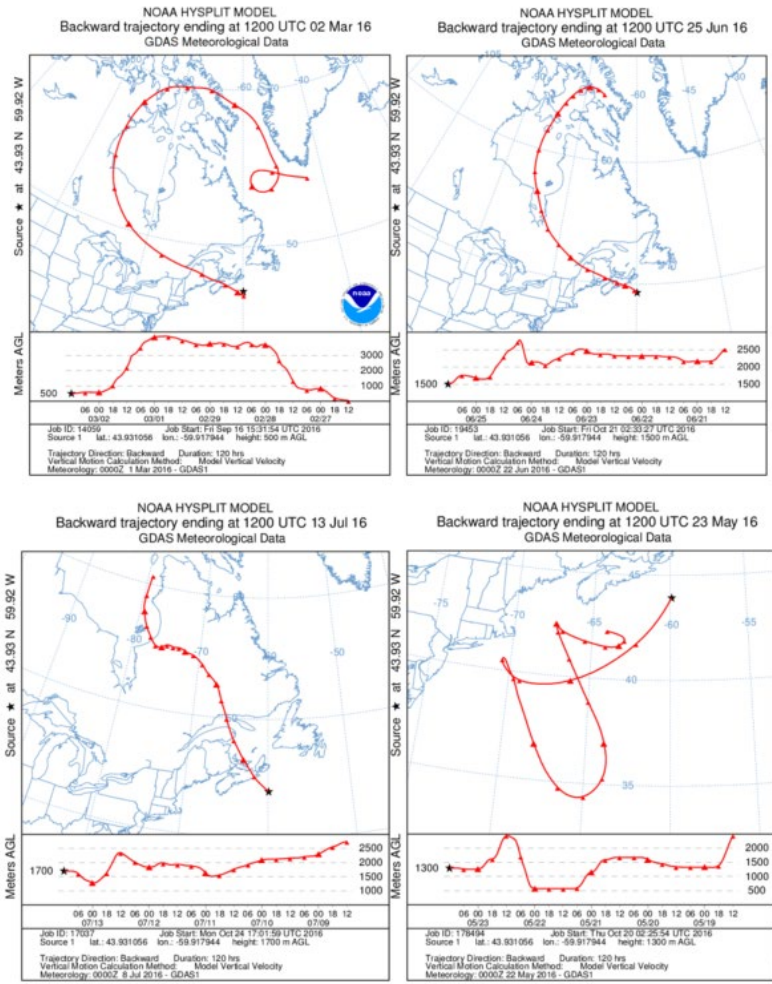
Figure 133 HYSPLIT 5-day air mass back trajectory associated with the Factor 1 contribution spikes shown in Figure 132
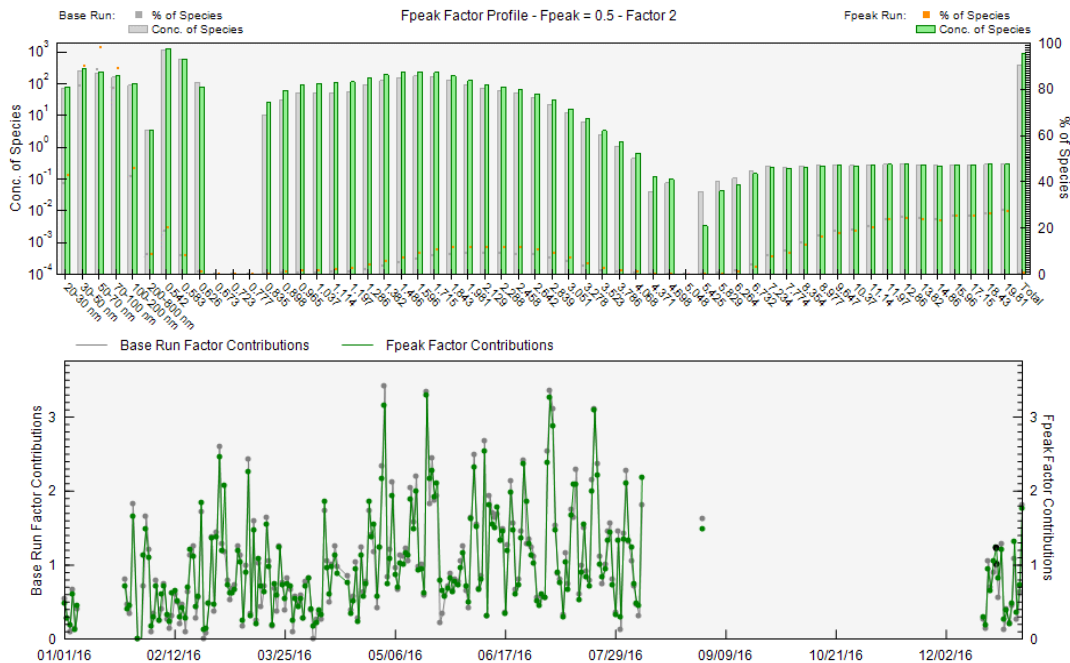
Figure 134 Factor 2 source profile (top panel) and mass contribution plot (bottom panel)

Figure 134 reveals the Factor 2 source species profile and factor contribution time series. From the knowledge of marine sources and ocean-atmosphere chemistry and physics, Factor 2 was chosen as biogenic marine secondary particles. From species percentage in the factor profile and time series in Figure 134, it can be determined that Factor 2 is dominated by more than 80% of UFP 20-200 nm, which is known to be only formed from fresh combustion gases or gas-to-particle conversion.

HYSPLIT air mass back trajectory (

Figure 135)

was also generated for spike days (2nd & 18th May, 4th & 21st Jul) in Factor 2 timeseries. There was a phytoplankton bloom in May 1st - 2nd around Sable Island (Figure 136), so phytoplankton VOC gas-to-particle conversion is the likely source.

169
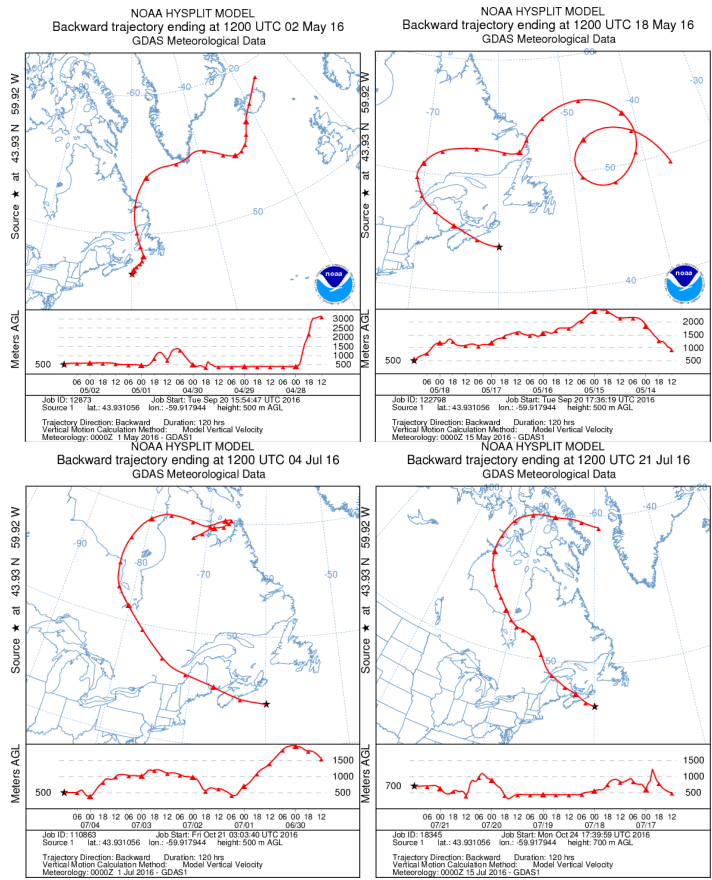
Figure 135 HYSPLIT 5-day air mass back trajectory for Factor 2 spikes
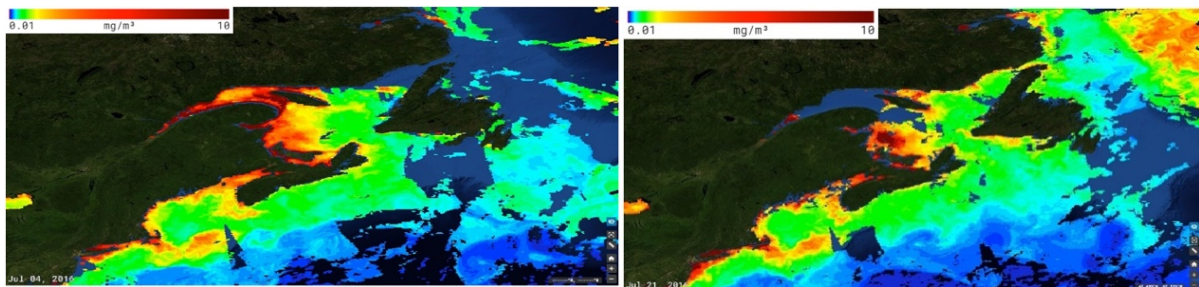
Figure 136 SOTO daily chlorophyll a concentration around Sable Island on Jul. 04th (left) and Jul. 21st (right)
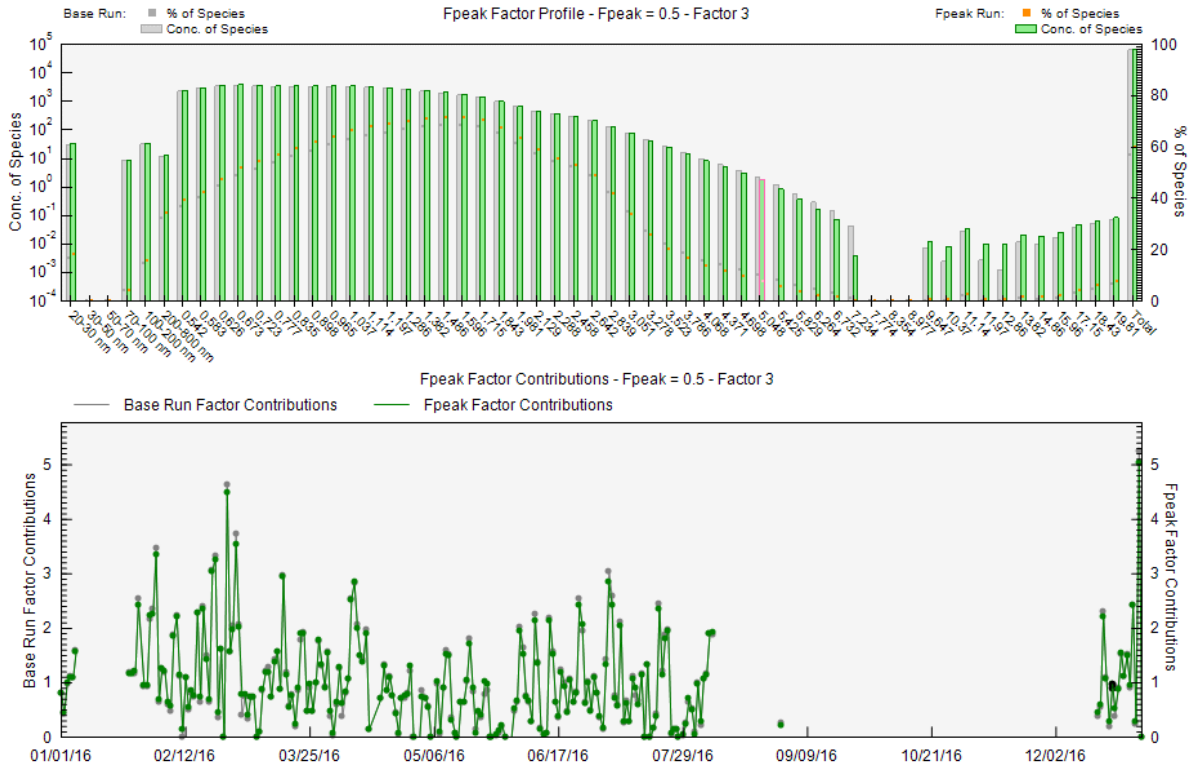
Figure 137 Factor 3 source profile (top panel) and mass contribution plot (bottom panel)

Figure 137 reveals the Factor 2 source species profile and factor contribution time series. With factor profile and the knowledge of coarse particles and their potential sources around Halifax, Factor 3 was identified as LRT. From species percentage in factor profile and time series in Figure 137, it can be determined that Factor 3 is dominated by $PM_{0.5-2.8}$, which are in accumulation mode and can exist in the atmosphere for few days or even weeks if not washed out by precipitation.

HYSPLIT air mass back trajectory (

Figure 138) was also generated for spike days (2nd, 26th & 29th Feb., 16th March, and 8th Jun) in Factor 3 time series. All of them, except Mar 16th, originated from west of Canada and they moved along Canada/US boundary from the NE US, which is an industrial source region.
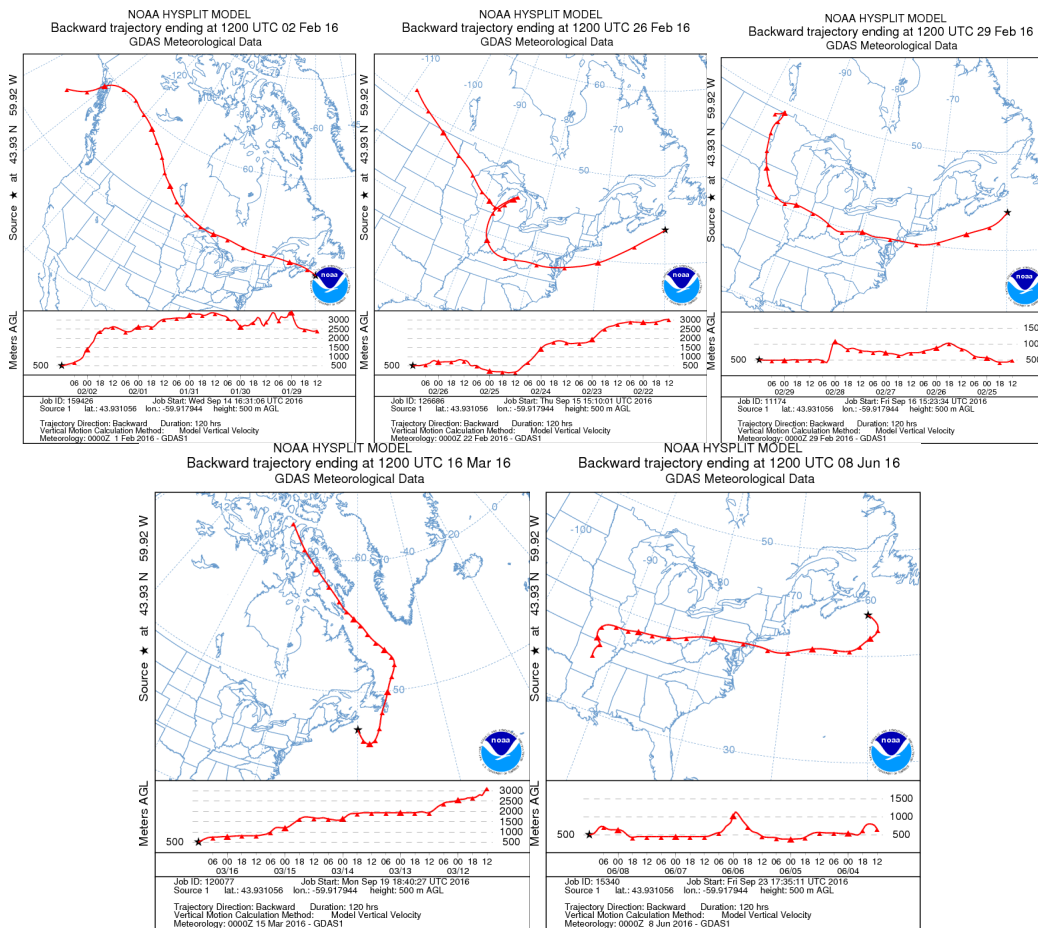
Figure 138 HYSPLIT 5-day air mass back trajectories associated with Figure 137 for Factor 3 (LRT) spikes
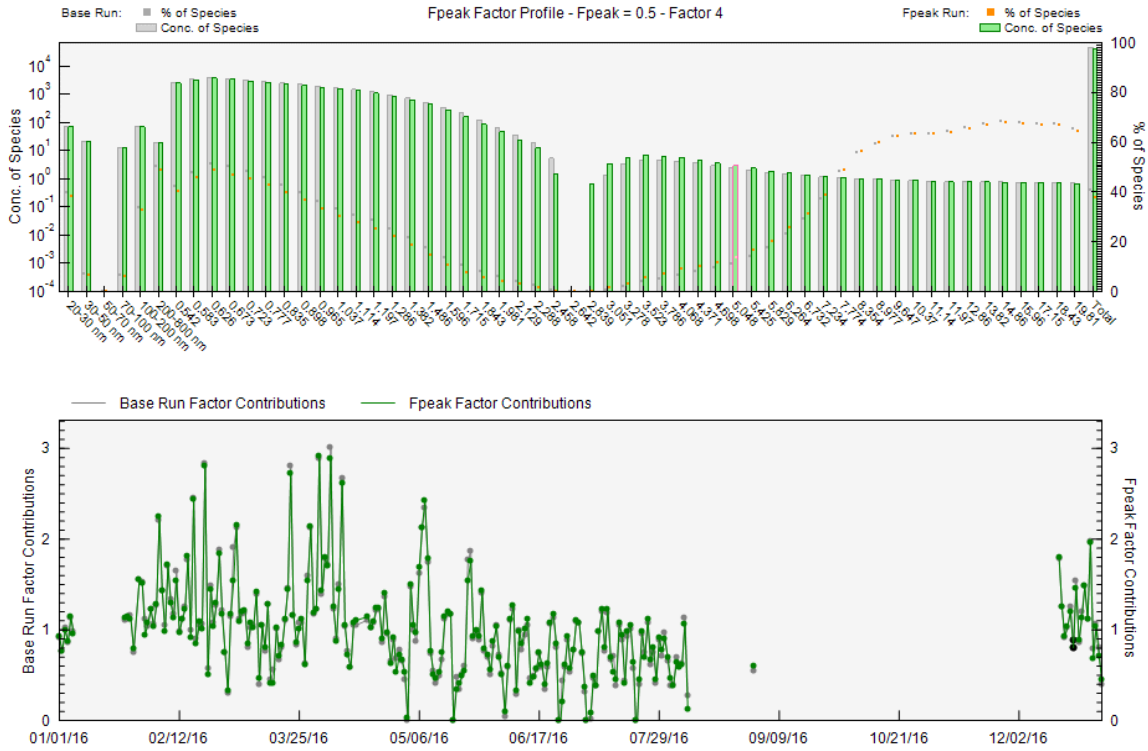
Figure 139 Factor 4 source profile (top panel) and mass contribution plot (bottom panel).

Figure 139 reveals the Factor 4 source species profile and factor contribution time series. It can be determined that Factor 4 is characterized by 50% of $PM_{0.2-1}$ & $PM_{>7.5}$ and UFP 20-30 μm. Therefore, the source of Factor 4 was identified as surface dust with contributions from aging UFP. $PM_{>7.5}$ are mostly from the break-up of large solids or droplets such as windblown dust, UFP 20-30 nm is likely from coagulation of freshly formed UFP.

HYSPLIT air mass back trajectory (

Figure 140) was also generated for spike days (17th Feb, 21st & 22nd March, 1st & 5th April, and 8th May) in Factor 4 timeseries. Three of them originated from the North part which is known to have relatively clean air (Gibson, Kundu, & Satish, 2013). All of the trajectories do pass the oil and gas field before arriving at Sable Island, which may bring some fresh combustion products to the site and cause a spike in UFP. This would require further investigation to confirm.

173
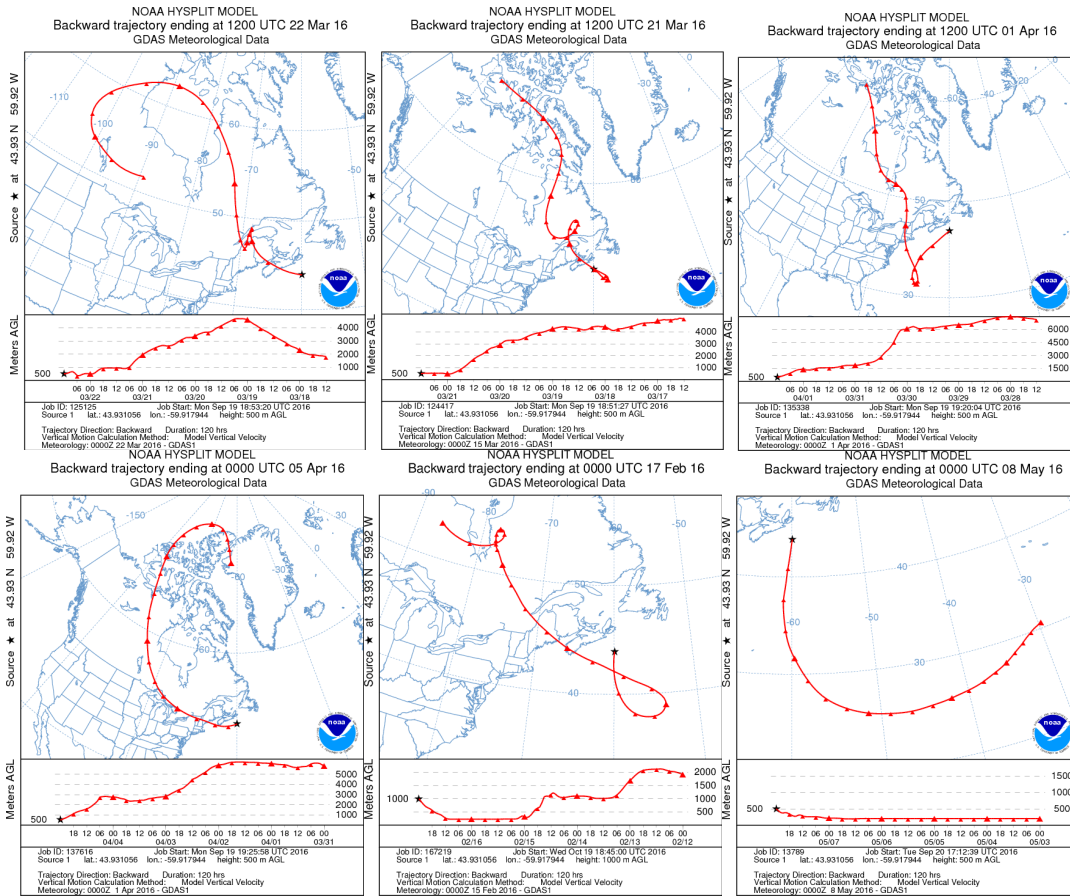
Figure 140 HYSPLIT 5-day air mass back trajectory for Factor 4 spikes
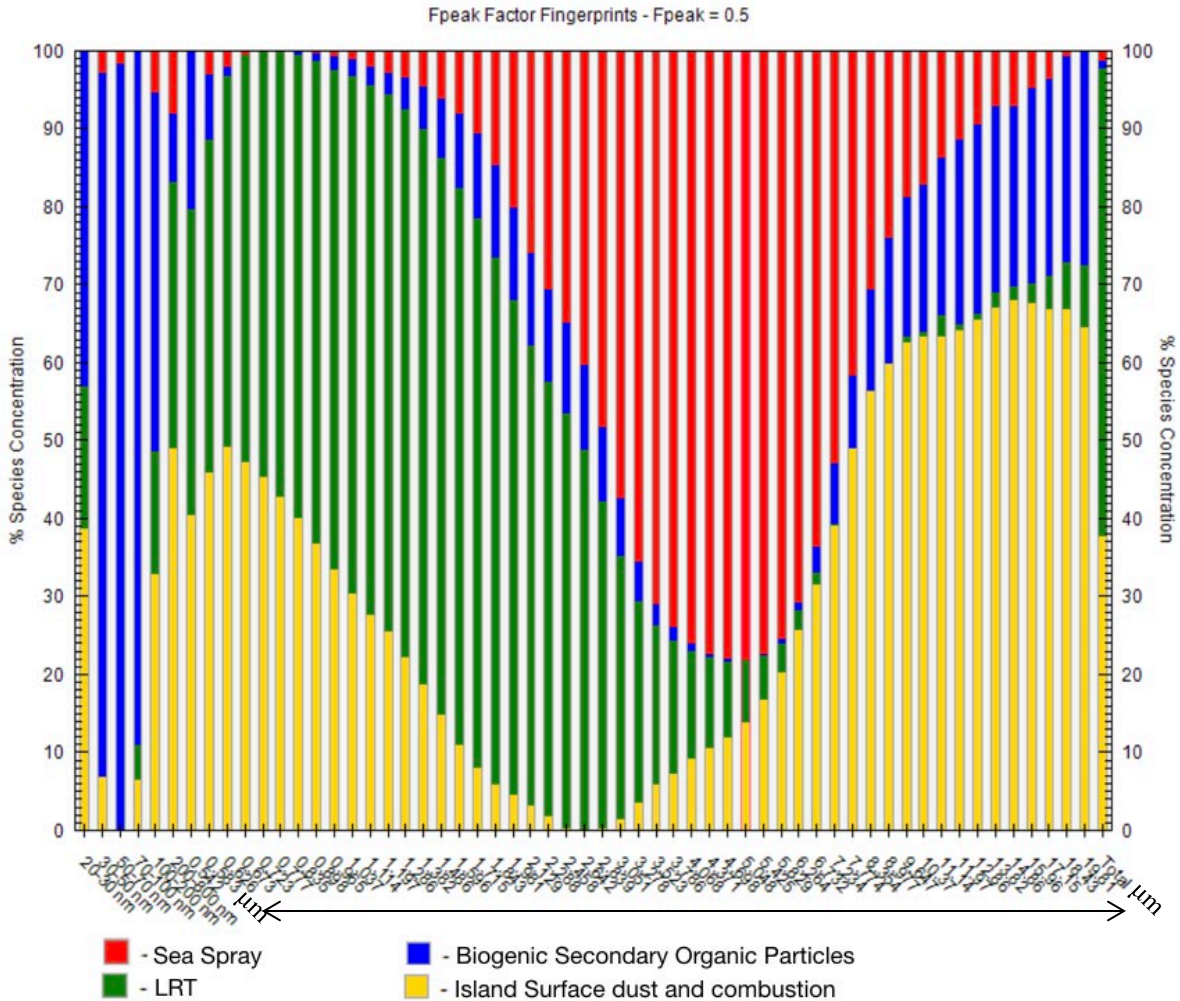
Figure 141 Factor (Source) attribution

Figure 141 shows factor source attribution for the PM number concentration, and presents the dominant factors for PM in different size fractions (20 nm – 20 μm). Coarse PM (2.5 – 10 μm) are dominating factor 1 (sea spray); UFP in the size of 20-200 nm are dominating Factor 2 (secondary marine biogenic particles); fine PM (0.2-4 μm) dominates Factor 3 (LRT); Factor 4 is mostly PM 20-30 nm, 0.1-2 μm and above 7.5 μm, which can be combustion fragments and dust from Sable Island surface and anthropogenic activities. In another feature of the data is that 90% of UFP 30-200 nm are marine secondary biogenic particles, more than 50% of $PM_{0.5-2.5}$ are LRT (the rest are from Sable Island surface dust), more than 50% of $PM_{2.5-8}$ are sea salt, and more than 50% of PM_{8-20} are Sable Island surface dust.

175

Figure 142 Pie chart of total UFP components

In Figure 142 it can be seen that the marine secondary biogenic particles account for 78.2% of total UFP; Sable Island surface dust account for 15% of total UFP, according to Figure 141, mostly UFP 200-800 nm; LRT and sea spray contribute to the rest 6% of total UFP. Figure 143 below provides a source contribution pie chart of total PM number concentration.
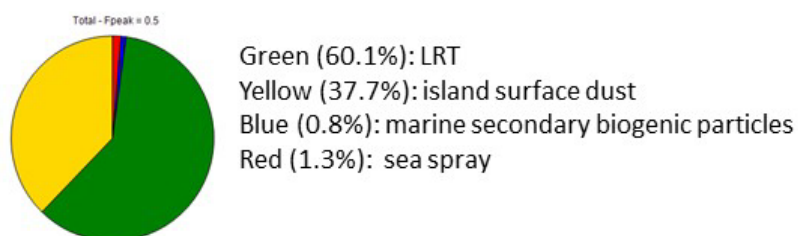
Figure 143 Pie chart of total PM components

From Figure 143, it can be seen that 60% of total PM (including UFP and $PM_{0.5-20}$) are from LRT, it is reasonable as fine PM have largest number counter; 37.7% of PM are from Sable Island surface dust and the rest 2% are attributable to marine. Table 27 below summarizes the source attributions of UFP and $PM_{0.5-20}$.

Table 27 Summary of sources for UFP and PM

	Sea Spray (%)	Marine Secondary biogenic particles (%)	LRT (%)	Sable Island dust (%)
20 – 30 nm	0.2	42.8	18.4	38.6
30 – 50 nm	2.7	90.3	0	6.9
50 – 70 nm	1.7	98.3	0	0

70 – 100 nm	0	89.1	4.5	6.4
100 – 200 nm	5.4	45.9	15.7	33.0
200 – 800 nm	8.0	8.8	34.2	49.0
UFP Total	2.2	78.2	4.4	15.2
PM Total	1.3	0.8	60.1	37.7

It can be seen in Table 27 that LRT accounts for most of the total number concentrations, which makes sense as fine particles coalesce around the 100nm size fraction (Hinds, W.C. 2012). Secondary marine biogenic particles account for 90% of UFP 30-50 nm. This, agrees with our mean monthly UFP vs *chl a* plot in later sections that shows the strong correlation between *chl a* and UFP in the 30 – 50 nm size range. The four size-resolved sources were sea spray (2.2% of total UFP, 1.3% of total PM), secondary marine biogenic particles (78.2% of total UFP, 0.8% of total PM), LRT (4.4% of total UFP, 60.1% of total PM) and Sable Island surface dusts (15.2% of total UFP, 37.7% of total PM), where secondary marine biogenic particles was the dominant contributor to UFP and LRT was the dominant contributor to coarse PM.

4.7.4 Ultrafine Particle Source Determination

Spikes appeared in annual cycle UFP number concentration plots (May 1st, May 11th, May 17th, Oct. 5th, and Oct 11th) were investigated for source apportionment. For each spike day, the hourly UFP number concentration, air mass back trajectory, *chl a* concentration along air mass pathway and satellite images (if necessary) were studied and gathered. The time that spike occurred in the day was set as arrival time when retrieving HYSPLIT air mass back trajectory from NOAA website. Hourly wind speed on spike days were also provided to assist source apportionment.

4.7.4.1 May 1st UFP Spike

Figure 144 below shows source apportionment analysis (hourly UFP number concentration plot, air mass back trajectory on arrival date and SOTO daily phytoplankton abundance) for UFP spike occurred on May 1st.
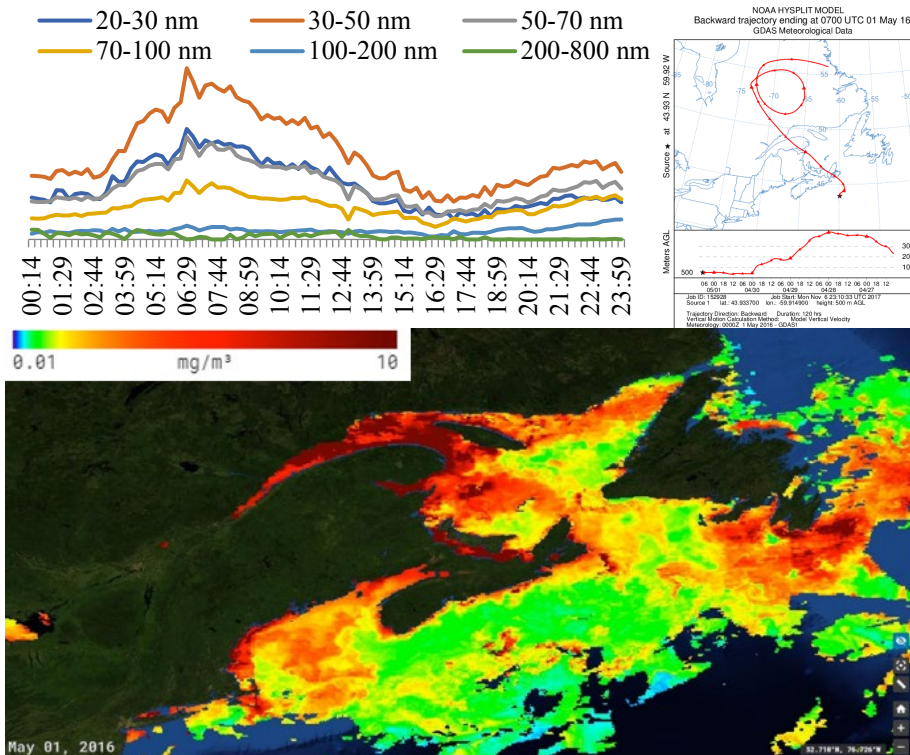
Figure 144 May 1st spike: hourly mean UFP plot (top left) and 5-day air mass back trajectory (top right), SOTO daily *chl a* concentration around the region (bottom).

From hourly mean UFP number counter plot shown in Figure 144, the May 1st UFP spike occurred at 6:30 am UTC where the 20-30, 30-50, 50-70, 70-100, 100-200 and 200-800 nm

number counts reached 1913, 2963, 1775, 1022, 239 and 0 particle/cm^3, respectively. Air mass originated from the Labrador coast and moved above Quebec at an altitude of 3000-4000 km (Figure 144), then lowered in altitude on approach to and crossing the St. Lawrence River. It then stayed at an altitude of 500 m until it left NS mainland crossing to Sable Island. The *chl a* concentration in St. Lawrence River and along NS coast were high at that time, implying that VOCs emitted by phytoplankton underwent gas-to-particle reactions forming UFP that generated the spike in number on Sable Island on May 1st.

4.7.4.2   *May 11th UFP Spike*

Figure 145 below shows source apportionment analysis (hourly UFP number concentration plot, air mass back trajectory on arrival date and SOTO daily phytoplankton abundance) for UFP spike occurred on May 11th – 12th.
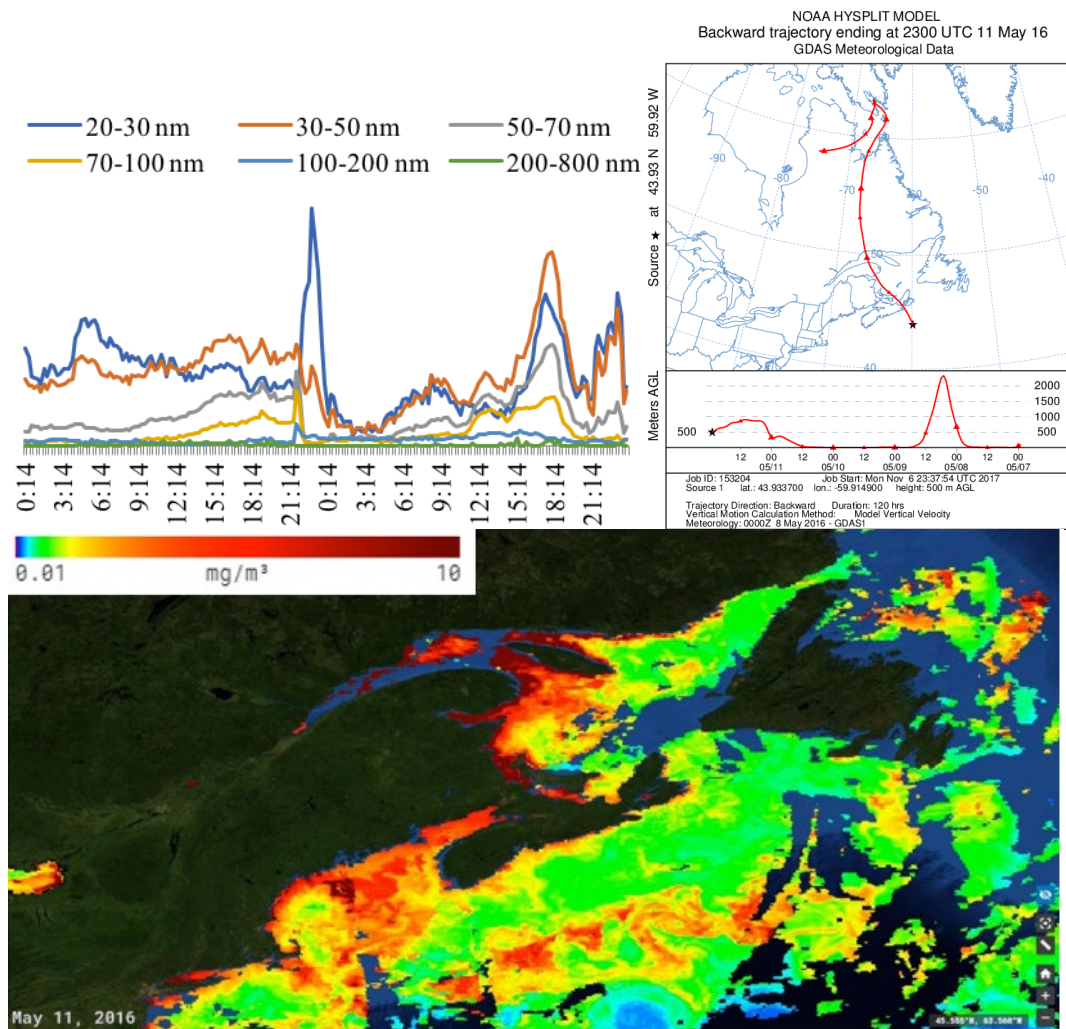
Figure 145 May 11ᵗʰ-12ᵗʰ spike: 48-hour hourly mean UFP plot (top left), 5-day air mass back trajectory ending at 23 pm 11ᵗʰ May 2016 (top right) and SOTO daily *chl a* concentration around the region (bottom).

From 48-hour hourly mean UFP plot shown in Figure 145, the spike on May 11ᵗʰ occurred at 22:30 UTC where the 20-30, 30-50, 50-70, 70-100, 100-200 and 200-800 nm number counts reached 3296, 1138, 91, 96, 191 and 0 particle/cm³, respectively; the second larger spike on May 12ᵗʰ occurred at 17:45 UTC where the 20-30, 30-50, 50-70, 70-100, 100-200 and 200-800 nm number counts reached 3096, 4120, 2134, 1037, 185 and 117 particle/cm³, respectively. It can be seen in Figure 145, air mass originated from Northern Quebec and moved at low altitude, then lowered in altitude further when approaching and crossing St. Lawrence River, after that it past PEI and went directly to Sable Island from NS mainland. The *chl a* concentration in PEI coastal area, St. Lawrence River and along NS coast were elevated at that time, and therefore

phytoplankton VOC emissions reacting in the atmosphere to form aerosols can be considered as the likely source of the UFP spike on Sable Island on May 11-12th.

4.7.4.3 *May 17th UFP Spike*

Figure 146 below shows source apportionment analysis (hourly UFP number concentration plot, air mass back trajectory on arrival date and SOTO daily phytoplankton abundance) for UFP spike occurred on May 17th – 18th.
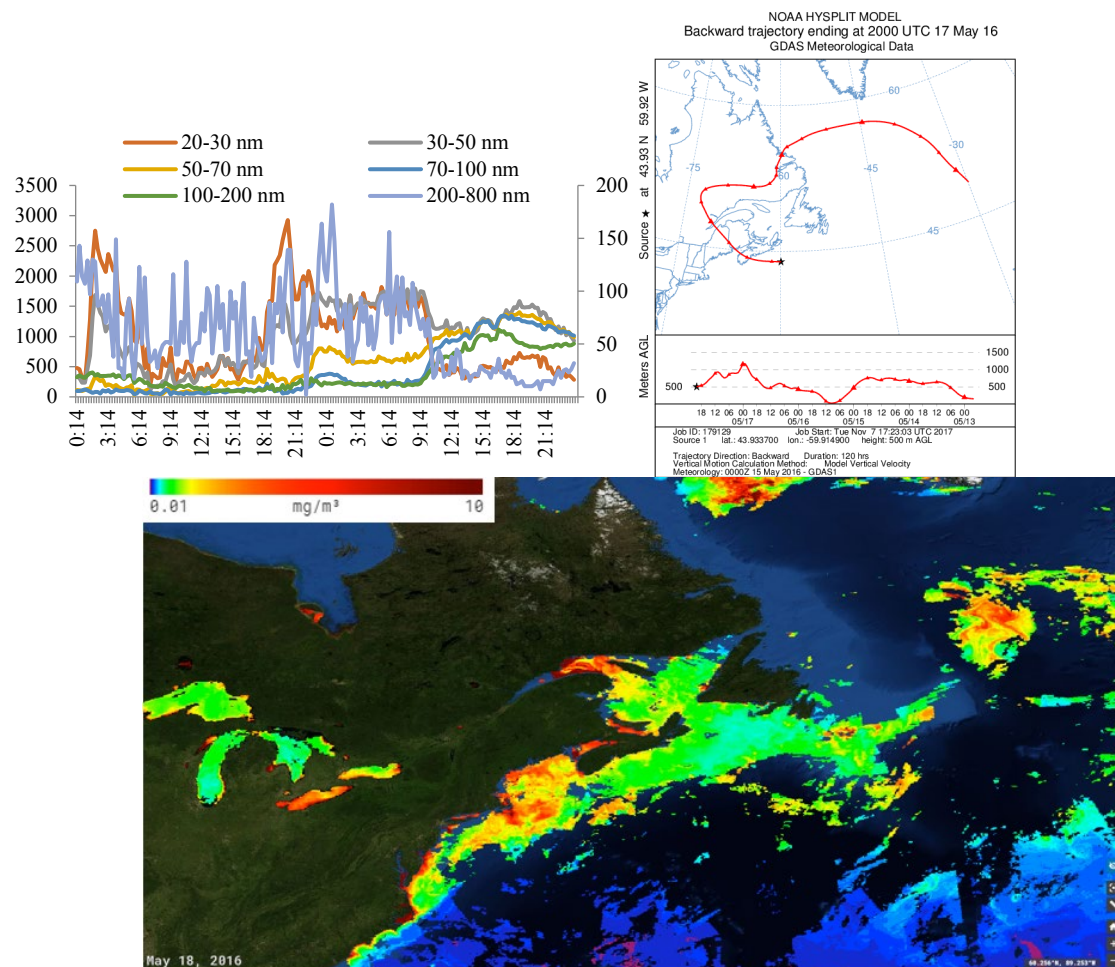
Figure 146 May 17th-18th spike: 48-hour hourly mean UFP plot (top left) and 5-day air mass back trajectory ending at 8 pm on 17th May (top right), Chlorophyll-a concentration around the region (bottom).

From 48-hour hourly mean UFP number counter plot shown in Figure 146, the UFP number counter spike on May 17-18th occurred at 2:00 and 20:15 UTC on May 17th where the 20-30, 30-50, 50-70, 70-100, 100-200 and 200-800 nm number counts reached 2776, 1535, 290, 67, 125 and 105 particle/cm^3, respectively at 20:15 on May 17th; the second larger spike on May 17th

occurred at 17:45 UTC where the 20-30, 30-50, 50-70, 70-100, 100-200 and 200-800 nm number counts reached 2752, 1686, 335, 80, 351 and 128 particle/cm^3, respectively. Air mass originated from middle of Atlantic Ocean (Figure 146), moved westward through Newfoundland and Quebec, and then went down southward across St. Lawrence River (19 hours before arrival on Sable Island) and Bay of Fundy (10 hours before arriving at Sable Island), after that arrived on Sable Island from NS mainland. The *chl a* concentration in St. Lawrence River, Bay of Fundy and NS coast was around 5.5 mg/m^3, and that can be considered as a source of UFP spike on Sable Island on May 17-18th. Furthermore, PM daily variance in May was also plotted, a spike (PM$_1$ reaching 24444 particle number/cm^3) was investigated on May 18th, which can be considered to be a result of coagulation of the UFPs.

4.7.4.4 Oct 5th UFP Spike

Figure 147 below shows source apportionment analysis (hourly UFP number concentration plot, air mass back trajectory on arrival date and SOTO daily phytoplankton abundance) for UFP spike occurred on Oct 5th.
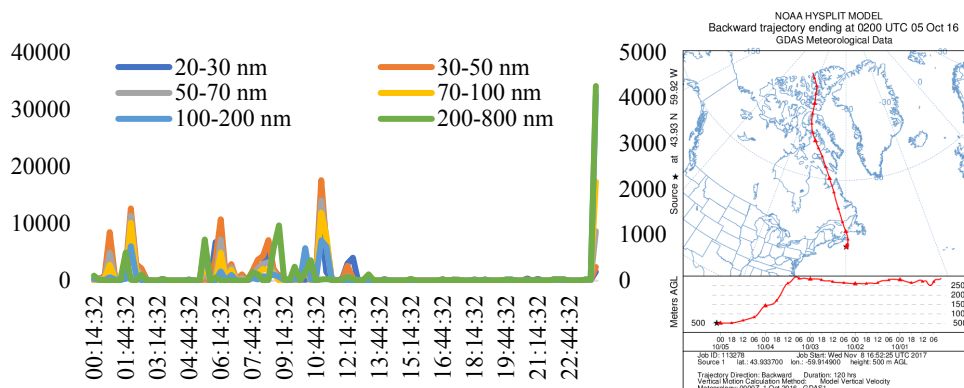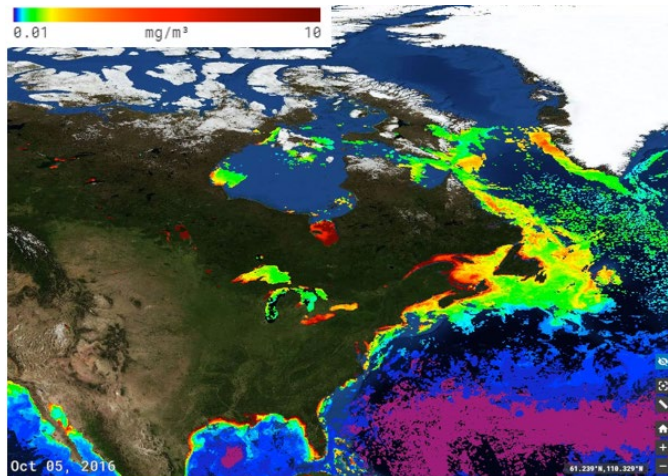
Figure 147 Oct 5ᵗʰ spike: hourly mean UFP plot (top left) and 5-day air mass back trajectory (top right), SOTO daily *chl a* concentration around the region (bottom)

From hourly mean UFP number counter plot shown in Figure 147, The spike on Oct 5ᵗʰ occurred several times during the morning where the 20-30, 30-50, 50-70, 70-100, 100-200 and 200-800 nm number counts reached 1136, 1480, 1124, 1089, 1111 and 162 particle/cm³, respectively. Air mass originated from arctic area, which does not have many anthropogenic sources. Then it moved straight south to Sable Island passing Gulf of St. Lawrence. The *chl a* concentration on that day was not significantly high enough to bring up a UFP spike; especially the sudden increase at 12 at night which pulls up the average of daily mean concentration for Oct 5ᵗʰ; it can be due to instrumental error adjustment. Figure 148 below shows source apportionment analysis (hourly UFP number concentration plot and hourly wind speed plot) for UFP spike occurred on Oct 11ᵗʰ – 13ᵗʰ.
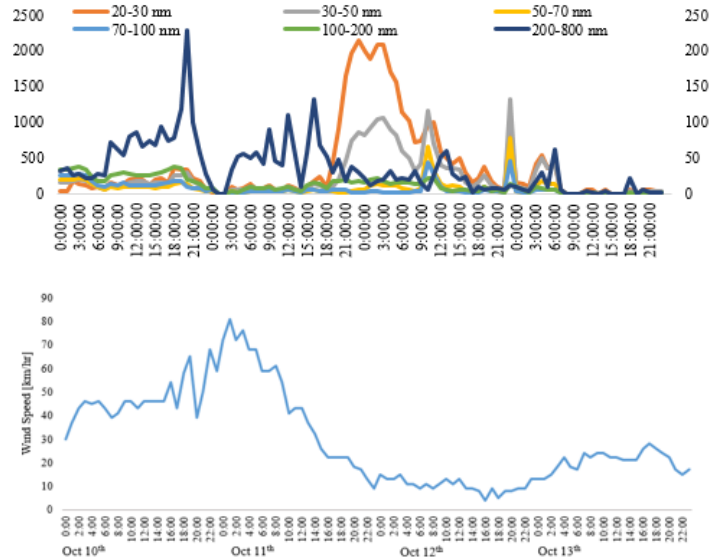
Figure 148 Oct 11th spike: Oct 10th – 13th 4-day hourly UFP number concentration [*#/cm³*] (top), and Oct 10th – 13th 4-day hourly wind speed (bottom)

In hourly mean UFP number counter plot shown in Figure 148, the spike on Oct 11th occurred at 23:00 where the 20-30, 30-50, 50-70, 70-100, 100-200 and 200-800 nm number counts reached 2147, 865, 65, 19, 175 and 31 particle/cm³, respectively. The hourly mean wind speed during Oct 10th – 13th was also plotted in Figure 148 (bottom panel), it can be seen that the wind speed was increasing and maintained in a rather high speed until Oct 11th morning; then few hours later in the afternoon, 20-30 nm and 30-50 nm UFP number counter began to increase.

4.7.4.5 *Oct 11th UFP spike*

Figure 149 below shows 72-hour HYSPLIT air mass back trajectory on arrival date and SOTO daily phytoplankton abundance for UFP spike source apportionment analysis occurred on Oct 11th – 13th.
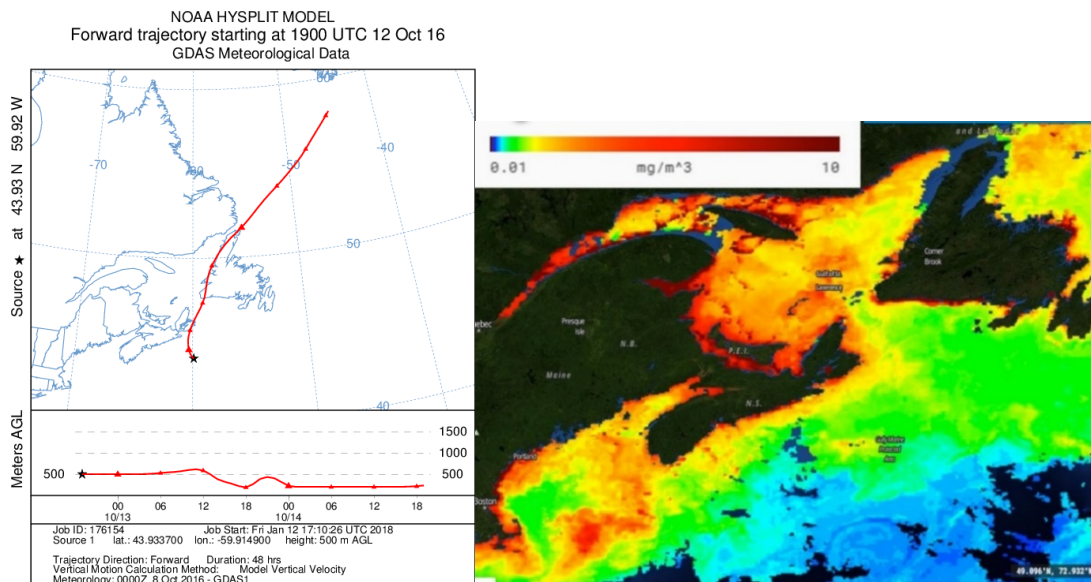
Figure 149 Oct 11ᵗʰ spike: 72-hour HYSPLIT 72-hour air mass back trajectory (left), Oct 12ᵗʰ SOTO daily chlorophyll-a concentration (right)

The 72-hr air mass back trajectory was generated for a better view of short-term air mass transport (Figure 149 left panel). From **Figure** 149 it can be seen that the back trajectory originated from the NE, crossing Newfoundland, crossing the Gulf of St. Lawrence, skirting the northeast corner of Cape Breton, finally crossing the ocean to Sable Island and with little anthropogenic input. The concentration of chlorophyll-a (Figure 149 right panel) along the path was approximately 7 (maximum was 10) mg/m^3 along NS coast and 4 mg/m^3 between NS mainland and Sable Island, confirming phytoplankton growth. Therefore, the spike at midnight on Oct 11-12 is likely due to gas-to-particle conversion of phytoplankton VOC emissions.

4.7.5 Fine and Course Particulate Matter Source Determination

The spikes that appeared in the annual time series PM concentration plots (Jan. 27ᵗʰ, Feb. 26ᵗʰ and Apr. 9ᵗʰ) were investigated. For each spike day, the hourly PM concentration, HYSPLIT air mass back trajectory and satellite images (if necessary) were studied and gathered. Both PM mass concentration and number concentration were presented, the time that spike occurred was set as arrival time of the 5-day air mass back trajectory.

185

4.7.5.1 Jan. 27th PM Spike

Figure 150 below shows source apportionment analysis (hourly PM number and mass concentration plot and air mass back trajectory on arrival date) for PM spike occurred on Jan. 27th.
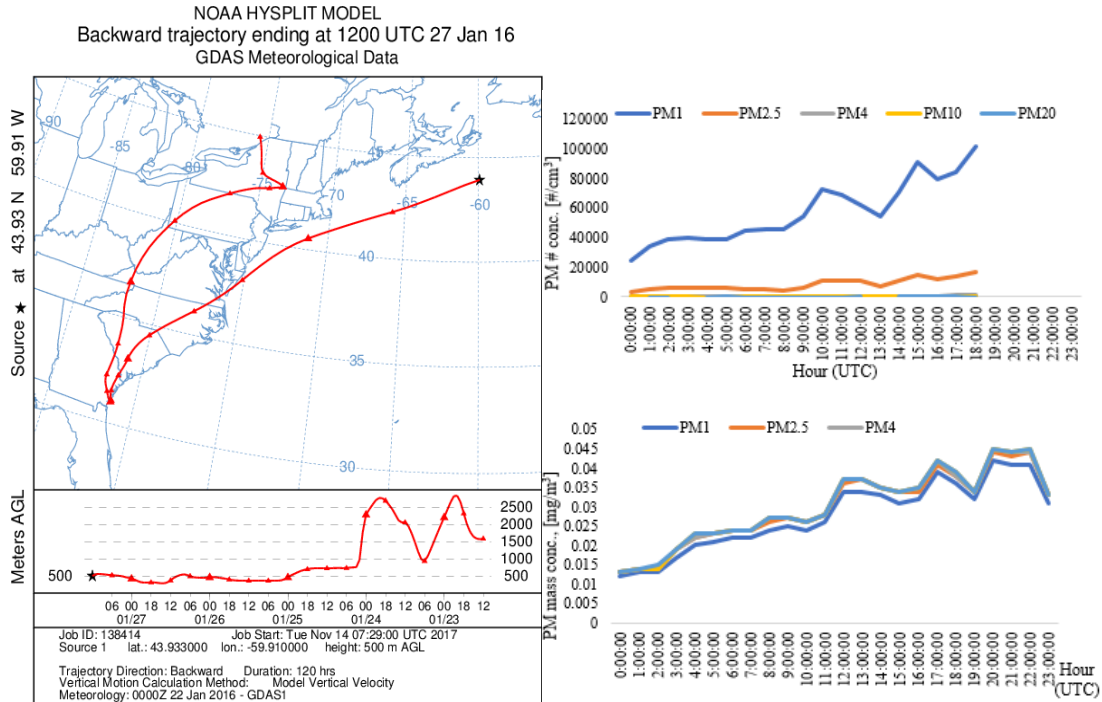
Figure 150 Jan. 27th spike: 120-hr air mass back trajectory (left), hourly PM number conc. (right top) and mass concentration (right bottom)

From hourly mean PM concentration plot shown in Figure 150, it can be seen that the PM mass and number concentration were increasing through the day until midnight. In 120-hr air mass back trajectory (Figure 150 left panel), it shows that the air mass originating in NE US, moving southward and then northeast passing industrial NE US again before landing at Sable Island. As mentioned previously, Pennsylvania, the Ohio Valley industrial zone, New York, I95 and port areas in Maryland have been identified as potential source regions for Halifax by Jeong et al. (2011) and Gibson et al. (2013), and are known to have many coal-fired power stations, vehicles and industry which suggests this spike may be due to LRT from this upwind source region. The air mass reaches an elevation of 2 000 m above the continent and drops to below 500 m over the Atlantic Ocean prior to reaching Sable Island. The air mass appears to pass close to the Deep Panuke and Thebaud oil and gas (O&G) platforms near Sable Island, indicating O&G as a potential additional source.

4.7.5.2 Feb. 26th PM Spike

Figure 151 and Figure 152 below shows source apportionment analysis (hourly PM number and mass concentration plot, HYSLPIT air mass back trajectory on arrival date and daily phytoplankton abundance) for PM spike occurred on Feb. 26th.
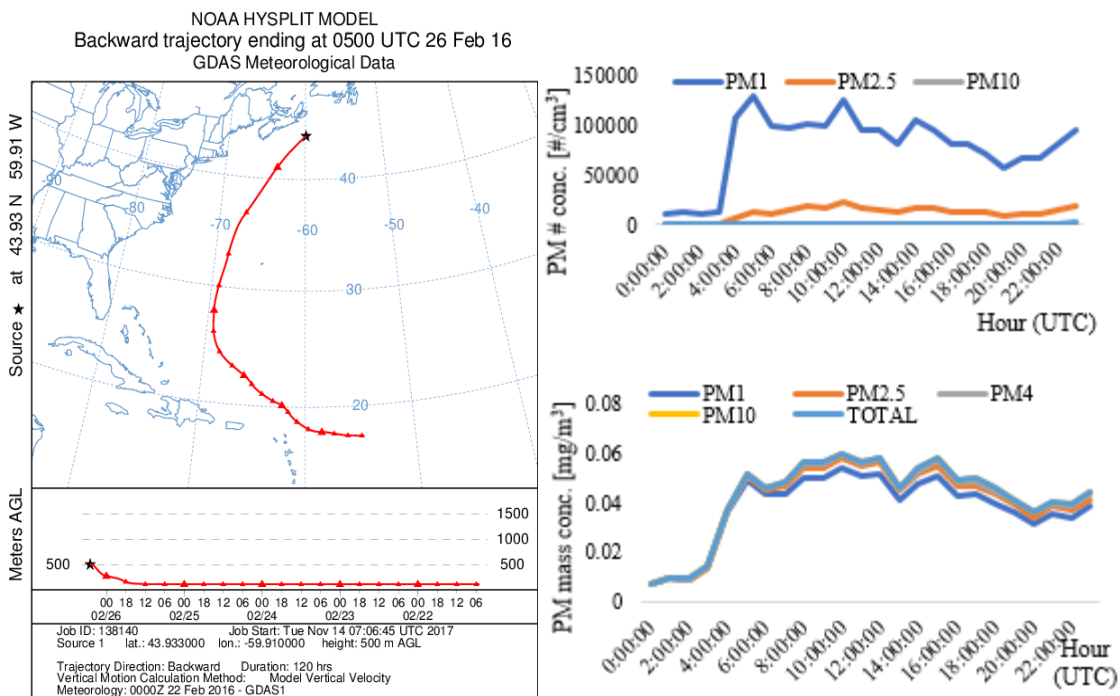
Figure 151 Feb. 26th spike: 120-hr air mass back trajectory (left), daily PM number (right top) and mass conc. hourly plot (right bottom)

The 120-hr air mass back trajectory, shown in Figure 151 left panel, shows that the air mass originated in a marine area and moved northward to Sable Island. LRT source from industrial NE US can be excluded. Also, the wind speed was 27.25 km/hr, which is around the mean wind speed experienced on Sable Island, with little wave action and therefore little wave-generated particles. PM_1 number counts were observed to increase higher than other size fractions. Furthermore, the PM_1 mass concentration was observed to be lower than other size fractions, which indicate that PM_1 was likely to be dominated by UFP on this day. UFP 20-30, 30-50, 50-70, 70-100, 100-200 and 200-800 nm number counts reached 656, 535, 284, 294, 512 and 114 particle/cm^3, respectively, all are much higher than February average of 341, 284, 161, 170, 296

and 71 particle/cm^3, respectively. In addition, phytoplankton abundance in the region was also obtained and shown in Figure 152.
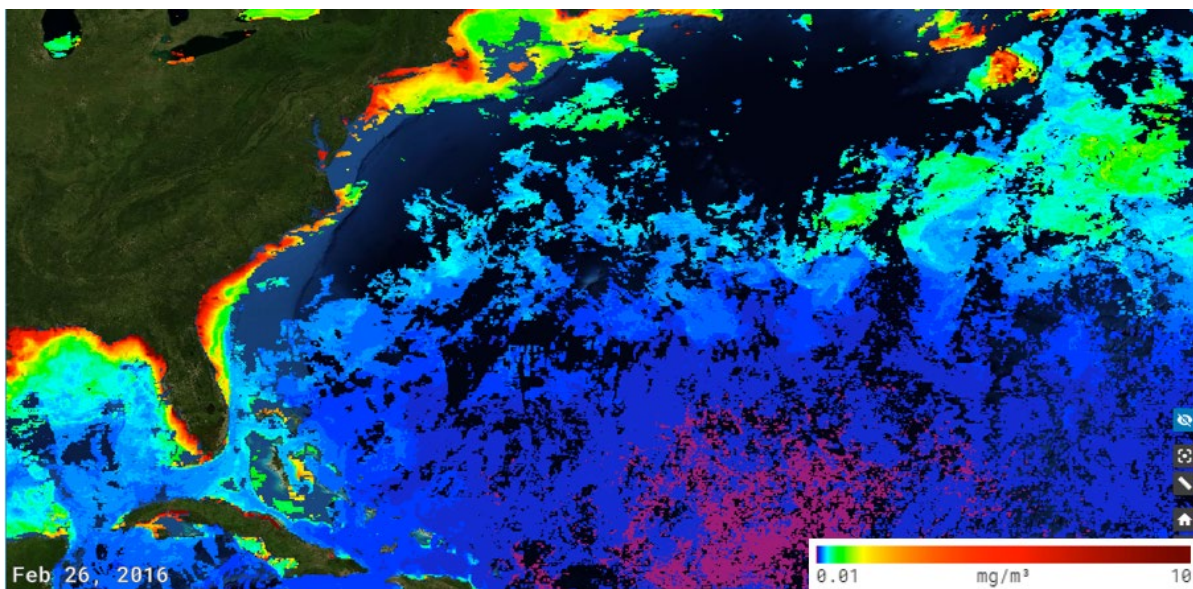
Figure 152 SOTO daily *Chl a* concentration in potential source region on February 25, 2016.

From Figure 152, it can be observed that daily *chl a* concentration was high along the air mass path to Sable Island, especially the altitude of airmass maintained at 500 m all the way. It is matching well with UFP number concentration shown in Figure 151. In this case, it can be assumed that the spike was likely to be the result of coagulation of UFP.

4.7.5.3 *Apr. 9th PM Spike*

Figure 153 below shows source apportionment analysis (hourly PM number and mass concentration plot, HYSLPIT air mass back trajectory on arrival date and daily phytoplankton abundance) for PM spike occurred on Apr. 9th.
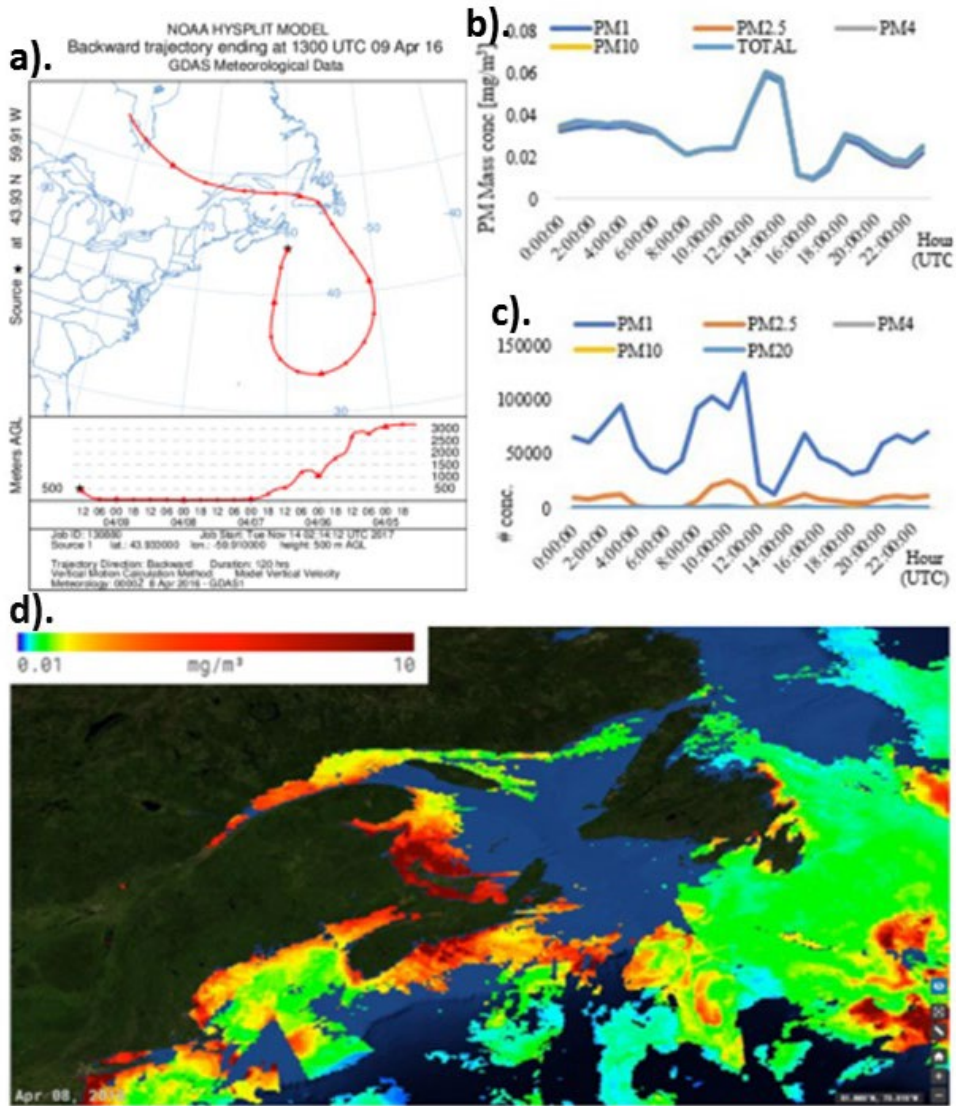
Figure 153 April 9th spike: a) 5-day air mass back trajectory; b) hourly PM mass concentration; c) hourly PM number concentration; and d) SOTO daily *chl a* concentration around Sable Island.

In Figure 153 a)HYSPLIT 5-day air mass back trajectory shows that the air mass originated from the James Bay area, which is a relatively clean area. PM mass concentration (Figure 153 b) shows that PM in each size fraction are consistent with each other, indicating that the source can be from island surface dust or ocean. Weather data was unavailable on that day so, it's hard to determine if it is windy. The air mass on that day was at the latitude of 500 meters, which is low, so it can be from the mixture of ocean emission and surface dust. However, to construct a more accurate conclusion, more details needed to be specified such as wind speed and weather condition as well as anthropogenic activities on the island.

189

4.8   Intra-study Comparison & Discussion

4.8.1   Seasonal variation

The p-value was investigated for PM in all size fractions (Table 28) to determine the seasonal variance in each size fraction with 95% confidence interval. In this study, seasons were divided in the following way: Spring: April, May, and June; Summer: July, August and September; Fall: October, November and December; Winter: January, February and March. p-value < 0.05 means there is a significant difference among four seasons; while p-value > 0.05 means there is no significant difference among four seasons.

Table 28 p-value for PM all size fraction seasonal variance

	Size fractions	p-value
UFP # concentration	20-30 nm	0.000
	30-50 nm	0.000
	50-70 nm	0.000
	70-100 nm	0.000
	100-200 nm	0.000
	200-800 nm	0.000
PM # concentration	PM_1	0.01
	$PM_{2.5}$	0.00
	PM_4	0.053
	PM_{10}	0.086
	PM_{20}	0.023
PM Mass concentration	PM_1	0.326
	$PM_{2.5}$	0.266
	PM_4	0.257
	PM_{10}	0.257
	TSP	0.258

As can be seen in Table 28, there is a season significant difference exhibited for UFP ($p < 0.000$), but no seasonal significant difference for $PM_{1/2.5/4/10/TSP}$ mass concentration and PM_4,

PM_{10} and PM_{20} number concentration. From Table 28, it can be observed that there is season significant difference for PM # concentration in the size fractions PM_1 and $PM_{2.5}$ (0.01 and 0.00 respectively).

4.8.2 UFP number concentration vs. total VOC concentration

Figure 154 and Figure 155 provide a monthly time series and a seasonal comparison plot of UFP and VOC's (averages of 15-minute measurements).
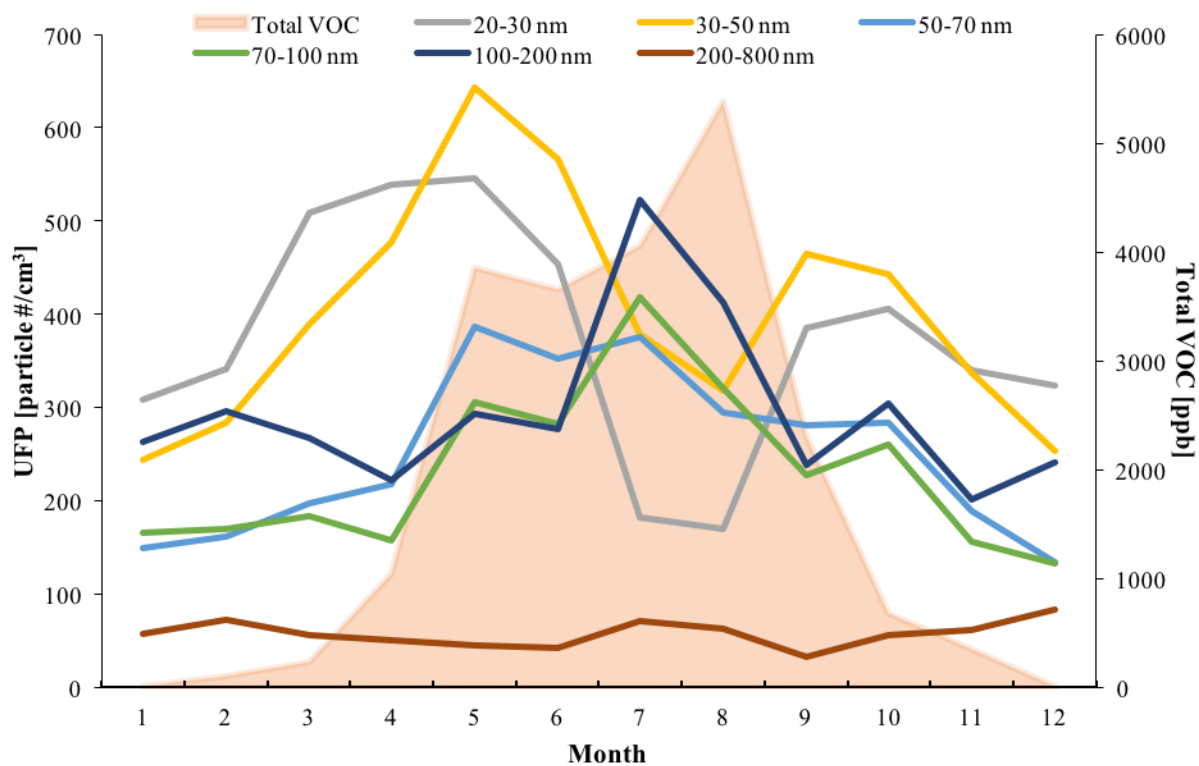
Figure 154 Monthly mean UFP number concentration (particle #/cm³) vs. mean monthly VOC concentration (ppb) on Sable Island in 2016.

Figure 154 shows the mean monthly UFP number concentration and VOC concentration. Line represents each UFP size fraction and shaded area indicates VOC concentration. From the chart, it can be seen that 20-30 and 30-50 nm UFP were increasing in April, May, September and October, the two distinct peaks occurring in May and September. 50-70 nm UFP began to increase in April and lasted until August. 70-100 nm UFP began to increase in April and reached peak in May, July and October. 100-200 nm UFP did not increase until July and then reduced quickly again in August and September followed by a minor peak in October. The 200-800 nm

UFP trend was too low to be seen clearly in this chart but is provided in the following section. The total VOC concentration increased in April and continued to increase through the summer, reaching a maximum in August, and then it diminished quickly into the fall and winter, following the seasonal continental vegetation and growth cycle. An overview of the seasonal mean UFP number concentration and total VOC concentration is provided below in Figure 155. The reason why VOC's do not covary with UFP can be explained by the fact that the local VOCs observed originating from the Ocean are also mixed with continental VOCs, whereas the UFP's are only from local sources due to their short lifetime in the atmosphere (Coe et al., 2000; Vaattovaara et al., 2006). Particles smaller than 10 nm have been detected frequently in marine air mass, so this particle size can be associated with VOC as they followed the trend of VOC concentration during the daytime, 30 - 90 min after the UV solar flux increased, their concentration increased sharply, then by early afternoon, the concentration returned to background concentrations (Coe et al., 2000; Vaattovaara et al., 2006).
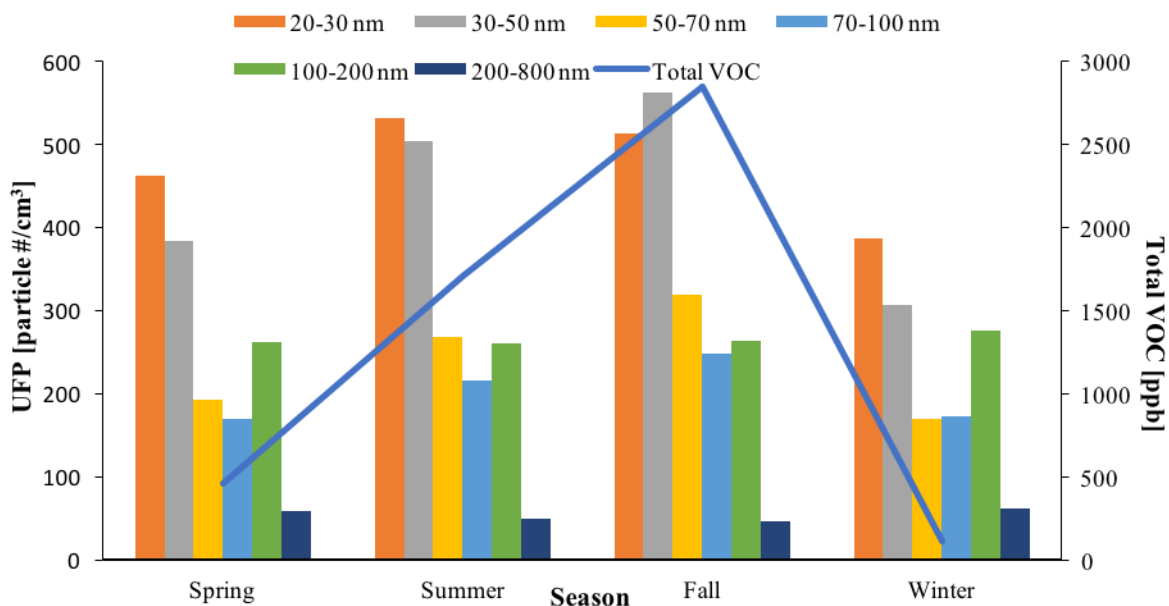
Figure 155 Seasonal mean UFP number concentration (particle #/cm^3) vs. mean seasonal total VOC concentration (ppb) on Sable Island in 2016.

Figure 155 reveals the mean seasonal trends of UFP number counts and total VOC concentrations (average of 15 minute data). It can be seen that total VOC seasonal mean concentration match well with UFP seasonal trends. The overall seasonal trend of total VOC and UFP number agree well, the total VOC concentration is seen to increase in February and decreases in November, in agreement with the UFP number concentration. In particular, VOC

192

co-varies with UFP 100-200 nm, which is the size range associated with the fast coagulation of fresh UFP. It is likely that UFP 100-200 nm is the coagulation products of both 20-30 nm and 30-50 nm UFP, which is assumed to be the gas-to-particle conversion product from VOCs. However, when looking at a monthly variance, the total VOC concentration and UFP number does not match very well, it can be due to several reasons; firstly, there are still other VOCs originating from either marine (halocarbons or isoprene) area or continental flows; secondly, due to instrument malfunction in August, which is the month that VOC reaches the maximum, UFP data is not available, resulting in an important UFP data loss for August. Because of reasons above, *chl a* concentration was investigated and used to run correlation test with UFP concentration in the following section.

4.8.3 UFP number concentration vs. chlorophyll-a concentration

Correlation between UFP and *chl a* concentration was also assessed. Monthly mean UFP number concentration was calculated from 15-minute measurement on Sable Island in 2016; the monthly mean chlorophyll-a concentration was retrieved from MODIS satellite observation via Giovanni data analysis system. Pearson's correlation test was also conducted in RStudio to show how they correlate with each other statistically. Figure 156 provides the comparison of monthly mean *chl a* concentration and UFP number concentration trends.
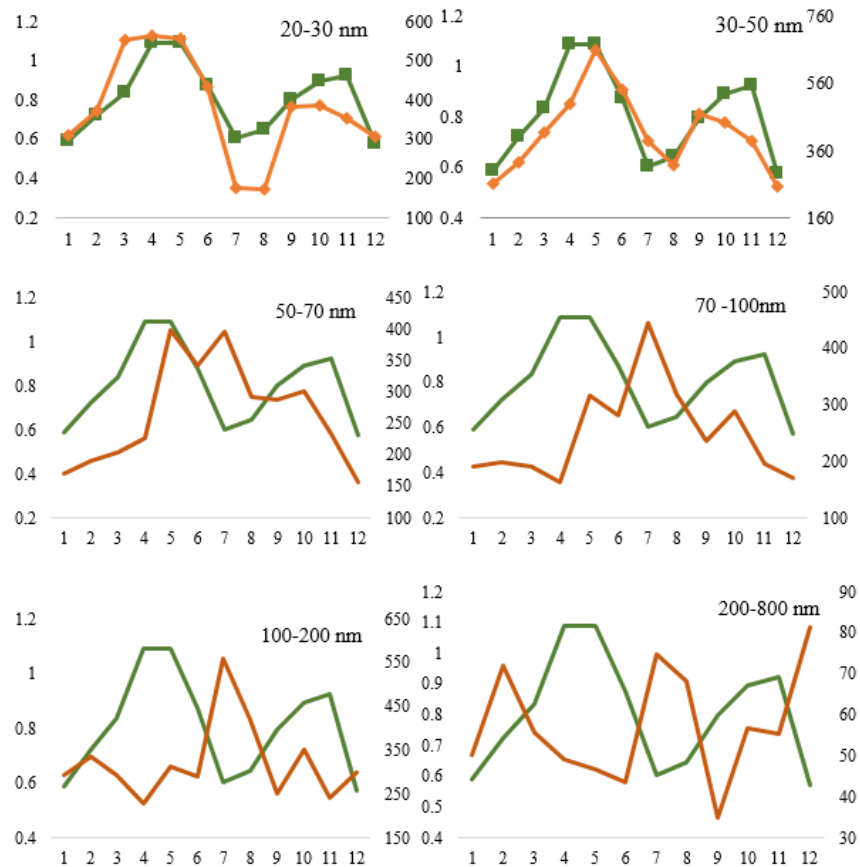
Figure 156 Comparison of monthly mean chlorophyll-a concentration and UFP (20-800 nm). Green line represents chlorophyll-a concentration; orange line represents different UFP sizes. Left vertical axis is *chl a* concentration [*mg/m³*], right vertical axis is UFP number counter [*#/cm³*], horizontal axis shows month in number.

In Figure 156, it reveals that 20-30 nm and 30-50 nm UFP number concentration trend matches very well with *chl a* concentration. They both have a major bloom in April and May and a second peak in October. Furthermore, the 100-200 nm and 200-800 nm UFP have very different trend to *chl a* concentration. In August, when *chl a* reached its maximum concentration, the 100-

800 UFP number counts instrument had a malfunction. A correlation test was run between *chl a* concentration and each UFP size fraction number concentration and shown in Figure 157.
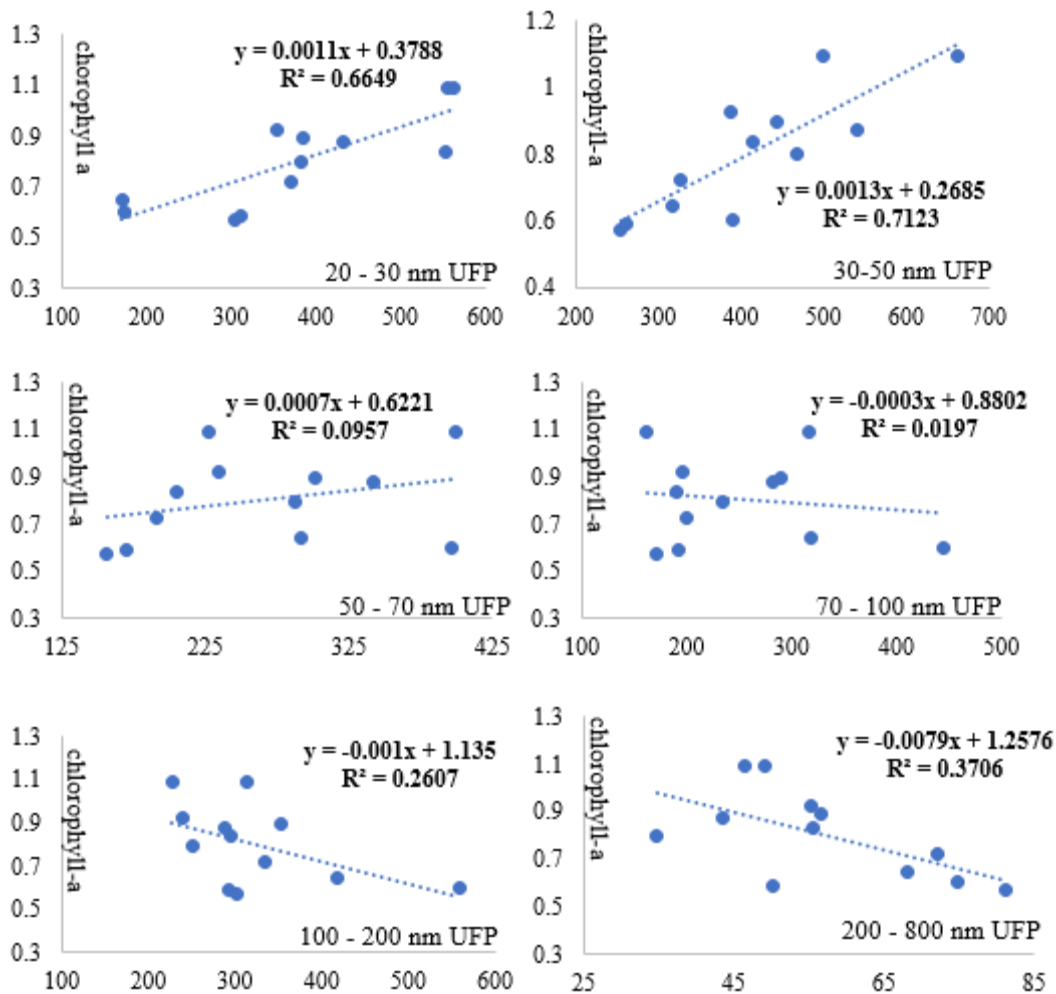
Figure 157 Correlation tests between UFP number concentrations for default size fractions versus chlorophyll-a monthly mean concentration.

It can be seen in Figure 157 that 20-30 nm and 30-50 nm UFP have the two highest R^2 value among six size fractions (0.6649 and 0.7123, respectively). In this case, 20-50 nm UFP are highly positively correlated to *chl a* concentration, and 200-800 nm UFP are negatively correlated to *chl a* concentration. This test result agrees with Pearson correlation test results shown in Table 29.

Table 29 Summary of correlation tests for UFP all size fractions and chlorophyll-a

Size fractions	Pearson correlation	p-value	R^2 value
20-30nm	0.815	0.01	0.6649
30-50 nm	0.844	0.01	0.7123
50-70 nm	0.309	0.328	0.0957
70-100 nm	-0.140	0.664	0.0197
100-200 nm	-0.511	0.09	0.2607
200-800 nm	-0.609	0.036	0.3706

Pearson test shown in Table 29 reveals good agreements with correlation tests shown in Figure 157, 20-30 nm and 30-50 nm UFP had the highest Pearson coefficient (0.815 and 0.844), showing the strong positive correlation between 20-50 nm UFP and phytoplankton abundance. In addition, the 200-800 nm UFP had the most negative Pearson coefficient (-0.609), showing the strong negative correlation between 200-800 nm UFP and *chl a* concentration. This is likely due to this size fraction being known to be associated with 'aged' aerosol and long-range transport from the continent and not local phytoplankton emissions (Gibson, M.D. et al., 2013).

In conclusion, Figure 156 presents the visual comparison of monthly *chl a* concentration and UFP number concentration trend over 12 months. It was found that here is good agreement between the *chl a* concentration and UFP (20-30 nm and 30-50 nm) number concentration, with significant correlation between the two variables (R^2 = 0.815 and 0.844) (Figure 156). Apart from these two size fractions, other UFP size fractions show weak correlation with *chl a* concentration (as would be expected being associated with LRT); further supported by the UFP 200-800 nm size fraction having a strong negative correlation with *chl a*. (Figure 157 & Table 29). This study provides similar results shown to previous studies (Craig et al., 2015; Shadwick et al., 2011), shown in Figure 158.
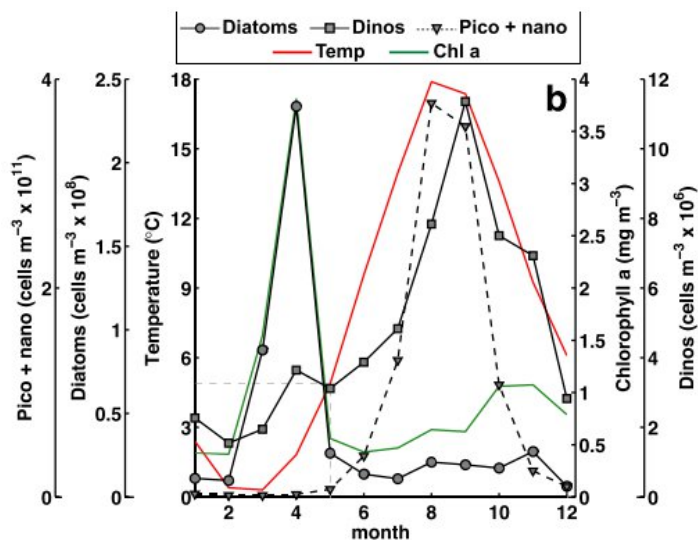
Figure 158 Seasonal cycle of temperature, *chl a*, diatoms, pico- & nanophytoplankton (Craig et al., 2015)

Figure 158 provides the annual cycle of diatoms, nanophytoplankton (nano), picophytoplankton (pico), pico and nano combined (pico+ nano) and dinoflagellates (dinos) concentrations measured in Bedford Basin (Craig et al., 2015). In the plot, it can be seen that diatoms concentration began to increase in March, reaching a peak in April, diminishing after that; pico+nano phytoplankton do not appear until July and June, then reached the peak in August and September. There is a variation in peak month between this study and Craig et al., 2015 study. This may be caused by the fact that monthly mean *chl a* concentration used in this study was calculated over a large area (including the Labrador Sea and Gulf of St. Lawrence) that extends into northern waters where the spring bloom occurs later in the season. The spatial averaging may have resulted in a peak that occurred later in the season and may, in large part, explain the disparity in spring peaks compared with the coastal and shelf sites studied by Craig et al., 2015. Visual comparison between total VOC and *chl a* was shown in Figure 159.
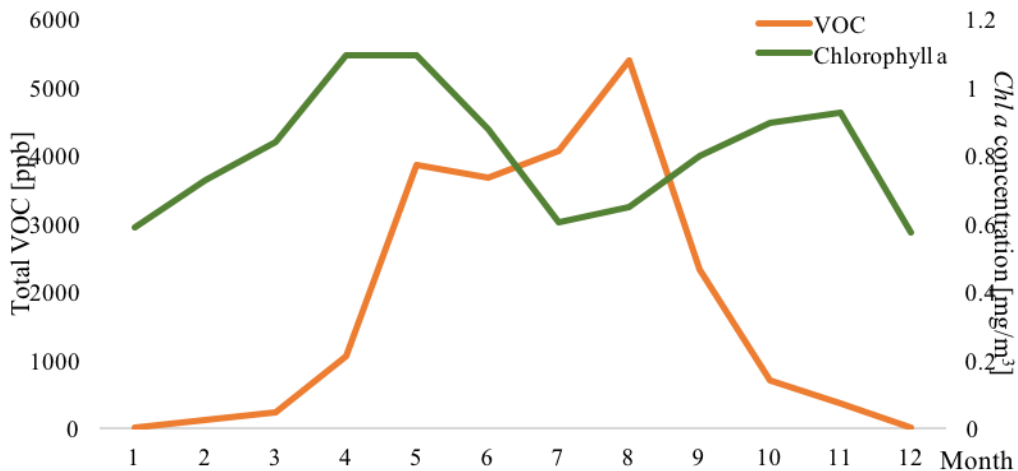
**Figure 159 Monthly mean *chl a* concentration (mg/m³)
in the ocean around Sable Island vs. mean monthly VOC concentration (ppb)**

As can be seen in Figure 159, the monthly trends do not match well. However, both of them began to increase in March. It is because that *chl a* is the representative of phytoplankton but not total VOC which can influence from continental outflow. In addition, it is not only phytoplankton that emit VOC but also other biomass such as zooplankton and fish. To summarize, UFP 20-50 nm trends coincided with *chl a* concentration, but the total VOC concentration did not, likely due to the mixing of continental VOC species.

4.8.4 Comparison with other ultrafine particle studies

Brace et al., 2014 found outdoor Halifax UFP number concentrations ranging from 7902 to 14,105 #/cm³. This compares with the UFP range observed on Sable Island of 666 #/cm³. The huge difference is because Brace conducted the measurement in Halifax urban area where there are significant anthropogenic sources (vehicles, industry etc.) while Sable Island has few sources of UFP and can be considered a pristine air zone.

PM_{10} mass concentration on Sable Island was compared with a study conducted on Cape Verde in 2007. During 14th May – 14th July, 2016, on Sable Island, PM_{10} = 12.8 (4.2:34.1 µg/m³); during 14th May – 14th July, 2007, at Cape Verde station, PM_{10} mass ranging from 15 to 332 µg/m³. The maximum PM_{10} mass concentration in Cape Verde is much higher, due to wind generated ocean spray and the influence of dust advected from the desert Sahara desert. Apart from mineral dust, 60% of 0.05-0.14 µm particles on Cape Verde were found to be organic matter, 10% were sulfate, and they were both from ocean biogenic emissions. On Sable Island,

90% of 0.05-0.2 µm particles were from ocean biogenic emissions. The higher percentage from ocean on Sable Island is because, compared to Cape Verde, it is more isolated and truly marine. Another study conducted by Yoon et al. in 2007 showed similar results, that marine secondary biogenic organic compounds dominate PM in nucleation modes. In Yoon et al., 2007 study, particles in Aitken mode was <0.1 µm and accumulation mode was 0.1-0.5 µm; while in this study, the Aitken mode was 20-50 µm and accumulation mode was 50-200 µm. Seasonal variation for size distribution, the Aitken mode particles increased from 0.031 µm in winter to 0.049 µm in summer, particle number increased from 137 /cm^3 to 327 /cm^3; the accumulation mode increased from 0.103 µm in winter to 0.177 µm in summer, particle number increase from 117 /cm^3 to 142 /cm^3 (Yoon et al., 2007). In this study, the Aitken mode particles increased from 0.045 µm in winter to 0.053 µm in summer, particle number increased from 609 /cm^3 to 674 /cm^3, the accumulation mode increased from 0.193 µm in winter to 0.214 µm in summer, particle number increased from 669 /cm^3 to 1113 /cm^3. Values vary between this study and Yoon et al. (2007) due to sampling taking place in different years, locations and using different instruments, but, importantly, the trends remain the same. Moreover, in the study conducted by Yoon et al., the seasonal variation in phytoplankton bloom from NW to NE was revealed, as well as the significant correlation between marine particles with the size below 0.5 µm and phytoplankton abundance.

Figure 160 below shows another UFP trend conducted in Mace Head during May 17th – May 20th, 1994. The relationships between UFP and UVA radiation and tides were investigated in the study. UFP number concentration and diurnal variation in Mace Head and Sable Island were compared.
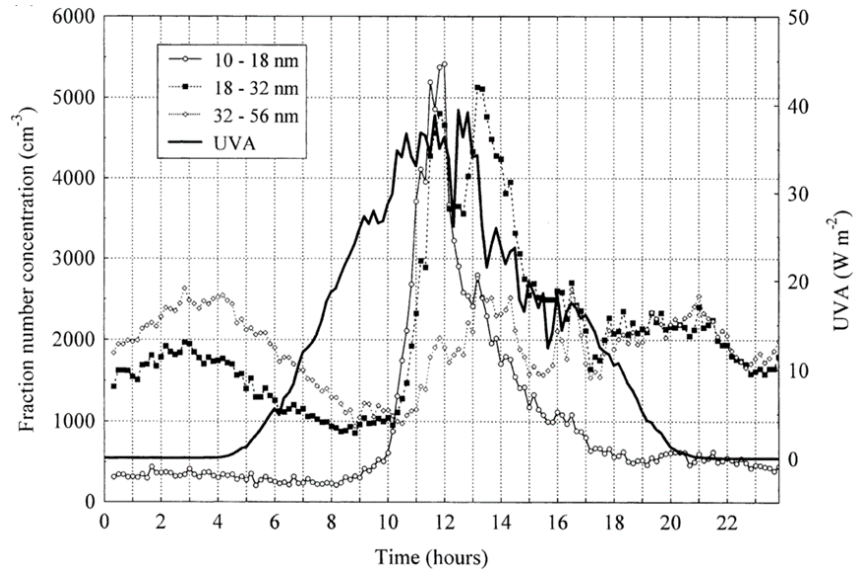
Figure 160 Mean fraction number concentrations, UVA radiation, and tide height categorized by time of day over May 17th – May 20th, 1994 (Vana, Jennings, Kleefeld, Mirme, & Tamm, 2002)

It can be seen from Figure 160 that UVA didn't increase until 5 am, which is earlier than the time of sunrise; five hours after UVA increase, 10-18 nm particles began to increase and reached maximum (5500 /cm^3) within 4 hours and maintaining this concentration for one hour; then half hour later the 10-18 nm began to increase, 18-32 nm particles began to increase, reaching a maximum (5000 /cm^3) about an hour after the 18-32 nm peak number concentration; 2 hours later the 18-32 nm began to increase, 32-56 nm particles began to increase and reached maximum (2750 /cm^3) in two hours. By way of comparison with this study, a mean 4-day period (May 17th – May 20th) particle number concentration during on Sable Island is shown in Figure 161.
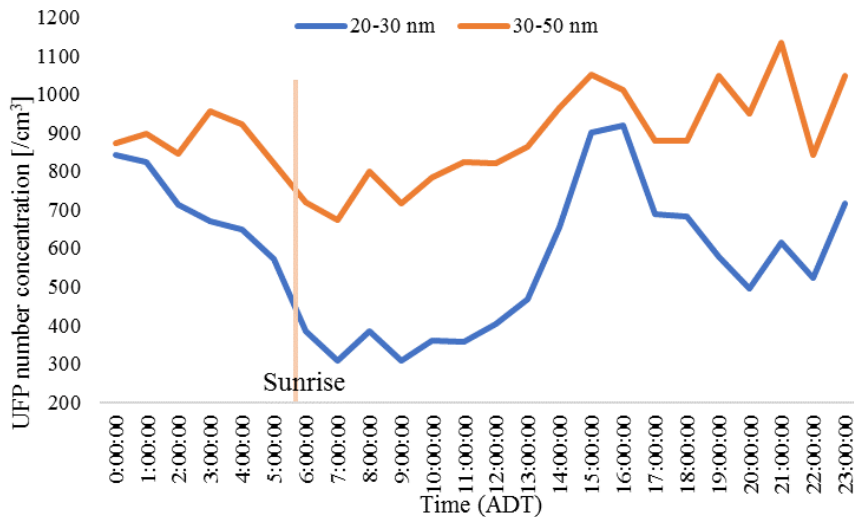
Figure 161 Mean fraction number concentration by time of day during May 17-20

It can be seen in Figure 161 that the sunrise time on Sable Island was around 5:45 am, almost same as Mace Head. Then, 5 hours later around 11 am, 20-30 nm and 30-50 nm particles began to increase until 15:00 they reached maximum (901 and 1050 /cm^3, respectively). The time difference between sunrise and spike time were similar, but UFP number on Sable Island was much less than UFP at Mace Head. Firstly, it can be due to that Sable Island is a more isolated island while Mace Head is closer to mainland anthropogenic influences. In addition, Mace Head is tidal whereas Sable Island is not as impacting by tiding action. The hourly mean water level in Halifax and Mace Head was calculated on the same period (May 17-20) in 2017, water level in Halifax ranged from 0.2 to 1 m, while Mace Head had water level ranged from -1.27 to 1.36 m. Low tide can stimulate the particle concentration events (Vana et al., 2002). Overall, the result of this study conducted on Sable Island in NW Atlantic Ocean matches well with results from some of study conducted in NE Atlantic Ocean, adding weight to the results of this ESRF funded study.

5   CONCLUSION AND RECOMMENDATIONS

5.1   Conclusions and Recommendations Based on Results Prior to 2016

5.1.1   Conclusions

The objective of this part of the ESRF study was to apportion the major sources of air pollution affecting the air quality on Sable Island to better understand the impacts of nearby offshore O&G activities, continental outflow (e.g. smog and wildfires) and marine emissions (e.g. sea salt spray, natural gaseous emissions directly from the ocean and if possible ship emissions). In particular, it focused on the effect of bringing a new O&G platform online through to production. This was achieved by performing source apportionment modelling. Real time sampling data was collected and then used to perform statistical analysis and run the USEPA PMF model. HYSPLIT back trajectories, satellite imagery, weather data, and pollution roses were used in support of the source apportionment modelling process.

The time series plots showed that total non-methane hydrocarbons (NMHC), black carbon (BC), hydrogen sulphide (H_2S), and sulphur dioxide (SO_2) concentrations tend to be generally low (compared to the NSE Air Quality Regulations, Canada-Wide Standards, and World Health Organization guidelines) with proportionally elevated concentrations occurring at specific times. These elevated concentrations are most likely linked to pollution events, linking NMHC, BC, H_2S, and SO_2 to sources with intermittent emissions. This was a conclusion reinforced by the PMF model outputs that identified flaring and off gassing from offshore O&G activity and also biogenic contributions from phytoplankton as their main source. Time series plots for particles with a median aerodynamic diameter ≤ 2.5 microns ($PM_{2.5}$), ozone (O_3), nitrogen monoxide (NO), nitrogen oxides (NO_x), and nitrogen dioxide (NO_2) were found to show more constant concentrations. Source apportionment modelling, with support from HYSPLIT and satellite data, showed the predominant likely source of NO_x was continental outflow advecting over Sable Island. Without chemical speciation of the $PM_{2.5}$ it is difficult to identify the source of the $PM_{2.5}$ affecting Sable Island, but is likely a heterogeneous mixture of sea salt spray, continental outflow, on island sources and with small inputs from O&G production activity.

Analysis of the descriptive statistics for the data found that the mean concentration for $PM_{2.5}$ was 14.1 $\mu g/m^3$. This is a rather high value considering Sable Island's remote location in the Atlantic. It was determined that sea salt is the likely cause of the higher than expected concentration.

The mean concentration for NMHCs was 0.034 ppm and for BC was 0.091 $\mu g/m^3$. Mean concentrations for SO_2, H_2S, O_3, NO_x, NO_2, and NO were 0.17 ppb, 0.36 ppb, 30.4 ppb, 2.17 ppb, 1.11 ppb, and 1.0 ppb respectively. The O_3 concentration of 30.4 observed over the course of the study on Sable Island is of a similar magnitude to the Canadian annual average concentration of O_3 of 33 ppb in 2011 (Environment Canada, 2013). This again is a reflection of the source of O_3 being associated with continental outflow of anthropogenic and natural O_3 sources in the North Atlantic (Gibson et al., 2013d, Gibson et al., 2009a). For H_2S, NO_2 and SO_2, all of the average and maximum concentrations fall below Canadian air quality regulations. Mean concentrations of $PM_{2.5}$ and O_3 are below the Canada-Wide Standards (24 hour average for $PM_{2.5}$ and 8 hour average for O_3). All recorded O_3 concentrations are below the Canada-Wide Standards.

The PMF model run identified 4 sources (Long Range Transport continental outflow, off-gassing of platform fugitive emissions, flaring, and on-site combustion) contributing to the air quality on Sable Island. However, the estimated source contributions to the total gaseous concentration and $PM_{2.5}$ mass concentration could not be determined due to insufficient chemical speciation data.

Source 1 was determined had high contributions from $PM_{2.5}$, O_3, NO_x, NO_2, and NO with low concentrations of SO_2. Pollution rose analysis and air mass back trajectory modelling supported Source 1 as being associated with Long Range Transport continental outflow (LRT).

Source 2 was determined to be off-gassing from O&G production facilities. Source 2 had low contributions from $PM_{2.5}$ and BC with higher contributions from NO_x and H_2S. O_3 was also strongly correlated with this factor which is likely due to its formation from the pre-cursor NO_2 and VOCs in the vicinity of Sable Island (Gibson et al 2009). It was found that VOC emissions from phytoplankton blooms might be contributing to this factor during periods of high biomass. However, without VOC chemical speciation data it is not possible to apportion VOC emissions from offshore O&G and that contribution from phytoplankton blooms. A Spearman rank order correlation was run in SigmaPlot and found that NMHC and H_2S concentrations were strongly correlated, further supporting the interpretation that production platforms as the main contributor to NMHC concentrations. Contributions from Source 2 can be seen to increase after July 22nd, which would fit well with off-gassing emissions associated with bringing new O&G production

activity online. Furthermore, the study was run mainly over the summer months, therefore likely missing the spring and part of the autumnal phytoplankton blooms. In 2016, GC-MS VOC speciation was conducted on Sable Island that improved the source apportionment estimate of phytoplankton emissions impacting the air quality on Sable Island.

Source 3 was determined to represent flaring from offshore O&G production activity. High contributions from $PM_{2.5}$, BC, H_2S, SO_2, and NO_x were present. H_2S is a strong marker of offshore O&G production as it is present in the production fields. NMHC concentrations are minimal, which is likely due to the fact that they would be combusted to CO_2 and H_2O during flaring. It can be seen from Figure 50 that contributions for Source Factor 3 increase drastically after July 22nd correlating with increased flaring from new offshore O&G activity. Pollution rose and HYSPLIT air mass back trajectory analysis also supports Source Factor 3 as representing O&G production flaring.

High contributions from $PM_{2.5}$, BC SO_2, NO_2, and NO were present in Source Factor 4. Source Factor 4 was estimated to be related to on-site combustion including local emissions such as transportation emissions to and from both the island and most importantly localized emissions on the island itself related to electricity generation and waste incineration. Contributions for on-site combustion decreased during the warmer summer months when less electricity was required for heating. Pollution rose and HYSPLIT air mass back trajectory analysis also supported Source Factor 4 as on-site combustion.

5.2   Episodic pollution events

Pollution events for NMHCs and $PM_{2.5}$ were examined using HYSPLIT air mass back trajectories and visible satellite images. The results enforced the conclusion that off-gassing and flaring from the production platforms is a major source of NMHCs on Sable Island with possible contributions from phytoplankton during certain time periods. Pollution events involving $PM_{2.5}$ were found to be associated with LRT continental outflow from the eastern seaboard of the United States and areas of eastern Canada. From this, it can be concluded that the O&G production facilities were most likely the main contributor to NMHCs during elevated concentrations, with potential contributions from phytoplankton. Pollution rose analysis and

HYSPLIT air mass back trajectory modelling supported the conclusion that the elevated $PM_{2.5}$ concentrations observed were likely due to continental outflow of man-made and natural air pollution sources.

5.3 Air quality comparison before and after O&G production coming online on July 22nd 2013

The data before and after July 22nd 2013 was compared in order to determine the potential effect of new offshore O&G activity commencing at this time. NMHC showed no statistically significant ($p > 0.05$) difference after July 22nd 2013. The median values and upper percentiles for BC, $PM_{2.5}$, NO, and NO_x showed decreases after July 22nd, while those for SO_2, H_2S, and NO_2 show increases. The descriptive statistics before and after July 22nd show that mean concentrations for SO_2 increased from 0.063 ppb to 0.24 ppb. Mean concentrations of H_2S increased from 0.21 ppb to 0.48 ppb. SO_2 and H_2S are the main components of the earlier source factor that was identified as flaring. Flaring would be associated with bringing online new O&G production activity. BC, It was determined from this analysis that bringing new offshore O&G production activity online produced a significant increase in SO_2 and H_2S concentrations. However, these changes were well below Canada Wide Standards. It would also be anticipated that initial increases in SO_2 and H_2S would decline sharply once the production is stabilized.

In conclusion, it was found that the air quality on Sable Island is good, with all concentrations for the sampling period falling well below Canada Wide Standards. Average $PM_{2.5}$ concentrations were higher than those found previously in Halifax (likely due to sea salt spray and continental outflow), and O_3 concentrations were found to be similar to the Canadian ambient annual average concentrations. The four main sources affecting the air quality on Sable Island are LRT continental outflow, off-gassing from offshore O&G activity (with potential contributions from phytoplankton blooms), flaring from offshore O&G production activity, and on-site combustion sources. New offshore O&G activity brought online July 22nd 2013 was found to cause a significant increase in SO_2 and H_2S, with concentrations well below Canada Wide Standards. Since this report was finished the positive drift in the SO_2 and H_2S analyzers was found to be due to instrumental drift and not due to local emissions from O&G production activity.

5.3.1 Recommendations from the 2013 monitoring

It is recommended that sampling on Sable Island, now a National Park, continue into the future as further characterization of the air quality would be beneficial to understand the impacts further O&G production activity may have on the air quality on Sable Island. In addition, new International Maritime Organization regulations governing the quality of marine fuel will result in significantly reduced emissions from shipping over the next 5-years, in turn changing the air pollution mixture in coastal waters (Sulphur oxides (SO_x) Regulation 14, 2014). Air quality monitoring on Sable Island will act as a sentinel to these changes in the source apportionment of air pollution impacting Sable Island. On a global scale, this air quality data on Sable Island will act as an emission inventory that can be fed into climate models, allowing improved predictions of climate change.

Unfortunately, due to practical constraints, this section of the study (pre-2016) did not capture seasonal trends or involve sampling during the winter months. A multi-year sampling campaign would further improve our understanding of the seasonal source apportionment of gases and $PM_{2.5}$ impacting Sable Island. In particular this would allow for sampling equipment to capture the annual spring and autumn phytoplankton blooms that are known to occur on the Scotian Shelf (Georges et al., 2014; Craig et al., 2012). Coupled with VOC speciation, data obtained using GC-MS, and greater sampling of particulate mass concentration species (using filter based sampling or aerosol monitors), this would allow for more in depth source apportionment modelling of the air quality on Sable Island.

5.4 Conclusions and Recommendations Based on 2016 Results

5.4.1 Conclusion

This part of the ESRF study found that the UFP (Ultra Fine Particle) and fine PM (Particle Matter) number concentrations were significantly different ($p<0.000$) between seasons. PM_1 and $PM_{2.5}$ number concentrations vary among seasons but interestingly, their mass concentration did not show significant differences ($p>0.05$). This is due to UFP's dynamic seasonal and diurnal variation compared with the fine or coarse particle mass concentrations.

The ocean *chlorophyll-a* (*chl a*) and UFP concentrations were highly correlated but total VOCs did not correlate with UFP. However, it is likely that phytoplankton emissions, as well as other

biogenic emissions from the ocean are the source of the UFP in the size-range encompassing 20-50 nm. This is because the particles in this size-range quickly (matter of minutes) coagulate to larger particle sizes and therefore cannot be associated with continental outflow.

This study tentatively identified and quantified four main sources of size-resolved PM number concentration on Sable Island in 2016. The four size-resolved sources that were apportioned included sea spray (2.2% of total UFP, 1.3% of total PM), secondary marine biogenic particles (78.2% of total UFP, 0.8% of total PM), Long Range Transport (LRT) (4.4% of total UFP, 60.1% of total PM) and wind-blown island surface dust (15.2% of total UFP, 37.7% of total PM), where secondary marine biogenic particles were the dominant contributor to UFP and LRT was the dominant contributor to coarse PM (> 2.5 microns). The discovery of the close correlation between UFP (20-30 nm and 30-50 nm) and *chl a* ($R^2 = 0.815$ and $R^2 = 0.815$, respectively) is a significant finding related to ocean-atmosphere dynamics and marine atmospheric chemistry over the North West Atlantic.

5.4.2 Recommendations

It is recommended that further monitoring be conducted to investigate multi-year associations between phytoplankton VOC emissions and their influence on the formation of freshly formed UFP in the 20-30nm size range. It is recommended that future research incorporates both particle species and gaseous species to better understand the ocean-atmosphere interactions and formation of UFP that act as cloud condensation nuclei that are so important in terms of mediating climate. This speciation data will also help to improve estimates of contributions from O&G production activity affecting Sable Island.

5.5 Overall Study Conclusions Overall Study

This project aimed to identify different sources of air pollution effecting the air quality on Sable Island, with the aim of better understanding the impacts of emissions from nearby offshore O&G production, directly from the ocean and from continental outflow of anthropic and biogenic emissions.

Gaseous and size-resolved particulate matter mass and number concentrations data was obtained from May 7th 2013, through project completion on December 31st 2017.

All of the average and maximum concentrations for the air pollutants measured fell below Canada Wide Standards.

During the early stages of the project (2013), four tentative sources contributing to the air quality on Sable Island were identified and included long range transport (LRT), offshore O&G production, marine emissions and on-island combustion. However, a lack of a full suite of continuous and 24-hr integrated operating instruments, caused by numerous contract amendments to replace instruments that were originally to have been supplied from research partners or removed from the Island by Nova Scotia Environment, meant that the mass contributions from these sources could not be determined due to insufficient aerosol and VOC chemical speciation data.

After the full suite of instruments were finally in place, in late 2015, monitoring was conducted for the entirety of 2016 (and still for $PM_{2.5}$, H_2S, SO_2, NO_x and O_3 still continues). The data completeness for 2016 was: UFP, and VOC instruments > 91.6%; NO_x, O_3, SO_2 and H_2S 66.7%; APS (fine to coarse PM number) 58%; only 5-days of BC data due to a capture error that went

undetected. The loss of BC is unfortunate, as it is a good marker for combustion of fossil fuels and wildfire smoke. None of the 'criteria' and regulated air pollutants ($PM_{2.5}$, O_3, SO_2, NO_x) were found to be above Provincial or National Air Quality Guidelines in 2016. Indeed, the concentrations are low and reflect the fact that Sable Island is located in a clean marine environment.

The 2016 data completeness for temperature, wind direction and wind speed was 96%, 100% and 99% respectively. The mean (min : max) temperature and wind speed was found to be 9.04 (-11.4 : 53.8°C), 25.39 km/h (0 : 84 km/h). It was found that the average wind vector for 2016 was found to be 256°, which is consistent with prevailing winds in the North West (NW) Atlantic.

In terms of off shore oil and gas production activity, Deep Panuke had several extended shutdown periods in 2016 for maintenance, repair and/or seasonal production (Jan 15-26; Mar 20-May 26; May 29-Jun 16; Oct 14-25 and Nov 1-8). ExxonMobil had a planned field-wide maintenance shutdown between September 15 and October 7 2016.

It terms of identifying potential O&G production emissions, there was a spike in H_2S of 6.01 ppbv on July 17th, 2106. However, this spike is well below the 1-hr Nova Scotia air quality objective of 30 ppbv. This H_2S spike is obviously linked to the elevated SO_2 level of 3.04 ppbv that occurred on the same day, and also well below the 1-hr Canada Ambient Air Quality Objectives threshold of 344 ppbv. Scrutiny of the air mass back trajectories for this day showed that air flow passed over both the Deep Panuke and Thebaud platforms preceding and during observations on Sable Island. The spike 'might' be associated with flaring of H_2S on the Deep Panuke platform at the time. On May 10th, 2016 there was a spike in NO_x concentration of 7.16 ppbv. This happened a few days after the ExxonMobil platform wide maintenance shutdown. The airflow during the spike observations was directly over the Thebaud platform. Therefore, it could be the source of the elevated NO_x observed on that date. However, this NO_x spike is well below the Canada Ambient Air Quality Objective of 213 ppbv.

The source apportionment of the size-resolved particle number and mass concentration yielded four source factors and included sea spray (2.2% UFP), secondary marine biogenic particles (78.2%), long range transport (4.4%) and island surface dust (15.2%).

The strong correlations between UFP (20-30 nm & 30-50 nm) and *chlorophyll a* ($R^2 = 0.815$ and $R^2 = 0.815$), was the most salient feature of this study and provides powerful insight into ocean-atmosphere dynamics that remain a high uncertainty in global climate research.

O&G production emissions were negligible over the course of the study (January 1st 2013 - December 31st 2016) and it was not possible to identify a definite O&G source 'factor' using PMF source apportionment modelling during 2016 as the emissions from O&G are extremely low, with intermittent 'spikes' that are dwarfed by continental and oceanic atmospheric gas and particle inputs.

The chief emissions sources impacting air quality on Sable Island are associated with the long-range transport continental outflow of anthropogenic and biogenic gases and particulate matter, VOCs associated with marine emissions. The VOCs emitted from the ocean undergo photochemical reactions forming secondary ultrafine particles. Major sources of particle number > 2.5 μm included sea salt spray and wind-blown sand.

REFERENCES

Acker, J. G., & Leptoukh, G. (2007). Online analysis enhances use of NASA Earth science data. Eos, Transactions American Geophysical Union, 88(2), 14–17. https://doi.org/10.1029/2007EO020003

Adventure Canada | Sable Island. (2017). Retrieved November 23, 2017, from http://www.adventurecanada.com/trip/sable-island-2017/

Andreae, M. O., & Crutzen, P. J. (1997). Atmospheric aerosols: Biogeochemical sources and role in atmospheric chemistry. Science, 276(5315), 1052-1058. doi:10.1126/science.276.5315.1052

Baker, A.R., Turner, S.M., Broadgate, W.J., Thompson, A., McFiggans, G.B., Vesperii, O., Nightengale, P.D., Liss, P.S., & Jickells, T.D., (2000). Distribution and sea– air fluxes of biogenic trace gases in the eastern Atlantic Ocean. Glob. Biogeochem. Cycles, 14 (3), 871– 886.

Barnett, T. C. (2016). The Source Apportionment of Airborne Particulate Matter Composition on Sable Island, Nova Scotia, Canada. Dalhousie University.

Batchelor, G.K. (1973). An Introduction to Fluid Dynamics. Cambridge University Press.

Bell, J. N. B., & Treshow, M. (2002). Air pollution and plant life (2nd ed. .). Chichester: Chichester : Wiley.

Bell, J. N. B., & Treshow, M. (2003). Air pollution and plant life (2nd ed.) John Wiley & Sons. doi:9780471490906.

Beranek, J., Imre, D., & Zelenyuk, A. (2012). Real-time shape-based particle separation and detailed in situ particle shape characterization. Analytical Chemistry, 84(3), 1459–1465. https://doi.org/10.1021/ac202235z

Beusse, R., & Hauck, E. (2013). EPA needs to improve air emissions data for the oil and natural gas production sector. (Review No. 13-P-0161). U.S. Environmental Protection Agency.

Beusse, R., Dunlap, C., Good, K., Hauck, E., Mcghee-lenart, R., & Narimatsu, J. (2013). EPA Needs to Improve Air Emissions Data for the Oil and Natural Gas Production Sector (Vol. P-0161). https://doi.org/13-P-0161

Bhattacharjee, H., Drescher, M., Good, T., Hartley, Z., Leza, J. D., Lin, B., Wu, D. (1999). Particulate matter in New Jersey. (Graduate Class Report). Princeton: Woodrow Wilson School of Public and International Affairs Princeton University.

Boney, A. D. (Arthur D. (1989). Phytoplankton (2nd ed. .). London: London : Edward Arnold.

Brace, M. D., Stevens, E., Taylor, S., Butt, S., Sun, Z., Hu, L., … Gibson, M. D. (2014). `The air that we breathe?: assessment of laser and electrosurgical dissection devices on operating theater air quality. Journal of Otolaryngology - Head & Neck Surgery = Le Journal D'oto-Rhino-Laryngologie et de Chirurgie Cervico-Faciale, 43(1), 39. https://doi.org/10.1186/PREACCEPT-7454522201323814

Brimblecombe, P. (1996). Air composition and chemistry. Cambridge (2nd ed. ., Vol. 11). Cambridge [Cambridgeshire] ; New York: Cambridge Cambridgeshire ; New York : Cambridge University Press. https://doi.org/10.1016/0160-9327(87)90266-3

Broadgate, W.J., Liss, P.S., & Penkett, S.A., (1997). Seasonal emissions of isoprene and other reactive hydrocarbon gases from the ocean. Geophys. Res. Lett., 24 (21), 2675– 2678.

Brook, R. D., Urch, B., Dvonch, T. J., Bard, R. L., Speck, M., Keeler, G., Brook, J. R. (2009). Insights into the mechanisms and mediators of the effects of air pollution exposure on blood pressure and vascular function in healthy humans. Hypertension Journal of the American Heart Association, 54, 659-667. doi:10.1161/HYPERTENSIONAHA.109.130237

Brown, S. G., Frankel, A. & Hafner, H. R. (2007). Source apportionment of VOCs in the Los Angeles area using positive matrix factorization. Atmospheric Environment, 41, 227-237.

Burkart, J., Willis, M. D., Bozem, H., Thomas, J. L., Law, K., Hoor, P., … Richard Leaitch, W. (2017). Summertime observations of elevated levels of ultrafine particles in the high Arctic marine boundary layer. Atmospheric Chemistry and Physics, 17(8), 5515–5535. https://doi.org/10.5194/acp-17-5515-2017

Calde On-garcidu Nas, L., Reed, W., Maronpot, R. R., Hen Iquez-rol, C. A., Delgado-chavez, R., Calde, A., … Swenberg, J. A. (2004). Brain Inflammation and Alzheimer's-Like Pathology in Individuals Exposed to Severe Air Pollution. Toxicologic Pathology, 32, 650–658. https://doi.org/10.1080/01926230490520232

Canada NS offshore Petroleum Board. (2013). Venture Thebaud. Retrieved November 8, 2017, from https://www.cnsopb.ns.ca/pdfs/sable_area_platforms.pdf

Carder, K.L., Steward, R.G., Harvey, G.R., & Ortner, P.B. (1989). Marine humic and fulvic acids: Their effects on remote sensing of ocean chlorophyll. Limnology and Oceanography, 34, 68-81.

Charlson, M. E., Pompei, P., Ales, K. L., & MacKenzie, C. R. (1987). A new method of classifying prognostic comorbidity in longitudinal studies: Development and validation. Journal of Chronic Diseases, 40(5), 373–383. https://doi.org/10.1016/0021-9681(87)90171-8

Claeys, M., Graham, B., Vas, G., Wang, W., Vermeylen, R., Pashynska, V., Maenhaut, W. (2004). Formation of secondary organic aerosols through photooxidation of isoprene. Science, 303, 1173-1176. doi:10.1126/science.1092805

Coe, H., Williams, P. I., McFiggans, G., Gallagher, M. W., Beswick, K. M., Bower, K. N., & Choularton, T. W. (2000). Behavior of ultrafine particles in continental and marine air masses at a rural site in the United Kingdom. Journal of Geophysical Research-Atmospheres, 105(D22), 26891–26905. https://doi.org/10.1029/2000jd900234

Cohen, A. J., Anderson, H. R., Ostro, B., Pandey, K. D., Krzyzanowski, M., Künzli, N., … Smith, K. (2005). The global burden of disease due to outdoor air pollution. Journal of Toxicology and Environmental Health - Part A, 68(13–14), 1301–1307. https://doi.org/10.1080/15287390590936166

Collins, D. B., Burkart, J., Chang, R. Y.-W., Lizotte, M., Boivin-Rioux, A., Blais, M., … Abbatt, J. P. D. (2017). Frequent Ultrafine Particle Formation and Growth in the Canadian Arctic Marine Environment. Atmospheric Chemistry and Physics Discussions, (June), 1–31. https://doi.org/10.5194/acp-2017-411

Colomb, A., Gros, V., Alvain, S., Sarda-Esteve, R., Bonsang, B., Moulin, C., Klupfel, T. & Williams, J. (2009). Variation of atmospheric volatile organic compounds over the Southern Indian Ocean (30-49ºS). Environmental Chemistry, 6, 70-82.

Colomb, A., Yasaa, N., Williams, J., Peeken, A., & Lochte, K. (2008). Screening volatile organic compounds (VOCs) emissions from five marine phytoplankton species by head space gas chromatography/mass spectrometry (HS-GC/MS). Journal of Environmental Monitoring, doi:10.1039/b715312k

Comero, S., Capitani, L., & Gawlik, B. M. (2009). Positive Matrix Factorisation (PMF) An introduction to the chemometric evaluation of environmental monitoring data using PMF. https://doi.org/10.2788/2497

Compounds, V. O., Devices, C., Sources, P., & Sources, N. (2007). Characterization of Greenhouse Gas Emissions Involved in Oil and Gas Exploration and Production Operations.

Conti, M. E., & Cecchetti, G. (2001). Biological monitoring: Lichens as bioindicators of air pollution assessment - a review. Environmental Pollution, 114(3), 471-492.

Craig, S. E., Jones, C.T., Li, W.K.W., Lazin, G., Horne, E., Caverhill, C., & Cullen, J.J. (2012). Deriving optical metrics of ecological variability from measurements of coastal ocean colour. Remote Sensing of Environment, 119, 72-83.

Craig, S. E., Thomas, H., Jones, C. T., Li, W. K. W., Greenan, B. J. W., Shadwick, E. H., & Burt, W. J. (2015). The effect of seasonality in phytoplankton community composition on

CO 2 uptake on the Scotian Shelf. Journal of Marine Systems, 147, 52–60. https://doi.org/10.1016/j.jmarsys.2014.07.006

Davidson, C. I., Phalen, R. F., & Solomon, P. A. (2005). Airborne particulate matter and human health: A review. Aerosol Science and Technology, 39(8), 737–749. https://doi.org/10.1080/02786820500191348

Davison, B., O'Dowd, C., Hewitt, C. N., Smith, M. H., Harrison, R. M., Peel, D. A., Wolf, E., Mulvaney, R., Schwikowski, M. & Baltenspergert, U. (1996). Dimethyl sulfide and its oxidation products in the atmosphere of the Atlantic and Southern Oceans. Atmospheric Environment

Deep Panuke Canada - Nova Scotia benefits. (2013). (Annual Report). Halifax, Nova Scotia: EnCana Corporation.

Deep Panuke gas production 'on track' for June. (2013). Retrieved 06/26, 2013, from http://www.cbc.ca/news/canada/nova-scotia/story/2013/05/23/ns-deep-panuke-june-production.html

Deep Panuke Offshore gas development environmental assessment report. (2006). (Environmental Assessment No. DMEN-X00-RP-RE-00-0005 Rev 01U). Halifax, Nova Scotia: EnCana Corporation.

Deep Panuke project newsletter. (December 2007). EnCana Corporation.

Dillon, P.J., Yan, N.D., Harvey, H.H., Schindler, D.W. (1984). Acidic deposition: Effects on aquatic ecosystems. CRC Critical Reviews in Environmental Control, 13(3), 167-194.

Dockery, D. W. (2009). Health Effects of Particulate Air Pollution. Annals of Epidemiology, 19(4), 257–263. https://doi.org/10.1016/j.annepidem.2009.01.018

Dockery, D. W., & Stone, P. H. (2007). Cardiovascular risks from fine particulate air pollution. New England Journal of Medicine, 356, 511-513.

Dockery, D. W., Pope, C. A., Xu, X., Spengler, J. D., Ware, J. H., Fay, M. E., … Speizer, F. E. (1993). An Association between Air Pollution and Mortality in Six U.S. Cities. New England Journal of Medicine, 329(24), 1753–1759. https://doi.org/10.1056/NEJM199312093292401

Dohoo, C., Guernsey, J. R., Gibson, M. D., & Vanleeuwen, J. (2013). Impact of biogas digesters on cookhouse volatile organic compound exposure for rural Kenyan farmwomen. Journal of Exposure Science and Environmental Epidemiology Advance Online Publication July, 31. https://doi.org/10.1038/jes.2013.42

Dominici, F., Peng, R., Bell, M., Pham, L., McDermott, A., Zeger, S., & Samet, J. (2006). Fine particulate air pollution and hospital admission for cardiovascular and respiratory

diseases. JAMA (Journal of the American Medical Association), 295(10), 1127–1134. https://doi.org/10.1001/jama.295.10.1127.Fine

Donaldson, K., Stone, V., Seaton, A., & MacNee, W. (2001). Ambient particle inhalation and the cardiovascular system: Potential mechanisms. Environmental Health Perspectives, 106, 523-527.

Duderstadt, K. A., Carroll, M. A., Sillman, S., Wang, T., Albercook, G. M., Feng, L., … Forbes, G. (1998). Photochemical production and loss rates of ozone at Sable Island, Nova Scotia during the North Atlantic Regional Experiment (NARE) 1993 summer intensive. Journal of Geophysical Research-Atmospheres, 103(D11), 13531–13555. https://doi.org/10.1029/98JD00397

Environment Canada: Ambient levels of ozone. (2013). Retrieved 12/7, 2013, from https://www.ec.gc.ca/indicateurs-indicators/default.asp?lang=en&n=9EBBCA88-1

Environment Canada: Canada-Wide Standards (CWS). (2013). Retrieved 1/7, 2014, from http://www.ec.gc.ca/rnspa-naps/default.asp?lang=En&n=07BC2AC0-1

Environment Canada: Canadian Ambient Air Quality Standards. (2013). Retrieved 1/7, 2014, from http://ec.gc.ca/default.asp?lang=En&n=56D4043B-1&news=A4B2C28A-2DFB-4BF4-8777-ADF29B4360BD

EPA. (2016). Health and Environmental Effects of Particulate Matter (PM). Retrieved November 4, 2017, from https://www.epa.gov/pm-pollution/health-and-environmental-effects-particulate-matter-pm

Evans, J. S., Tosteson, T., & Kinney, P. L. (1984). Cross-sectional mortality studies and air pollution risk assessment. Environment International, 10(1), 55-83. doi:10.1016/0160-4120(84)90233-2

Fountoukis, C., Riipinen, I., Denier Van Der Gon, H. A. C., Charalampidis, P. E., Pilinis, C., Wiedensohler, A., … Pandis, S. N. (2012). Simulating ultrafine particle formation in Europe using a regional CTM: Contribution of primary emissions versus secondary formation to aerosol number concentrations. Atmospheric Chemistry and Physics, 12(18), 8663–8677. https://doi.org/10.5194/acp-12-8663-2012

Fournier, R. O., Marra, J., Bohrer, R., & Det, M. Van. (1977). Plankton Dynamics and Nutrient Enrichment of the Scotian Shelf. Journal of the Fisheries Research Board of Canada, 34(7), 1004–1018. https://doi.org/10.1139/f77-153

Franklin, J.E., Drummond, J.R., Griffin, D., Pierce, J.R., Waugh, D.L., Palmer, P.I., Parrington, M.P., Lee, J.D., Lewis, A.C., Rickard, A.R., Taylor, J.W., Allan, J.D., Coe, H., Chisholm, L., Duck, T.J., Hopper, J.T., Gibson, M.D., Curry, K.R., Sakamoto, K.M., Lesins, G., Walker, K.A., Dan, L., Kliever, J., & Saha, A. (2014) A case study of aerosol depletion in

a biomass burning plume over Eastern Canada during the 2011 BORTAS field experiment. Atmospheric Chemistry and Physics Discussions. acp-2014-31

Friends of Sable Island Society | A Brief History of Sable Island. (2012). Retrieved November 21, 2017, from http://sableislandfriends.ca/?p=148

Fuzzi, S., Baltensperger, U., Carslaw, K., Decesari, S., Denier Van Der Gon, H., Facchini, M. C., … Gilardoni, S. (2015). Particulate matter, air quality and climate: Lessons learned and future needs. Atmospheric Chemistry and Physics, 15(14), 8217–8299. https://doi.org/10.5194/acp-15-8217-2015

Georges, A.A., El-Swais, H., Craig, S.E., Li, W.K.W & Walsh, D.W. (2014) Metaproteomic analysis of a winter to spring succession in coastal northwest Atlantic Ocean microbial plankton. International Society for Microbial Ecology, 14, 1751-7362.

Gibson, M. D., & Hopper, J. T. (2013b). Sable island study. Retrieved 10/28, 2013, from http://afrg.peas.dal.ca/sableisland/index.php

Gibson, M. D., Guernsey, J. R., Beauchamp, S., Waugh, D., Heal, M. R., Brook, J. R., … Terashima, M. (2009). Journal of the Air & Waste Management Association Quantifying the Spatial and Temporal Variation of Ground-Level Ozone in the Rural Annapolis Valley, Nova Scotia, Canada Using Nitrite-Impregnated Passive Samplers Quantifying the Spatial and Temporal V. Journal of the Air & Waste Management Association, 593, 310–320. https://doi.org/10.3155/1047-3289.59.3.310

Gibson, M. D., Haelssig, J., Pierce, J. R., Parrington, M., Franklin, J. E., Hopper, J. T., … Ward, T. J. (2015). A comparison of four receptor models used to quantify the boreal wildfire smoke contribution to surface PM2.5 in Halifax, Nova Scotia during the BORTAS-B experiment. Atmospheric Chemistry and Physics, 15(2), 815–827. https://doi.org/10.5194/acp-15-815-2015

Gibson, M. D., Heal, M. R., Bache, D. H., Hursthouse, A. S., Beverland, I. J., Craig, S. E., … Jones, C. (2009). Using Mass Reconstruction along a Four-Site Transect as a Method to Interpret PM10 in West-Central Scotland,United Kingdom. Journal of the Air & Waste Management Association, 59(12), 1429–1436. https://doi.org/10.3155/1047-3289.59.12.1429

Gibson, M. D., Heal, M. R., Li, Z., Kuchta, J., King, G. H., Hayes, A., & Lambert, S. (2013). The spatial and seasonal variation of nitrogen dioxide and sulfur dioxide in Cape Breton Highlands National Park, Canada, and the association with lichen abundance. Atmospheric Environment, 64, 303–311. https://doi.org/10.1016/j.atmosenv.2012.09.068

Gibson, M. D., Kundu, S., & Satish, M. (2013). Dispersion model evaluation of PM2.5, NOx and SO2 from point and major line sources in Nova Scotia, Canada using AERMOD Gaussian plume air dispersion model. Atmospheric Pollution Research, 4(2), 157–167. https://doi.org/10.5094/APR.2013.016

Gibson, M. D., Pierce, J. R., Waugh, D., Kuchta, J. S., Chisholm, L., Duck, T. J., … Palmer, P. I. (2013). Identifying the sources driving observed PM2.5 temporal variability over Halifax, Nova Scotia, during BORTAS-B. Atmospheric Chemistry and Physics, 13(14), 7199–7213. https://doi.org/10.5194/acp-13-7199-2013

Gibson, M. D., Ward, T. J., Wheeler, A. J., Guernsey, J. R., Seaboyer, M. P., Bazinet, P., King, G. H., Brewster, N. B., Kuchta, J., Potter, R. & Stieb, D. M. (2010). Woodsmoke source apportionment in the Rural Annapolis Valley, Nova Scotia, Canada. Conference Proceedings of the 103rd Annual Conference of the Air and Waste Management Association, Calgary.

Government of Canada, P. C. A.-S. A. P. (2014). Parks Canada - Internal Audit and Evaluation Documents. Retrieved from https://www.pc.gc.ca/leg/docs/pc/rpts/rve-par/88/index_e.asp

Government of Canada. (2016). Environment and Climate Change Canada. Retrieved November 3, 2017, from https://ec.gc.ca/meteoaloeil-skywatchers/default.asp?lang=En&n=7884CDEA-1

Greenan, B. J. W., Petrie, B. D., Harrison, W. G., & Oakey, N. S. (2004) Are the spring and fall blooms on the Scotian Shelf related to short-term physical events? Continental Shelf Research. 24, 603-625, 10.1016/j.csr.2003.11.006.

Guenther, A., Geron, C., Pierce, T., Lamb, B., Harley, P., & Fall, R. (2000). Natural emissions of non-methane volatile organic compounds, carbon monoxide, and oxides of nitrogen from North America. Atmospheric Environment, 34 (12-14), 2205-2230. doi:10.1016/S1352-2310(99)00465-3

Guo, H., Wang, T., & Louie, P. K. K. (2004). Source apportionment of ambient non-methane hydrocarbons in Hong Kong: Application of a principal component analysis/absolute principal component scores (PCA/APCS) receptor model. Environmental Pollution, 129, 489-498.

Ha, S., Sundaram, R., Louis, G. M. B., Nobles, C., Seeni, I., Sherman, S., & Mendola, P. (2017). Ambient air pollution and the risk of pregnancy loss: a prospective cohort study. https://doi.org/10.1016/j.fertnstert.2017.09.037

Hader, D., & Schafer, J. (1995). Photosynthetic Oxygen Production in Macroalgae and Phytoplankton under Solar Irradiation.

Halsey, K. H., Giovannoni, S. J., Graus, M., Zhao, Y., Landry, Z., Thrash, J. C., … de Gouw, J. (2017). Biological cycling of volatile organic carbon by phytoplankton and bacterioplankton. Limnology and Oceanography, 62(6), 2650–2661. https://doi.org/10.1002/lno.10596

Hannah, C.G., Shore, J.A., Loder, J.W., & Naimie, C.E. (2001). Seasonal Circulation on the Western and Central Scotian Shelf. Journal of Physical Oceanography, 31.

Hansen, J., Sato, M., Kharecha, P., & Von Schuckmann, K. (2011). Earth's energy imbalance and implications. Atmospheric Chemistry and Physics, 11(24), 13421–13449. https://doi.org/10.5194/acp-11-13421-2011

Harrison, R. M. (1990). Pollution : causes, effects, and control. (3rd ed. .). Cambridge: Cambridge : Royal Society of Chemistry Information Services. Retrieved from http://silk.library.umass.edu/login?url=http://search.ebscohost.com/login.aspx?direct=true&db=cat06087a&AN=umass.000759019&site=eds-live&scope=site

Harrison, R. M., Beddows, D. C. S. & Dall'Osto, M. (2011). PMF Analysis of Wide-Range Particle Size Spectra Collected on a Major Highway. Environmental Science & Technology, 45, 5522-5528

Harrison, R. M., Deacon, A. R., & Jones, M. R. (1997). Sources and processes affecting concentrations of PM10 and PM2.5 particulate matter in Birmingham (U.K.). Atmospheric Environment, 31(24), 4103-4117. doi:1352-2310/97

Hayes, A. (2014). Source Apportionment of the Air Quality on Sable Island. Dalhousie University.

Henson, S. A., Dunne, J. P., & Sarmiento, J. L. (2009). Decadal variability in North Atlantic phytoplankton blooms. Journal of Geophysical Research: Oceans, 114(4), 1–11. https://doi.org/10.1029/2008JC005139

Hillemann, L., Zschoppe, A., & Caldow, R. (2007). Aerosol mobility spectrometry based on diffusion charging. Retrieved from http://www.tsi.com/uploadedFiles/_Site_Root/Products/Literature/Posters/UFIPOLNET_EAC07_Hillemann_lecture.pdf

Hinds, W. C. (1999). Aerosol technology: Properties, Behavior, and Measurement of Airborne Particles. Wiley-Interscience Publication (2nd ed. ., Vol. 70). New York: New York : Wiley. https://doi.org/10.1016/0021-8502(83)90049-6

Hobbs, P. V. (1993). Aerosol--cloud--climate interactions. San Diego: San Diego : Academic Press.

Hoffmann, T., Bandur, R., Marggraf, U., & Linscheid, M. (2012). Molecular composition of organic aerosols formed in the α-pinene/O3 reaction: Implications for new particle formation processes. Journal of Geophysical Research: Atmospheres, 103(D19), 25569-25578. doi:10.1029/98JD01816

Holgate, S.T., Samet, J.M., Koren, H.S., & Maynard, R.L. (1999) Air Pollution and Health (pp 1-2). Academic Press.

Hondula, D. M., Sitka, L., Davis, R. E., Knight, D. B., Gawtry, S. D., Deaton, M. L., … Stenger, P. J. (2010). A back-trajectory and air mass climatology for the Northern Shenandoah

Valley, USA. International Journal of Climatology, 30(4), 569–581. https://doi.org/10.1002/joc.1896

Huang, Y., Shen, H., Chen, H., Wang, R., Zhang, Y., Su, S., … Tao, S. (2014). Quantification of global primary emissions of PM$_{2.5}$, PM$_{10}$, and TSP from combustion and industrial process sources. Environmental Science and Technology, 48(23), 13834–13843. https://doi.org/10.1021/es503696k

Hubert, L., Meulman, J., & Heiser, W. (2000). Two purposes for matrix factorization: A historical appraisal. Society for Industrial and Applied Mathematics, 42(1), 68-82. doi: PII: S0036144598340483

HYSPLIT - hybrid single particle lagrangian integrated trajectory model. (2012). Retrieved 10/28, 2013, from http://www.arl.noaa.gov/HYSPLIT_info.php

IPCC. (2014). Climate Change 2013 - The Physical Science Basis. Climate Change 2013: The Physical Science Basis. Contribution of Working Group I to the Fifth Assessment Report of the Intergovernmental Panel on Climate Change. https://doi.org/10.1017/CBO9781107415324

Jabre, L. (2017). Source Sector Analysis of Marine and Other Volatile Organic Compounds on Sable Island, Nova Scotia, Canada. Dalhousie University.

Jacob, C., Field, B. D., Jin, E. M., Bey, I., Li, Q., Logan, J. A., … Jacob, D. J. (2002). Atmospheric budget of acetone. Journal of Geophysical Research, 107(D10). https://doi.org/10.1029/2001JD000694

Jacob, D. J. (1999). Ozone air pollution. Introduction to atmospheric chemistry (pp. 231-242). Princeton, New Jersey: Princeton University Press.

Jaeckals, J. M., Bae, M.S. & Schauer, J. J. (2007). Positive Matrix Factorization (PMF) Analysis of Molecular Marker Measurements to Quantify the Sources of Organic Aerosols. Environmental Science & Technology, 41, 5763-5769.

Jeong, C., McGuire, M. L., Herod, D., Dann, T., Dabek–Zlotorzynska, E., Wang, D., … Evans, G. (2011). Receptor model based identification of PM2.5 sources in Canadian cities. Atmospheric Pollution Research, 2(2), 158–171. https://doi.org/10.5094/APR.2011.021

Jeong, C., McGuire, M., Herod, D., Dann, T., Dabek-Zlotorzynska, E., Wang, D., Evans, G. (2011). Receptor model based identification of PM2.5 sources in Canadian cities Atmospheric Pollution Research, 2, 158-171. doi:10.5094/APR.2011.021

Johnson, C., Harrison, G., Head, E., Spry, J., Pauley, K., Maass, H., Kennedy, M., Porter, C., Yashayaeva, I., and Casault, B. (2012). Optical, chemical and biological conditions in the maritimes resion in 2009 and 2010. Canadian Science Advisory Secretariat (CSAS). Bedford Institute of Oceanography

Jones, A. M., Harrison, R. M., & Baker, J. (2010). The wind speed dependence of the concentrations of airborne particulate matter and NOx. Atmospheric Environment, 44(13), 1682–1690. https://doi.org/10.1016/j.atmosenv.2010.01.007

Kearns, J. (BHP P., Armstrong, K. (Chevron), Shirvill, L. (Shell), Garland, E. (Elf), Simon, C. (Texaco), & Monopolis, J. (Exxon). (2000). Flaring & venting in the oil & gas exploration & production industry. IOGP Publications. https://doi.org/Report No. 2.79/288

Kearns, J., Armstrong, K., Shirvill, L., Garland, E., Simon, C., & Monopolis, J. (2000). Flaring & venting in the oil and gas exploration & production industry. (No. 2.79/288). International Association of Oil and Gas Producers.

Khoo, H. H., & Tan, R. B. H. (2006). Environmental impact evaluation of conventional fossil fuel production (oil and natural gas) and enhanced resource recovery with potential CO2 sequestration. Energy and Fuels, 20, 1914-1924. doi:10.1021/ef060075+

Kim, K. D., & Lee, E. J. (2005). Potential tree species for use in the restoration of unsanitary landfills. Environmental Management, 36(1), 1–14. https://doi.org/10.1007/s00267-004-1089-3

Kim, Y. M., Harrad, S., & Harrison, R. M. (2001). Concentrations and sources of VOCs in urban domestic and public microenvironments. Environmental Science and Technology, 35(6), 997-1004. doi:10.1021/es000192y

Krewski, D., Burnett, R., Goldberg, M., Hoover, K., Siemiatycki, J., Abrahamowicz, M., & White, W 2005b. Reanalysis of the Harvard Six Cities Study, Part I: Validation and Replication. Inhalation toxicology, 17, 335-342.

Kulmala, M., Dal Maso, M., Mäkelä, J. M., Pirjola, L., Väkevä, M., Aalto, P., … O'Dowd, C. D. (2001). On the formation, growth and composition of nucleation mode particles. Tellus, Series B: Chemical and Physical Meteorology, 53(4), 479–490. https://doi.org/10.3402/tellusb.v53i4.16622

Kulmala, M., Vehkamäki, H., Petäjä, T., Dal Maso, M., Lauri, A., Kerminen, V. M., … McMurry, P. H. Formation and growth rates of ultrafine atmospheric particles: A review of observations, 35 Journal of Aerosol Science § (2004). Pergamon. https://doi.org/10.1016/j.jaerosci.2003.10.003

Levy, M. A. (1993). In Haas P. M., Keohane R. O. and Levy M. A. (Eds.), European acid rain: The power of tote-board diplomacy (Institution for the Earth ed.). Massachusetts: The MIT Press.

Mahowald, N., Ward, D. S., Kloster, S., Flanner, M. G., Heald, C. L., Heavens, N. G., … Chuang, P. Y. (2011). Aerosol Impacts on Climate and Biogeochemistry. Annual Review

of Environment and Resources, 36(1), 45–74. https://doi.org/10.1146/annurev-environ-042009-094507

McNeilly, J. D., Heal, M. R., Beverland, I. J., Howe, A., Gibson, M. D., Hibbs, L. R., … Donaldson, K. (2004). Soluble transition metals cause the pro-inflammatory effects of welding fumes in vitro. Toxicology and Applied Pharmacology, 196(1), 95–107. https://doi.org/10.1016/j.taap.2003.11.021

Mills, N. L., Robinson, S. D., Fokkens, P. H. B., Leseman, D. L. A. C., Miller, M. R., Anderson, D., Cassee, F. R. (2008). Exposure to concentrated ambient particles does not affect vascular function in patients with coronary heart disease. Environmental Health Perspectives, 116, 709-715.

Model 5012 instruction manual. (2009). Franklin, MA: Thermo Scientific.

Model 55i instruction manual. (2008). Franklin, MA: Thermo Scientific.

MODIS Web. (2015). Retrieved August 1, 2017, from http://modis.gsfc.nasa.gov/sci_team/pubs/abstract_new.php?id=19776

Monitoring, A. Q. (2014). Model 3031200 Environmental Sampling System Field Setup with Model 3031 Ultrafine Particle Monitor. Retrieved from http://www.tsi.com/uploadedFiles/_Site_Root/Products/Literature/Application_Notes/UFP-002_Model_3031200_Env_Samp_Sys.pdf

Monks, P. S., Granier, C., Fuzzi, S., Stohl, A., Williams, M. L., Akimoto, H., … von Glasow, R. (2009). Atmospheric composition change - global and regional air quality. Atmospheric Environment, 43(33), 5268–5350. https://doi.org/10.1016/j.atmosenv.2009.08.021

Moore, R. M., Oram, D. E., & Penkett, S. A. (1994). Production of isoprene by marine phytoplankton cultures. Geophysical Research Letters, 21(23), 2507–2510. https://doi.org/10.1029/94GL02363

MSFC, J. W. : (2009). NASA - Giovanni: An Easier Way to Visualize Earth Science Data. Retrieved November 7, 2017, from http://www.nasa.gov/audience/foreducators/9-12/features/giovanni-an-easier-way.html

NASA Ocean Biology Processing Group. (2015). MODIS-Aqua Level 3 Binned Chlorophyll Data Version 2014. Greenbelt, MD, USA: NASA Ocean Biology DAAC. https://doi.org/10.5067/AQUA/MODIS/L3B/CHL/2014

Niinemets, U., Loreto, F., & Reichstein, M. (2004). Physiological and physicochemical controls on foliar volatile organic compound emissions. Trends in Plant Science, 9(4), 180-186. doi:10.1016./j.tplants..2004.02.006

NOAA. (2017). Visible Infrared Imaging Radiometer Suite (VIIRS). Retrieved August 1, 2017, from https://ncc.nesdis.noaa.gov/VIIRS/

Norris, G., Duvall, R., Brown, S., & Bai, S. (2014). EPA Positive Matrix Factorization (PMF) 5.0 Fundamentals and User Guide, 136. https://doi.org/EPA/600/R-14/108

Norris, G., Vedantham, R., Wade, K., Brown, S., Prouty, J., & Foley, C. (2008). EPA positive Matrix Factorization (PMF) 3.0 fundamentals & user guide. U.S. Environmental Protection Agency.

Nova Scotia ambient air quality monitoring network. (2010). Retrieved 10/28, 2013, from https://www.novascotia.ca/nse/air/docs/AirMonitoringNetworkMap.pdf

Nova Scotia Environment: Air quality regulations, Environment Act U.S.C. 12 (2010).

Nova Scotia Offshore Petroleum Board. (2000). Technical Summaries of Scotian Shelf Significant and Commercial Discoveries (Technical Summary). Canada.

Nova Scotia Offshore Petroleum Board. (2011). A synopsis of Nova Scotia's offshore oil and gas environmental effects monitoring programs (Summary). Canada.

Novak, C. (2004). The oxford dictionary of statistical terms Dodge Y (ed). Pharmaceutical Statististics. doi: 10.1002/pst.128.

Novakov, T., & Penner, J. E. (1993). Large contribution of organic aerosols to cloud-condensation-nuclei concentrations. Nature, 365, 823-826. doi:10.1038/365823a0

O'Dowd, C. D., Facchini, M. C., Cavalli, F., Ceburnis, D., Mircea, M., Decesari, S., Fuzzi, S., Yoon, Y. J. & Putaud, J.P. (2004). Biogenically driven organic contribution to marine aerosol. Nature, 431, 676-680.

O'Dowd, C. D., Aalto, P., Hmeri, K., Kulmala, M., & Hoffmann, T. (2012). Aerosol formation: Atmospheric particles from organic vapours. Nature, 416(6880), 497-498. doi:10.1038/416497a

O'Dowd, C., Ceburnis, D., Ovadnevaite, J., Vaishya, A., Rinaldi, M., & Facchini, M. C. (2014). Do anthropogenic, continental or coastal aerosol sources impact on a marine aerosol signature at Mace Head? Atmospheric Chemistry and Physics, 14(19), 10687–10704. https://doi.org/10.5194/acp-14-10687-2014

O'Dowd, C.D., & Leeuw, G. (2007). Marine aerosol production: a review of the current knowledge. Philosophical Transactions of the Royal Society A, 365, 1753 – 1774. doi: 10.1098/rsta.2007.2043

Palmer, P. I., & Shaw, S. L. (2005). Quantifying global marine isoprene fluxes using MODIS chlorophyll observations. Geophysical Research Letters, 32(L09805) doi:10.1029/2005GL022592

Palmer, P. I., Parrington, M., Lee, J. D., Lewis, A. C., Rickard, A. R., Bernath, P. F., … Young, J. C. (2013). Quantifying the impact of Boreal forest fires on Tropospheric oxidants over the Atlantic using Aircraft and Satellites (BORTAS) experiment: Design, execution and science overview. Atmospheric Chemistry and Physics, 13(13), 6239–6261. https://doi.org/10.5194/acp-13-6239-2013

Paterson, K. G., Sagady, J. L., Hooper, D. L., Bertman, S. B., Carroll, M. A., & Shepson, P. B. (1999). Analysis of air quality data using positive matrix factorization. Environmental Science and Technology, 33(4), 635-641.

Pelucchi, C., Negri, E., Gallus, S., Boffetta, P., Tramacere, I., & La Vecchia, C. (2009). Long-term particulate matter exposure and mortality: a review of European epidemiological studies. BMC Public Health, 9, 453. https://doi.org/10.1186/1471-2458-9-453

Pen, T., Hingston, M., Waugh, D., Keast, S., Mcpherson, J., Worthy, D., & Forbes, G. (2009). Sable Island air monitoring program report: 2003-2006 (Technical Report). Meteorological Service of Canada Atlantic Region Science.

Piccot, S. D., Watson, J. J., & Jones, J. W. (1992). A global inventory of volatile organic compound emissions from anthropogenic sources. Journal of Geophysical Research, 97(D9), 9897-9912. doi:0148-0227/92/92JD-006825

Pierce, J. R. & Adams, P. J. (2009). Uncertainty in global CCN concentrations from uncertain aerosol nucleation and primary emission rates. Atmospheric Chemistry and Physics, 9, 1339-1356.

Pilling, M., ApSimon, H., Carruthers, D., Carslaw, D., Colvile, R., Derwent, R., Stevenson, K. (2005). Particulate matter in the United Kingdom: Summary. London, U.K.: Air Quality Expert Group.

Pope III, C. A., Burnett, R. T., Thun, M. J., Calle, E. E., Krewski, D., Ito, K., & Thurston, G. D. (2002). Lung Cancer, Cardiopulmonary Mortality, and Long-term Exposure to Fine Particulate Air Pollution. JAMA, 287(9), 1132. https://doi.org/10.1001/jama.287.9.1132

Pope, C. A., Burnett, R. T., Thun, M. J., Calle, E. E., Krewski, D., Ito, K., & Thurston, G. D. (2002). Lung cancer, cardiopulmonary mortality, and long-term exposure to fine particulate air pollution. The Journal of the American Medical Association, 287, 1132-1141.

Qeurol, X., Alastuey, A., Ruiz, C. R., Artinano, B., Hansson, H. C., Harrison, R. M., Buringh, E., Ten Brink, H. M., Lutz, M., Bruckmann, P., Straehl, P. & Schneider, J. 2004. Speciation

and origin of PM10 and PM2.5 in selected European cities. Atmospheric Environment, 38, 6547-6555.

Quinn, P. K., & Bates, T. S. (2011). The case against climate regulation via oceanic phytoplankton sulphur emissions. Nature, 480(7375), 51–56. https://doi.org/10.1038/nature10580

Ramadan, Z., Song, X. H., & Hopke, P. K. (2000). Identification of sources of phoenix aerosol by positive matrix factorization. Journal of the Air and Waste Management Association, 50(8), 1308–1320. https://doi.org/10.1080/10473289.2000.10464173

Reimer, D.D., Milne, P.J., Zika, R.G., & Pos, W.H. (2000). Photoproduction of nonmethane hydrocarbons (NMHC) in seawater. Marine Chemistry. 71, 177– 198.

Rosselli, R., Fiamma, M., Deligios, M., Pintus, G., Pellizzaro, G., Canu, A., … Cappuccinelli, P. (2015). Microbial immigration across the Mediterranean via airborne dust. Scientific Reports, 5(1), 16306. https://doi.org/10.1038/srep16306

Rumchev, K., Spickett, J., Bulsara, M., Phillips, M., & Stick, S. (2004). Association of domestic exposure to volatile organic compounds with asthma in young children. Thorax, 59, 746-751. doi:10.1136/thx.2003.013680

Ryerson, T. B., Trainer, M., Angevine, W. M., Brock, C. A., Dissly, R. W., Fehsenfeld, F. C., Sueper, D. T. (2003). Effect of petrochemical industrial emissions of reactive alkenes and NOx on tropospheric ozone formation in Houston, TX. Journal of Geophysical Research: Atmospheres, 108(D8), 27. doi:10.1029/2002JD003070

Sable Aviation - Aircraft Charter to Sable Island. (2017). Retrieved November 23, 2017, from http://www.sableaviation.ca/

Sable Island national park reserve: Park establishment. (2012). Retrieved 06/03, 2013, from http://www.pc.gc.ca/eng/pn-np/ns/sable/plan/plan01.aspx

Sable Island: A story of survival. (2001). Retrieved 06/03, 2013, from http://museum.gov.ns.ca/mnh/nature/sableisland/english_en/index_en.htm

Saltzman, E. S., & Cooper, W. J. (1989). Biogenic Sulfur in the Environment. Environmental Chemistry. Washington, DC: Washington, DC : American Chemical Society. https://doi.org/10.1021/bk-1989-0393

Schawrtz, J., & Marcus, A. (1990). Mortality and air pollution in London: A time series analysis. American Journal of Epidemiology, 131, 185-194.

Seinfeld, J. H., & Pandis, S. N. (2006). Atmospheric chemistry and physics - from air pollution to climate change (2nd ed.) John Wiley & Sons. Retrieved from:

http://www.knovel.com/web/portal/browse/display?_EXT_KNOVEL_DISPLAY_bookid =2126&VerticalID=0

Seinfeld, J., & Pandis, S. (2016). Atmospheric Chemistry and Physics: From Air Pollution to Climate Change (Third edit). Hoboken, New Jersey: John Wiley & Sons, Inc. Retrieved from Chemistry%5Cnand%5CnPhysics-1709322496/Atmospheric%5CnPhysics.pdf

Shadwick, E. H., Thomas, H., Azetsu-Scott, K., Greenan, B. J. W., Head, E., & Horne, E. (2011). Seasonal variability of dissolved inorganic carbon and surface water pCO2 in the Scotian Shelf region of the Northwestern Atlantic. Marine Chemistry, 124(1–4), 23–37. https://doi.org/10.1016/j.marchem.2010.11.004

Shaw, S. L., Gantt, B. & Meskhidze, N. (2010). Production and Emissions of Marine Isoprene and Monoterpenes: A Review. Advances in Meteorology, 2010.

Shaw, S.L., Chisholm, S.W., Prinn, R.G. (2003). Isoprene production by Prochlorococcus, a marine cyanobacterium, and other phytoplankton. Marine Chemistry, 80, 227– 245.

Shwartz, J., & Dockery, D. W. (1992). Increased mortality in Philadelphia associated with daily air pollution concentrations. The American Review of Respiratory Diseases, 145, 600-604.

Siegel, D. A., Doney, S. C., & Yoder, J. A. (2002). The North Atlantic Spring Phytoplankton Bloom and Sverdrup's Critical Depth Hypothesis. Science, 296(5568), 730 LP-733. Retrieved from http://science.sciencemag.org/content/296/5568/730.abstract

Singh, H. B., Kanakidou, M., Crutzen, P. J., & Jacob, D. J. (1995). High concentrations and photochemical fate of oxygenated hydrocarbons in the global troposphere. Nature, 378(6552), 50–54. https://doi.org/10.1038/378050a0

Sioutas, C., Delfino, R. J., & Singh, M. (2005). Exposure assessment for atmospheric Ultrafine Particles (UFPs) and implications in epidemiologic research. Environmental Health Perspectives. https://doi.org/10.1289/ehp.7939

Slingo, A. (1990). Sensitivity of the Earth's radiation budget to changes in low clouds. Nature, 343(6253), 49–51. https://doi.org/10.1038/343049a0

Slowik, J. G., Stainken, K., Davidovits, P., Williams, L. R., Jayne, J. T., Kolb, C. E., … Jimenez, J. L. (2004). Particle morphology and density characterization by combined mobility and aerodynamic diameter measurements. Part 2: Application to combustion-generated soot aerosols as a function of fuel equivalence ratio. Aerosol Science and Technology, 38(12), 1206–1222. https://doi.org/10.1080/027868290903916

Snider, G., Weagle, C. L., Murdymootoo, K. K., Ring, A., Ritchie, Y., Stone, E., … Martin, R. V. (2016). Variation in global chemical composition of PM2.5: emerging results from

SPARTAN. Atmospheric Chemistry and Physics, 16(15), 9629–9653. https://doi.org/10.5194/acp-16-9629-2016

Solomon, P. a., & Hopke, P. K. (2008). The U . S . Environmental Protection Agency ' s Particulate Matter Supersites Program : An Integrated Synthesis of Scientific Findings and Policy- and Health-Relevant Insights. Journal of the Air & Waste Management Association, 58, 1–2. https://doi.org/10.3155/1047-3289.58.13.S-1

Solomon, S.D., Qin, M., Manning, Z., Chen, M., Marquis, K.B., Averyt, M., Tignor, & Miller, H.L. (2007). Contribution of Working Group I to the Fourth Assessment Report of the Intergovernmental Panel on Climate Change. Cambridge University Press.

Stieb, D. M., Burnett, R. T., Smith-Doiron, M., Brion, O., Shin, H. H., & Economou, V. (2008). No-threshold air quality health index based on short-term associations observed in daily time-series analyses. Journal of the Air and Waste Management Association, 58, 435-450. doi:10.3155/1047-3289.58.3.435

Stieb, D. M., Judek, S., & Burnett, R. T. (2002). Meta-analysis of time-series studies of air pollution and mortality: Effects of gases and particles and the influence of cause of death, age, and season. Journal of the Air and Waste Management Association, 52, 470-484.

Stohl, A. (2002). Chapter 21 Computation, accuracy and applications of trajectories- a review and bibliography. Developments in Environmental Science, 1(C), 615–654. https://doi.org/10.1016/S1474-8177(02)80024-9

Stohl, A., Haimberger, L., Scheele, M. P., & Wernli, H. (2001). An intercomparison of results from three trajectory models. Meteorological Applications, 8(2), 127–135. https://doi.org/10.1017/S1350482701002018

Sulphur oxides (Sox) Regulation 14. (2014). International Maritime Organization. Retrieved from: http://www.imo.org/OurWork/Environment/PollutionPrevention/ AirPollution/Pages/Sulphur-oxides-(SOx)-%E2%80%93-Regulation-14.aspx.

Targino, A. C., Gibson, M. D., Krecl, P., Rodrigues, M. V. C., dos Santos, M. M., & de Paula Corrêa, M. (2016). Hotspots of black carbon and PM2.5 in an urban area and relationships to traffic characteristics. Environmental Pollution, 218, 475–486. https://doi.org/10.1016/j.envpol.2016.07.027

Tassia Owen. (2017). MODIS | Terra. Retrieved August 1, 2017, from https://terra.nasa.gov/about/terra-instruments/modis

Teather, K., Hogan, N., Critchley, K., Gibson, M. D., Craig, S., & Hill, J. (2013). Examining the links between air quality, climate change and respiratory health in Qatar. Avicenna, 2013(1). https://doi.org/10.5339/avi.2013.9

The new dustrak II and DRX aerosol monitors (2011). TSI Incorporated.

The spatial and seasonal variation of nitrogen dioxide and sulphur dioxide in Cape Breton Highlands National Park, Canada, and the association with lichen abundance. Atmospheric Environment, 64, 303-311. doi:10.1016/j.atmosenv.2012.09.068

Thurston, G. D. & Spengler, J. D. (1985). A Quantitative Assessment of Source Contributions to Inhalable Particulate Matter Pollution in Metropolitan Boston. Atmospheric Environment (1967), 19, 9-25.

TSI Incorporated. (2012a). Aerodynamic ParTicle sizer® model 3321. USA. Retrieved from http://www.tsi.com/uploadedFiles/_Site_Root/Products/Literature/Brochures/3321 Operation brochure US-5001468_WEB.pdf

TSI Incorporated. (2012b). DustTrak DRX Aerosol Monitor Theory of Operation. Retrieved from http://www.tsi.com/uploadedFiles/_Site_Root/Products/Literature/Application_Notes/EX PMN-002_DustTrak_DRX_Theory_of_Operation.pdf

TSI Incorporated. (2015). FAST MOBILITY PARTICLE SIZER TM SPECTROMETER MODEL 3091 AEROSOL PARTICLES IN REAL-TIME IDEAL FOR A WIDE RANGE OF. Retrieved from http://www.tsi.com/uploadedFiles/_Site_Root/Products/Literature/Spec_Sheets/3091FMP S.pdf

Vaattovaara, P., Huttunen, P. E., Yoon, Y. J., Joutsensaari, J., Lehtinen, K. E. J., O'Dowd, C. D., & Laaksonen, A. (2006). The composition of nucleation and Aitken modes particles during coastal nucleation events: evidence for marine secondary organic contribution. Atmospheric Chemistry and Physics Discussions, 6(2), 3337–3379. https://doi.org/10.5194/acpd-6-3337-2006

Volatile organic compounds (VOCs). (2012). Retrieved 06/04, 2013, from: http://www.ec.gc.ca/air/default.asp?lang=En&n=15B9B65A-1

Wang, S., Nan, J., Shi, C., Fu, Q., Gao, S., Wang, D., … Zhou, B. (2015). Atmospheric ammonia and its impacts on regional air quality over the megacity of Shanghai, China. Scientific Reports, 5(1), 15842. https://doi.org/10.1038/srep15842

Ward, T. J. (2007). The Missoula, Montana PM2.5 source apportionment research Study. The University of Montana – Missoula Center for Environmental Health Sciences.

Ward, T. J. & Noonan, C. (2008). Results of a residential indoor PM2.5 sampling program before and after a woodstove changeout. Indoor Air, 18, 408-415.

Ward, T. J., Hamilton JR, R. F., Dixon, R. W., Paulsen, M. & Simpson, C. D. (2006a). Characterization and evaluation of smoke tracers in PM: Results from the 2003 Montana wildfire season. Atmospheric Environment, 40, 7005-7017.

Ward, T. J., Rinehart, L. R., & Lange, T. (2006b). Aerosol Science and Technology, The 2003/2004 Libby, Montana PM2.5 source apportionment research Study, 40, 166-177.

Ward, T., Trost, B., Conner, J., Flanagan, J., & Jayanty, R. K. M. (2012). Source apportionment of PM2.5 in a subarctic airshed - Fairbanks, Alaska. Aerosol and Air Quality Research, 12, 536-543.

Ware, J. H., Spengler, J. D., Neas, L. M., Samet, J. M., Wagner, G. R., Coultas, D., Schwab, M. (1993). Respiratory and irritant health effects of ambient volatile organic compounds. American Journal of Epidemiology, 137(12), 1287-1301.

Wark, K., Warner, C. F., & Davis, W. T. (1977). Air pollution. Its origin and control. Environmental Pollution (1970) (3rd ed., Vol. 13). https://doi.org/10.1016/0013-9327(77)90079-9

Watson, J. G., Robinson, N. F., Fujita, E. M., Chow, J. C., Pace, T. G., Lewis, C. & Coulter, T. (1998). CMB8 Applications andValidation Protocol for PM2.5 and VOCs. Report No. 1808.2D1 Reno, Nevada: Desert Research Institute.

Waugh, D., Inkpen, D. T., Hingston, M., Keast, S., McPherson, J., Worthy, D., & Forbes, G. (2010). Sable island air monitoring program report: 2003-2006. (No. 181). Dartmouth: Environmental Studies Research Funds.

Waugh, D., Inkpen, T., Hingston, M., Keast, S., Mcpherson, J., Worthy, D., & Forbes, G. (2003). Sable Island Air Monitoring Program Report: 2003-2006. Environmental Studies Research Funds Report (Vol. 56). Retrieved from http://publications.gc.ca/collections/collection_2016/one-neb/NE22-4-181-eng.pdf

Weekly operations report EnCana Deep Panuke production status. (2013). Canada - Nova Scotia Offshore Petroleum Board.

Wheeler, A. J., Gibson, M. D., MacNeill, M., Ward, T. J., Wallace, L. A., Kuchta, J., … Stieb, D. M. (2014). Impacts of air cleaners on indoor air quality in residences impacted by wood smoke. Environmental Science and Technology, 48(20), 12157–12163. https://doi.org/10.1021/es503144h

WHO, (2005). Air quality guidelines for particulate matter, ozone, nitrogen dioxide and sulphur dioxide. (Summary of risk assessment). World Health Organization.

WHO, 2002. World Health Report: Reducing Risks, Promoting Healthy Life. World Health Organization, Geneva, Switzerland.

WHO. (2013). Health Effects of Particulate Matter. https://doi.org/10.5124/jkma.2007.50.2.175

Will-Wolf, S., & Neitlich, P. (2010). Development of lichen response indexes using a regional gradient modelling approach for large-scale monitoring of forests (General Technical Report No. PNW-GTR- 807).United States Department of Agriculture.

Wilson, W. E., & Suh, H. H. (1997). Fine particles and coarse particles: Concentration relationships relevant to epidemiologic studies. Journal of the Air and Waste Management Association, 47(12), 1238–1249. https://doi.org/10.1080/10473289.1997.10464074

World Health Organization. (2013). Health Effects of Particulate Matter: Policy implications for countries in eastern Europe, Caucasus and central Asia. Journal of the Korean Medical Association, 50(2), 20. https://doi.org/10.5124/jkma.2007.50.2.175

Yang, C., Wang, J., Chan, C., Chen, P., Huang, J., & Chengs, M. (1997). Respiratory and irritant health effects of a population living in a petrochemical-polluted area in Taiwan. Environmental Research, 74, 145-149. doi:0013-9351/97

Yin, J., & Harrison, R. M. (2008). Pragmatic mass closure study for PM1.0, PM2.5 and PM10 at roadside, urban background and rural sites. Atmospheric Environment, 42, 980-988.

Yin, J., Allen, A. G., Harrison, R. M., Jennings, S. G., Wright, E., Fitzpatrick, M., McCusker, D. (2005). Major component composition of urban PM10 and PM2.5 in Ireland. Atmospheric Research, 78, 149-165.

Yoon, Y. J., Ceburnis, D., Cavalli, F., Jourdan, O., Putaud, J. P., Facchini, M. C., … O'Dowd, C. D. (2007). Seasonal characteristics of the physicochemical properties of North Atlantic marine atmospheric aerosols. Journal of Geophysical Research Atmospheres, 112(4), 1– 14. https://doi.org/10.1029/2005JD007044

Zahniser, A. (2007). Characterization of greenhouse gas emissions involved in oil and gas exploration and production operations. California Air Resources Board.